UNIVERSITÀ DEGLI STUDI DI PADOVA

Dipartimento di Fisica e Astronomia “Galileo Galilei”

Master Degree in Physics

Final Dissertation

Model-independent on-shell amplitude methods for one-loop Higgs production via gluon fusion

Thesis supervisor

Prof. Ramona Groeber

Candidate

Giuseppe Rizzi

Academic Year 2025/2026

Abstract

In this thesis, we use the on-shell amplitude method to derive a loop-induced amplitude without referring to a Lagrangian to determine the interaction rules. As an example, we study Higgs production via gluon fusion, for which we derive the amplitude for a subset of the contributing diagrams. This framework therefore encodes, in a model-independent way, all possible beyond-the-Standard-Model effects compatible with general principles such as Lorentz invariance and little-group scaling of the amplitude. The amplitude obtained is then matched onto its Standard Model Effective Field Theory (SMEFT) counterpart, and complete agreement is found. The results of this thesis lay the groundwork for systematically extending the on-shell amplitude approach to the one-loop level, providing a general algorithm for the construction and evaluation of loop amplitudes.

Contents

1 Introduction **1**

2 Motivations for physics beyond the Standard Model **7**
- 2.1 Experimental reasons 7
- 2.2 Theoretical reasons 9

3 Effective field theories as tools to probe BSM physics . . . **11**
- 3.1 Top-down and bottom-up approaches 12
  - 3.1.1 Power counting 14
- 3.2 SMEFT 15

4 The on-shell way **19**
- 4.1 The massless spinor helicity formalism 19
  - 4.1.1 Spinor notation 21
  - 4.1.2 Properties of angle and square spinors 23
  - 4.1.3 Polarization vectors 28
  - 4.1.4 The little group scaling 31
  - 4.1.5 Three-point amplitudes from little-group scaling 33
- 4.2 The massive spinor helicity formalism 38
  - 4.2.1 $h\bar{q}q$ amplitude from massless to massive 40
  - 4.2.2 Little group scaling in the massive case 43

5 Amplitude method at tree level **47**
- 5.1 Bootstrapping and gluing on-shell amplitudes 48
  - 5.1.1 Bootstrapping hgg 50
  - 5.1.2 Bootstrapping $ht\bar{t}$ 54
  - 5.1.3 Bootstrapping $\bar{t}tg$ 56

6 One-loop amplitudes and generalized unitarity **61**
- 6.1 Basic properties of one-loop integrals 61
  - 6.1.1 Example: reduction of a rank-two bubble integral 64

6.1.2 Passarino–Veltman reduction pattern 67
6.2 Implications of unitarity 69
6.3 Generalized unitarity 73
6.3.1 The van Neerven–Vermaseren basis 75
6.3.2 Integrand reduction in D dimensions 87

7 Higgs production via gluon-fusion at one-loop 91
7.1 Extending the analysis to one loop 91
7.1.1 Obtaining the SM contribution 95
7.2 Implementation of a generalized unitarity algorithm 98
7.3 SM amplitude 102
7.4 BSM amplitude at LO 105
7.4.1 Computation of the SM-like numerator 106
7.4.2 Computation of the pure BSM factor 107
7.4.3 Complete amplitude 108
7.4.4 Matching onto SMEFT 111

8 Conclusions 113

A SMEFT conventions and Feynman rules of interest 115
A.1 The Standard Model 115
A.2 $gg \to h$ at leading order in SMEFT 118
A.2.1 Computational implementation 120

B Representations of the Lorentz group 125
B.1 The Lorentz group 125
B.1.1 Left- and right-handed spinor fields 127
B.2 Particles in quantum field theory 131
B.2.1 Little group 132

C Massive spinor conventions 135
C.1 Useful relations among massive spinors 135
C.2 The high energy limit 136
C.3 Massive polarization vectors 137
C.4 Identity for an amplitude with two massive and one massless leg 139

D Explicit computations for hgg at one loop 141
D.1 Computation of SM integrand 141
D.1.1 SM integrand–way 1 141
D.1.2 SM amplitude–way 2 144
D.2 Loop-momentum parametrization 146
D.3 Implementation of the generalized unitarity algorithm for the b_{01} coefficient 147
D.3.1 Physical interpretation of the double cut (01) 149
D.3.2 Explicit evaluation 150
D.4 Computation of BSM integrand 153

Chapter 1

Introduction

The standard approach to compute scattering amplitudes relies on determining the set of Feynman rules from the Lagrangian of a chosen theory. These rules represent the basic building blocks for constructing scattering amplitudes and are conveniently expressed in terms of Feynman diagrams. Once we specify the process of interest, we systematically enumerate all allowed diagrams and sum them to obtain the corresponding scattering amplitude. When the relevant couplings permit a perturbative treatment, we end up with a power-series expansion in small coupling constants. The evaluation of these diagrams becomes highly non-trivial when loop contributions are involved, as we must deal with complicated integrals over the loop momenta and we must also take into account the regularization and renormalization of the theory [1–3].

The Standard Model (SM) of particle physics provides the theoretical framework in which such calculations can be consistently performed. However, it is widely recognized as an incomplete theory since, for instance, it fails to describe the mass of neutrinos, has no viable dark matter candidate and cannot generate the excess of baryons over antibaryons in the universe. Indeed, it is commonly interpreted as a low-energy effective description of an unknown more fundamental ultraviolet (UV) theory. A systematic and model-independent way to describe potential new physics is to extend the SM by higher-dimensional operators, leading to a more general description known as the Standard Model Effective Field Theory (SMEFT). In this approach, we supplement the SM Lagrangian by an infinite tower of higher-dimensional operators, each multiplied by a so-called Wilson coefficient whose structure remains unknown. We construct these local operators using the SM fields and asking to satisfy fundamental symmetry requirements, in particular invariance under the SM gauge group, $SU(3)_c \times SU(2)_L \times U(1)_Y$, as well as

Lorentz invariance. Moreover, we take the fields to transform exactly as in they do in the SM. The effects of heavy degrees of freedom, which are not directly accessible at current energies, are encoded into the Wilson coefficients, suppressed by a characteristic energy scale Λ, associated with the scale of new physics. In general an effective theory is valid in the regime where the typical energy of the process satisfies $E \ll \Lambda$ [4, 5].

Within this scheme, a key strategy to probe beyond-the-Standard-Model (BSM) physics is to analyze experimental data collected at high-energy particle accelerators by performing fits to observables, such as cross sections, computed in SMEFT. In particular, global fits are performed [6–9] for the Wilson coefficients that can give a guideline on where new physics can show up and how. These fits identify which deformations of SM interactions remain experimentally allowed and help prioritize future measurements. The SMEFT framework is though limited. Not only does it assume that new physics completely decouples, but also that the Higgs boson is part of an $SU(2)$ doublet, which is just an assumption and not an experimentally proven fact. The so-called Higgs Effetive Field Theory (HEFT) relaxes the assumption of a linearly realized Higgs doublet. The electroweak Goldstone bosons are described nonlinearly, while the physical Higgs is treated as an independent scalar singlet under the nonlinear realization. Its expansion is more complicated and organized by an appropriate chiral or HEFT power counting [10,11].

In this context, the amplitude approach provides a robust framework that can yield broader theoretical insights. In particular, the on-shell approach parametrizes interactions directly in terms of amplitudes, without choosing an off-shell operator basis. Its construction is instead organized by the assumed particle content, symmetries, locality and power counting. This comes with many advantages, namely that no $SU(2)$ structure of the scalar fields need to be assumed, it avoids ambiguities from field redefinitions and allows to write down process-specific all-order expressions in the EFT.

The first step to implement the amplitude method is to identify the physical process one wishes to study. In this thesis, we focus on gluon-gluon fusion into a Higgs boson, which represents the dominant Higgs production mechanism at the LHC and can therefore be probed with high precision experimentally. In the amplitude method we rely on more general arguments with respect to using a specific BSM theory. The amplitude is indeed bootstrapped from Lorentz invariance, little-group scaling, dimensional analysis, locality arguments, symmetry considerations, and possible factorization properties. Furthermore, the on-shell approach can describe both decoupling effects of the SMEFT type and non-decoupling effects characteristic of HEFT, without assuming that the Higgs belongs to a linearly realized electroweak doublet. In the non-decoupling case, the low-energy expansion must be organized using an appropriate HEFT or chiral power counting. Moreover, it avoids issues related to field redefinitions and operator choices, as well as unphysical degrees of freedom like ghosts or issues related to gauge fixing.

An important aspect of this construction is that we must specify the helicities of the external massless particles from the outset for the amplitude method to work properly. As a consequence, the contribution of each helicity configuration becomes naturally manifest at the amplitude level. Why is this important? At the High Luminosity Large Hadron Collider (HL-LHC) due to the large amount of data, we will be able to test kinematic features via multi-dimensional distributions, where we might be sensitive precisely to effects that carry helicity suppressions from non-interference with the SM. Furthermore, we get more and more sensitive to measurements that really probe helicities and polarisation, or spin correlations link in quantum observables [12, 13].

In general, the amplitude method outlined above works remarkably well at tree-level. At this order, in fact, scattering amplitudes display a relatively simple analytic structure: as functions of the external momenta, they can be characterised at most by the simple poles associated with the internal propagators. Moreover, assuming locality, the residues at these poles factorize into products of lower-point on-shell amplitudes, hence we can decompose a generic tree-level amplitude into the sum of a factorizable part, obtained by gluing lower-point amplitudes through factorization channels, and a non-factorizable part, which is instead bootstrapped from the general arguments mentioned above. The contact interaction of the amplitude can be naturally written by making its Lorentz- and little-group structure manifest. To this end, the spinor-helicity formalism is implemented, as it allows to write the momenta and polarization vectors in terms of spinors whose transformation properties under Lorentz- and little-group are well-defined. As a result of this, the possible singularities of the amplitude are contained in the factorizable piece, whereas the coefficients that parametrize the bootstrapped section can only be polynomial functions of the Mandelstam variables, hence admit a Taylor expansion in the relevant variables. The energy dimension of these coefficients is determined through dimensional analysis which forces us to introduce a cut-off scale that is can be chosen as the minimal energy at which unitarity would be violated. This clearly establishes a connection between the on-shell scattering amplitudes and EFTs: each coefficient in the amplitude expansion would in fact be related to a certain combination of Wilson coefficients of the chosen EFT [14].

What about loop corrections? In this case, the amplitudes are no longer merely meromorphic functions of the external kinematics. Instead, they develop a richer analytic structure, including branch cuts and logarithmic singularities generated by loop integrations. These non-analytic features encode the discontinuities of the amplitude and may be systematically studied through unitarity methods [15].

This thesis to our knowledge gives the first application of an agnostic amplitude basis to the one-loop case, build on bootstrapped contact terms and general on-shell $ht\bar{t}$ and $g\bar{t}t$ three-point structures. Accomplishing this extension represents a major step forward, as it allows us not only capture the well-established SM contributions to a given amplitude, but also to probe all possible Beyond-the-Standard-Model physics effects in a model-independent way beyond tree-level. Qualitatively, the general procedure to achieve this goal can be summarized in the following steps. We first construct the model-independent one-loop amplitude starting from the relevant model-independent tree-level lower-point amplitudes entering the process. This point relies crucially on the implementation of both massless and massive spinor-helicity formalism. Then, we expand this amplitude into a sum over the chosen basis of scalar loop integrals, together with the rational term contribution, each multiplied by an a priori unknown coefficient. Finally, by exploiting generalized unitarity techniques [15, 16], we determine the precise expression for all these coefficients. In this last step, performing 4-dimensional cuts over the internal propagators of the relevant Feynman diagrams of the process ensures the determination of only the cut-constructible part of the amplitude. By promoting the cuts to d dimensions [15, 17], the rational term is also properly captured. Needless to say, the resulting expression must contain the SM contribution, providing a valuable and controlled benchmark for the calculation.

The thesis work is structured as follows. In Ch. 2 we summarize the main problems of the SM of particle physics. We account for both experimental and theoretical reasons. This is the starting point for the search for BSM physics. Then, in Ch. 3 we review the traditional approach to probe BSM physics. Hence, after briefly introducing the general grounds of EFTs, we discuss SMEFT. We concentrate on the dimension-6 operators relevant for the $gg \to h$ process in the Warsaw basis. Then, by means of SmeftFR v3.03 [18–20], FeynArts [21], and FeynCalc [22–24], we reproduce the LO SMEFT amplitude for the process of interest. We recover the result reported in Ref. [25].

In Ch. 4, we introduce both the massless and massive spinor-helicity formalisms. We adopt a hands-on approach by providing some relevant examples. The aim of this chapter is to establish the power of little-group transformations in deriving on-shell tree-level amplitudes in a bottom-up approach. Then, in Ch. 5 we specialize this technology to evaluate the tree-level on-shell amplitude for the process hgg, as well as those for $ht\bar{t}$ and $\bar{t}tg$. These latter two amplitudes are the building blocks for evaluating the one-loop $gg \to h$ diagrams.

In order to move from tree-level to one-loop amplitude methods, in Ch. 6 we review the main amplitude techniques to compute one-loop amplitudes and establish the connection with generalized unitarity. In this context, we introduce the van Neerven–Vermaseren basis, which can be implemented to efficiently reconstruct an amplitude by performing unitarity cuts.

Finally, in Ch. 7 we have all the tools required to perform the calculation of one-loop Higgs production via gluon fusion. For the scope of this thesis, we perform the calculation considering the two SM-like diagrams with top quarks circulating in the loops. We first simplify the evaluation by benchmarking the algorithm against the SM contribution, which is correctly reproduced. We then promote the approach to the BSM structures at first order in the $1/\Lambda$ expansion. Here, generalized unitarity methods are implemented computationally by means of MATHEMATICA [26] and its interface with the package SMaSH [27]. Finally, we provide the matching of the amplitude we obtain with the one derived in the SMEFT framework. The correct implementation of the amplitude method allows this matching to work properly. Finally, Ch. 8 provides a summary and outlook.

Chapter 2

Motivations for physics beyond the Standard Model

Although the SM has been extremely successful in describing a wide range of experimental data, there are several reasons to believe that it cannot be the final theory of fundamental interactions [28]. These motivations can be divided into experimental observations and theoretical considerations.

2.1 Experimental reasons

- **Neutrino masses and oscillations.** In the SM, neutrinos are massless particles. This is because of the restricted particle content of the SM: it does not contain right-handed neutrino fields, and therefore neutrinos cannot acquire a Dirac mass through the Higgs mechanism. However, neutrino oscillation experiments have shown that neutrinos produced in a given flavor state can change their flavor during propagation [29, 30]. This implies that the flavor eigenstates do not coincide with the propagation eigenstates, namely the mass eigenstates. It turns out that neutrinos are much lighter than the other SM fermions, suggesting that their masses may originate from a different mechanism. Moreover, the ordering of the neutrino mass eigenstates is still under investigation and is usually referred to as the neutrino mass ordering.

  Different solutions have been proposed in order to give mass to neutrinos. A minimal extension of the SM consists in adding right-handed neutrinos and Yukawa interactions, so that neutrinos acquire a mass through the Higgs mechanism. We consider the right-handed neutrinos as singlets under $SU(3)_c \times SU(2)_L \times U(1)_Y$, hence they are sterile and can only be probed indirectly. So far, no conclusive evidence for right-handed neutrinos has been found. Moreover, following this strategy, we end up with an exceedingly small Yukawa coupling, especially when compared to the top Yukawa coupling.

Another possibility is that neutrinos are Majorana particles. In the minimal SM, this possibility is forbidden by the lepton-number conservation which emerges as an accidental global symmetry of theory. In particular, the see-saw mechanism introduces a heavy right-handed Majorana neutrino which is still sterile under the SM gauge group. This time, however, we are able to provide a small mass to the neutrinos without assuming an unnaturally small value of the Yukawa coupling. From an experimental point of view, if neutrinos are Majorana particles, neutrinoless double-β decay provides a possible probe. The observation of this process would therefore establish lepton-number violation and, under very general assumptions, imply a Majorana mass component for neutrinos.

- **Dark matter.** Galaxy rotation curves and gravitational lensing observations suggest the existence of a form of matter that interacts gravitationally but is invisible to electromagnetic radiation. This component is known as dark matter and accounts for approximately 84% of the total matter content of the Universe [31].

  In terms of particles, the SM does not provide a viable candidate for dark matter. In particular, the only SM particles with the right qualitative features are neutrinos, since they are neutral and weakly interacting. However, their small masses make them relativistic at decoupling and until late times, corresponding to hot dark matter. Their free streaming out of gravitational potential wells suppresses the formation of structures on small scales, making them incompatible with the observed large-scale structure if they constituted all of the dark matter. They can therefore account for only a small fraction of the observed dark matter relic density. Therefore, a particle-physics explanation of dark matter requires new degrees of freedom beyond the SM.

- **Matter–antimatter asymmetry.** It is known that the observable Universe contains much more matter than antimatter. In order to dynamically generate such an asymmetry, the Sakharov conditions must be satisfied: baryon-number violation, C and CP violation, and a departure from thermal equilibrium [32]. In this regards, the amount of CP violation introduced by the minimal SM is not sufficient. Therefore, the SM cannot account for the observed baryon asymmetry of the Universe. This suggests the presence of additional sources of baryon-number violation and CP violation, together with a new mechanism for departure from thermal equilibrium, beyond the SM.

2.2 Theoretical reasons

- **Naturalness and the hierarchy problem.** One of the main theoretical motivations for physics beyond the SM is the hierarchy between the electroweak scale and much higher energy scales. In particular, the SM may remain valid up to energies close to the Planck scale,

$$\Lambda_{\mathrm{Pl}} \sim 10^{19}\,\mathrm{GeV},$$

while electroweak symmetry breaking occurs at the much lower scale

$$v \simeq 246\,\mathrm{GeV}.$$

The Higgs sector is particularly sensitive to this large separation of scales. Because the Higgs mass parameter is not protected by a symmetry, particles at a heavy scale M that couple to the Higgs generally induce corrections proportional to M^2. If such scales are far above the electroweak scale, obtaining $v \simeq 246$ GeV can require cancellations among independent contributions. This requires a large amount of fine tuning among various contributions which ask for an explanation. This sensitivity is the electroweak hierarchy or naturalness problem.

- **Triviality and vacuum stability.** The Higgs sector may also develop problems when the SM is extrapolated to very high energies. In particular, the Higgs self-interaction changes with the energy scale because of quantum effects. For present central values of the Higgs and top-quark masses and the strong coupling constant, high-order SM calculations typically place the electroweak vacuum in the metastable region, with a tunnelling lifetime vastly longer than the age of the Universe. The distinction between absolute stability and metastability remains sensitive to the above-mentioned parameters [33].

- **The cosmological constant problem.** Another important theoretical problem concerns the extremely small observed value of the cosmological constant. The vacuum-energy density inferred from cosmological observations is tiny compared with the values we would naturally expect from the energy scales of particle physics, and even more so when compared with the Planck scale. The enormous difference between the observed value and theoretical expectations represents one of the most striking hierarchy and naturalness problems in fundamental physics.

- **Unexplained flavor structure.** The SM successfully describes the masses and interactions of quarks and leptons, but it does not explain why these parameters take the values observed in nature. Fermion masses span a very wide range, and the patterns of mixing among quarks and leptons are also remarkably different. These quantities are introduced in the SM as free parameters determined experimentally. The origin of this flavor structure therefore remains unexplained and may point toward additional symmetries, interactions, or organizing principles beyond the SM.

- **Strong CP problem.** At the renormalizable level, the SM Lagrangian must contain the term

$$\mathcal{L}_{\mathrm{SM}} \supset \theta \frac{g_s^2}{32\pi^2} G^{a,\mu\nu} \widetilde{G}^a_{\mu\nu}, \tag{2.1}$$

with θ being a dimensionless parameter, and $\widetilde{G}^a_{\mu\nu} = \frac{1}{2}\epsilon_{\mu\nu\rho\sigma} G^{a,\rho\sigma}$. This operator violates CP in the QCD sector of the SM Lagrangian. In particular, measurements of the electric dipole moment of the neutron lead to the bound $|\theta| \lesssim 10^{-10}$ [34], implying that CP violation in the strong interactions is extremely small. The exceedingly small value of θ is known as the strong CP problem.

Many possible solutions to these problems have been proposed, including new particles, new symmetries, new interactions, unification mechanisms, and extended Higgs sectors. However, no direct evidence for a specific BSM model has been found so far. For this reason, effective field theories provide a useful framework to describe possible new-physics effects [35, 36], if the new physics is assumed to be much heavier than the electroweak scale. We present the groundwork of EFTs in the next chapter.

Chapter 3

Effective field theories as tools to probe BSM physics

Effective Field Theories (EFTs) provide a general framework to describe the physics of a system at a given energy scale without requiring the full knowledge of its dynamics. The basic idea is that, if one is interested in processes occurring at energies much smaller than a certain high-energy scale Λ, the details of the dynamics above Λ do not need to be known explicitly. We encode their effects in a systematic expansion in powers of small parameters, such as E/Λ or m/Λ, where E is the typical energy of the process and m denotes a light mass scale [37–41].

An EFT must be constructed in such a way to fulfill the general requirements of the system under study, such as its symmetries. In this sense, an EFT is the most general field theory describing the relevant low-energy degrees of freedom, which is organized according to a given power counting prescription. More explicitly, an EFT is specified by:

- the set of light fields, together with their transformation properties under the symmetries of the system;
- the symmetries that determine which interactions are allowed;
- a power-counting rule, which organizes the Lagrangian as an expansion in small parameters.

In principle an EFT receives contributions from an infinite tower of higher-dimensional operators. Hence, how can such a theory be predictive? In general only a finite number of them contributes at any fixed order in the expansion. Therefore, physical observables can be computed to a given precision in terms of a finite number of parameters, which can either be measured experimentally or derived from a more fundamental theory.

3.1 Top-down and bottom-up approaches

In QFT, we typically use Lagrangians to encode the behaviour of a theory. In this context, an EFT Lagrangian acts as a bridge between a high-energy theory and low-energy observables. This connection can be used in two complementary ways.

Top-down approach. In the top-down approach, one starts from a known ultraviolet theory and derives the corresponding low-energy EFT. Suppose that the full theory contains light fields ϕ_ℓ, with masses $m_\ell \ll \Lambda$, and heavy fields ϕ_h, with masses $m_h \gtrsim \Lambda$. The ultraviolet theory can be schematically written in terms of an action of fields

$$\mathcal{S}_{\rm UV}(\phi_\ell, \phi_h) = \int d^4x\, \mathcal{L}_{\rm UV}(\phi_\ell, \phi_h, c), \tag{3.1}$$

where c parametrizes the coupling constants of the high-energy theory.

Therefore, the generating functional of the full theory reads

$$Z_{\rm UV}[J_\ell, J_h] = \int \mathcal{D}\phi_\ell \mathcal{D}\phi_h \exp\left[i\left(\mathcal{S}_{\rm UV}(\phi_\ell, \phi_h) + \int d^4x J_\ell\phi_\ell + \int d^4x J_h\phi_h\right)\right], \tag{3.2}$$

where J_ℓ and J_h are the light and heavy external sources, respectively.

Conversely, the low energy theory can be described by an action of light fields only

$$\mathcal{S}_{\rm IR}(\phi_\ell) = \int d^4x\, \mathcal{L}_{\rm IR}(\phi_\ell, c'). \tag{3.3}$$

Notice that the Lagrangian depends on specific IR parameters, denoted with c', which are commonly referred to as Wilson coefficients. The path integral of this theory can be straightforwardly written as

$$Z_{\rm IR}[J_\ell] = \int \mathcal{D}\phi_\ell \exp\left[i\left(\mathcal{S}_{\rm IR}(\phi_\ell) + \int d^4x J_\ell\phi_\ell\right)\right], \tag{3.4}$$

where the heavy external source has been switched off. Now, since in the IR region the two theories must give the same predictions, this implies

$$Z_{\rm IR}[J_\ell] = Z_{\rm UV}[J_\ell, J_h = 0]. \tag{3.5}$$

This relation means that, since the heavy fields cannot be produced on-shell in the low energy theory, they are removed from the complete spectrum by integrating them out. It is enough to require that

$$e^{iS_{\rm IR}(\phi_\ell)} \equiv \int \mathcal{D}\phi_h\, e^{iS_{\rm UV}(\phi_\ell, \phi_h)}, \tag{3.6}$$

in order to guarantee the above relation. We define the Wilsonian action as

$$S_{\rm W}(\phi_\ell) \equiv S_{\rm IR}(\phi_\ell), \tag{3.7}$$

which governs the low energy behaviour of the light fields.

In general, the task of determining this action is not trivial. Integrating out the heavy fields gives, in general, a non-local description. However, at energies much smaller than the heavy scale, $E \ll \Lambda$, the effects associated with the heavy degrees of freedom admit an expansion in powers of $1/\Lambda$. This can be seen straightforwardly at tree level. For instance, the propagator of a heavy particle can be expanded as

$$\frac{1}{p^2 - \Lambda^2} = -\frac{1}{\Lambda^2}\left(1 + \frac{p^2}{\Lambda^2} + \frac{p^4}{\Lambda^4} + \cdots\right), \qquad p^2 \ll \Lambda^2, \tag{3.8}$$

so that the exchange of the heavy particle is reproduced by a tower of local interactions with increasing numbers of derivatives. A similar argument applies at loop level, see e.g., [42]. Therefore, at low energies, the effects of the heavy degrees of freedom can be encoded in a local expansion in inverse powers of the heavy scale. The corresponding EFT Lagrangian can then be written as

$$\mathcal{L}_{\mathrm{IR}}(\phi_\ell, c') = \sum_n \mathcal{L}_{\mathrm{IR}}^{(n)}(\phi_\ell, c'), \tag{3.9}$$

where each term contains the appropriate power of $1/\Lambda$. The procedure that determines the low-energy Wilson coefficients c' by comparing the UV theory and the EFT is called matching.

After matching, the Wilson coefficients are evolved from the high scale down to the low-energy scale at which measurements are performed. This evolution is governed by renormalization-group equations and is called running. Finally, the EFT is used to compute physical observables at low energies.

Bottom-up approach. In the bottom-up approach, the ultraviolet theory is not specified. Instead, one constructs the most general low-energy Lagrangian compatible with the known degrees of freedom and symmetries. For example, if Lorentz invariance and gauge invariance are imposed, all operators consistent with these symmetries must be included.

The bottom-up EFT therefore takes the form

$$\mathcal{L}_{\mathrm{IR}}(\phi_\ell, c') = \sum_n \mathcal{L}_{\mathrm{IR}}^{(n)}(\phi_\ell, c'), \tag{3.10}$$

where the expansion is organized according to the chosen power-counting rule, and as before, the required precision determines where the expansion has to be truncated. In this case however, the Wilson coefficients are treated as free parameters and are constrained by experimental data.

This approach is particularly useful when the underlying high-energy theory is unknown, or when matching from the UV theory is too difficult to perform explicitly. In particular, a bottom-up approach is usually employed to parametrize BSM physics. In EFT approaches to new physics, the SM is augmented with higher-dimensional operators compatible with the symmetries of the theory. In this case the low-energy fields are the SM fields themselves and local interactions are required.

In this context, the scale of new physics, as well as the pattern and relative size of the Wilson coefficients associated with the different effective operators, are among the big open questions in particle physics. In the next section, we will provide a parametrization of BSM physics by means of SMEFT.

We should briefly comment on the role of field redefinitions in an EFT Lagrangian. In particular, the S-matrix equivalence theorem states that S-matrix elements do not depend on the choice of interpolating fields [43]. They are indeed invariant under local field redefinitions. This can be understood from the LSZ reduction formula, which relates momentum-space Green's functions to physical S-matrix elements [2]. Although field redefinitions can modify the Green's functions and their residues, these changes do not affect the resulting S-matrix elements. This allows us to employ the equations of motion of the fields to eliminate redundant operators in the EFT expansion. This point is particularly important since, at a fixed order in the expansion of an EFT Lagrangian, some of the operators that we would naively write in a bottom-up approach may instead be related by field redefinitions. This is, in general, a non-trivial task and requires fixing a basis of operators to work with. More on this will be provided in the context of the SMEFT operators.

3.1.1 Power counting

As discussed above, we need a rule that allows us to organize the EFT expansion. This is known as power counting. Qualitatively, it dictates which operators must be kept at a given order [43]. More explicitly, consider a scattering amplitude normalized to have mass dimension zero. If the relevant energy scale of the process is E, the insertion of a single operator of dimension $n > 4$ gives a contribution of order

$$\mathcal{M} \sim \left(\frac{E}{\Lambda}\right)^{n-4} . \tag{3.11}$$

Here, it is assumed that all the relevant light kinematic scales are of order E and that no additional suppressions are present. This follows from dimensional analysis, since the coefficient of a dimension-n operator has mass dimension $4 - n$ and is therefore suppressed by Λ^{n-4}.

More generally, if several higher-dimensional operators are inserted, the amplitude scales as

$$\mathcal{M} \sim \left(\frac{E}{\Lambda}\right)^{N} , \tag{3.12}$$

where

$$N = \sum_i (n_i - 4) , \tag{3.13}$$

and the sum runs over all inserted operators.

This formula shows how the EFT expansion is organized when the power counting is based on the canonical dimension of the operators, as in SMEFT [43]. Other EFTs may require a different power counting scheme. For instance, in HEFT the loop expansion also enters the power counting [10]. At leading order one keeps only the renormalizable part of the Lagrangian which is given by operators of dimension equal or lower to n. Corrections of order E/Λ instead arise from one insertion of a dimension-five operator. Corrections of order $(E/\Lambda)^2$ can arise either from one insertion of a dimension-six operator or from two insertions of dimension-five operators, and so on.

The same logic applies at loop level. For instance, if a loop diagram with two insertions of dimension-five operators is divergent, the corresponding counterterm has the structure of a dimension-six operator. This reflects the fact that EFTs are non-renormalizable in the traditional sense: renormalization requires an infinite tower of higher-dimensional operators.

Fortunately, this does not spoil predictivity. At any fixed accuracy in the expansion, only a finite number of operators contributes. Therefore, we can use EFTs as well-defined and predictive framework for describing low-energy phenomena without knowing the detailed dynamics at energies of order Λ or above.

3.2 SMEFT

Up to now, we have provided the basic tools for understanding the EFT framework without relying on a specific theory. In this section, we use this technology to describe BSM effects in SMEFT.

SMEFT provides a model-independent description of possible deviations from the Standard Model at energies below the characteristic scale of new physics which we still call Λ. As for the general case, the main assumption is that the high-energy effects are encoded by significantly heavier degrees of freedom with respect to those at the electroweak scale. This means that the former can be integrated out. This results in an expansion encoded in a tower of higher-dimensional local operators constructed exclusively from Standard Model fields and invariant under the gauge SM group

$$SU(3)_c \times SU(2)_L \times U(1)_Y. \tag{3.14}$$

In SMEFT, the Higgs field is assumed to belong to an $SU(2)_L$ doublet, so that electroweak symmetry breaking is linearly realized as in the Standard Model.

The SMEFT Lagrangian is obtained exploiting a bottom-up approach, and is organized as an expansion in inverse powers of the new-physics scale Λ,

$$\mathcal{L}_{\mathrm{SMEFT}} = \mathcal{L}_{\mathrm{SM}} + \sum_{d>4} \mathcal{L}^{(d)}, \qquad \mathcal{L}^{(d)} = \sum_i \frac{C_i^{(d)}}{\Lambda^{d-4}} Q_i^{(d)}, \tag{3.15}$$

where $\mathcal{L}_{\rm SM}$ is provided in Appendix A.1, $Q_i^{(d)}$ are gauge-invariant operators of dimension d, while $C_i^{(d)}$ are the corresponding Wilson coefficients. These parametrize the high-energy content which has been integrated out from the unknown ultraviolet (UV) completion. These coefficients are taken to be dimensionless since their mass dimension is made explicit via the Λ parameter.

In this work we focus on dimension-six operators only, and use the first non-redundant operator basis determined in the literature, namely the so-called Warsaw basis [44]. The construction of this basis was achieved by making field redefinitions on the SM fields, use integration by parts identities as well as Fierz identities. In particular, The Warsaw basis is constructed such as to remove as many derivative operators as possible. Clearly, as already pointed out many field redefinitions are possible and one should fix a preferable one from the outset. More on this can be found in [45].

We do not attempt a comprehensive review of SMEFT here. Instead, we retain only the dimension-6 operators relevant to the analysis of Higgs production through gluon fusion, which is the main production mode at the LHC. In particular, the SM contribution to this process is loop induced, and, at leading order, the dominant contribution is generated by a top-quark triangle. In SMEFT, this process receives both modifications of the top-mediated amplitude and genuinely new contributions. In principle, loops involving lighter quarks may also contribute in SMEFT, however, in the following we restrict our analysis to the top-quark contribution and neglect light-quark loops. The operators that directly generate the relevant interaction structures are [20]

$$
\begin{aligned}
Q_{\varphi G} &= \left(\varphi^\dagger\varphi\right) G^a_{\mu\nu} G^{a\mu\nu}, \\
Q_{\varphi \widetilde{G}} &= \left(\varphi^\dagger\varphi\right) G^a_{\mu\nu} \widetilde{G}^{a\mu\nu}, \\
Q_{uG}^{33} &= (\bar{q}_3 \sigma^{\mu\nu} T^a t_R)\, \widetilde{\varphi}\, G^a_{\mu\nu}, \\
Q_{u\varphi}^{33} &= \left(\varphi^\dagger\varphi\right) (\bar{q}_3 t_R \widetilde{\varphi}), \\
Q_{\varphi\Box} &= \left(\varphi^\dagger\varphi\right) \Box \left(\varphi^\dagger\varphi\right), \\
Q_{\varphi D} &= \left(\varphi^\dagger D^\mu\varphi\right)^* \left(\varphi^\dagger D_\mu\varphi\right).
\end{aligned}
\tag{3.16}
$$

where

$$
\widetilde{\varphi} = i\sigma_2\varphi^*, \qquad \widetilde{G}^a_{\mu\nu} = \frac{1}{2}\epsilon_{\mu\nu\rho\sigma} G^{a\rho\sigma}, \tag{3.17}
$$

$q_3 = (t_L, b_L)^T$ is the third-generation left-handed quark doublet, and the covariant derivative is defined in Eq. (A.7).

Therefore, we are interested in the following part of the SMEFT Lagrangian

$$\begin{aligned}\mathcal{L}^{(6)}_{\text{SMEFT}} \supset \frac{1}{\Lambda^2}\Big[&C_{\varphi G}Q_{\varphi G} + C_{\varphi\widetilde{G}}Q_{\varphi\widetilde{G}} \\ &+ \left(C^{33}_{uG}Q^{33}_{uG} + C^{33}_{u\varphi}Q^{33}_{u\varphi} + \text{h.c.}\right) \\ &+ C_{\varphi\Box}Q_{\varphi\Box} + C_{\varphi D}Q_{\varphi D}\Big].\end{aligned} \tag{3.18}$$

Here, the coefficients $C_{\varphi G}$ and $C_{\varphi\widetilde{G}}$ are real. These two operators are responsible for the non-vanishing tree level amplitude for $gg \to h$, which is absent in the SM case. $C_{\varphi G}$ produces a CP-even interaction, whereas $C_{\varphi\widetilde{G}}$ produces its CP-odd counterpart.

The latter four operators in the list contribute only to the loop diagrams. The first one, Q^{33}_{uG}, provides a genuinely new contribution by modifying the top-gluon vertices and is usually referred to as the chromomagnetic dipole operator. The remaining three operators modify the top-Higgs interaction. In particular, $Q_{\varphi\Box}$, $Q_{\varphi D}$, and $\text{Re}\left(Q^{33}_{u\varphi}\right)$ modify the CP-even top Yukawa coupling, while a non-zero $\text{Im}\left(Q^{33}_{u\varphi}\right)$ generates a CP-odd pseudoscalar top-Higgs interaction. Consequently, the Higgs coupling to top quarks contains both CP-even and CP-odd components, leading to CP violation.

In Appendix A.2, we first provide the relevant Feynman rules for the process $gg \to h$ at one loop. Then, we summarize the steps required to obtain computationally the SMEFT amplitude at leading order (LO) in the EFT expansion, i.e. at $\mathcal{O}(1/\Lambda^2)$. Considering the CP-even part of the amplitude, we obtain

$$\boxed{\mathcal{M}^{\text{SMEFT}}(g(p_1) + g(p_2) \to h) = i\,\frac{\alpha_s}{3\pi v}\,\delta^{ab}\,\varepsilon_{1\mu}\varepsilon_{2\nu}\left[p_1^\nu p_2^\mu - (p_1\cdot p_2)g^{\mu\nu}\right]F(\tau),} \tag{3.19}$$

with

$$\boxed{F(\tau) = c_t F_1(\tau) + c_g(\mu_R)F_2(\tau) + \text{Re}(c_{tg})\frac{m^2}{v^2}F_3(\tau).} \tag{3.20}$$

The expressions for the coefficients c_t, c_g, and c_{tg} in terms of the Wilson coefficients are given in Eq. (A.32), whereas the form factors $F_1(\tau)$, $F_2(\tau)$, and $F_3(\tau)$ are given in Eq. (A.31), with $\tau \equiv 4m^2/m_h^2$ and m the top mass. The above result coincides with that of Ref. [25].

Chapter 4

The on-shell way

Effective field theories, such as SMEFT and HEFT, provide a systematic way to parametrize the unknown effects of physics beyond the Standard Model. However, they unavoidably rely on the assumptions made when constructing the Lagrangian. A possible way to describe BSM effects without relying on a specific BSM Lagrangian, is to use on-shell amplitude methods. In this framework, the fundamental object is the scattering amplitude itself rather than the Lagrangian, which is not explicitly specified. These amplitudes can be constructed by relying on general principles such as Lorentz invariance, little-group scaling, and locality.

In this section, we introduce the spinor-helicity formalism, which provides the mathematical language needed to parametrize model-independent on-shell amplitudes. Both the massless and massive versions of the formalism are discussed, together with some useful examples that establish the notation and illustrate the underlying working principles.

4.1 The massless spinor helicity formalism

The spinor-helicity formalism is commonly employed in the calculation of scattering amplitudes. Compared to the conventional four-vector formalism, it has several advantages, as it makes the helicity structure of an amplitude manifest from the outset. In the case of massless particles, helicity is conserved under free time evolution and is also invariant under Lorentz transformations. It therefore serves as a quantum number that labels an irreducible representations of the Poincaré group. For this reason, it is convenient to start from the massless case, where the formalism is more naturally defined, and then extend it to the massive case.

We begin the discussion with Dirac spinors and later extend it to spin-1 particles. In Appendix B, we introduce the notation used in this section.

By reviewing the representations of the Lorentz group, we introduce left- and right-handed spinors as the objects of its first two non-trivial irreducible representations. We denote by $D^{(j_L,j_R)}$ the $(2j_L+1)(2j_R+1)$-dimensional representation of the Lorentz group, where j_L and j_R label the representations associated with the two independent $SU(2)$ algebras introduced in Eq. (B.11). Therefore, we denote by

$$D^{(\frac{1}{2},0)} \qquad \text{and} \qquad D^{(0,\frac{1}{2})}, \tag{4.1}$$

the left- and right-handed Weyl representations, respectively. These representations act on left-handed spinors $\psi_a(x)$ and right-handed spinors $\psi^\dagger_{\dot{a}}(x)$, respectively. Here, undotted and dotted indices each take two values, since both representations are two dimensional. By convention, undotted indices transform in the left-handed representation, while dotted indices transform in the right-handed one. In this context, a Dirac field is a four-dimensional completely reducible representation of the Lorentz group, given by

$$D_{\text{Dirac}} = D^{(\frac{1}{2},0)} \oplus D^{(0,\frac{1}{2})}. \tag{4.2}$$

On the other hand, the vector representation is provided by their tensor product,

$$D^{(\frac{1}{2},\frac{1}{2})} = D^{(\frac{1}{2},0)} \otimes D^{(0,\frac{1}{2})}. \tag{4.3}$$

This is a 4-dimensional irreducible representation of the Lorentz group. In fact, although under rotations only the spatial components of a four-vector are mixed, the presence of boosts ensures that all components are mixed with each other. A natural question arises: are we sure that this is actually the Lorentz vector representation? The other possible candidates may be the representations $(\frac{3}{2},0)$ and $(0,\frac{3}{2})$, which have the correct dimension. However, these two contain only angular momentum $j=\frac{3}{2}$, whereas $(\frac{1}{2},\frac{1}{2})$ contains $j=0$ and $j=1$, which coincides with the behavior of a Lorentz vector under rotations. This property allows us to make a general statement about the structure of a Dirac field.

Consider a field carrying one undotted and one dotted index, $A_{a\dot{a}}(x)$. Such a field belongs to the $\left(\frac{1}{2},\frac{1}{2}\right)$ representation, namely to the Lorentz vector representation. A field in the vector representation is usually written as $A^\mu(x)$, where μ is a Minkowski index. Therefore, there must exist a dictionary relating the components of $A_{a\dot{a}}(x)$ to those of $A^\mu(x)$. This relation can be written as [3]

$$A_{a\dot{a}}(x) = \sigma^\mu_{a\dot{a}} A_\mu(x), \tag{4.4}$$

and analogously

$$A^{\dot{a}a}(x) = \bar{\sigma}^{\mu\,\dot{a}a} A_\mu(x), \tag{4.5}$$

where the symbols $\sigma^\mu_{a\dot{a}}$ and $\bar{\sigma}^{\mu\,\dot{a}a}$ contain the Pauli matrices and are defined in Eqs. (B.31) and (B.34).

We specialize the two relations above to the case of a momentum four-vector, since we generally work in momentum space:

$$p^\mu = \left(p^0, p^i\right) = \left(E, p^i\right), \qquad p^\mu p_\mu = m^2. \tag{4.6}$$

By contracting it with the gamma matrices in the chiral-basis representation of Eq. B.40, we can write

$$\not{p} = \begin{pmatrix} 0 & p_{a\dot{a}} \\ \bar{p}^{\dot{a}a} & 0 \end{pmatrix}, \tag{4.7}$$

with

$$p_{a\dot{a}} \equiv p_\mu \left(\sigma^\mu\right)_{a\dot{a}} = \begin{pmatrix} p^0 - p^3 & -p^1 + ip^2 \\ -p^1 - ip^2 & p^0 + p^3 \end{pmatrix}, \tag{4.8}$$

and similarly

$$\bar{p}^{\dot{a}a} \equiv p_\mu \left(\bar{\sigma}^\mu\right)^{\dot{a}a}. \tag{4.9}$$

The momentum bispinors $p_{a\dot{a}}$ and $\bar{p}^{\dot{a}a}$ can be regarded as 2×2 matrices. Their determinant is Lorentz invariant and satisfies

$$\det p = p^\mu p_\mu = m^2. \tag{4.10}$$

4.1.1 Spinor notation

The momentum-space Dirac equation reads

$$\left(\not{p} - m\right) u(p) = 0 \qquad \text{and} \qquad \left(\not{p} + m\right) v(p) = 0. \tag{4.11}$$

Here, $u(p)$ and $v(p)$ denote the Dirac wave functions in momentum space, linear combinations of which form a Dirac field,

$$\Psi(x) \sim u(p)e^{-ip\cdot x} + v(p)e^{ip\cdot x}, \tag{4.12}$$

which satisfies the Dirac equation in coordinate space. To work in the chiral representation, which distinguishes left- and right-handed representations, we introduce the chirality projectors

$$\mathbb{P}_\pm = \frac{\mathbb{1} \pm \gamma_5}{2}, \tag{4.13}$$

with $\gamma_5 = i\gamma_0\gamma_1\gamma_2\gamma_3$. Here, we consistently employ the chiral representation of the gamma matrices provided in Appendix B.1.1.

We now label the left- and right-handed representations by $\pm$, referring to the two possible values of the helicity of the fermionic particle, $h = \pm\frac{1}{2}$. This can be done, since we consider for now the massless limit, in which chirality and helicity coincide. In our notation, chirality is actually opposite to helicity only for antiparticles, as is evident in Eqs. (4.14) and (4.15). In the massless case, helicity becomes a Lorentz-invariant quantity.

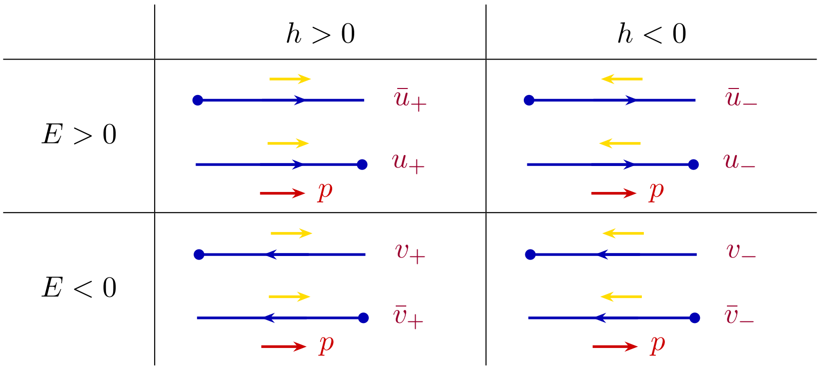

Table 4.1: Relation between the sign of the energy, helicity, and the corresponding chiral spinors. The yellow arrow indicates the spin direction, while the red arrow indicates the momentum direction.

As mentioned above, a massless particle is completely specified by its helicity and by the sign of its energy, since $[\hat{H}, \hat{h}] = 0$, where $\hat{H}$ is the Dirac Hamiltonian and $\hat{h}$ is the helicity operator. In this context, $u(p)$ represents positive-energy solutions, while $v(p)$ represents negative-energy solutions. We further specify their chirality and helicity by defining the chiral spinors as

$$u_\pm(p) = \mathbb{P}_\pm u(p), \qquad v_\mp(p) = \mathbb{P}_\pm v(p), \tag{4.14}$$

$$\bar{u}_\pm(p) = \bar{u}(p)\mathbb{P}_\mp, \qquad \bar{v}_\mp(p) = \bar{v}(p)\mathbb{P}_\mp. \tag{4.15}$$

In Tab. 4.1, we provide a diagrammatic representation of the chiral spinors and their Dirac adjoints. Each spinor is identified by its helicity and by the sign of its energy. The yellow arrows represent the direction of the spin, whereas the red arrows represent the momentum flow, which is conventionally chosen from left to right.

Moreover, crossing symmetry, namely incoming $\leftrightarrow$ outgoing and fermions $\leftrightarrow$ antifermions, exchanges the wave functions and flips the sign of the helicity. Therefore, in the massless case the wave functions are related as

$$u_\pm = v_\mp \quad \text{and} \quad \bar{v}_\pm = \bar{u}_\mp. \tag{4.16}$$

The last step is to introduce an explicit representation of the wave functions. This is done in terms of angle and square spinors, which are the central objects of the spinor-helicity formalism:

$$\begin{aligned} u_+(p) = v_-(p) &= \begin{pmatrix} 0 \\ |p]^{\dot{a}} \end{pmatrix}, & u_-(p) = v_+(p) &= \begin{pmatrix} |p\rangle_a \\ 0 \end{pmatrix}, \\ \bar{u}_+(p) = \bar{v}_-(p) &= \begin{pmatrix} \langle p|^a & 0 \end{pmatrix}, & \bar{u}_-(p) = \bar{v}_+(p) &= \begin{pmatrix} 0 & [p|_{\dot{a}} \end{pmatrix}. \end{aligned} \tag{4.17}$$

These spinors must satisfy the massless Dirac equation in momentum space, namely

$$\not{p}\, u_\pm(p) = \not{p}\, v_\pm(p) = \bar{u}_\pm(p)\not{p} = \bar{v}_\pm(p)\not{p} = 0; \tag{4.18}$$

this requires the angle and square spinors to satisfy

$$\bar{p}^{\dot{a}a}|p\rangle_a = 0, \qquad p_{a\dot{a}}|p]^{\dot{a}} = 0, \qquad [p|_{\dot{a}}\bar{p}^{\dot{a}a} = 0, \qquad \langle p|^a p_{a\dot{a}} = 0, \tag{4.19}$$

where the representation of $\not{p}$ in Eq. (4.7) has been used. These equations are the massless Weyl equations.

4.1.2 Properties of angle and square spinors

In this section we present the main properties of the angle and square spinors which will be necessary for later applications.

Reality conditions. The Dirac-conjugate field $\bar{\Psi}$ is obtained from Ψ by Dirac conjugation. When this operation is applied to the momentum-space Dirac equations, it relates the spinors associated with particles and antiparticles. This relation, however, holds only if the momentum p^μ is real, namely if all its components are real numbers. In that case, angle and square spinors are not independent, but are related by complex conjugation:

$$p^\mu \in \mathbb{R}: \qquad (|p\rangle_a)^* = [p|_{\dot{a}}, \qquad \left(|p]^{\dot{a}}\right)^* = \langle p|^a. \tag{4.20}$$

For complex momenta, instead, this reality condition is lost; in this case, angle and square spinors must be treated as independent variables. Let us verify the first equality as a consistency check. Using the definition of the Dirac adjoint and the γ^0 defined in Eq. (B.40), we obtain

$$\begin{aligned} \bar{u}_+(p) &= u_+^\dagger(p)\gamma^0 \\ &= \begin{pmatrix} 0 & \left(|p]^{\dot{a}}\right)^* \end{pmatrix} \begin{pmatrix} 0 & \mathbb{1} \\ \mathbb{1} & 0 \end{pmatrix} \\ &= \begin{pmatrix} \left(|p]^{\dot{a}}\right)^* & 0 \end{pmatrix}. \end{aligned} \tag{4.21}$$

On the other hand, from Eq. (4.17),

$$\bar{u}_+(p) = \begin{pmatrix} \langle p|^a & 0 \end{pmatrix}. \tag{4.22}$$

Comparing the two expressions, we find

$$\left(|p]^{\dot{a}}\right)^* = \langle p|^a, \tag{4.23}$$

as required.

Completeness relation. Consider the spin-sum completeness relations for Dirac's wavefunctions

$$\sum_{h=\pm} u_h(p)\bar{u}_h(p) = \not{p}, \qquad \sum_{h=\pm} v_h(p)\bar{v}_h(p) = \not{p}, \tag{4.24}$$

where we have set $m = 0$. By employing the explicit forms of the chiral wave functions in Eq. (4.17) and of $\not{p}$ in Eq. (4.7), we obtain

$$p_{a\dot{a}} = |p\rangle_a [p|_{\dot{a}}, \qquad \bar{p}^{\dot{a}a} = |p]^{\dot{a}} \langle p|^a. \tag{4.25}$$

These two expressions are 2×2 matrices that occupy the two off-diagonal blocks of a larger 4×4 matrix. For this reason, we can employ the following abuse of notation, which will be used extensively in what follows:

$$\boxed{\not{p} \equiv |p\rangle[p| + |p]\langle p|} \tag{4.26}$$

where the 4×4 matrix $\not{p}$ is written as the sum of its two 2×2 components. Notice we have also suppressed the Weyl indices.

Angle and square spinor brackets. Given two massless momenta p and q, we define the Lorentz-invariant spinor products

$$\langle pq\rangle \equiv \langle p|^a |q\rangle_a, \qquad [pq] \equiv [p|_{\dot{a}} |q]^{\dot{a}}, \tag{4.27}$$

where we have introduced the NW–SE $\searrow$ contraction rule for undotted Weyl indices and the SW–NE $\nearrow$ contraction rule for dotted Weyl indices. Since the spinor indices are contracted with the two-component Levi-Civita tensors ϵ^{ab} and $\epsilon^{\dot{a}\dot{b}}$ defined in Eq. (B.25), these products are antisymmetric by construction

$$\langle pq\rangle = -\langle qp\rangle, \qquad [pq] = -[qp]. \tag{4.28}$$

Moreover,

$$\langle pp\rangle = 0, \qquad [pp] = 0. \tag{4.29}$$

In case of mixed contractions between angle and square spinors, they do not define Lorentz scalars, because they carry different types of spinor indices. In this sense, one writes

$$\langle p|q] = \langle p|^a |q]^{\dot{a}} = 0, \qquad [p|q\rangle = [p|_{\dot{a}} |q\rangle_a = 0. \tag{4.30}$$

More precisely, these expressions are not allowed scalar contractions unless an object carrying one dotted and one undotted index, such as $\sigma^\mu_{a\dot{a}}$, is inserted. We will address this point later.

A very useful identity relates spinor products to the scalar product of the two momenta:

$$\langle pq\rangle[qp] = 2p \cdot q = (p+q)^2, \tag{4.31}$$

where in the last passage we used that the particle is massless. This relation can be proved in the following way

$$
\begin{aligned}
\langle pq\rangle[qp] &= \langle p|^a|q\rangle_a\,[q|_{\dot a}|p]^{\dot a} \\
&= \bar p^{\dot a a} q_{a\dot a} \\
&= p_\mu\,(\bar\sigma^\mu)^{\dot a a}\,q_\nu\,(\sigma^\nu)_{a\dot a} \\
&= p_\mu q_\nu\,\mathrm{Tr}(\bar\sigma^\mu\sigma^\nu) \\
&= 2p_\mu q_\nu g^{\mu\nu} \\
&= 2p\cdot q,
\end{aligned}
\tag{4.32}
$$

where we used Eqs. (4.25), (4.8), (4.26) and (B.36).

Moreover, we adopt the following convention for negative spinor momenta

$$|-p\rangle = -|p\rangle, \qquad |-p] = +|p]. \tag{4.33}$$

Momentum conservation. In amplitude calculations, we use the all-incoming convention, so that momentum conservation for an n-particle process reads

$$\sum_{i=1}^{n} p_i^\mu = 0. \tag{4.34}$$

In the spinor-helicity formalism this condition can be written by contracting the momentum-conservation equation with arbitrary massless reference spinors $\langle q|$ and $|k]$. Using the spinorial representation of a massless momentum, one obtains

$$\sum_{i=1}^{n}\langle qi\rangle[ik] = 0, \tag{4.35}$$

for any lightlike momenta q and k. This form is often very useful because it allows to rewrite spinor products using momentum conservation directly.

Spinor bilinears. In amplitude calculations it is common to deal with spinor bilinears which are constructed employing Pauli matrices in such a way to properly contract all dotted and undotted indices.

With a similar notation abuse implemented in Eq. (4.108) we can write the 4-dimensional gamma matrices as the sum of its 2-dimensional Pauli matrices components

$$\gamma^\mu \equiv \sigma^\mu + \bar\sigma^\mu, \tag{4.36}$$

in accordance with Eq. (B.40). With this object we can build spinors bilinears like

$$[k|\gamma^\mu|p\rangle \quad \text{and} \quad \langle k|\gamma^\mu|p], \tag{4.37}$$

with k^μ and p^μ two different massless momenta. Note these expressions combine the 2-component spinors with the 4×4 gamma matrices. We interpret these expressions thinking that the 2-component spinors act as projectors which single out the matching sigma-matrix contained in γ^μ. Explicitly we have

$$[k|\gamma^\mu|p\rangle \equiv [k|_{\dot a}\,(\bar\sigma^\mu)^{\dot a a}\,|p\rangle_a \quad \text{and} \quad \langle k|\gamma^\mu|p] \equiv \langle k|^a\,(\sigma^\mu)_{a\dot a}\,|p]^{\dot a}. \tag{4.38}$$

Some useful relations hold for spinors bilinears:

- *Momentum reconstruction*:

$$\boxed{\langle k|\gamma^\mu|k] = 2k^\mu.} \tag{4.39}$$

Contracting both sides with an arbitrary four-vector q_μ, we find

$$\begin{aligned} q_\mu\langle k|\gamma^\mu|k] &= \langle k|\not{q}|k] \\ &= \langle k|q\rangle[q|k] \\ &= 2k^\mu q_\mu. \end{aligned} \tag{4.40}$$

- *Same-chirality contractions*:

$$\boxed{\langle p|\gamma^\mu|k\rangle = 0, \qquad [p|\gamma^\mu|k] = 0.} \tag{4.41}$$

Following the discussion we have just presented, it is not possible in this case to project the γ-matrix onto a Pauli-matrix whose indices contract consistently with the spinors. In particular

$$\langle p|\gamma^\mu|k\rangle = \langle p|^a\,(\sigma^\mu)_{a\dot a}\,|k\rangle_a, \qquad [p|\gamma^\mu|k] = [p|_{\dot a}\,(\bar\sigma^\mu)^{\dot a a}\,|k]^{\dot a}. \tag{4.42}$$

In both cases, one spinor index remains of the wrong type, so no Lorentz-covariant contraction can be formed. Hence these same-chirality contractions vanish.

- *Charge conjugation*:

$$\boxed{[k|\gamma^\mu|p\rangle = \langle p|\gamma^\mu|k].} \tag{4.43}$$

Contracting both sides with an arbitrary four-vector q_μ, we find

$$\begin{aligned} q_\mu[k|\gamma^\mu|p\rangle &= [k|\not{q}|p\rangle \\ &= [k|\,(|q]\langle q|)\,|p\rangle \\ &= [kq]\langle qp\rangle \\ &= [qk]\langle pq\rangle \\ &= \langle p|\not{q}|k] \\ &= q_\mu\langle p|\gamma^\mu|k]. \end{aligned} \tag{4.44}$$

Since this relation holds for an arbitrary q_μ, the identity follows. Notice that the compact notation introduced above allows us to avoid displaying the Lorentz indices explicitly.

- *Fierz identity*:

$$\boxed{[i|\gamma^\mu|j\rangle[k|\gamma_\mu|l\rangle = 2[ik]\langle lj\rangle.} \tag{4.45}$$

Using charge conjugation,

$$[k|\gamma_\mu|l\rangle = \langle l|\gamma_\mu|k], \tag{4.46}$$

so that it is enough to prove

$$[i|\gamma^\mu|j\rangle\langle l|\gamma_\mu|k] = 2[ik]\langle lj\rangle. \tag{4.47}$$

To this end, consider on the one hand that

$$[i|\gamma^\mu \not{p}_j \not{p}_l \gamma_\mu|k] = [i|\gamma^\mu|j\rangle[jl]\langle l|\gamma_\mu|k], \tag{4.48}$$

on the other hand

$$\begin{aligned}[i|\gamma^\mu \not{p}_j \not{p}_l \gamma_\mu|k] &= p_{j,\alpha} p_{l,\beta} [i|\gamma^\mu\gamma^\alpha\gamma^\beta\gamma_\mu|k] \\ &= 4p_j\cdot p_l\,[ik] \\ &= -2[jl]\langle jl\rangle[ik] \\ &= 2[jl]\langle lj\rangle[ik].\end{aligned} \tag{4.49}$$

In the second line we used the four-dimensional γ-matrix identity

$$\gamma^\mu\gamma^\alpha\gamma^\beta\gamma_\mu = 4g^{\alpha\beta}\,\mathbb{1}, \tag{4.50}$$

which holds in $d = 4$ spacetime dimensions.

Therefore,

$$[i|\gamma^\mu|j\rangle[jl]\langle l|\gamma_\mu|k] = 2[jl]\langle lj\rangle[ik], \tag{4.51}$$

and, after cancelling the common factor $[jl]$, we obtain

$$[i|\gamma^\mu|j\rangle\langle l|\gamma_\mu|k] = 2[ik]\langle lj\rangle. \tag{4.52}$$

- *Schouten identity*:

$$\boxed{|i\rangle\langle jk\rangle + |j\rangle\langle ki\rangle + |k\rangle\langle ij\rangle = 0.} \tag{4.53}$$

This identity follows from the simple fact that any three two-component spinors are linearly dependent. Therefore, given three spinors $|i\rangle$, $|j\rangle$, and $|k\rangle$, one can write

$$|k\rangle = a|i\rangle + b|j\rangle. \tag{4.54}$$

Contracting this relation with $\langle i|$ and $\langle j|$, respectively, gives

$$\begin{aligned}\langle ik\rangle &= b\langle ij\rangle, \quad b = \frac{\langle ik\rangle}{\langle ij\rangle}, \\ \langle jk\rangle &= a\langle ji\rangle, \quad a = \frac{\langle jk\rangle}{\langle ji\rangle} = -\frac{\langle jk\rangle}{\langle ij\rangle}.\end{aligned} \tag{4.55}$$

Hence,

$$|k\rangle = -\frac{\langle jk\rangle}{\langle ij\rangle}|i\rangle + \frac{\langle ik\rangle}{\langle ij\rangle}|j\rangle. \tag{4.56}$$

Multiplying by $\langle ij\rangle$ and using $\langle ik\rangle = -\langle ki\rangle$, we obtain

$$|i\rangle\langle jk\rangle + |j\rangle\langle ki\rangle + |k\rangle\langle ij\rangle = 0, \tag{4.57}$$

which proves the Schouten identity.

Contracting the identity with a fourth spinor $\langle r|$, one obtains the more commonly used form

$$\langle ri\rangle\langle jk\rangle + \langle rj\rangle\langle ki\rangle + \langle rk\rangle\langle ij\rangle = 0. \tag{4.58}$$

An analogous identity holds for square spinors:

$$[ri][jk] + [rj][ki] + [rk][ij] = 0. \tag{4.59}$$

4.1.3 Polarization vectors

For a massless vector boson with momentum k, we introduce an arbitrary massless reference momentum r, with $r \neq k$, and define the polarization vectors as in [46]

$$\varepsilon^+_\mu(k;r) := \frac{[k|\gamma_\mu|r\rangle}{\sqrt{2}\,\langle kr\rangle}, \qquad \varepsilon^-_\mu(k;r) := \frac{\langle k|\gamma_\mu|r]}{\sqrt{2}\,[kr]}, \tag{4.60}$$

where the usage of γ_μ in place of the Pauli matrices is understood.

The arbitrariness in the choice of r reflects gauge invariance: changing the reference spinor changes the polarization vector by a term proportional to the momentum k_μ, which does not affect gauge-invariant on-shell amplitudes.

The polarization vectors must satisfy some fundamental properties.

- *Transversality*:

$$k^\mu\varepsilon^\pm_\mu(k;r) = 0, \qquad r^\mu\varepsilon^\pm_\mu(k;r) = 0. \tag{4.61}$$

Indeed,

$$\begin{aligned} k^\mu\varepsilon^+_\mu(k;r) &= \frac{[k|\not{k}|r\rangle}{\sqrt{2}\,\langle kr\rangle} = 0, \quad r^\mu\varepsilon^+_\mu(k;r) = \frac{[k|\not{r}|r\rangle}{\sqrt{2}\,\langle kr\rangle} = 0,\\ k^\mu\varepsilon^-_\mu(k;r) &= \frac{\langle k|\not{k}|r]}{\sqrt{2}\,[kr]} = 0, \quad r^\mu\varepsilon^-_\mu(k;r) = \frac{\langle k|\not{r}|r]}{\sqrt{2}\,[kr]} = 0. \end{aligned} \tag{4.62}$$

These relations follow from the massless Weyl Eqs. (4.19) for the spinors associated with k and r.

- *Slashed polarization vectors*:

$$\not\varepsilon^{\,+}(k;r) = \frac{\sqrt{2}}{\langle kr\rangle}\left(|k]\langle r| + |r\rangle[k|\right), \qquad \not\varepsilon^{\,-}(k;r) = \frac{\sqrt{2}}{[kr]}\left(|k\rangle[r| + |r]\langle k|\right). \tag{4.63}$$

These relations connect the 4-dimensional slashed polarization vectors with the 2-dimensional spinor variables. Hence, they encode the notation abuse we have already encountered before.

For example, by inserting $\not\varepsilon^{\,+}$ between two external spinors, one finds

$$\begin{aligned}\langle i|\not\varepsilon^{+}(k;r)|j] &= \langle i|\gamma^{\mu}|j]\,\varepsilon^{+}_{\mu}(k;r)\\ &= \frac{\langle i|\gamma^{\mu}|j]\,[k|\gamma_{\mu}|r\rangle}{\sqrt{2}\,\langle kr\rangle}\\ &= \frac{\sqrt{2}}{\langle kr\rangle}\langle ir\rangle[kj]\\ &= \langle i|\left[\frac{\sqrt{2}}{\langle kr\rangle}|r\rangle[k|\right]|j].\end{aligned} \tag{4.64}$$

By exploiting this strategy the slashed polarization vectors are correctly reproduced.

- *Complex conjugation*: for real momenta,

$$\left(\varepsilon^{+}_{\mu}(k;r)\right)^{*} = \varepsilon^{-}_{\mu}(k;r). \tag{4.65}$$

Indeed, for real k and r, angle and square spinors are related by complex conjugation. Therefore,

$$\begin{aligned}\left(\varepsilon^{+}_{\mu}(k;r)\right)^{*} &= \left(\frac{[k|\gamma_{\mu}|r\rangle}{\sqrt{2}\,\langle kr\rangle}\right)^{*}\\ &= \frac{\langle k|\gamma_{\mu}|r]}{\sqrt{2}\,[kr]}\\ &= \varepsilon^{-}_{\mu}(k;r).\end{aligned} \tag{4.66}$$

- *Normalization*:

$$\varepsilon^{+}(k;r)\cdot\varepsilon^{-}(k;r) = -1. \tag{4.67}$$

Indeed,

$$\begin{aligned}\varepsilon^{+}(k;r)\cdot\varepsilon^{-}(k;r) &= -\frac{1}{2}\frac{[k|\gamma_{\mu}|r\rangle\langle k|\gamma^{\mu}|r]}{\langle kr\rangle[kr]}\\ &= -\frac{1}{2}\frac{2\langle kr\rangle[kr]}{\langle kr\rangle[kr]}\\ &= -1.\end{aligned} \tag{4.68}$$

where the Fierz identity was implemented.

- *Same-helicity contractions*:

$$\varepsilon^+(k;r)\cdot\varepsilon^+(k;r)=0,\qquad \varepsilon^-(k;r)\cdot\varepsilon^-(k;r)=0. \tag{4.69}$$

For the positive-helicity case,

$$\begin{aligned}\varepsilon^+(k;r)\cdot\varepsilon^+(k;r) &= -\frac{1}{2}\frac{[k|\gamma_\mu|r\rangle[k|\gamma^\mu|r\rangle}{\langle kr\rangle^2}\\ &= -\frac{[kk]\langle rr\rangle}{\langle kr\rangle^2}\\ &= 0.\end{aligned} \tag{4.70}$$

Similarly,

$$\begin{aligned}\varepsilon^-(k;r)\cdot\varepsilon^-(k;r) &= -\frac{1}{2}\frac{\langle k|\gamma_\mu|r]\langle k|\gamma^\mu|r]}{[kr]^2}\\ &= -\frac{\langle kk\rangle[rr]}{[kr]^2}\\ &= 0.\end{aligned} \tag{4.71}$$

- *Gauge transformations*: changing the reference spinor changes the polarization vector by a term proportional to the external momentum k^μ. For the positive-helicity polarization, one finds

$$\begin{aligned}\varepsilon^+_\mu(k;\tilde r)-\varepsilon^+_\mu(k;r) &= \frac{[k|\gamma_\mu|\tilde r\rangle}{\sqrt{2}\,\langle k\tilde r\rangle}-\frac{[k|\gamma_\mu|r\rangle}{\sqrt{2}\,\langle kr\rangle}\\ &= \frac{\langle kr\rangle[k|\gamma_\mu|\tilde r\rangle-\langle k\tilde r\rangle[k|\gamma_\mu|r\rangle}{\sqrt{2}\,\langle k\tilde r\rangle\langle kr\rangle}\\ &= \frac{[k|\gamma_\mu\left(\langle kr\rangle|\tilde r\rangle-\langle k\tilde r\rangle|r\rangle\right)}{\sqrt{2}\,\langle k\tilde r\rangle\langle kr\rangle}\\ &= -\frac{\langle r\tilde r\rangle}{\sqrt{2}\,\langle k\tilde r\rangle\langle kr\rangle}[k|\gamma_\mu|k\rangle\\ &= -\sqrt{2}\,\frac{\langle r\tilde r\rangle}{\langle k\tilde r\rangle\langle kr\rangle}k_\mu.\end{aligned} \tag{4.72}$$

where in the fourth step we have employed the Schouten identity (4.58), while in the last step we have used Eq. (4.40). Therefore,

$$\varepsilon^+_\mu(k;\tilde r)=\varepsilon^+_\mu(k;r)+C_+(r,\tilde r)\,k_\mu,\qquad C_+(r,\tilde r)=-\sqrt{2}\,\frac{\langle r\tilde r\rangle}{\langle k\tilde r\rangle\langle kr\rangle}. \tag{4.73}$$

Hence two polarization vectors with different reference spinors differ only by a gauge transformation. If the amplitude satisfies the Ward identity [2]

$$k_\mu\,\mathcal{M}^\mu=0, \tag{4.74}$$

then the physical quantity $\varepsilon^\pm_\mu(k;r)\,\mathcal{M}^\mu$ is independent of the choice of the reference spinor.

Remark. For each external vector boson, one is free to choose the corresponding reference spinor r_i, with $r_i \neq k_i$. However, this choice must be kept fixed in all diagrams contributing to the same process. After summing over all diagrams, the final on-shell amplitude is independent of the reference spinors r_i.

4.1.4 The little group scaling

In this section, we present a powerful tool that can be used together with the spinor-helicity formalism to infer the form of an on-shell scattering amplitude, namely the little group. A somewhat formal discussion of the little group can be found in Appendix B.2.1. In this section, instead, we provide a more direct and intuitive approach, starting from the simple case of massless particles.

The discussion of the spinor helicity formalism in the previous sections, allowed us to disentangle the presence of left- and right-handed indices belonging to the two non-equivalent 2-dimensional irreducible representations of Lorentz group. This relation was given in Eq. (4.25) as

$$p_{a\dot{a}} = |p\rangle_a [p|_{\dot{a}}, \qquad \bar{p}^{\dot{a}a} = |p]^{\dot{a}} \langle p|^a. \tag{4.75}$$

The introduction of little-group techniques follows from noticing that these relations are invariant under the scaling

$$|p\rangle \to w\,|p\rangle, \qquad |p] \to w^{-1}|p], \tag{4.76}$$

which is indeed a little-group transformation, as it leaves the massless momentum p^μ invariant. As reported in Eq. (B.56), the little group of the momentum p^μ does not change the momentum itself, but acts at most on the internal labels, which we denoted collectively by σ in the Appendix. In the present massless case, the physically relevant non-trivial part of the little group is $U(1)$. From a physical point of view, we can straightforwardly justify this statement. For a massless particle, we can choose a frame in which $p^\mu = (E, 0, 0, E)$. The transformations that leave this vector invariant form the Euclidean group in two dimensions, denoted by $\mathbb{E}(2)$. This group contains rotations in the transverse (x, y)-plane, together with two translation-like generators. The physically relevant finite-dimensional representations are obtained by requiring the translation-like generators to act trivially on the states. Therefore, the non-trivial part of the massless little group is its rotational subgroup,

$$SO(2) \simeq U(1). \tag{4.77}$$

In particular, in the spinor representation of a massless momentum, the little-group transformation is realized as the scaling in Eq. (4.76). For real momenta, w must be a complex phase, so that the reality condition relating angle and square spinors is preserved. For complex momenta, instead, angle and square spinors are independent, and therefore w can be taken to be any non-zero complex number.

The invariance of an on-shell massless momentum under the $U(1)$ little group allows one to constrain an on-shell tree-level amplitude without specifying a Lagrangian. In fact, a Feynman amplitude essentially consists of propagators, vertices, and external-line factors. However, the momenta appearing in propagators and vertices are invariant under little-group transformations. More explicitly, only the wave functions associated with the incoming and outgoing particles transform under the little group.

Suppose we write a scattering amplitude involving massless particles entirely in terms of spinor variables. Let $i = 1, 2, \dots, n$ label the external particles involved, so that we can denote the amplitude as

$$\mathcal{M}_n\left(1^{h_1}, \dots, i^{h_i}, \dots, n^{h_n}\right), \tag{4.78}$$

where we have specified the helicity of each particle and denoted each momentum p_i simply by its label i. Now, the little-group scaling of the external states is then fixed as follows:

- a scalar external state carries no little-group weight, thus it does not scale;
- for massless Weyl fermions, the external spinors scale with weight w^{-2h}, where $h = \pm\frac{1}{2}$;
- for massless spin-1 bosons, the polarization vectors have little-group weight w^{-2h}, with $h = \pm 1$. Indeed, under the scaling in Eq. (4.76), the massless vector bosons in Eq. (4.60) transform as

  $$\varepsilon_\mu^\pm(p; r) \longrightarrow w^{\mp 2}\varepsilon_\mu^\pm(p; r) = w^{-2h}\varepsilon_\mu^\pm(p; r), \qquad h = \pm 1. \tag{4.79}$$

  This transformation is the little-group transformation associated with the external leg of momentum p; the chosen reference spinors are held fixed. A separate rescaling of the reference spinors would cancel between the numerator and denominator and leaves the polarization vector hence unchanged.

Thus, for amplitudes involving only massless particles, little-group covariance gives a strong constraint. Under the little-group scaling of the spinors associated with each external particle, the on-shell amplitude must transform homogeneously with weight $-2h_i$, where h_i is the helicity of the i-th particle. Therefore [47],

$$\boxed{\mathcal{M}_n\left(1^{h_1}, \dots, i^{h_i}, \dots, n^{h_n}\right) = w_i^{-2h_i}\mathcal{M}_n\left(1^{h_1}, \dots, i^{h_i}, \dots, n^{h_n}\right)} \tag{4.80}$$

This result can be applied to all the n massless particles involved in the process of interest.

4.1.5 Three-point amplitudes from little-group scaling

We now apply the discussion developed so far to the case of three-point amplitudes. We consider both a top-down and a bottom-up approach. The former relies on the specification of a Lagrangian, which in this case is the simple QED Lagrangian. In particular, we use the explicit representation of the wave functions in terms of spinor variables, Eq. (4.17), together with the explicit form of the polarization vectors in Eq. (4.60), in order to implement the spinor-helicity formalism.

Conversely, from a bottom-up perspective, we will eventually recover the same result, but starting from more general principles. In particular, we will implement little-group scaling, dimensional analysis, and locality arguments.

Top-down derivation from QED. Consider the three-point QED amplitude involving a massless electron e, a massless positron $\bar{e}$, and a photon γ. We choose the following helicity configuration and momentum assignments

$$e^-(p_1), \qquad \bar{e}^+(p_2), \qquad \gamma^-(p_3),$$

where all momenta are taken to be incoming. The SM Feynman rule reads [2]

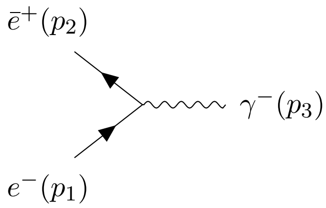

$$= ie\gamma^\mu. \tag{4.81}$$

Using the QED vertex and the negative-helicity polarization vector, the amplitude can be obtained in the spinor helicity formalism

$$\begin{aligned}
\mathcal{M}_3\big(1^-_{e^-}, 2^+_{\bar{e}^+}, 3^-_\gamma\big) &= ie\,\bar{v}_+(p_2)\gamma_\mu u_-(p_1)\,\varepsilon^\mu_-(p_3;q) \\
&= ie\,[2|\gamma^\mu|1\rangle\,\frac{\langle 3|\gamma_\mu|q]}{\sqrt{2}\,[3q]} \\
&= ie\,\frac{1}{\sqrt{2}\,[3q]}\,2\langle 31\rangle[2q] \\
&= -ie\sqrt{2}\,\frac{\langle 13\rangle[2q]}{[3q]},
\end{aligned} \tag{4.82}$$

where in the third line we used the Fierz identity. The result still depends on the reference spinor q, but this dependence must cancel in the final on-shell amplitude. Indeed, using momentum conservation, $p_1 + p_2 + p_3 = 0$ one can eliminate q as follows:

$$\begin{aligned}\langle 13\rangle[2q] &= \frac{\langle 13\rangle}{\langle 12\rangle}\langle 1|p_2|q] \\ &= -\frac{\langle 13\rangle}{\langle 12\rangle}\langle 1|(p_1+p_3)|q] \\ &= -\frac{\langle 13\rangle}{\langle 12\rangle}\langle 1|p_3|q] \\ &= -\frac{\langle 13\rangle^2}{\langle 12\rangle}[3q]. \end{aligned} \tag{4.83}$$

Substituting this expression into Eq. (4.82), we obtain

$$\mathcal{M}_3\big(1^-_{e^-}, 2^+_{\bar{e}^+}, 3^-_{\gamma}\big) = ie\sqrt{2}\,\frac{\langle 13\rangle^2}{\langle 12\rangle}. \tag{4.84}$$

Notice that this final result depends only on angle brackets. This is a special feature of three-point kinematics with massless external particles. This fact becomes clear from

$$\langle 12\rangle[21] = 2p_1\cdot p_2 = (p_1+p_2)^2 = p_3^2 = 0. \tag{4.85}$$

Two important consequences follow:

- *Three-point amplitudes depend either on angle brackets or on square brackets.*

  Since
  $$\langle 12\rangle[21] = 0, \tag{4.86}$$
  either $\langle 12\rangle = 0$ or $[21] = 0$. The same reasoning applies to the other pairs of external particles.

  Suppose, for instance, that $\langle 12\rangle \neq 0$. Then $[12] = 0$. Moreover, using momentum conservation,
  $$0 = \langle 1|(\not{p}_1 + \not{p}_2 + \not{p}_3)|3] = \langle 12\rangle[23], \tag{4.87}$$
  and therefore
  $$[23] = 0. \tag{4.88}$$
  Similarly, one obtains $[13] = 0$. Hence, if the angle brackets are non-vanishing, all square brackets vanish:
  $$[12] = [13] = [23] = 0. \tag{4.89}$$
  Conversely, if the square brackets are non-vanishing, all angle brackets vanish:
  $$\langle 12\rangle = \langle 13\rangle = \langle 23\rangle = 0. \tag{4.90}$$
  Therefore, a non-vanishing three-point amplitude involving only massless particles can depend either on angle brackets or on square brackets, but not on both.

- *Non-vanishing three-point amplitudes require complex momenta.*

  For real momenta, angle and square spinors are related by complex conjugation. Therefore, if all square brackets vanish, the corresponding angle brackets must vanish as well, and vice versa. This would make any massless three-point amplitude vanish.

  Non-trivial massless three-point amplitudes are therefore naturally defined with complex momenta. In this case, angle and square spinors become independent variables, and the two kinematic branches are independent.

Bottom-up derivation from little-group scaling. At this point, we want to use the spinor-helicity formalism to obtain the tree-level on-shell three-particle amplitude in a model-independent way, namely without *a priori* knowledge of a Lagrangian that dictates the interactions. Suppose that the amplitude depends only on angle brackets; we will comment on this point later. The most general three-point ansatz is

$$\mathcal{M}_3\left(1^{h_1}, 2^{h_2}, 3^{h_3}\right) = c\,\langle 12\rangle^{x_{12}}\langle 13\rangle^{x_{13}}\langle 23\rangle^{x_{23}}, \tag{4.91}$$

where c is an overall constant. The amplitude scales in the following way:

$$\mathcal{M}_3 \;\longrightarrow\; \begin{cases} w_1^{-2h_1}\, w_2^{-2h_2}\, w_3^{-2h_3}\, \mathcal{M}_3 & \text{(using Eq. (4.80))}, \\ w_1^{x_{12}+x_{13}}\, w_2^{x_{12}+x_{23}}\, w_3^{x_{13}+x_{23}}\, \mathcal{M}_3 & \text{(using Eq. (4.76))}. \end{cases}$$

Equating the two scalings gives

$$\begin{cases} x_{12} + x_{13} = -2h_1, \\ x_{12} + x_{23} = -2h_2, \\ x_{13} + x_{23} = -2h_3. \end{cases} \tag{4.92}$$

The solution is

$$x_{12} = h_3 - h_1 - h_2, \qquad x_{13} = h_2 - h_3 - h_1, \qquad x_{23} = h_1 - h_2 - h_3. \tag{4.93}$$

Therefore little-group scaling fixes the angle-bracket three-point amplitude to be

$$\boxed{\mathcal{M}_3\left(1^{h_1}, 2^{h_2}, 3^{h_3}\right) = c\,\langle 12\rangle^{h_3-h_1-h_2}\langle 13\rangle^{h_2-h_3-h_1}\langle 23\rangle^{h_1-h_2-h_3}.} \tag{4.94}$$

Applying this formula to

$$h_1 = -\frac{1}{2}, \qquad h_2 = +\frac{1}{2}, \qquad h_3 = -1,$$

one immediately obtains

$$\mathcal{M}_3\left(1^-_{e^-}, 2^+_{\bar{e}^+}, 3^-_\gamma\right) = c\,\frac{\langle 13\rangle^2}{\langle 12\rangle}, \tag{4.95}$$

in agreement with the top-down calculation, with

$$c = ie\sqrt{2}.$$

We can now comment further on the procedure just described.

- *Dimensional analysis provides an additional selection rule.*

  Let us evaluate the mass dimension of the parameter c appearing in the amplitude of Eq. (4.94). First, recall that in four spacetime dimensions an n-point amplitude has mass dimension [47]

  $$[\mathcal{M}_n] = 4 - n. \tag{4.96}$$

  For a three-point amplitude this gives $[\mathcal{M}_3] = 1$. Since each spinor bracket has mass dimension one, the coupling in the angle-bracket solution has dimension

  $$[c] = 1 + h_1 + h_2 + h_3. \tag{4.97}$$

  For the QED amplitude above this gives $[c] = 0$, as expected for the dimensionless electric charge. Other helicity assignments may require a coupling with non-zero mass dimension; if such a coupling is not present in the theory, the corresponding amplitude is absent. In particular, if we set $h_1 = h_2 = h$, we must have $[c] \neq 0$, which means that

  $$\mathcal{M}_3\left(1^+_{e^-}, 2^+_{\bar{e}^+}, 3^\pm_\gamma\right) = \mathcal{M}_3\left(1^-_{e^-}, 2^-_{\bar{e}^+}, 3^\pm_\gamma\right) = 0. \tag{4.98}$$

  This result is expected from the fact that QED interactions preserve chirality. In the massless limit, this means that the two outgoing fermions must have equal chirality, namely opposite helicities[1].

  Let us observe another important point related to the mass dimension of c. If we set

  $$h_1 = +\frac{1}{2}, \qquad h_2 = -\frac{1}{2}, \qquad h_3 = +1, \tag{4.99}$$

  and try to use the angle-bracket solution, the coupling would have non-zero mass dimension, namely $[c] = 2$. This would seem to suggest that this amplitude cannot be generated by the dimension-four QED interaction. However, this cannot be the case. How do we solve this issue?

[1] Recall that, in our notation, helicity coincides with chirality for particles, while it is opposite to chirality for antiparticles.

Instead of starting from the ansatz in Eq. (4.91), we can consider its parity conjugate[2]

$$\mathcal{M}_3\Big(1^{h_1}, 2^{h_2}, 3^{h_3}\Big) = \tilde{c}\,[12]^{\tilde{x}_{12}}[13]^{\tilde{x}_{13}}[23]^{\tilde{x}_{23}}. \tag{4.100}$$

Following steps analogous to those above, one finds that little-group scaling fixes the square-bracket exponents in terms of the helicities of the external particles,

$$\boxed{\mathcal{M}_3\Big(1^{h_1}, 2^{h_2}, 3^{h_3}\Big) = \tilde{c}\,[12]^{-h_3+h_1+h_2}[13]^{-h_2+h_3+h_1}[23]^{-h_1+h_2+h_3}.} \tag{4.101}$$

Specializing this equation to the case of the QED vertex, we find the parity-conjugate QED amplitude

$$\mathcal{M}_3\big(1^+_{e^-}, 2^-_{\bar{e}^+}, 3^+_\gamma\big) = \tilde{c}\,\frac{[13]^2}{[12]}, \tag{4.102}$$

with $[\tilde{c}] = 0$, as expected. The remaining non-vanishing helicity configurations can be obtained straightforwardly from Eqs. (4.94) and (4.101). The configurations with equal fermion and antifermion helicities vanish, as discussed above.

A natural question arises at this point. If we do not require the overall coefficient of the amplitude, here denoted by c, to have vanishing mass dimension, namely if we also allow amplitudes generated by higher-dimensional operators, how do we know whether the ansatz should be written in terms of angle brackets or square brackets?

- *The role of locality.*

To answer the question above, we need to take into account the locality of the operators that generate a given amplitude. Again, we provide an example that illustrates the issue. We consider a three-gluon amplitude with two negative-helicity gluons and one positive-helicity gluon. Using Eq. (4.94), we find

$$\mathcal{M}_3\big(1^-_g 2^-_g 3^+_g\big) = c\,\frac{\langle 12\rangle^3}{\langle 13\rangle\langle 23\rangle}. \tag{4.103}$$

For brevity, we omit the fully antisymmetric color factor $f^{a_1a_2a_3}$, which ensures Bose symmetry under the exchange of the identical gluons 1 and 2. This amplitude has the correct mass dimension with a dimensionless coupling c.

[2]Parity reverses the spatial momentum of a particle. This also flips the sign of the helicity, which in turn implies that, in order to provide the correct little-group weight, angle brackets must be exchanged with square brackets and vice versa: $\langle\cdot\,\cdot\rangle \leftrightarrow [\cdot\,\cdot]$.

Now, let us try to build the same helicity configuration using the square-bracket amplitude in Eq. (4.101). This yields

$$\mathcal{M}_3\big(1_g^- 2_g^- 3_g^+\big) = \tilde{c}\,\frac{[13][23]}{[12]^3}. \tag{4.104}$$

In this case, the coefficient has non-zero mass dimension, $[\tilde{c}] = 2$.

Therefore, what is the correct physical amplitude between the two? From Eq. (4.103), we see that the momentum dependence scales as M^1, since spinor brackets carry mass dimension one. This is compatible with the fact that the amplitude comes from the local $c\,AA\partial A$ interaction contained in $\mathrm{Tr}\,F_{\mu\nu}F^{\mu\nu}$. On the other hand, in Eq. (4.104) the momentum dependence scales as M^{-1}. This means that such an amplitude would have to come from an interaction term of the form

$$\tilde{c}\,AA\frac{\partial}{\Box}A.$$

However, this cannot originate from a local Lagrangian. Therefore, we discard the amplitude in Eq. (4.104) as unphysical.

By now, the importance of little-group scaling as a tool to determine model-independent scattering amplitudes should be clear. Moreover, we observed that dimensional analysis provides an additional selection rule for the determination of an amplitude, together with the requirement that it must be generated by local operators. These general arguments uniquely fix the massless three-particle amplitude and can also be used in more complicated cases that will be explored in the following.

4.2 The massive spinor helicity formalism

Up to this point, we have discussed how to use the spinor helicity formalism to determine tree-level scattering amplitudes. This was done both in a top-down and a bottom-up approach, applied to three particle scattering processes. Now, we wish to extend the formalism to include massive momenta. This will allow us to consider more complicated scattering processes involving both massless and massive particles, such as Higgs bosons and quarks.

Some of the techniques discussed in the previous sections for the massless case can also be directly applied to the massive case. We will point out these similarities when needed.

A straightforward extension to the massive case can be obtained through the following argument. Given a massive momentum P^μ, such that $P^2 = m^2$, and two non-collinear massless momenta q^μ and k^μ, such that $q^2 = k^2 = 0$, we can write

$$P^\mu \equiv q^\mu + \frac{m^2}{2q\cdot k}\,k^\mu. \tag{4.105}$$

The idea is that, by decomposing a massive momentum as the sum of two massless momenta, we can reuse many of the tools developed for the massless spinor-helicity formalism. In particular, from the equation above, we may write

$$\not{P} = \not{q} + \frac{m^2}{\langle kq\rangle[qk]}\,\not{k}. \tag{4.106}$$

Although this provides a straightforward extension to massive momenta, the formalism is not particularly efficient. In particular, the covariance of an amplitude under little-group transformations of the massive momentum is obscured. To see this, notice that the definition provided in Eq. (4.105) contains three redundant real degrees of freedom. In fact, both massless and massive momenta possess three real degrees of freedom, given by their four components subject to the corresponding on-shell condition. These three spurious degrees of freedom are related to the massive little group, which in four dimensions is $SO(3)$, or equivalently its double cover $SU(2)$ for particles with spin. Therefore, just as the invariance of a massless momentum $\not{p}$ under the $U(1)$ little group is manifest in Eq. (4.76), we can make the analogous property manifest in the massive case as well.

To this end, it is convenient to introduce a new set of spinors $|p^I\rangle, |p_I]$ which carry a manifest $SU(2)$ index I. Explicitly, we can define the momentum spinor variables as

$$p_{a\dot{a}} = |p^I\rangle_a [p_I|_{\dot{a}}, \qquad \bar{p}^{\dot{a}a} = |p_I]^{\dot{a}}\langle p^I|^a. \tag{4.107}$$

Therefore, we can also write a massive momentum p^μ employing

$$\boxed{\not{p} \equiv |p^I\rangle[p_I| + |p_I]\langle p^I|.} \tag{4.108}$$

This momentum is now manifestly invariant under the transformations

$$|p^I\rangle \;\to\; W^I{}_J\,|p^J\rangle, \qquad [p_I| \;\to\; \left(W^{-1}\right)^J{}_I\,[p_J|, \tag{4.109}$$

where W_I^J is a matrix in the $SU(2)$ little group. To raise and lower these indices we can employ the 2-dimensional Levi-Civita tensor defined in Eq. (B.25), where we simply replace the Lorentz indices with the $SU(2)$ little group ones, ϵ^{IJ}.

Following the conventions of Ref. [46] we write the explicit expressions of the massive Dirac wavefunctions as

$$\begin{aligned} u^I(p) &= \begin{pmatrix} |p\rangle_a^I \\ |p]^{I,\dot{a}} \end{pmatrix}, \qquad & v^I(p) &= \begin{pmatrix} |p\rangle_a^I \\ -|p]^{I,\dot{a}} \end{pmatrix}, \\ \bar{u}_I(p) &= \begin{pmatrix} -\langle p|_I^a & [p|_{I,\dot{a}} \end{pmatrix}, & \bar{v}_I(p) &= \begin{pmatrix} \langle p|_I^a & [p|_{I,\dot{a}} \end{pmatrix}. \end{aligned} \tag{4.110}$$

Plugging these objects into the momentum Dirac equation (4.11), yields the massive Weyl equations

$$\begin{aligned} p_{a\dot{a}}\,|p^I]^{\dot{a}} &= m\,|p^I\rangle_a, & \bar{p}^{\dot{a}a}\,|p^I\rangle_a &= m\,|p^I]^{\dot{a}}, \\ [p^I|_{\dot{a}}\,\bar{p}^{\dot{a}a} &= -m\,\langle p^I|^a, & \langle p^I|^a\,p_{a\dot{a}} &= -m\,[p^I|_{\dot{a}}. \end{aligned} \tag{4.111}$$

For brevity, we collect in Appendix C.1 all the other relevant relations among massive spinors which we use to set the notation.

4.2.1 $h\bar{q}q$ amplitude from massless to massive

As an intermediate example between the massless and massive spinor helicity formalisms, let us consider the Yukawa interaction between the Higgs boson and a quark–antiquark pair. We take

$$h(p_1), \quad \bar{q}_j(p_2), \quad q_i(p_3), \qquad \text{with} \qquad p_1 = -p_2 - p_3, \qquad p_2^2 = p_3^2 = m_q^2, \tag{4.112}$$

where i, j are colour indices, and the momenta all incoming .

The corresponding Standard Model Feynman rule gives [2]

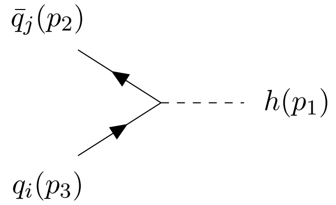

$$= -i\,\delta_{ij}\,\frac{y_q}{\sqrt{2}}, \tag{4.113}$$

where $y_q = \frac{\sqrt{2}\,m_q}{v}$ is the yukawa coupling of the quark q. In this section, we first evaluate the squared modulus of the amplitude for this process, $\big|\mathcal{M}\big(h, \bar{q}, q\big)\big|^2$, in the massless case and then extend the calculation to the massive case using the spinor-helicity formalism. This provides a useful example for understanding the connection between the massless and massive formulations and will also be relevant for the subsequent calculation of Higgs production in gluon fusion. Finally, as a consistency check, we compare the resulting amplitude with the one obtained using standard Dirac-spinor techniques.

Massless helicity amplitudes. When the two external fermions are treated as massless, the only non-vanishing helicity amplitudes are those with equal helicities, since the Higgs–quark interaction flips chirality:

$$\mathcal{M}\big(1_h, 2^+_{\bar{q}_i}, 3^+_{q_j}\big) = -i\,\delta_{ij}\,\frac{y_q}{\sqrt{2}}\,[32], \tag{4.114}$$

$$\mathcal{M}\big(1_h, 2^-_{\bar{q}_i}, 3^-_{q_j}\big) = -i\,\delta_{ij}\,\frac{y_q}{\sqrt{2}}\,\langle 32\rangle, \tag{4.115}$$

$$\mathcal{M}\big(1_h, 2^+_{\bar{q}_i}, 3^-_{q_j}\big) = \mathcal{M}\big(1_h, 2^-_{\bar{q}_i}, 3^+_{q_j}\big) = 0. \tag{4.116}$$

These on-shell tree-level amplitudes can be obtained in two equivalent ways:

- **Bottom-up approach.** Take Eqs. (4.94) and (4.101), and specialize them to the present process by setting $h_1 = 0$, $h_2 = -\frac{1}{2}$ and $h_3 = -\frac{1}{2}$ in the former equation, and $h_1 = 0$, $h_2 = -\frac{1}{2}$ and $h_3 = -\frac{1}{2}$ in the latter[3]. Then you just need to match the generic coupling c to the SM one of Eq. (4.113), obtaining $c = -i\delta_{ij}\frac{y_q}{\sqrt{2}}$.
- **Top-down approach.** Start directly from the helicity amplitudes of the process $\mathcal{M}\big(1_h, 2^{\pm}_{\bar{q}_i}, 3^{\pm}_{q_j}\big) = -i\delta_{ij}\frac{y_q}{\sqrt{2}}\bar{v}_{\pm}(p_2)u_{\pm}(p_3)$ and use the explicit form of the Dirac wave functions in terms of spinor-helicity variables, namely Eq. (4.17).

This being said, we can easily evaluate the squared amplitude by summing over all helicities and colors of the particles involved:

$$\begin{aligned}
\overline{\big|\mathcal{M}\big(h, \bar{q}, q\big)\big|^2}_{\text{massless}} &= \sum_{\text{hel., col.}} |\mathcal{M}|^2_{\text{massless}} \\
&= N_c \frac{y_q^2}{2} \left([32]\langle 23\rangle + \langle 32\rangle [23]\right) \\
&= N_c \frac{y_q^2}{2} \left(2p_2 \cdot p_3 + 2p_2 \cdot p_3\right) \\
&= 2N_c \, y_q^2 \, p_2 \cdot p_3 .
\end{aligned} \tag{4.117}$$

Here, we have implemented Eq. (4.31) to convert the spinor products into momentum dot products, and also Eq. (4.20) when evaluating the complex conjugated amplitudes.

Massive amplitude. Let us now turn to the most interesting case, namely the massive one. As already discussed, in the massive spinor-helicity formalism, helicity is replaced by an $SU(2)$ little-group index. We assign the index I to leg 3 and the index J to leg 2, and obtain the massive amplitude in a *top-down approach*,

$$\begin{aligned}
\mathcal{M}^I_J &\equiv \mathcal{M}\big(1_h, 2_{\bar{q}_i, J}, 3^I_{q_j}\big) \\
&= -i\,\delta_{ij}\,\frac{y_q}{\sqrt{2}}\,\bar{v}_J(p_2)\,u^I(p_3) \\
&= i\,\delta_{ij}\,\frac{y_q}{\sqrt{2}}\,\left(\langle 3^I 2_J\rangle + [3^I 2_J]\right) .
\end{aligned} \tag{4.118}$$

where the explicit form of the massive Dirac wavefunctions Eq. (4.110) was used. Clearly, also here a bottom-up approach can be used; however we have not yet developed the needed tools.

[3]Notice we are using Eqs. (4.94) and (4.101) as if all particles involved were massless, though the Higgs boson its clearly not. From a practical point of view this is completely fine as the Higgs is a scalar, therefore it does not bring about any little group index that would spoil the equations we are using here.

Since each external fermion has spin 1/2, each leg carries only one little-group index, and no symmetrization is required. We will address this point more accurately later. By exploiting the high-energy limit as prescribed in Appendix C.2 we correcly reproduce the massless components:

$$\mathcal{M}_1^1 \xrightarrow{m_q \to 0} -i\,\delta_{ij}\,\frac{y_q}{\sqrt{2}}\,[32], \qquad \mathcal{M}_2^2 \xrightarrow{m_q \to 0} -i\,\delta_{ij}\,\frac{y_q}{\sqrt{2}}\,\langle 32\rangle, \tag{4.119}$$

Notice we are taking the massless limit of the kinematic mass, thus we are keeping the Yukawa coupling constant. We can now proceed to evaluate the squared modulus of the amplitude by summing over the two little group indices I, J and color. First, exploiting Eq. (C.3) we obtain

$$\big(\langle 3^I 2_J\rangle\big)^\dagger = -[2^J 3_I], \quad \big([3^I 2_J]\big)^\dagger = -\langle 2^J 3_I\rangle. \tag{4.120}$$

$$\begin{aligned}
\sum_{\text{spin, col.}} \left|\mathcal{M}^I_J\right|^2 &= -N_c\,\frac{y_q^2}{2}\,\big(\langle 3^I 2_J\rangle + [3^I 2_J]\big)\big([2^J 3_I] + \langle 2^J 3_I\rangle\big) \\
&= -N_c\,\frac{y_q^2}{2}\bigg[\langle 3^I 2_J\rangle[2^J 3_I] + [3^I 2_J]\langle 2^J 3_I\rangle \\
&\qquad + \langle 3^I 2_J\rangle\langle 2^J 3_I\rangle + [3^I 2_J][2^J 3_I]\bigg].
\end{aligned} \tag{4.121}$$

Each of the four terms can be evaluated using Eq. (4.107) and the identities reported in Eq. (C.1). The relevant contractions are

$$\begin{aligned}
\langle 3^I 2_J\rangle[2^J 3_I] &= \langle 3^I|^a \left(|2_J\rangle_a [2^J|_{\dot a}\right) |3_I]^{\dot a} \\
&= -\langle 3^I|^a (p_2)_{a\dot a} |3_I]^{\dot a} \\
&= -(p_2)_{a\dot a}(\bar p_3)^{\dot a a} \\
&= -2 p_2 \cdot p_3.
\end{aligned} \tag{4.122}$$

$$\begin{aligned}
[3^I 2_J]\langle 2^J 3_I\rangle &= [3^I|_{\dot a} \left(|2_J]^{\dot a} \langle 2^J|^a\right) |3_I\rangle_a \\
&= [3^I|_{\dot a} (\bar p_2)^{\dot a a} |3_I\rangle_a \\
&= -(\bar p_2)^{\dot a a}(p_3)_{a\dot a} \\
&= -2 p_2 \cdot p_3.
\end{aligned} \tag{4.123}$$

$$\begin{aligned}
\langle 3^I 2_J\rangle\langle 2^J 3_I\rangle &= \langle 3^I|^a \Big(|2_J\rangle_a \langle 2^J|^b\Big) |3_I\rangle_b \\
&= m_q\,\langle 3^I|^a \delta_a^b |3_I\rangle_b \\
&= m_q\,\langle 3^I|3_I\rangle \\
&= -m_q\,\langle 3_I|3^I\rangle \\
&= m_q^2\,\delta_I^I \\
&= 2m_q^2.
\end{aligned} \tag{4.124}$$

$$
\begin{aligned}
[3^I 2_J][2^J 3_I] &= [3^I|_{\dot a}\left(|2_J]^{\dot a}[2^J|_{\dot b}\right)|3_I]^{\dot b} \\
&= -m_q\,[3^I|_{\dot a}\delta^{\dot a}_{\dot b}|3_I]^{\dot b} \\
&= -m_q\,[3^I|3_I] \\
&= m_q\,[3_I|3^I] \\
&= m_q^2\,\delta^I_I \\
&= 2m_q^2.
\end{aligned} \tag{4.125}
$$

Therefore, we obtain

$$
\begin{aligned}
\overline{\left|\mathcal{M}\big(h,\bar q,q\big)\right|^2} &= N_c\,\frac{y_q^2}{2}\left(4p_2\cdot p_3 - 4m_q^2\right) \\
&= 2N_c\,y_q^2\left(p_2\cdot p_3 - m_q^2\right).
\end{aligned} \tag{4.126}
$$

As a benchmark for the calculation, we can evaluate the same object using standard Dirac-spinor techniques, obtaining

$$
\begin{aligned}
\overline{\left|\mathcal{M}\big(h,\bar q,q\big)\right|^2} = \sum_{\text{spin, col.}}|\mathcal{M}|^2 &= N_c\,\frac{y_q^2}{2}\,\mathrm{Tr}\left[\left(\not{p}_3+m_q\right)\left(\not{p}_2-m_q\right)\right] \\
&= N_c\,\frac{y_q^2}{2}\left(4p_2\cdot p_3 - 4m_q^2\right) \\
&= 2N_c\,y_q^2\left(p_2\cdot p_3 - m_q^2\right).
\end{aligned} \tag{4.127}
$$

This equation is exactly the same of Eq. (4.126). Hence, we have managed to obtain the correct amplitude in case of massive quarks using the massive spinor helicity formalism.

We conclude that the result in Eq. (4.117) therefore misses the term proportional to m_q^2, because the external fermions were treated as massless when performing the polarization sum.

This example provided a first introduction to massive calculations within the spinor-helicity framework and made the connection with the massless formalism explicit. Moreover, we derived the massive amplitude for this process using a top-down approach. In the following section, we will instead focus on the bottom-up construction of massive amplitudes based on little-group covariance.

4.2.2 Little group scaling in the massive case

As already pointed out, the massive little group in four spacetime dimensions is $SU(2)$. Therefore, massive particles of spin s transform in spin-s representations of $SU(2)$. In the notation of [48], these representations are described by the states

$$|p, s_z\rangle,$$

where

$$\mathbf{J}^2|p,s_z\rangle = s(s+1)|p,s_z\rangle, \qquad J_3|p,s_z\rangle = s_z|p,s_z\rangle, \tag{4.128}$$

and $\mathbf{J}$ is the total angular momentum operator of the particle. See Appendix B.2 for further discussion on particle states. Here, s labels the irreducible representation of $SU(2)$, whose dimension is

$$2s+1. \tag{4.129}$$

Namely, a spin-s representation is spanned by

$$\{|p,s_1\rangle,\ldots,|p,s_{2s+1}\rangle\}\,. \tag{4.130}$$

For our purposes, however, it is more convenient to label the spin-s representation by a symmetric rank-$2s$ tensor of $SU(2)$,

$$\psi^{I_1\cdots I_{2s}}, \tag{4.131}$$

where each index $I_i = 1,2$ is a little-group index. The generators of $SU(2)$ act on this object as [48]

$$(J^a\psi)^{I_1\cdots I_{2s}} = \left(\frac{\sigma^a}{2}\right)^{I_1}{}_{J_1}\psi^{J_1 I_2\cdots I_{2s}} + \cdots + \left(\frac{\sigma^a}{2}\right)^{I_{2s}}{}_{J_{2s}}\psi^{I_1\cdots I_{2s-1}J_{2s}}. \tag{4.132}$$

In this way, the spin-s representation is obtained as the completely symmetric product of $2s$ spin-$\frac{1}{2}$ representations. This implies that any massive spin representation can be built by combining spin-$\frac{1}{2}$ representations, and the massive helicity spinors introduced above are precisely $SU(2)$ doublets.

For instance, an amplitude involving a massive fermion of momentum p_1 and a massive spin-2 particle of momentum p_2 must carry one little-group index for the fermion and four symmetrized little-group indices for the other particle. If particles 3 and 4 are massless with helicities $h_3 = \frac{3}{2}$ and $h_4 = -1$, respectively, the amplitude can be written schematically as

$$\mathcal{M}(1^I, 2^{\{J_1,J_2,J_3,J_4\}}, 3^{+\frac{3}{2}}, 4^{-1}), \tag{4.133}$$

where the $SU(2)$ little-group indices label massive particles, whereas massless particles are identified by their helicities. Here, as in the massless case, we abbreviate the spinor associated with the external leg i as $|p_i] \to |i]$ or $|p_i\rangle \to |i\rangle$.

Under a little-group transformation, this amplitude transforms as

$$\begin{aligned}\mathcal{M}(1^I, 2^{\{J_1,J_2,J_3,J_4\}}, 3^{+\frac{3}{2}}, 4^{-1}) \longrightarrow (W_1)^I{}_{I'}\,(W_2)^{J_1}{}_{J_1'}\,(W_2)^{J_2}{}_{J_2'}\,(W_2)^{J_3}{}_{J_3'}\,(W_2)^{J_4}{}_{J_4'} \\ \times\, w_3^{-2\left(\frac{3}{2}\right)} w_4^{-2(-1)} \mathcal{M}(1^{I'}, 2^{\{J_1',J_2',J_3',J_4'\}}, 3^{+\frac{3}{2}}, 4^{-1}),\end{aligned} \tag{4.134}$$

where we employ Eqs. (4.109) and (4.80) for the massive and massless little-group scalings, respectively. Notice that we use curly brackets to indicate that the indices J_1, J_2, J_3, J_3, J_4 must be symmetrized. From this relatively simple example, we can understand the advantage of employing explicit little-group indices when defining massive momenta.

More generally, an amplitude with a massive spin-s particle of momentum p_1^μ can be written as [48]

$$\boxed{\begin{aligned}\mathcal{M}(1^{\{I_1 \cdots I_{2s}\}}, \dots) &= |1\rangle_{a_1}^{\{I_1} \cdots |1\rangle_{a_{2s}}^{I_{2s}\}} \, M^{\{a_1,\dots,a_{2s}\}} \\ &= |1]^{\dot{a}_1,\{I_1} \cdots |1]^{I_{2s}\},\dot{a}_{2s}} \, \tilde{M}_{\{\dot{a}_1,\dots,\dot{a}_{2s}\}}\end{aligned}}, \tag{4.135}$$

since, as seen in the previous example, the little-group indices must be manifest for the scaling to work properly. The reduced amplitudes M and $\tilde{M}$ do not carry any massive little group index and are equivalent, as one can switch between dotted and undotted spinors by exploiting Eqs. (4.111). Moreover, they are totally symmetric in the a or $\dot{a}$ indices; again, this is conventionally indicated by curly brackets.

Let us now give a “legal” expression for the amplitude in the previous example, namely an expression with the correct little-group transformation properties.

Again, consider an amplitude with particles 1 and 2 massive, of spin 1/2 and 2, respectively, and particles 3 and 4 massless, with helicities $h_3 = \frac{3}{2}$ and $h_4 = -1$. For the massless particles, little-group covariance fixes the required weights. Since particle 3 has helicity $h_3 = 3/2$, the amplitude must scale as

$$\mathcal{M} \to w_3^{-2h_3}\mathcal{M} = w_3^{-3}\mathcal{M}. \tag{4.136}$$

This implies that the amplitude must contain 3 square spinors of momenum p_3, namely $|3]^3$.

Similarly, since particle 4 has helicity $h_4 = -1$, the amplitude must scale as

$$\mathcal{M} \longrightarrow w_4^{-2h_4}\mathcal{M} = w_4^{2}\mathcal{M}. \tag{4.137}$$

Hence, the amplitude must also contain 2 square spinors of momenum p_3, namely $|4]^2$.

For the massive particles, the amplitude must carry the appropriate $SU(2)$ little-group indices. Therefore, for particle 1 we need one index I, while for particle 2 we need four symmetrized indices J_1, J_2, J_3, J_4.

Two possible legal structures, which reproduce the correct little-group weights but do not exhaust all the possibilities, are then

$$\begin{aligned}\mathcal{M}(1^I, 2^{\{J_1,J_2,J_3\}}, 3^{+\frac{3}{2}}, 4^{-1}) = & \, c_1 \, [2^{J_1}3] \, [2^{J_2}3] \, [2^{J_3}3] \, \langle 4 \, 2^{J_4} \rangle \langle 1^I 4 \rangle \\ & + c_2 \, [2^{J_1}3] \, [2^{J_2}3] \, [2^{J_3}3] \, \langle 1^I 2^{J_4} \rangle \langle 4 | \not{p}_1 \not{p}_2 | 4 \rangle \\ & + \text{symmetrization over } \{J_1, J_2, J_3, J_4\},\end{aligned} \tag{4.138}$$

where we require symmetrization over the J_i with $i \in 1,2,3,4$ little group indices. It would clearly be notationally cumbersome to keep all explicit $SU(2)$ little-group indices in our expressions. Fortunately, this is not necessary. We will denote massive spinor-helicity variables in boldface and suppress their $SU(2)$ little-group indices. Since these indices are always completely symmetrized, they can be restored unambiguously whenever needed. With this convention, expressions such as the one above can be written in the compact form

$$\mathcal{M}(\mathbf{1}^{s=\frac{1}{2}}, \mathbf{2}^{s=2}, 3^{+\frac{3}{2}}, 4^{-1}) = [\mathbf{2}3]^3 \left(c_1 \, \langle 4\mathbf{2} \rangle \langle \mathbf{1}4 \rangle + c_2 \, \langle \mathbf{12} \rangle \langle 4 | \not{p}_1 \not{p}_2 | 4 \rangle \right). \tag{4.139}$$

This expression would otherwise be written as

$$[2^{\{J_1,J_2,J_3} \, 3]^3 \left(c_1 \, \langle 4 \, 2^{J_1,J_2,J_3\}} \rangle \langle 1^{\{I} 4 \rangle + c_2 \, \langle 1^{I\}} \, 2^{J_1,J_2,J_3\}} \rangle \langle 4 | \not{p}_1 \not{p}_2 | 4 \rangle \right). \tag{4.140}$$

It is important to stress that, for massive particles, there is no analogue of the usual massless helicity weight. Therefore, expressions involving massive spinors may look, from a purely massless point of view, as if they were combining terms with different helicity weights. This is not a problem. The massive spinors transform as $SU(2)$ little-group tensors, and the suppressed little-group indices ensure that the full expression has the correct transformation properties.

Chapter 5

Amplitude method at tree level

What we aim to do in this thesis is to extend the "amplitude method" to the one-loop level, in the case of Higgs production via gluon fusion. In this section, we review what we exactly mean by "amplitude method", looking at tree-level examples. Understanding the working mechanism at tree level is indeed necessary for its later extension to one loop. Moreover, the former case is well established in the literature, for instance, in Refs. [49–51].

As presented in Sec. 4.1.5, little-group scaling efficiently constrains massless tree-level amplitudes, together with dimensional analysis and the locality of the operators. In this section, we want to focus on this subject and extend the discussion to the massive case. To this end, we will explicitly implement the massive little-group scaling presented in Sec. 4.2.2, for which no examples were given. Although not explicitly implemented in this thesis, we will also give some hints on how to treat higher-point tree-level amplitudes. Special care must be taken when treating these amplitudes. The point is that their form is determined not only by the general principles stated above, giving the so-called "bootstrapped" part, but also by a "factorizable" part, which comes from gluing together the lower-point on-shell amplitudes they are made of. Mastering these two methods makes it possible to derive on-shell scattering amplitudes from a bottom-up perspective, without relying on prior knowledge of a Lagrangian. In this sense, we usually call these amplitudes model-independent. What we have just discussed is exactly what we mean by the "amplitude method".

The program of this section is therefore to first present a general discussion on the topic and then compute some scattering amplitudes of interest at tree level. The first is the hgg process, for which we provide a matching onto SMEFT. Thereafter, we will apply the amplitude method to the processes $ht\bar{t}$ and $\bar{t}tg$. These are of fundamental importance for the extension of the amplitude method to one loop in the hgg process.

Finally, we stress that we will not explicitly compute amplitudes which require a factorizable part. To see how factorizable contributions are evaluated in higher-point amplitudes, see for instance Refs. [2, 46, 49, 50].

5.1 Bootstrapping and gluing on-shell amplitudes

As briefly reviewed in Sec. 3, effective field theories provide a systematic description of possible new physics arising at high energy and parametrized through an expansion in inverse powers of a heavy scale Λ. In the conventional Lagrangian approach, this requires the construction of a complete set of independent local operators, followed by the derivation of the corresponding Feynman rules, similarly to what was described for SMEFT in Sec. 3.2. What we do here is to change this perspective. Since the quantities that ultimately enter physical observables are on-shell scattering amplitudes, it is more natural to formulate the EFT expansion directly at the level of amplitudes.

An on-shell amplitude is constrained by Lorentz invariance, little-group covariance and locality. unitarity and the statistics of identical particles. These principles can be used to determine the allowed kinematic structures without referring explicitly to a Lagrangian or to a particular choice of operator basis. In this formulation, redundancies associated with field redefinitions are absent from the outset, since they do not affect the physical S-matrix.

A general n-point on-shell amplitude may be written schematically as

$$\mathcal{M}_n = \mathcal{T} \sum_{\alpha} c_\alpha\big(\{s_{ij}\}\big)\, \langle \ldots \rangle^{A_\alpha} [\ldots]^{B_\alpha}, \tag{5.1}$$

where $\mathcal{T}$ denotes an invariant tensor carrying the internal quantum numbers of the external states, e.g. color, whereas $\langle \ldots \rangle$ and $[\ldots]$ represent contracted helicity spinor structures. Their exponents are fixed by the little-group weights of the external states, both for massless and massive particles. The coefficients c_α are Lorentz-invariant functions of the generalized Mandelstam variables

$$s_{ij} = (p_i + p_j)^2, \tag{5.2}$$

or, more generally, of independent multiparticle invariants. Throughout this discussion, all external momenta are taken to be incoming. Eq. (5.1) is what we mean by the bootstrapping of an amplitude. We have already seen that the main ingredient we use here is little-group scaling, as shown in Eqs. (4.80) and (4.135), for the massless and massive cases, respectively.

Let us now focus on the so-called factorizable part of the amplitude. At tree level, locality implies that the only singularities of the amplitude are simple poles associated with physical internal propagators. Notice that this point is one of the most evident differences between tree-level and loop-level amplitudes, since in the latter a much more complicated non-analytic structure emerges from the integrations over the loop momenta. Sticking to tree-level amplitudes, consider a channel with momentum P_i; the residue at the pole $P_i^2 = m_i^2$ must factorize into a product of lower-point on-shell amplitudes,

$$\operatorname*{Res}_{P_i^2=m_i^2} \mathcal{M}_n = \sum_{\sigma_i} \mathcal{M}_L\big(\ldots, i^{\sigma_i}\big)\mathcal{M}_R\big(\widetilde{i}^{-\sigma_i}, \ldots\big), \tag{5.3}$$

where the sum runs over the physical polarization or little-group states of the exchanged particle. Clearly, the state $\widetilde{i}$ carries momentum opposite to that of i.

It is therefore useful to decompose the full tree-level amplitude as

$$\mathcal{M}_n = \mathcal{M}_n^{\mathrm{F}} + \mathcal{M}_n^{\mathrm{NF}}, \tag{5.4}$$

where $\mathcal{M}_n^{\mathrm{F}}$ is the factorizable contribution containing all physical poles, whereas $\mathcal{M}_n^{\mathrm{NF}}$ is a local, non-factorizable contribution with no poles. Obtaining both parts is what we mean by the “amplitude method”.

The two parts are constructed in different but complementary ways. The factorizable part is obtained by *gluing* lower-point amplitudes across all allowed physical channels, while the non-factorizable part is obtained by *bootstrapping* all local spinor structures compatible with the quantum numbers and symmetries of the process, as shown in Eq. (5.1).

For example, the factorizable contribution to a four-point amplitude can be constructed as

$$\mathcal{M}_4^{\mathrm{F}}(\psi_1, \psi_2, \psi_3, \psi_4) = -\sum_{\text{channels}} \sum_{\sigma_V} \frac{\mathcal{M}_3(\psi_i, \psi_j, \psi_V^{\sigma_V})\,\mathcal{M}_3(\psi_k, \psi_\ell, \widetilde{\psi}_V^{\sigma_V})}{s_{ij} - m_V^2}, \tag{5.5}$$

where $i, j, k, \ell \in \{1, 2, 3, 4\}$, ψ_V is the particle of mass m_V being exchanged, and σ_V labels its little-group states. The first sum runs over all possible factorization channels, while the second implements the contraction over the little-group indices of the internal particle. Here, $\widetilde{\psi}_V$ denotes the same particle as ψ_V, but with opposite helicity and momentum, since each three-point amplitude requires all particles to be incoming. This prescription allows the full amplitude to reproduce the correct poles and residues. For higher-point amplitudes, the same principle can be applied recursively, although additional care is needed to organize the different factorization channels and avoid overcounting.

The remaining contribution, $\mathcal{M}_n^{\mathrm{NF}}$, contains the information that cannot be reconstructed from lower-point amplitudes. Since all singularities are already contained in $\mathcal{M}_n^{\mathrm{F}}$, its coefficients are analytic functions of the independent Mandelstam invariants. They can therefore be expanded as

$$\begin{aligned} c_\alpha\big(\{s_{ij}\}\big) = c_\alpha^{(0)} &+ \frac{1}{\Lambda^2} \sum_{i<j} c_{\alpha,ij}^{(1)} s_{ij} \\ &+ \frac{1}{\Lambda^4} \sum_{\substack{i<j \\ k<\ell}} c_{\alpha,ij;k\ell}^{(2)} s_{ij} s_{k\ell} + \cdots , \end{aligned} \tag{5.6}$$

where the powers of $1/\Lambda$ displayed explicitly account only for the additional suppression associated with increasing powers of the Mandelstam invariants. Depending on the spinor-helicity structure labelled by α, the leading coefficient $c_\alpha^{(0)}$ may itself start at order $1/\Lambda^n$, with n fixed by dimensional analysis. This expansion naturally organizes the amplitude according to its energy growth. Terms containing higher powers of the Mandelstam invariants correspond to interactions of increasing canonical dimension and must be accompanied by increasing powers of the EFT suppression scale. At this stage, Bose symmetry can also be imposed: if identical particles are present among the external states, invariance of the amplitude under their exchange relates some of the coefficients appearing in the expansion. When matched to a Lagrangian description, the independent coefficients appearing in the on-shell amplitude are related to linear combinations of Wilson coefficients.

As a final comment, notice that gauge redundancy does not enter explicitly in this construction because the amplitudes are written directly in terms of physical on-shell states. For external massless gauge bosons, the combination of little-group covariance, locality and consistent factorization ensures that the final result possesses the correct gauge-invariant physical content. In this sense, gauge invariance is implemented directly at the level of the observable amplitude.

In the following, the "amplitude method" is illustrated through explicit examples.

5.1.1 Bootstrapping hgg

Let us consider the three-point amplitude involving one massive scalar and two massless gluons. The most general ansatz built out of square brackets is

$$\mathcal{M}\left(h, 1_g^{a,h_1}, 2_g^{b,h_2}\right) = \delta^{ab}[12]^n c_{-d}(s_{12}, \Lambda), \tag{5.7}$$

where a and b are color indices and c_{-d} is an analytic function of the generalized Mandelstam variables, which in this case reduce to the Higgs mass squared,

$$s_{12} = (p_1 + p_2)^2 = m_h^2, \tag{5.8}$$

and of Λ, which parametrizes the scale of an unknown high-energy theory. The mass dimension of c_{-d} is

$$[c_{-d}] = -d = 1 - n. \tag{5.9}$$

Under little-group transformations, the amplitude scales in two equivalent ways:

$$\mathcal{M}_3 \longrightarrow \begin{cases} t_1^{-2h_1}\, t_2^{-2h_2}\, \mathcal{M}_3 & \text{(using Eq. (4.80))}, \\ t_1^{-n}\, t_2^{-n}\, \mathcal{M}_3 & \text{(using Eq. (4.76))}. \end{cases} \tag{5.10}$$

Notice that the scalar particle does not contribute any little-group weight. Comparing the two scaling behaviours gives

$$n = 2h_1 = 2h_2, \tag{5.11}$$

and therefore

$$h_1 = h_2. \tag{5.12}$$

Thus, the amplitude vanishes for opposite-helicity gluons, while for $h_1 = h_2 = +1$ one finds $n = 2$. This has a straightforward physical interpretation in terms of total angular momentum conservation in a scattering process. For convenience, consider a Higgs boson at rest and picture its decay into two gluons in the center-of-mass frame. Since the Higgs boson is a spin-0 particle, the total angular momentum of the final state must also vanish. This can be achieved if the spins of the two gluons, which are emitted with opposite three-momenta due to momentum conservation, either both point along their respective momentum directions or both point opposite to them. In other words, the only possible helicity configurations are precisely those predicted by the spinor-helicity formalism.

The positive-helicity amplitude is therefore

$$\mathcal{M}\left(h, 1_g^{a,+}, 2_g^{b,+}\right) = \delta^{ab}[12]^2 c_{-1}(s_{12}, \Lambda). \tag{5.13}$$

Here, since the coefficient c of the amplitude has mass dimension of -1, we can write

$$c(m_h^2, \Lambda) = \frac{1}{\Lambda}\widetilde{c}\left(\frac{m_h^2}{\Lambda^2}\right), \tag{5.14}$$

where $\widetilde{c}$ is dimensionless. Locality implies that $\widetilde{c}$ is analytic and can be expanded as

$$\widetilde{c}\left(\frac{m_h^2}{\Lambda^2}\right) = \sum_{n=0}^{\infty} c_n \left(\frac{m_h^2}{\Lambda^2}\right)^n. \tag{5.15}$$

Absorbing this expansion into the effective coefficient c_{hgg}^{++}, the most general three-point amplitude becomes

$$\boxed{\mathcal{M}\left(h, 1_g^{a,+}, 2_g^{b,+}\right) = \delta^{ab}\frac{c_{hgg}^{++}}{\Lambda}[12]^2.} \tag{5.16}$$

Notice that, with respect to the discussion in Sec. 4.1.5, here we allow for a non-zero mass dimension of the coefficient c. This hints at the presence of a higher-dimensional operator, specifically one of dimension 6, which generates this amplitude in the first place. Before looking at the connection between the amplitude and the EFT operators from which it may be generated, let us first comment on the other non-vanishing helicity configuration of the amplitude.

As already pointed out in the general discussion of three-point on-shell amplitudes in Sec. 4.1.5, the negative-helicity configuration requires a different ansatz from the one in Eq. (5.7), namely one built out of angle brackets. If we used the square bracket ansatz instead, a manifestly non-local amplitude would be generated and should therefore be discarded.

In particular, for the negative-helicity configuration, we should instead start from

$$\mathcal{M}\left(h, 1_g^{a,-}, 2_g^{b,-}\right) = \delta^{ab}\langle 12\rangle^n \tilde{c}_{-d}(s_{12}, \Lambda). \tag{5.17}$$

In this case, following steps similar to those above, we readily obtain

$$\boxed{\mathcal{M}\left(h, 1_g^{a,-}, 2_g^{b,-}\right) = \delta^{ab}\frac{c_{hgg}^{--}}{\Lambda}\langle 12\rangle^2.} \tag{5.18}$$

As expected, this amplitude is the parity conjugate of the positive-helicity configuration. This is, again, a confirmation of the correct implementation of the spinor-helicity formalism. Notice that the coefficient c_{hgg}^{++} can be in general different from c_{hgg}^{--}. On considering a purely CP-even theory, the two coefficients must be equal to each other. This is for example the case of the SM in which

$$\left|\mathcal{M}^{\rm SM}\left(h, 1_g^{a,+}, 2_g^{b,+}\right)\right|^2 = \left|\mathcal{M}^{\rm SM}\left(h, 1_g^{a,-}, 2_g^{b,-}\right)\right|^2. \tag{5.19}$$

Matching onto SMEFT. We now consider for simplicity the amplitude with all positive helicity configuration. We saw that the emergence on the inverse of the EFT scale Λ must hint to the presence of dimension-6 operators. In this context, SMEFT provides this kind of contribution through a subset of operators we already pointed out in Sec. 3.2 which are

$$Q_{\varphi G} = \left(\varphi^\dagger\varphi\right) G_{\mu\nu}^A G^{A\mu\nu}, \qquad Q_{\varphi\widetilde{G}} = \left(\varphi^\dagger\varphi\right) G_{\mu\nu}^A \widetilde{G}^{A\mu\nu}. \tag{5.20}$$

The relevant Feynman rule that can be obtained from these operators is reported in Eq. (A.17). These two operators are CP-even and CP-odd, respectively.

Now, we can match the SMEFT Wilson coefficients $C_{\varphi G}$ and $C_{\varphi\widetilde{G}}$ onto the c_{hgg}^{++} coefficient appearing in the bootstrapped amplitude. We can do this analytically in two steps; first evaluate the SMEFT amplitude in the spinor helicity formalism, then confront what we obtained with Eq. (5.16). Notice we must declare the helicities of the gluons from the outset.

$$\mathcal{M}\big(h, 1_g^{a,+}, 2_g^{b,+}\big)_{\text{SMEFT}} =$$

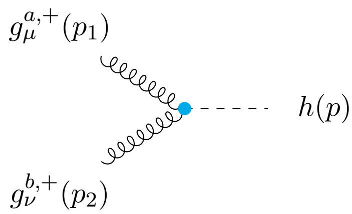

$$\begin{aligned}
&= \frac{4iv}{\Lambda^2}\,\delta^{ab}\Big[C_{\varphi G}\left(-p_1\cdot p_2\, g^{\mu\nu} + p_1^\nu p_2^\mu\right) + C_{\varphi\widetilde{G}}\epsilon^{\mu\nu\rho\sigma}p_{1\rho}p_{2\sigma}\Big]\epsilon_\mu^+(p_1)\,\epsilon_\nu^+(p_2)\\
&= \frac{1}{\Lambda^2}\left[4iv\,\delta^{ab}C_{\varphi G}\left(-\frac{m_h^2}{2}\right)\frac{[12]^2}{m_h^2} + 2v\,\delta^{ab}C_{\varphi\widetilde{G}}[12]^2\right]\\
&= \frac{\delta^{ab}[12]^2}{\Lambda^2}\left(-2iv\,C_{\varphi G} + 2v\,C_{\varphi\widetilde{G}}\right)\\
&= -\frac{2iv}{\Lambda^2}\,\delta^{ab}[12]^2\left(C_{\varphi G} + iC_{\varphi\widetilde{G}}\right).
\end{aligned} \tag{5.21}$$

where we used the following relations

- $p_1\cdot p_2 = \frac{m_h^2}{2}$ from the kinematics of the process;
- $\epsilon^+(p_1;p_2)\cdot\epsilon^+(p_2;p_1) = \frac{[12]^2}{m_h^2}$. Using the definition of the polarization vectors in Eq. (4.60), and choosing the reference momenta as $r_1 = p_2$ and $r_2 = p_1$, we obtain

$$\begin{aligned}
\varepsilon^+(p_1;p_2)\cdot\varepsilon^+(p_2;p_1) &= \frac{1}{2}\,\frac{[1|\gamma^\mu|2\rangle[2|\gamma^\mu|1\rangle}{\langle 21\rangle\langle 12\rangle}\\
&= \frac{[12]\cancel{\langle 12\rangle}}{\langle 21\rangle\cancel{\langle 12\rangle}}\\
&= \frac{[12]^2}{\langle 21\rangle[12]}\\
&= \frac{[12]^2}{m_h^2},
\end{aligned} \tag{5.22}$$

  where Eqs. (4.45) and (4.31) were used.

- $p_{1\rho}p_{2\sigma}\varepsilon_\mu^+(p_1)\varepsilon_\nu^+(p_2)\epsilon^{\mu\nu\rho\sigma} = -\frac{i}{2}[12]^2$. A proof is provided in Appendix B.1.1.

The result in Eq. (5.22) can be now matched onto the general on-shell parametrization derived above in Eq. (5.16). Comparing this expression with the SMEFT amplitude, we obtain the matching relation

$$c_{hgg}^{++} = -\frac{2iv}{\Lambda}\left(C_{\varphi G} + iC_{\varphi\widetilde{G}}\right). \tag{5.23}$$

This result makes explicit how the dimension-five on-shell interaction is generated, within the SMEFT, by dimension-six gauge-invariant operators after electroweak symmetry breaking. In particular, the factor v/Λ originates from the insertion of the Higgs vacuum expectation value in $Q_{\varphi G}$ and $Q_{\varphi\widetilde{G}}$. For a matching onto SMEFT up to order $1/\Lambda^2$ see also Ref. [49].

By following a similar calculation, one finds that the matching of the all negative-helicity amplitude onto SMEFT yields

$$c_{hgg}^{--} = -\frac{2iv}{\Lambda}\left(C_{\varphi G} - iC_{\varphi\widetilde{G}}\right), \tag{5.24}$$

which differs from c_{hgg}^{++} by a sign difference on $C_{\varphi\widetilde{G}}$. This is expected from the fact that in a CP-even theory $c_{hgg}^{++} = c_{hgg}^{--}$, which implies at the level of SMEFT that $C_{\varphi\widetilde{G}} = 0$.

5.1.2 Bootstrapping $ht\bar{t}$

We now consider the three-point $ht\bar{t}$ amplitude, which will serve as one of the building blocks for the gluon-fusion Higgs-production amplitude discussed in Ch. 7. Here, we derive its general on-shell form. As for the hgg amplitude, $ht\bar{t}$ does not have a factorizable part, being a three-particle amplitude. Therefore, all we need to do is bootstrap its non-factorizable part. To this end, we exploit Eq. (4.135), which constrains the amplitude to be of the following form

$$\boxed{\mathcal{M}(\mathbf{1}_h, \mathbf{2}_{t_i}, \mathbf{3}_{\bar{t}_j}) = \delta_{ij}\left(c_{ht\bar{t}}^{LL}\langle\mathbf{32}\rangle + c_{ht\bar{t}}^{RR}[\mathbf{32}]\right).} \tag{5.25}$$

Here, we are implementing the bold notation to avoid showing explicitly the little-group indices of t and $\bar{t}$. It is natural to ask whether a structure of the form

$$\langle\mathbf{3}|\not{p}_1|\mathbf{2}] \tag{5.26}$$

should also be considered, as $\not{p}_1$ is invariant under little-group transformations. We can recast this term in the following form

$$\begin{aligned}\langle\mathbf{3}|\not{p}_1|\mathbf{2}] &= \langle 3^K|(-\not{p}_2 - \not{p}_3)|2^J] \\ &= -\langle 3^K|\not{p}_2|2^J] - \langle 3^K|\not{p}_3|2^J] \\ &= -m_t\langle\mathbf{32}\rangle + m_t[\mathbf{32}].\end{aligned} \tag{5.27}$$

Here, m_t is the top-quark mass, and we have exploited momentum conservation, Eqs. (4.26), and the massive Weyl equations (4.111). Hence, the independent bootstrapped structures contained in Eq. (5.25) already account for a term such as $\langle\mathbf{3}|\not{p}_1|\mathbf{2}]$.

What is different with respect to the SM amplitude? In Sec. 4.2.1, we already encountered the amplitude involving a Higgs and two quarks. There, we made use of a top-down approach, starting from the SM interaction vertex.

We report here the result obtained in Eq. (4.118), adapting the momentum definitions:

$$\mathcal{M}(\mathbf{1}_h, \mathbf{2}_{t_i}, \mathbf{3}_{\bar{t}_j}) = -i\,\delta_{ij}\,\frac{y_t}{\sqrt{2}}\,(\langle\mathbf{32}\rangle + [\mathbf{32}])\,. \tag{5.28}$$

We straightforwardly notice that matching to the SM provides the following values for the coefficients $c^{LL}_{ht\bar{t}}$ and $c^{RR}_{ht\bar{t}}$ of the bootstrapped amplitude:

$$\boxed{\text{SM}: \qquad c^{LL}_{ht\bar{t}} = c^{RR}_{ht\bar{t}} = -i\frac{y_t}{\sqrt{2}}.} \tag{5.29}$$

The fact that in the SM the two coefficients are equal to each other reflects the parity conservation of the interaction. The SM operator $h\bar{t}t$ is indeed parity conserving; therefore, applying a parity transformation to Eq. (5.28), thus exchanging angle and square brackets, leaves the amplitude unchanged. Conversely, the model-independent expression for the amplitude allows for a more general interaction in which parity can also be violated, for instance via an operator of the form $ih\bar{t}\gamma^5 t$. This can be seen more explicitly by recasting Eq. (5.25) as

$$\mathcal{M}(\mathbf{1}_h, \mathbf{2}_{t_i}, \mathbf{3}_{\bar{t}_j}) = \delta_{ij}\left[\frac{c^{RR}_{ht\bar{t}} + c^{LL}_{ht\bar{t}}}{2}\,(\langle\mathbf{32}\rangle + [\mathbf{32}]) + \frac{c^{RR}_{ht\bar{t}} - c^{LL}_{ht\bar{t}}}{2}\,(-\langle\mathbf{32}\rangle + [\mathbf{32}])\right]. \tag{5.30}$$

The second term on the right-hand side is precisely the parity-violating term, which changes sign under a parity transformation. Also, as expected, if the two coefficients $c^{LL}_{ht\bar{t}}$ and $c^{RR}_{ht\bar{t}}$ are equal, as in the SM, the parity-violating term vanishes.

Let us now comment on the choice of notation for the coefficients of the amplitude, which coincides with that of [46]. In $c^{RR}_{ht\bar{t}}$ and $c^{LL}_{ht\bar{t}}$, the RR and LL chirality pairs give rise to chirality-violating terms, which is consistent with the fact that the Higgs boson flips chirality in this interaction. We stick to this notation since it makes the chiral structure of the spinors manifest. More explicitly, $\langle\mathbf{32}\rangle$ and $[\mathbf{32}]$ are Lorentz-invariant contractions of spinors transforming in the left- and right-handed Weyl representations, respectively. Although their Lorentz indices are fully contracted, they retain the suppressed $SU(2)$ little-group indices associated with the two massive external particles.

As a final remark, we highlight the fact that the amplitude of Eq. (5.25) can be matched onto its SMEFT counterpart, whose Feynman rule is reported in Eq. (A.18). From a qualitative comparison, we can see that the combination $(c^{RR}_{ht\bar{t}} + c^{LL}_{ht\bar{t}})/2$ should account for a simple modification of the Yukawa coupling due to the presence of the real part of the Wilson coefficient $C^{33}_{u\varphi}$, whereas the parity-violating coefficient $(c^{RR}_{ht\bar{t}} - c^{LL}_{ht\bar{t}})/2$ can be matched onto the imaginary part of the same Wilson coefficient. We will not make the matching explicit here, as it will be performed in Ch. 7 when matching the one-loop Higgs production via gluon-fusion process. Here, we only wanted to make a qualitative connection with SMEFT.

5.1.3 Bootstrapping $\bar{t}tg$

The last on-shell amplitude we want to determine via bootstrapping is the interaction between a gluon and a pair of top and anti-top quarks. This amplitude will be of fundamental importance when studying the one-loop production of a Higgs via gluon fusion. We start from the positive-helicity configuration,

$$\mathcal{M}\big(\mathbf{1}_{\bar{t}_i}, \mathbf{2}_{t_j}, 3_g^{a,+}\big), \tag{5.31}$$

As before, we use the bold notation to keep the massive little-group indices implicit. Since particles 1 and 2 are massive spin-1/2 states, each of them carries one $SU(2)$ little-group index. To bootstrap this amplitude, we implement the square-spinor representation of Eq. (4.135); the amplitude can therefore be written as

$$\mathcal{M}\big(\mathbf{1}_{\bar{t}}, \mathbf{2}_t, 3_g^+\big) = |\mathbf{1}]^{\dot{a}}|\mathbf{2}]^{\dot{b}} M_{\dot{a}\dot{b}}, \tag{5.32}$$

where all the dependence on the massless particle is contained in $M_{\dot{a}\dot{b}}$. Moreover, we are omitting the color factor $(T^a)_{ji}$ that will be restored at the end of the derivation.

The reduced amplitude $M_{\dot{a}\dot{b}}$ is strongly constrained by the massless little group, which dictates the scaling of the square and angle spinors as reported in Eq. (4.76). In particular, under

$$|3\rangle \longrightarrow w_3|3\rangle, \qquad |3] \longrightarrow w_3^{-1}|3], \tag{5.33}$$

an amplitude containing a particle of helicity h_3 must transform as

$$\mathcal{M} \longrightarrow w_3^{-2h_3}\mathcal{M}. \tag{5.34}$$

We say that particle 3 carries helicity weight h_3. For a positive-helicity gluon, $h_3 = +1$, and therefore

$$\mathcal{M}\big(\mathbf{1}_{\bar{t}}, \mathbf{2}_t, 3_g^+\big) \longrightarrow w_3^{-2}\mathcal{M}\big(\mathbf{1}_{\bar{t}}, \mathbf{2}_t, 3_g^+\big). \tag{5.35}$$

Since the massive spinors $|\mathbf{1}]$ and $|\mathbf{2}]$ are unaffected by the massless little-group transformation of particle 3, the entire weight w_3^{-2} must be carried by $M_{\dot{a}\dot{b}}$.

A first possibility is immediate. The tensor

$$M_{\dot{a}\dot{b}} = [3|_{\dot{a}}[3|_{\dot{b}} \tag{5.36}$$

has precisely the required weight, since each $|3]$ transforms as w_3^{-1}. It therefore generates the legal structure

$$\mathcal{M}\big(\mathbf{1}_{\bar{t}}, \mathbf{2}_t, 3_g^+\big) \supset [3\mathbf{1}][3\mathbf{2}]. \tag{5.37}$$

However, this is not the only possible structure. In two-component spinor space, a rank-two dotted tensor can also contain an antisymmetric part proportional to $\epsilon_{\dot{a}\dot{b}}$. Since $\epsilon_{\dot{a}\dot{b}}$ itself carries no little-group weight, it has to be multiplied by a scalar quantity transforming as w_3^{-2}. Such a quantity naturally arises from the special kinematics of the three-point amplitude.

To see this, consider the following two objects

$$|3\rangle, \qquad \not{p}_1|3]. \tag{5.38}$$

Their spinor contraction vanishes:

$$\begin{aligned}\langle 3|\not{p}_1|3] &= p_1^\mu \langle 3|\gamma_\mu|3] \\ &= 2p_1 \cdot p_3 \\ &= (p_1+p_3)^2 - p_1^2 - p_3^2 \\ &= (-p_2)^2 - m_t^2 \\ &= 0.\end{aligned} \tag{5.39}$$

Here we have used momentum conservation assuming all particles to be incoming and on shell,

$$p_1 + p_2 + p_3 = 0, \qquad p_1^2 = p_2^2 = m_t^2, \qquad p_3^2 = 0. \tag{5.40}$$

The above condition implies that $|3\rangle$ and $\not{p}_1|3]$ are not independent. We can therefore define a scalar quantity x through

$$\not{p}_1|3] = x\,|3\rangle. \tag{5.41}$$

The proportionality coefficient can be extracted by introducing an arbitrary auxiliary spinor $|r\rangle$. Contracting the previous relation with $\langle r|$ gives

$$x = \frac{\langle r|\not{p}_1|3]}{\langle r3\rangle}. \tag{5.42}$$

Under the little-group transformation, we have

$$x \longrightarrow w_3^{-2} x, \tag{5.43}$$

since the numerator contains one $|3]$ and therefore scales as w_3^{-1}, whereas the denominator contains one $|3\rangle$ and scales as w_3. Thus, x carries exactly the helicity weight required for a positive-helicity gluon. We can consequently construct the second possible tensor structure as

$$M_{\dot{a}\dot{b}} = \frac{\langle r|\not{p}_1|3]}{\langle r3\rangle}\,\epsilon_{\dot{a}\dot{b}}, \tag{5.44}$$

which gives

$$\mathcal{M}\big(\mathbf{1}_{\bar{t}}, \mathbf{2}_t, 3_g^+\big) \supset [\mathbf{12}]\frac{\langle r|\not{p}_1|3]}{\langle r3\rangle}, \tag{5.45}$$

Therefore, up to scalar coefficients, the positive-helicity amplitude contains two independent structures,

$$[\mathbf{13}][\mathbf{23}], \qquad [\mathbf{12}]\,\frac{\langle r|\not{p}_1|3]}{\langle r3\rangle}. \tag{5.46}$$

Before putting together these two structures, we can work further on the latter. One can make use of the following identity

$$[\mathbf{12}]\,\frac{\langle r|\not{p}_1|3]}{\langle r3\rangle} = m_t\,\frac{\langle r\mathbf{1}\rangle[3\mathbf{2}] + \langle r\mathbf{2}\rangle[3\mathbf{1}]}{\langle r3\rangle} + [\mathbf{1}3][\mathbf{2}3]. \tag{5.47}$$

whose derivation is reported in Appendix C.4. Making use of the positive-helicity slashed polarization vectors defined in Eq. (4.63), the previous relation reads

$$[\mathbf{12}]\frac{\langle r|\not{p}_1|3]}{\langle r\rangle} = \frac{m_t}{\sqrt{2}}\left(\langle\mathbf{1}|\not{\epsilon}_3^+|\mathbf{2}] + \langle\mathbf{2}|\not{\epsilon}_3^+|\mathbf{1}]\right) + [\mathbf{1}3][\mathbf{2}3], \tag{5.48}$$

Hence, instead of using $[\mathbf{12}]x$ and $[\mathbf{1}3][\mathbf{2}3]$ as a basis, we may equivalently choose the polarization-dependent structure and the pure square-bracket structure. The general positive-helicity amplitude can then be parametrized as

$$\boxed{\mathcal{M}\big(\mathbf{1}_{\bar{t}_i}, \mathbf{2}_{t_j}, 3_g^{a,+}\big) = (T^a)_{ji}\left(c_{g\bar{t}t}\left(\langle\mathbf{1}|\not{\epsilon}_3^+|\mathbf{2}] + \langle\mathbf{2}|\not{\epsilon}_3^+|\mathbf{1}]\right) + c_{g\bar{t}t}^{RRR}[\mathbf{1}3][\mathbf{2}3]\right).} \tag{5.49}$$

Here, we have also restored the color structure with $(T^a)_{ji}$.

The negative-helicity amplitude follows from an entirely analogous argument. In this case the required massless little-group weight is w_3^{+2}, and the roles of angle and square spinors are exchanged. One can define the corresponding quantity

$$\tilde{x} = \frac{[r|\not{p}_1|3\rangle}{[r3]}, \qquad \tilde{x} \longrightarrow w_3^{+2}\tilde{x}, \tag{5.50}$$

and construct the two independent structures

$$\langle\mathbf{13}\rangle\langle\mathbf{23}\rangle, \qquad \langle\mathbf{12}\rangle\,\tilde{x}. \tag{5.51}$$

Equivalently, choosing again a basis involving the polarization vector, the negative-helicity amplitude can be written as

$$\boxed{\mathcal{M}\big(\mathbf{1}_{\bar{t}_i}, \mathbf{2}_{t_j}, 3_g^{a,-}\big) = (T^a)_{ji}\left(c_{g\bar{t}t}\left(\langle\mathbf{1}|\not{\epsilon}_3^-|\mathbf{2}] + \langle\mathbf{2}|\not{\epsilon}_3^-|\mathbf{1}]\right) + c_{g\bar{t}t}^{LLL}\langle\mathbf{13}\rangle\langle\mathbf{23}\rangle\right).} \tag{5.52}$$

Let us further analyze the amplitudes we obtained. Using dimensional analysis, the couplings $c_{g\bar{t}t}^{RRR}$ and $c_{g\bar{t}t}^{LLL}$ have mass dimension -1, which hints at the presence of a dimension-6 operator generating these couplings, hence a BSM interaction. Indeed, as can be inferred from the SMEFT Feynman rule reported in Eq. (A.19), an additional structure with respect to the SM is generated by the so-called chromomagnetic operator. Conversely, the coefficient $c_{g\bar{t}t}$ is dimensionless, hinting that the operator that generates it is the renormalizable QCD interaction vertex.

What we do now, instead, is match the bootstrapped amplitude onto the SM one. This will be important in order to benchmark the future computation of hgg at one loop. We can do this using the explicit expressions for the Dirac wavefunctions in the massive formalism given in Eq. (4.110):

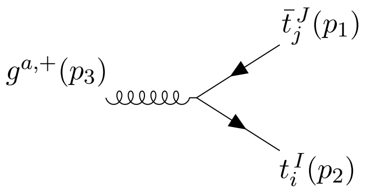

$$
\begin{aligned}
&= -ig_s\,(T^a)_{ji}\,\bar{u}_I(2)\gamma_\mu v^J(1)\,\varepsilon^\mu_+(p_3,r)\\
&= -ig_s\,(T^a)_{ji}\begin{pmatrix} -\langle 2|^{\alpha}_{I} & [2|_{I,\dot{\alpha}}\end{pmatrix}\begin{pmatrix} 0 & (\sigma^\mu)_{\alpha\dot{\beta}} \\ (\bar{\sigma}^\mu)^{\dot{\alpha}\beta} & 0\end{pmatrix}\begin{pmatrix} |1\rangle^J_\beta \\ -|1]^{J,\dot{\beta}}\end{pmatrix}\varepsilon^\mu_+(p_3,r)\\
&= -ig_s\,(T^a)_{ji}\,\left(\langle\mathbf{2}|\not{\varepsilon}^+_3|\mathbf{1}] + \langle\mathbf{1}|\not{\varepsilon}^+_3|\mathbf{2}]\right). \qquad (5.53)
\end{aligned}
$$

In the calculation, we assigned the $SU(2)$ little-group indices I and J to particles 2 and 3, respectively. The matching between Eq. (5.52) and Eq. (5.53) then reads

$$\boxed{\text{SM}: \qquad c_{g\bar{t}t} = -ig_s, \qquad c^{RRR}_{g\bar{t}t} = 0.} \qquad (5.54)$$

The fact that $c^{RRR}_{g\bar{t}t} = 0$ in the SM confirms our predictions. In the case of negative-helicity gluons, we clearly obtain

$$\boxed{\text{SM}: \qquad c^{LLL}_{g\bar{t}t} = 0.} \qquad (5.55)$$

Chapter 6

One-loop amplitudes and generalized unitarity

It is now time to go beyond tree level and consider one-loop amplitudes. In this section, we aim to review some of the main results concerning one-loop amplitudes, such as the possibility of expressing them in terms of a basis of only four types of scalar integrals. This result is of fundamental importance for introducing generalized unitarity methods, which in fact aim at determining the coefficients of this expansion, thus effectively evaluating the one-loop amplitude.

Before doing so, we will first briefly focus on the so-called Passarino–Veltman (PV) reduction, which is a powerful tool that allows tensor integrals to be reduced to scalar integrals, since the former are the ones that usually emerge from one-loop diagram computations. We then proceed by reviewing the cutting rules, making contact with the well-known optical theorem. This is done in order to introduce the generalized unitarity method in a natural way.

To systematize the use of this method, it is convenient to introduce the van Neerven–Vermaseren parametrization of the loop momentum. We present it for a generic N-point amplitude in D dimensions in order to be as general as possible. A particularly useful feature of the van Neerven–Vermaseren basis is that it provides a natural bridge between integrand reduction and generalized D-dimensional unitarity.

6.1 Basic properties of one-loop integrals

In general, when going from tree level to loop level, the main difference is the emergence of the so-called Feynman integrals. These are integrals over the loop momenta of a given diagram and require specific techniques in order to be evaluated. Here, we do not provide an exhaustive discussion of the subject, but only introduce the theoretical tools needed for this thesis.

Given an N-point one-loop amplitude, the following type of integral naturally emerges in the computation:

$$I_N \sim \int \frac{\mathrm{d}^D l}{(2\pi)^D} \frac{\mathcal{N}(l)}{\left[(l+q_0)^2 - m_1^2\right]\left[(l+q_1)^2 - m_2^2\right]\cdots\left[(l+q_{N-1})^2 - m_N^2\right]}, \tag{6.1}$$

where the momenta q_j are obtained from the external momenta p_j as follows

$$q_j = \sum_{k=1}^{j} p_k, \qquad q_0 = 0, \qquad \text{with} \qquad \sum_{k=1}^{N} p_k = 0, \tag{6.2}$$

and $\mathcal{N}(l)$ is a polynomial in the loop momentum l and in the external kinematic variables. Throughout, the Feynman $+i\epsilon$ prescription is understood in all propagator denominators and will be suppressed unless explicitly needed. Fig. 6.1 provides the diagrammatic representation of this loop integral. We define a scalar integral as the special case in which $\mathcal{N}(l) = 1$. The general goal is to compute I_N efficiently.

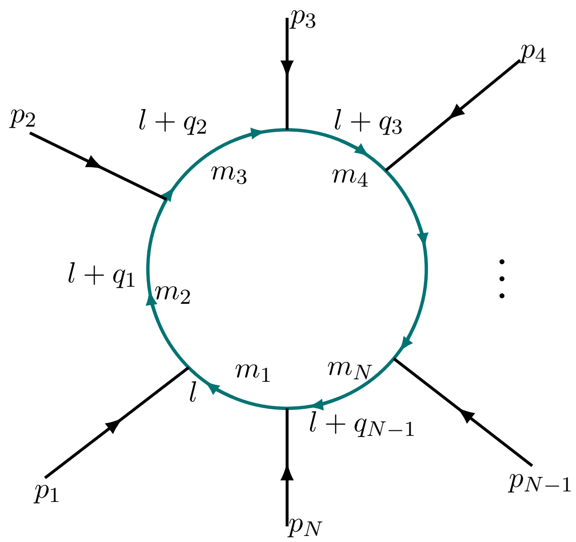

Figure 6.1: Generic one-loop N-point diagram. All external momenta are taken to be incoming, with $q_j = \sum_{k=1}^{j} p_k$.

An important feature of one-loop integrals is that Feynman integrals may be UV divergent. In particular, if the polynomial $\mathcal{N}(l)$ contains a sufficiently high power of the loop momentum, the Feynman integral may diverge in the ultraviolet (UV) region. From simple power counting, we can observe that I_N is UV divergent if it contains tensor integrals of rank r with $r \geq 2N-4$. This follows from the fact that each propagator in the denominator of I_N contributes two powers of the loop momentum l. This immediately implies that only one-point and two-point scalar integrals are UV divergent. Moreover, the highest rank of an N-point one-loop diagram is $r = N$ in renormalizable theories such as the SM [15]. This implies that only one-, two-, three-, and four-point one-loop integrals can be UV divergent, whereas five- and higher-point one-loop integrals are necessarily ultraviolet finite.

An important point concerning loop amplitudes is how to deal with the resulting divergences. Loop integrals require the so-called regularization and renormalization procedures in order to obtain a completely finite result for a given process of interest. There exist different kinds of regularization for divergent diagrams and different renormalization schemes. We refer to standard textbooks for a detailed discussion of these subjects [1, 2]. Commonly, one employs dimensional regularization, as it provides an economical tool to deal with divergences in loop integrals. In this case, the dimensionality of spacetime is set to $D = 4-2\epsilon$, with ϵ a small positive parameter. In this way, UV divergences arise as poles in the variable ϵ and can therefore be removed in a straightforward way once a renormalization scheme has been defined.

Up to the required order in ϵ, a generic one-loop integral with four-dimensional external kinematics can be reduced to a linear combination of scalar one-, two-, three-, and four-point integrals, together with a rational contribution [15],

$$I_N = \sum_j c_{4,j} D_0^{(j)} + \sum_j c_{3,j} C_0^{(j)} + \sum_j c_{2,j} B_0^{(j)} + \sum_j c_{1,j} A_0^{(j)} + \mathcal{R} + \mathcal{O}(D-4). \tag{6.3}$$

Here, the coefficients $c_{n,j}$ contain the process-dependent kinematic information and are evaluated in $D = 4$, namely, they do not depend on ϵ. Moreover, $\mathcal{R}$ denotes the rational part whose contribution originates from information that is lost if the loop momentum and numerator algebra are restricted to four dimensions. For instance explicit D-dependence in tensor or spin algebra, generates dimension-shifted integrals and $O(\epsilon)$ coefficients. When combined with ultraviolet or infrared poles, these terms can leave finite rational remainders. The integrals appearing in the expansion, D_0, C_0, B_0, A_0, carry a subscript 0, indicating that they are scalar integrals. They are called box, triangle, bubble, and tadpole scalar integrals, respectively. These names clearly refer to the associated scalar Feynman diagrams; hence, a diagrammatic representation of this one-loop decomposition can also be provided. Notice that the index j encodes the different combinations of the external momenta p_i entering the corresponding q_i.

In order to perform this decomposition, it is necessary to reduce tensor integrals to scalar integrals. Recall that, in a renormalizable theory, the rank r of a tensor integral of the form given in Eq. (6.1) is bounded by $r \leq N$. Therefore, we shall consider the following tensor integrals, defined with the same normalization adopted for the scalar integrals above and with $D = 4-2\epsilon$:

$$A_0(m_1^2) = \int \frac{\mathrm{d}^D l}{(2\pi)^D} \frac{\mu^{2\epsilon}}{d_1}, \tag{6.4}$$

$$B_0;\, B^{\mu};\, B^{\mu\nu}\left(p_1; m_1^2, m_2^2\right)$$
$$= \int \frac{\mathrm{d}^D l}{(2\pi)^D} \frac{\mu^{2\epsilon}\,(1;\, l^{\mu};\, l^{\mu}l^{\nu})}{d_1 d_2}, \tag{6.5}$$

$$C_0;\, C^{\mu};\, C^{\mu\nu};\, C^{\mu\nu\alpha}\left(p_1, p_2; m_1^2, m_2^2, m_3^2\right)$$
$$= \int \frac{\mathrm{d}^D l}{(2\pi)^D} \frac{\mu^{2\epsilon}\,(1;\, l^{\mu};\, l^{\mu}l^{\nu};\, l^{\mu}l^{\nu}l^{\alpha})}{d_1 d_2 d_3}, \tag{6.6}$$

$$D_0;\, D^{\mu};\, D^{\mu\nu};\, D^{\mu\nu\alpha};\, D^{\mu\nu\alpha\beta}\left(p_1, p_2, p_3; m_1^2, m_2^2, m_3^2, m_4^2\right)$$
$$= \int \frac{\mathrm{d}^D l}{(2\pi)^D} \frac{\mu^{2\epsilon}\left(1;\, l^{\mu};\, l^{\mu}l^{\nu};\, l^{\mu}l^{\nu}l^{\alpha};\, l^{\mu}l^{\nu}l^{\alpha}l^{\beta}\right)}{d_1 d_2 d_3 d_4}. \tag{6.7}$$

where we use a shortened notation for the denominators,

$$d_i = \left(l + \sum_{k=1}^{i-1} p_k\right)^2 - m_i^2, \qquad i = 1, \ldots, 4. \tag{6.8}$$

Moreover, we have introduced a factor $\mu^{2\epsilon} = \mu^{4-D}$, where μ is an arbitrary mass scale, so that the mass dimensions of the integrals coincide with their corresponding dimensions in $D = 4$.

We now introduce an algorithm that allows tensor integrals to be reduced to combinations of scalar integrals, namely the PV decomposition [52]. We specialize it to the specific case of a rank-two bubble integral and then apply it to the gluon self-energy as a hands-on example.

6.1.1 Example: reduction of a rank-two bubble integral

As a simple example of the PV procedure, we consider the massless rank-two integral

$$I^{\mu\nu}(p) = \int \frac{\mathrm{d}^D \ell}{(2\pi)^D} \frac{\mu^{2\epsilon}(\ell + p)^{\mu}\ell^{\nu}}{d_1 d_2}, \tag{6.9}$$

where

$$d_1 = \ell^2, \qquad d_2 = (\ell + p)^2. \tag{6.10}$$

Since p^{μ} is the only external momentum available, Lorentz covariance implies that the tensor integral can be decomposed as

$$I^{\mu\nu}(p) = g^{\mu\nu}\,\mathbf{a}(p^2) + p^{\mu}p^{\nu}\,\mathbf{b}(p^2), \tag{6.11}$$

where $\mathbf{a}(p^2)$ and $\mathbf{b}(p^2)$ are scalar form factors.

The two form factors can be determined by contracting Eq. (6.11) with $g_{\mu\nu}$ and $p_\mu p_\nu$. This gives

$$g_{\mu\nu} I^{\mu\nu} = D\,\mathbf{a} + p^2\,\mathbf{b} = \int \frac{\mathrm{d}^D\ell}{(2\pi)^D}\,\frac{\mu^{2\epsilon}\,\ell\cdot(\ell+p)}{d_1 d_2} \equiv I_1, \tag{6.12}$$

$$p_\mu p_\nu I^{\mu\nu} = p^2\,\mathbf{a} + p^4\,\mathbf{b} = \int \frac{\mathrm{d}^D\ell}{(2\pi)^D}\,\frac{\mu^{2\epsilon}(\ell\cdot p)\,[p\cdot(\ell+p)]}{d_1 d_2} \equiv I_2. \tag{6.13}$$

To evaluate the first contraction, we use

$$\ell\cdot(\ell+p) = \frac{1}{2}\left(d_1 + d_2 - p^2\right). \tag{6.14}$$

Therefore,

$$\begin{aligned} I_1 &= \frac{1}{2}\int \frac{\mathrm{d}^D\ell}{(2\pi)^D}\,\mu^{2\epsilon}\left(\frac{1}{d_1} + \frac{1}{d_2} - \frac{p^2}{d_1 d_2}\right) \\ &= -\frac{p^2}{2} B_0(p;0,0). \end{aligned} \tag{6.15}$$

where we used the scalar bubble

$$B_0(p;0,0) = \int \frac{\mathrm{d}^D\ell}{(2\pi)^D}\,\frac{\mu^{2\epsilon}}{\ell^2(\ell+p)^2}, \tag{6.16}$$

and that the one-propagator integrals appearing in the first line are scaleless tadpoles and hence vanish in dimensional regularization.

For the second contraction, one can write

$$\ell\cdot p = \frac{1}{2}\left(d_2 - d_1 - p^2\right), \qquad p\cdot(\ell+p) = \frac{1}{2}\left(d_2 - d_1 + p^2\right). \tag{6.17}$$

It follows that

$$(\ell\cdot p)\,[p\cdot(\ell+p)] = \frac{1}{4}\left[(d_2 - d_1)^2 - p^4\right]. \tag{6.18}$$

Consequently,

$$\begin{aligned} I_2 &= \frac{1}{4}\int \frac{\mathrm{d}^D\ell}{(2\pi)^D}\mu^{2\epsilon}\left(\frac{d_2}{d_1} + \frac{d_1}{d_2} - 2 - \frac{p^4}{d_1 d_2}\right) \\ &= -\frac{p^4}{4} B_0(p;0,0), \end{aligned} \tag{6.19}$$

where the first three terms vanish because they reduce to scaleless integrals.

The form factors therefore satisfy

$$\begin{pmatrix} D & p^2 \\ p^2 & p^4 \end{pmatrix} \begin{pmatrix} \mathbf{a} \\ \mathbf{b} \end{pmatrix} = \begin{pmatrix} -\dfrac{p^2}{2} B_0(p;0,0) \\ -\dfrac{p^4}{4} B_0(p;0,0) \end{pmatrix}. \tag{6.20}$$

Solving this system gives

$$\mathbf{a}(p^2) = \frac{p^2}{4(1-D)} B_0(p;0,0), \qquad \mathbf{b}(p^2) = \frac{D-2}{4(1-D)} B_0(p;0,0). \tag{6.21}$$

For a two-point function, there is only one independent external momentum, so the corresponding Gram matrix is one-dimensional and proportional to p^2. In this context, the standard PV reduction assumes that the Gram matrix of the independent external momenta is invertible. Exceptional kinematics with a vanishing Gram determinant must be treated separately, while small Gram determinants may lead to numerical instabilities. In the present case the system can be straightforwardly solved:

$$I^{\mu\nu}(p) = \frac{B_0(p;0,0)}{4(1-D)} \left[p^2 g^{\mu\nu} + (D-2) p^\mu p^\nu \right]. \tag{6.22}$$

Application to the gluon self-energy As an application of the rank-two bubble reduction derived above, we consider the fermion-loop contribution to the gluon self-energy. Among the different one-loop contributions to the gluon two-point function, this is the one generated by the n_f quark flavours circulating in the loop. We assume that the quarks are massless. The corresponding diagram is reported in Fig. 6.2.

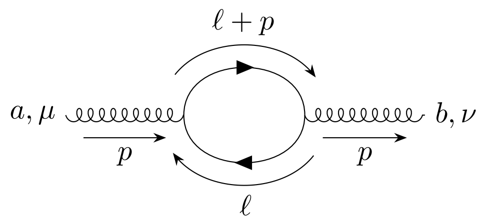

Figure 6.2: Fermion-loop contribution to the gluon self-energy.

Using $\mathrm{Tr}(t^a t^b) = T_F \delta^{ab}$, and including the minus sign associated with a closed fermion loop, the diagram gives

$$i\Pi_q^{ab,\mu\nu}(p) = -g^2\, n_f T_F \delta^{ab}\ \mathrm{Tr}\Big(\gamma^\mu \gamma^\alpha \gamma^\nu \gamma^\beta\Big)\, I_{\alpha\beta}(p), \tag{6.23}$$

where

$$I^{\alpha\beta}(p) = \int \frac{\mathrm{d}^D \ell}{(2\pi)^D} \frac{\mu^{2\epsilon}\, (\ell+p)^\alpha \ell^\beta}{\ell^2 (\ell+p)^2}. \tag{6.24}$$

Using the rank-two bubble reduction derived above, one immediately finds

$$I^{\alpha\beta}(p) = \frac{B_0(p;0,0)}{4(1-D)} \Big[p^2 g^{\alpha\beta} + (D-2) p^\alpha p^\beta \Big], \tag{6.25}$$

The Dirac algebra and all contracted Lorentz indices are treated in D dimensions, with $\mathrm{Tr}(\mathbf{1}) = 4$. Now, using

$$\mathrm{Tr}\Big(\gamma^\mu \gamma^\alpha \gamma^\nu \gamma^\beta\Big) = 4 \Big(g^{\mu\alpha} g^{\nu\beta} - g^{\mu\nu} g^{\alpha\beta} + g^{\mu\beta} g^{\nu\alpha} \Big), \tag{6.26}$$

we obtain

$$\mathrm{Tr}\Big(\gamma^\mu\gamma^\alpha\gamma^\nu\gamma^\beta\Big)\, I_{\alpha\beta}(p) = \frac{2(D-2)}{D-1}\, B_0(p;0,0)\, \big(p^2 g^{\mu\nu} - p^\mu p^\nu\big)\,. \tag{6.27}$$

Therefore,

$$i\Pi_q^{ab,\mu\nu}(p) = g^2 n_f T_F \delta^{ab}\, \frac{2(D-2)}{D-1}\, B_0(p;0,0)\, \big(p^\mu p^\nu - p^2 g^{\mu\nu}\big)\,. \tag{6.28}$$

Notice that the result is manifestly transverse:

$$p_\mu \Pi_q^{ab,\mu\nu}(p) = 0. \tag{6.29}$$

Clearly, this result contains a UV divergence, which must be renormalized in order for the diagram to be completely finite.

This example illustrates the power of the PV reduction: once we know how to decompose any tensor integral, it is only a matter of computing scalar integrals to obtain the desired one-loop amplitude.

6.1.2 Passarino–Veltman reduction pattern

As shown in the previous section, the PV algorithm allows us to decompose a tensor integral in terms of scalar integrals. We have provided the simple example of a rank-two tensor bubble integral. In general, a rank-r form factor of an N-point integral is expressed in terms of lower-rank coefficients of the same topology and coefficients of integrals with one propagator removed. The latter are $(N-1)$-point functions. Repeating the procedure eventually reduces every tensor integral to scalar tadpole, bubble, triangle, and box integrals. In Tab. 6.1, we summarize the reduction pattern for all tensor integrals. For a precise definition of the coefficients appearing in the table, see Ref. [15]. Though we do not explicitly derive all form factors, we summarize through the following steps the PV reduction algorithm:

- contract the tensor integral with all independent external momenta and, when necessary, with the metric tensor;
- rewrite the scalar products involving the loop momentum in terms of inverse propagators and kinematic invariants, allowing propagator-like denominators to be canceled;
- solve the resulting linear system of equations for the scalar form factors.

By applying these steps recursively, tensor integrals are reduced to lower-rank tensor integrals and, eventually, to scalar one-loop integrals.

Form factor		Lower-rank form factors and scalar integrals
D_{ijkl}	$\longrightarrow$	D_{00ij}, D_{ijk}, C_{ijk}, C_{ij}, C_i, C_0
D_{00ij}	$\longrightarrow$	D_{ijk}, D_{ij}, C_{ij}, C_i
D_{0000}	$\longrightarrow$	D_{00i}, D_{00}, C_{00}
D_{ijk}	$\longrightarrow$	D_{00i}, D_{ij}, C_{ij}, C_i
D_{00i}	$\longrightarrow$	D_{ij}, D_i, C_i, C_0
D_{ij}	$\longrightarrow$	D_{00}, D_i, C_i, C_0
D_{00}	$\longrightarrow$	D_i, D_0, C_0
D_i	$\longrightarrow$	D_0, C_0
C_{ijk}	$\longrightarrow$	C_{00i}, C_{ij}, B_{ij}, B_i
C_{00i}	$\longrightarrow$	C_{ij}, C_i, B_i, B_0
C_{ij}	$\longrightarrow$	C_{00}, C_i, B_i, B_0
C_{00}	$\longrightarrow$	C_i, C_0, B_0
C_i	$\longrightarrow$	C_0, B_0
B_{11}	$\longrightarrow$	B_{00}, B_1, A_0
B_{00}	$\longrightarrow$	B_1, B_0, A_0
B_1	$\longrightarrow$	B_0, A_0

Table 6.1: Reduction chains in the PV procedure. Tensor form factors of rank r are expressed in terms of lower-rank form factors and scalar integrals.

6.2 Implications of unitarity

The basic mathematical object of scattering processes in QFT (quantum field theory) is the S-matrix. It maps asymptotic incoming states into asymptotic outgoing states, after they have interacted in a certain way described by the underlying theory at play. It is conventionally written as

$$S = \mathbb{1} + iT, \tag{6.30}$$

where T is the transition matrix and contains the non-trivial part of the scattering process. Its matrix elements define the scattering amplitude through

$$\langle f|T|i\rangle = (2\pi)^4 \delta^{(4)}(p_i - p_f)\, \mathcal{M}(i \to f), \tag{6.31}$$

where p_i and p_f denote the total initial- and final-state momenta, respectively.

Conservation of probability requires the S-matrix to be unitary,

$$S^\dagger S = \mathbb{1}. \tag{6.32}$$

Using Eq. (6.30), this condition becomes

$$\mathbb{1} = \left(\mathbb{1} - iT^\dagger\right)(\mathbb{1} + iT)\,. \tag{6.33}$$

Notice that the transition matrix is not, in general, Hermitian: $T^\dagger \neq T$. To express Eq. (6.33) in terms of scattering amplitudes, we insert a complete set of intermediate states,

$$\mathbb{1} = \sum_x \int \mathrm{d}\Pi_x\, |x\rangle\langle x|, \tag{6.34}$$

where the sum runs over all possible intermediate states, including their discrete quantum numbers, and

$$\mathrm{d}\Pi_x = \prod_{j\in x} \frac{\mathrm{d}^3\mathbf{p}_j}{(2\pi)^3\, 2E_j} \tag{6.35}$$

is the multiparticle phase-space measure.

Taking the matrix element of Eq. (6.33) between $\langle f|$ and $|i\rangle$, the left-hand side gives

$$\begin{aligned}\langle f|i(T^\dagger - T)|i\rangle &= i\langle i|T|f\rangle^* - i\langle f|T|i\rangle \\ &= i(2\pi)^4\delta^{(4)}(p_i - p_f)\,[\mathcal{M}^*(f\to i) - \mathcal{M}(i\to f)]\,. \end{aligned}\tag{6.36}$$

The right-hand side instead reads

$$\begin{aligned}\langle f|T^\dagger T|i\rangle &= \sum_x \int \mathrm{d}\Pi_x\, \langle f|T^\dagger|x\rangle\langle x|T|i\rangle \\ &= \sum_x \int \mathrm{d}\Pi_x\, (2\pi)^4\delta^{(4)}(p_f - p_x)(2\pi)^4\delta^{(4)}(p_x - p_i) \\ &\qquad \times \mathcal{M}(i\to x)\mathcal{M}^*(f\to x). \end{aligned}\tag{6.37}$$

After factoring out the overall momentum-conserving delta function, one obtains the generalized optical theorem,

$$\mathcal{M}(i \to f) - \mathcal{M}^*(f \to i) = i \sum_x \int \mathrm{d}\Pi_x \, (2\pi)^4 \delta^{(4)}(p_i - p_x) \, \mathcal{M}(i \to x)\mathcal{M}^*(f \to x). \tag{6.38}$$

Sums over the spin, polarization and internal quantum numbers of the intermediate particles are implicit.

For forward scattering, $f = i$, the generalized relation reduces to the well-known optical theorem:

$$\boxed{2 \,\mathrm{Im}\, \mathcal{M}(i \to i) = \sum_x \int \mathrm{d}\Pi_x \, (2\pi)^4 \delta^{(4)}(p_i - p_x) \, |\mathcal{M}(i \to x)|^2}. \tag{6.39}$$

An important feature of this equation is that it relates the imaginary part of a scattering amplitude to products of amplitudes of lower perturbative order. This relation provides the theoretical basis of unitarity-cut methods, in which selected internal propagators are placed on shell and a loop amplitude is reconstructed from products of on-shell amplitudes.

If the initial state consists of a single particle A, its partial decay width into an arbitrary multiparticle state x is

$$\Gamma(A \to x) = \frac{1}{2m_A} \int \mathrm{d}\Pi_x \, (2\pi)^4 \delta^{(4)}(p_A - p_x) \, |\mathcal{M}(A \to x)|^2 \, . \tag{6.40}$$

It then follows from Eq. (6.39) that

$$\mathrm{Im}\, \mathcal{M}(A \to A) = m_A \sum_x \Gamma(A \to x) = m_A \Gamma_{\mathrm{tot}}. \tag{6.41}$$

Similarly, for a two-particle initial state $A = a + b$, the total cross-section in the centre-of-mass frame is related to the forward scattering amplitude by

$$\mathrm{Im}\, \mathcal{M}(A \to A) = 2E_{\mathrm{CM}} |\mathbf{p}_i| \sum_x \sigma(A \to x), \tag{6.42}$$

which is the usual optical theorem for the forward cross-section.

Now, Eq. (6.39) admits a simple diagrammatic interpretation which we report in Eq. (6.43): the imaginary part of a scattering amplitude can be obtained by summing over all possible on-shell intermediate states x that cut the diagram into two lower-order amplitudes.

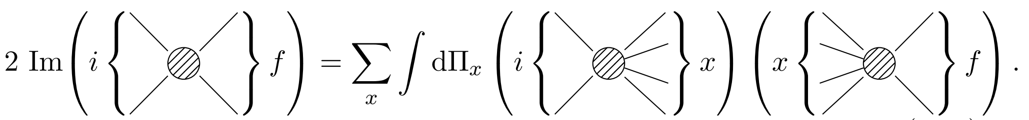

(6.43)

The precise connection between the imaginary part of an amplitude and unitarity cuts, are given by the cutting rules [2] that can be summarized as follows:

1. Cut the diagram in every possible way such that all cut propagators can be simultaneously placed on shell without violating momentum conservation.

2. For each cut propagator, perform the replacement

$$\frac{1}{p^2 - m^2 + i\epsilon} \quad \longrightarrow \quad -2\pi i\, \delta\big(p^2 - m^2\big)\, \theta\big(p^0\big)\,. \tag{6.44}$$

3. Sum over all possible cuts.

4. The resulting expression gives the discontinuity of the diagram, with

$$\mathrm{Disc}(i\mathcal{M}) \equiv \lim_{\epsilon \to 0^+} \left[i\mathcal{M}(s + i\epsilon) - i\mathcal{M}(s - i\epsilon)\right] = -2\ \mathrm{Im}\,\mathcal{M}. \tag{6.45}$$

Notice that rule number 2 provides a precise physical interpretation of a unitarity cut: cutting a propagator means placing the corresponding particle on shell. This is indeed enforced by the Dirac delta function, which requires that $p^2 = m^2$ [53].

Relation between optical theorem and unitarity cuts: the muon decay. As a simple example of the relation between the optical theorem and unitarity cuts, let us consider muon decay in the Fermi theory, including only QED corrections. The effective Lagrangian of interest reads

$$\mathcal{L}^{\mathrm{CC}}_{\mathrm{Fermi}} \; = \; -\frac{4G_F}{\sqrt{2}}\left[(\bar{e}_L\gamma^\mu\mu_L)(\bar{\nu}_{\mu,L}\gamma_\mu\nu_{e,L}) + (\bar{\mu}_L\gamma^\mu e_L)(\bar{\nu}_{e,L}\gamma_\mu\nu_{\mu,L})\right]. \tag{6.46}$$

Here, terms involving only muonic or electronic fields have been neglected, and the Fierz identity [2] has been applied. The first term in Eq. (6.46) can annihilate a left-handed muon and create a left-handed electron together with a muon neutrino and a right-helicity electron antineutrino state created by the left-chiral neutrino field. This generates Feynman diagrams in which the muon is annihilated. By similar reasoning, the second term in the Lagrangian, i.e. its Hermitian conjugate, is also required, as it generates Feynman diagrams in which the outgoing muon is created. We will need both contributions for the purposes of this section.

The optical theorem for forward muon scattering reads

$$2\ \mathrm{Im}\,\mathcal{M}(\mu \to \mu) = \sum_X \int \mathrm{d}\Pi_X\ (2\pi)^4\delta^{(4)}(p_\mu - p_X)\left|\mathcal{M}(\mu \to X)\right|^2. \tag{6.47}$$

In the present case the sum over intermediate states naturally includes

$$X = \{X_0 = e^-\,\bar{\nu}_e\,\nu_\mu,\ X_1 = e^-\,\bar{\nu}_e\,\nu_\mu\,\gamma,\ ...\}. \tag{6.48}$$

Suppose we are interested in the QED corrections up to relative order α. Then, it is sufficient to retain the first two decay channels, namely the three-particle state X_0 and the four-particle state X_1. The inclusion of both virtual corrections to X_0 and real-photon emission through X_1 is also required for the cancellation of infrared divergences, in accordance with the KLN theorem [2].

Let us focus on the process $\mathcal{M}(\mu \to X_0)$ only. This can be expanded in the following way

$$\mathcal{M}(\mu \to X_0) = \mathcal{M}_0 + \mathcal{M}_{\mathrm{virt}} + \mathcal{O}(\alpha^2), \tag{6.49}$$

where $\mathcal{M}_0$ is the tree-level Fermi amplitude, while $\mathcal{M}_{\mathrm{virt}}$ denotes the one-loop QED virtual correction at first order in α. In relative power counting one has

$$\mathcal{M}_0 \sim \mathcal{O}(1), \qquad \mathcal{M}_{\mathrm{virt}} \sim \mathcal{O}(\alpha). \tag{6.50}$$

From a diagrammatic point of view we have

$\mathcal{M}(\mu \to X_0) =$

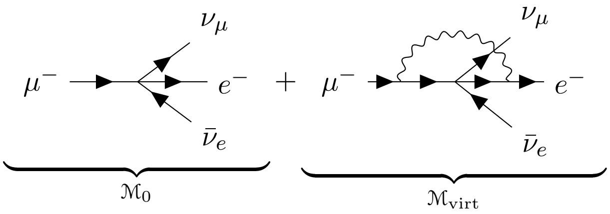

$+ \ \mathcal{O}(\alpha^2).$ (6.51)

Since the optical theorem holds at any order in perturbation theory, we can write that at relative order $\mathcal{O}(1)$ we have

$$2\ \mathrm{Im}\,\mathcal{M}(\mu \to \mu)\Big|_{\mathcal{O}(1)} = \int \mathrm{d}\Pi_{X_0}\,(2\pi)^4\delta^{(4)}(p_\mu - p_{X_0})\big|\mathcal{M}_0\big|^2. \tag{6.52}$$

Conversely, at relative order $\mathcal{O}(\alpha)$ the optical theorem yields

$$\begin{aligned} 2\ \mathrm{Im}\,\mathcal{M}(\mu \to \mu)\Big|_{\mathcal{O}(\alpha)} &= \int \mathrm{d}\Pi_{X_0}\,(2\pi)^4\delta^{(4)}(p_\mu - p_{X_0})\Big[\mathcal{M}_0\mathcal{M}^*_{\mathrm{virt}} + \mathcal{M}_{\mathrm{virt}}\mathcal{M}^*_0\Big] \\ &\quad + \left(\int \mathrm{d}\Pi_{X_1}\,(2\pi)^4\delta^{(4)}(p_\mu - p_{X_1})\big|\mathcal{M}(\mu^- \to X_1)\big|^2\right)\Big|_{\mathcal{O}(\alpha)}. \end{aligned} \tag{6.53}$$

The two interference terms are precisely the virtual corrections of relative order α.

Let us now make contact with unitarity cuts. The $\mathcal{O}(1)$ relation in Eq. (6.52), contains the squared modulus of $\mathcal{M}_0$, which directly corresponds to a *three-particle cut* through the X_0 intermediate state. Hence, Eq. (6.52) has the following diagrammatic interpretation

$2\ \mathrm{Im}\,\mathcal{M}(\mu \to \mu)\Big|_{\mathcal{O}(1)} \sim$

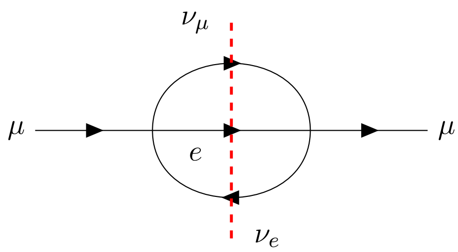

. (6.54)

Conversely, let us consider Eq. (6.53). The first line corresponds to two different *three-particle cuts* which pass through the X_0 intermediate state and contains the virtual QED correction to the decay. The second line corresponds instead to the *four-particle cuts* and represents real photon emission, $\mu \to e\,\bar{\nu}_e\,\nu_\mu\gamma$, namely the X_1 intermediate state. In the present discussion we only focus on the first contribution. Explicitly, Eq. (6.53) naturally allows for the following diagrammatic interpretation

$$2\,\mathrm{Im}\,\mathcal{M}(\mu \to \mu)\Big|_{\mathcal{O}(\alpha)} \sim$$

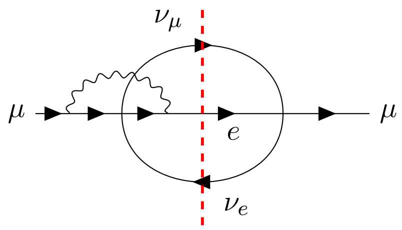

$$+$$

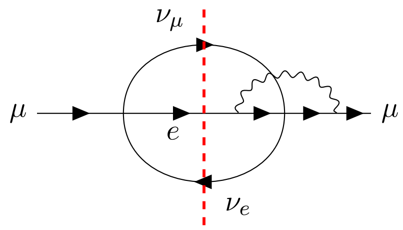

$$+\ \big(\text{4-particle cuts}\big). \qquad (6.55)$$

In summary, this example explicitly illustrates the connection between the optical theorem and unitarity cuts. The imaginary part of the forward amplitude $\mu \to \mu$ is obtained by summing over all allowed on-shell cuts. At order α, the three-particle cuts reproduce the interference between the tree-level decay amplitude and the virtual QED corrections, while the four-particle cuts account for real photon emission. This is the simplest manifestation, within the Fermi theory, of the general statement that cuts extract the discontinuity of a loop amplitude and relate it to products of lower-order on-shell amplitudes.

6.3 Generalized unitarity

Up to this point, we have explored the relation between the imaginary part of an amplitude and on-shell unitarity cuts. In this section, we see how the latter can provide further insights into the structure of a scattering amplitude.

We refer to this extension as generalized unitarity. The basic idea is that, by taking more than one cut of a one-loop amplitude, we can reconstruct its complete behaviour in terms of the scalar integrals defined in Eqs. (6.4), (6.5), (6.6), and (6.7), thus bypassing the PV-reduction algorithm. Multiple cuts indeed act as projectors onto specific integral topologies and can be used to determine their coefficients recursively. In order to illustrate the working principle schematically, we consider a 4-point amplitude and decompose it in terms of scalar integrals:

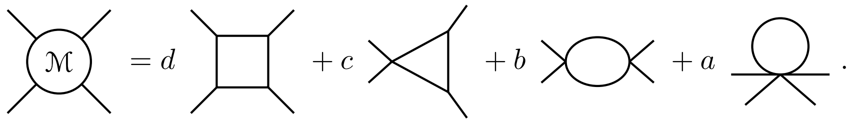

(6.56)

Notice that the above decomposition matches the one reported in Eq. (6.3), but this time the scalar integrals are sketched as Feynman diagrams. Actually, in this expansion we are missing the rational term $\mathcal{R}$, which requires more care to be extracted and will be discussed in the following sections.

Let us now exploit generalized unitarity with the aim of finding all the coefficients multiplying the different topologies. We first cut as many internal propagators as possible; in this case, we should perform a quadruple cut. Clearly, this puts four internal propagators on shell. By cutting the left-hand side of Eq. (6.56) along its four internal propagators, only one term in the expansion on the right-hand side survives, namely the box contribution. This is because, in the case of the triangle, bubble, and tadpole topologies, we cannot possibly take four cuts, since there are not enough internal propagators. Diagrammatically, this translates into:

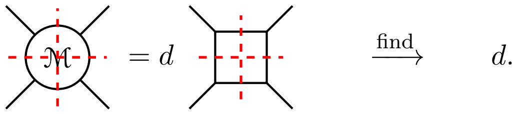

(6.57)

Let us consider now triple cuts. This time, cutting through three internal propagators is allowed for both the box and triangle integrals. Since the triple cut is shared by the box and triangle topologies, we can obtain the coefficient c by subtracting from the triple cut of $\mathcal{M}$ the remaining contribution from the triple cut of the box diagram. Diagrammatically, this can be written as follows:

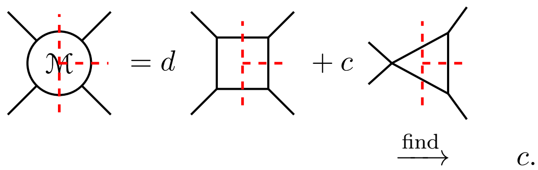

(6.58)

Similarly, a double cut receives contributions from boxes, triangles and bubbles. After subtracting the already known box and triangle contributions, the remaining term determines the bubble coefficient b:

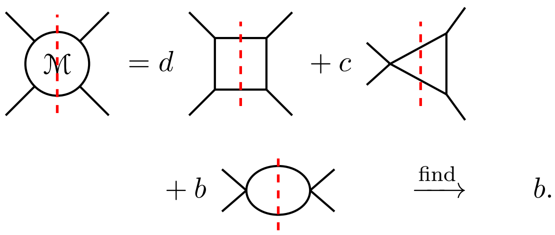

(6.59)

Finally, a single cut can receive contributions from all the integral topologies. Once the coefficients d, c and b have been determined, their contributions can be removed and the remaining term isolates the coefficient a:

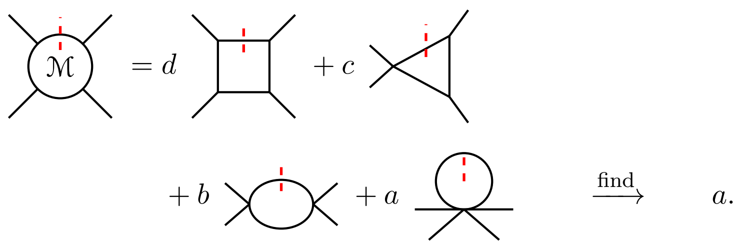

(6.60)

The derivation of the coefficients is clearly recursive. In particular, cutting the highest possible number of internal propagators is usually relatively easy from a computational point of view. However, going down to the tadpole contributions requires much more care, and therefore an automation through some software is usually preferred.

We will apply this mechanism to the evaluation of the gluon-fusion Higgs production process, in which we implement this cut construction of the amplitude by means of a Mathematica [26] package called SMaSH [27].

A convenient way of exploiting the generalized unitarity method just outlined, is by expanding the loop momentum in some four-momentum basis before taking the cuts. This is because, as prescribed in Eq. (6.44), taking a cut means substituting an internal propagator with a delta function whose argument $p^2 - m^2$ depends on the loop momentum of the amplitude itself. If we manage to parametrize the loop momentum in some basis, each delta function basically constrains one of the coefficients of this expansion. In this way, the set of delta functions in the loop integral, which corresponds to the set of propagators that have been cut, allows us to determine the constrained loop momentum that can flow through the cut diagram. We will see that this point significantly reduces the computational effort, since, in the end, we will not need to perform the actual loop integrals, but only to determine the constraints on the loop momentum imposed by the Dirac delta functions.

The central point is: in which basis should we expand the loop momentum? The answer is actually not trivial, since it generally depends on both the dimensionality of spacetime, which plays a fundamental role in the determination of the rational term $\mathcal{R}$, and the external momenta involved in the process. In the following section, we will provide the fundamental tools needed to perform this loop-momentum expansion.

6.3.1 The van Neerven–Vermaseren basis

The implementation of generalized unitarity requires a convenient parametrization of the loop momentum. In particular, it is useful to separate the components of the loop momentum that are determined by the external kinematics from those belonging to the transverse space. The van Neerven–Vermaseren basis provides a natural framework for performing this decomposition [54].

A fundamental constraint is provided by the Schouten identity. In 4-dimensional space-time, a totally antisymmetric rank-five tensor necessarily vanishes since 2 of its indices must be repeated. Therefore, in $D = 4$ the following holds

$$\begin{aligned}\ell^\lambda \epsilon^{\mu_1\mu_2\mu_3\mu_4} = &\ell^{\mu_1}\epsilon^{\lambda\mu_2\mu_3\mu_4} + \ell^{\mu_2}\epsilon^{\mu_1\lambda\mu_3\mu_4} \\ &+ \ell^{\mu_3}\epsilon^{\mu_1\mu_2\lambda\mu_4} + \ell^{\mu_4}\epsilon^{\mu_1\mu_2\mu_3\lambda},\end{aligned} \tag{6.61}$$

where l is the loop momentum. We use this relation as the starting point of the discussion as it makes the linear dependence of sufficiently large sets of momenta explicit.

We will actually only present the result of the expansion of the loop momentum in D-dimensions, while showing the working mechanism in a simpler situation, namely in a 2-dimensional space-time.

The two-dimensional basis. To introduce the basic idea, consider a two-dimensional vector space spanned by two linearly independent, but not orthogonal, vectors q_1^μ and q_2^μ. Their linear independence requires

$$\epsilon^{q_1 q_2} \equiv \epsilon^{\mu\nu} q_{1,\mu} q_{2,\nu} \neq 0. \tag{6.62}$$

If q_1 and q_2 were parallel, $\epsilon^{q_1 q_2}$ would vanish and they would not span the two-dimensional space, so the construction below would not be well defined. An arbitrary vector ℓ^μ belonging to this space can be written as

$$\ell^\mu = c_1 q_1^\mu + c_2 q_2^\mu. \tag{6.63}$$

However, since q_1 and q_2 are not orthogonal, the coefficients c_i cannot be obtained directly by contracting ℓ^μ with q_i^μ. For instance,

$$q_1 \cdot \ell = c_1 q_1^2 + c_2 (q_1 \cdot q_2), \tag{6.64}$$

which depends on both coefficients.

Let us consider the Schouten identity in two dimensions

$$\ell^\lambda \epsilon^{\mu\nu} = \ell^\mu \epsilon^{\lambda\nu} + \ell^\nu \epsilon^{\mu\lambda}. \tag{6.65}$$

Contracting this equation with $q_{1,\mu} q_{2,\nu}$, one obtains

$$\ell^\lambda \epsilon^{q_1 q_2} = (\ell \cdot q_1)\epsilon^{\lambda q_2} + (\ell \cdot q_2)\epsilon^{q_1 \lambda}. \tag{6.66}$$

It is therefore natural to introduce the dual vectors

$$v_1^\lambda \equiv \frac{\epsilon^{\lambda q_2}}{\epsilon^{q_1 q_2}}, \qquad v_2^\lambda \equiv \frac{\epsilon^{q_1 \lambda}}{\epsilon^{q_1 q_2}}, \tag{6.67}$$

in terms of which

$$\boxed{\ell^\lambda = (\ell \cdot q_1) v_1^\lambda + (\ell \cdot q_2) v_2^\lambda,} \tag{6.68}$$

which is obtained from Eq. (6.66) by dividing by $\epsilon^{q_1 q_2}$. The two sets of vectors are dual, since

$$v_i \cdot q_j = \delta_{ij}. \tag{6.69}$$

The vectors v_i^μ are not, in general, orthonormal among themselves,

$$v_i \cdot v_j \neq \delta_{ij}. \tag{6.70}$$

Nevertheless, they define a useful coordinate system because the coefficient of v_i^μ in Eq. (6.68) is precisely the projection $\ell \cdot q_i$.

Suppose now that the vectors q_i appear as shifts of the loop momentum in the inverse propagators

$$d_i = (\ell + q_i)^2 - m_i^2, \qquad d_0 = \ell^2 - m_0^2, \qquad q_0 = 0. \tag{6.71}$$

Here, we are clearly still referring to the momentum configuration presented in Fig. 6.1, where the vectors q_i are combinations of the external momenta p_i. The difference between the two denominators read

$$d_i - d_0 = 2\ell \cdot q_i + q_i^2 - m_i^2 + m_0^2, \tag{6.72}$$

and hence

$$\ell \cdot q_i = \frac{1}{2}\left[d_i - d_0 - q_i^2 + m_i^2 - m_0^2\right]. \tag{6.73}$$

This is the crucial property of the basis: factors of the loop momentum along the physical directions can be traded for differences of inverse propagators, which may subsequently cancel against the denominators of the integrand.

The same construction can be reformulated without explicitly referring to the Levi–Civita tensor in order to set the stage for arbitrary dimensional space-time. First, in two dimensions, we can use the identity

$$\epsilon^{\mu_1\mu_2}\epsilon_{\nu_1\nu_2} = \delta^{\mu_1\mu_2}_{\nu_1\nu_2}, \tag{6.74}$$

with all other components fixed by antisymmetry. where the rank-two generalized Kronecker symbol is defined as

$$\delta^{\mu_1\mu_2}_{\nu_1\nu_2} \equiv \det\begin{pmatrix} \delta^{\mu_1}_{\nu_1} & \delta^{\mu_1}_{\nu_2} \\ \delta^{\mu_2}_{\nu_1} & \delta^{\mu_2}_{\nu_2} \end{pmatrix} = \delta^{\mu_1}_{\nu_1}\delta^{\mu_2}_{\nu_2} - \delta^{\mu_1}_{\nu_2}\delta^{\mu_2}_{\nu_1}. \tag{6.75}$$

We can now rewrite the dual vectors introduced in Eq. (6.67). Starting from

$$v_1^\mu = \frac{\epsilon^{\mu q_2}}{\epsilon^{q_1 q_2}}, \tag{6.76}$$

we multiply both numerator and denominator by $\epsilon_{q_1 q_2}$, obtaining

$$\begin{aligned} v_1^\mu &= \frac{\epsilon_{q_1 q_2}\,\epsilon^{\mu q_2}}{\epsilon_{q_1 q_2}\,\epsilon^{q_1 q_2}} \\ &= \frac{\epsilon_{\rho\sigma}\epsilon^{\mu\nu} q_1^\rho q_2^\sigma q_{2,\nu}}{\epsilon_{\rho\sigma}\epsilon^{\alpha\beta} q_1^\rho q_2^\sigma q_{1,\alpha} q_{2,\beta}}. \end{aligned} \tag{6.77}$$

Using Eq. (6.74), the numerator becomes

$$\begin{aligned} \epsilon_{\rho\sigma}\epsilon^{\mu\nu} q_1^\rho q_2^\sigma q_{2,\nu} &= \delta^{\mu\nu}_{\rho\sigma} q_1^\rho q_2^\sigma q_{2,\nu} \\ &\equiv \delta^{\mu q_2}_{q_1 q_2}. \end{aligned} \tag{6.78}$$

Expanding the generalized Kronecker symbol explicitly,

$$\begin{aligned} \delta^{\mu q_2}_{q_1 q_2} &= \left(\delta^\mu_\rho \delta^\nu_\sigma - \delta^\mu_\sigma \delta^\nu_\rho\right) q_1^\rho q_2^\sigma q_{2,\nu} \\ &= q_1^\mu q_2^2 - q_2^\mu (q_1 \cdot q_2). \end{aligned} \tag{6.79}$$

Similarly,

$$\delta^{q_1 \mu}_{q_1 q_2} = q_1^2 q_2^\mu - (q_1 \cdot q_2) q_1^\mu. \tag{6.80}$$

Whereas, the common denominator reads

$$\begin{aligned} \Delta_2 &\equiv \epsilon_{q_1 q_2}\epsilon^{q_1 q_2} \\ &= \delta^{q_1 q_2}_{q_1 q_2} \\ &= \delta^{\mu\nu}_{\rho\sigma} q_{1,\mu} q_{2,\nu} q_1^\rho q_2^\sigma \\ &= \left(\delta^\mu_\rho \delta^\nu_\sigma - \delta^\mu_\sigma \delta^\nu_\rho\right) q_{1,\mu} q_{2,\nu} q_1^\rho q_2^\sigma \\ &= q_1^2 q_2^2 - (q_1 \cdot q_2)^2. \end{aligned} \tag{6.81}$$

This is precisely the so-called Gram determinant associated with the two vectors q_1 and q_2.

The dual vectors can therefore be written as

$$\boxed{v_1^\mu = \frac{\delta^{\mu q_2}_{q_1 q_2}}{\Delta_2} = \frac{q_2^2 q_1^\mu - (q_1 \cdot q_2) q_2^\mu}{q_1^2 q_2^2 - (q_1 \cdot q_2)^2}, \qquad v_2^\mu = \frac{\delta^{q_1 \mu}_{q_1 q_2}}{\Delta_2} = \frac{q_1^2 q_2^\mu - (q_1 \cdot q_2) q_1^\mu}{q_1^2 q_2^2 - (q_1 \cdot q_2)^2}.} \tag{6.82}$$

The duality relations can now be verified directly. For instance,

$$v_1 \cdot q_1 = \frac{q_2^2 q_1^2 - (q_1 \cdot q_2)^2}{\Delta_2} = 1, \tag{6.83}$$

$$v_1 \cdot q_2 = \frac{q_2^2 (q_1 \cdot q_2) - (q_1 \cdot q_2) q_2^2}{\Delta_2} = 0, \tag{6.84}$$

and analogously

$$v_2 \cdot q_1 = 0, \qquad v_2 \cdot q_2 = 1. \tag{6.85}$$

Hence,

$$v_i \cdot q_j = \delta_{ij}. \tag{6.86}$$

In what sense are we avoiding using the Levi-Civita tensor in this new construction? Notice that though Eq. (6.74) holds in a 2-dimensional space-time only, the generalized Kronecker symbol $\delta^{\mu_1\mu_2}_{\nu_1\nu_2}$ can be easily extended up to a n-dimensional space-time. Explicitly, we have shifted from the dual vectors in Eq. (6.67) defined using the ϵ tensor, to those in Eq. (6.82), which can belong to any chosen dimensional space-time. This is important since it allows the construction to be extended to generic one-loop configurations.

Before seeing how the van Neerven–Vermaseren decomposition makes it particularly convenient to impose generalized unitarity conditions, we first need to provide the D-dimensional extension of the case just discussed.

Physical and transverse spaces. We now consider a generic N-particle scattering amplitude in a renormalizable quantum field theory in D-dimensional space-time. Each one-loop Feynman diagram contributing to the amplitude can be described by an integrand of the form

$$\mathcal{I}_N(p_1,\ldots,p_N;\ell) = \frac{\mathcal{N}_{\mathcal{I}}(p_1,\ldots,p_N;\ell)}{d_1 d_2 \cdots d_R}, \tag{6.87}$$

where R denotes the number of loop-momentum-dependent propagators and

$$d_i = (\ell + q_i)^2 - m_i^2, \qquad i = 1,\ldots,R, \tag{6.88}$$

where we are slightly changing the notation with respect to the one adopted in the previous section. The vectors q_i will be referred to as the *propagator momenta*.

Associated with the R propagators there is a set of R inflow momenta k_i, defined by

$$k_i = q_i - q_{i-1}. \tag{6.89}$$

The k_i are either external momenta p_j or linear combinations of them,

$$k_i = \sum_{j=1}^{N} \alpha_{ij} p_j, \tag{6.90}$$

where the coefficients α_{ij} depend on the particular diagram. Momentum conservation implies

$$\sum_{i=1}^{R} k_i = 0. \tag{6.91}$$

A suitable diagrammatic representation is shown in Fig. 6.3[1].

The vector space spanned by the inflow momenta k_i is called the *physical space*. Since Eq. (6.91) implies that at most $R-1$ of them are linearly independent, its dimension is

$$D_P = \min(D, R-1). \tag{6.92}$$

[1]With respect to Fig. 6.1 we use the notation adopted in this section

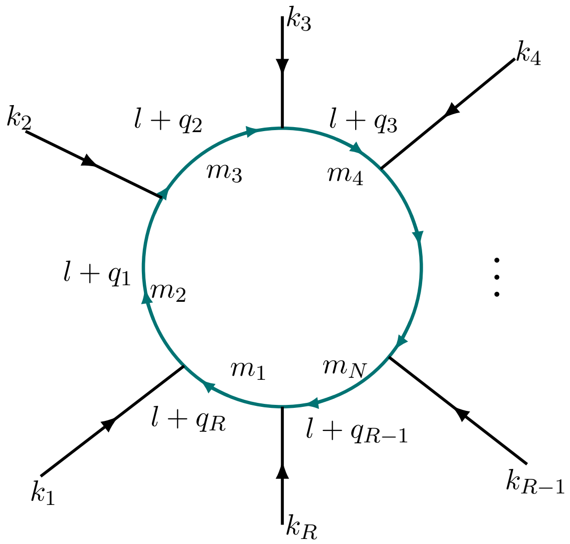

Figure 6.3: Generic one-loop N-point diagram. All external momenta are taken to be incoming.

The orthogonal complement of the physical space defines the *transverse space*, whose dimension is therefore

$$D_T = D - D_P = \max(0, D-(R-1)). \tag{6.93}$$

Thus,

$$D = D_P + D_T. \tag{6.94}$$

In particular, if $R > D$, the physical space spans the entire D-dimensional space and

$$D_T = 0. \tag{6.95}$$

This was the case of the 2-dimensional parametrization provided above. The inflow momenta define a natural, although in general non-orthogonal, coordinate system in the physical space. In order to construct the corresponding dual basis, we introduce the generalized Kronecker symbol

$$\delta^{\mu_1\cdots\mu_s}_{\nu_1\cdots\nu_s} \equiv \det\begin{pmatrix} \delta^{\mu_1}_{\nu_1} & \delta^{\mu_1}_{\nu_2} & \cdots & \delta^{\mu_1}_{\nu_s} \\ \delta^{\mu_2}_{\nu_1} & \delta^{\mu_2}_{\nu_2} & \cdots & \delta^{\mu_2}_{\nu_s} \\ \vdots & \vdots & \ddots & \vdots \\ \delta^{\mu_s}_{\nu_1} & \delta^{\mu_s}_{\nu_2} & \cdots & \delta^{\mu_s}_{\nu_s} \end{pmatrix}. \tag{6.96}$$

The Gram determinant associated with a set of s vectors is then defined as

$$\Delta(k_1, \ldots, k_s) \equiv \delta^{k_1\cdots k_s}_{k_1\cdots k_s} = \det(k_i \cdot k_j)\,. \tag{6.97}$$

The generalized Kronecker symbol vanishes whenever the number of antisymmetrized indices exceeds the dimensionality of the vector space. For the special case in which the number of indices equals D, it can be expressed in terms of two Levi–Civita tensors,

$$\delta^{\mu_1\cdots\mu_D}_{\nu_1\cdots\nu_D} = \epsilon^{\mu_1\cdots\mu_D}\epsilon_{\nu_1\cdots\nu_D}, \tag{6.98}$$

up to the sign convention associated with the metric and the Levi–Civita tensor.

We can now construct the van Neerven–Vermaseren basis of the physical space. Choosing D_P independent inflow momenta, the dual vectors are defined by

$$v_i^\mu(k_1,\ldots,k_{D_P}) \equiv \frac{\delta^{k_1\cdots k_{i-1}\,\mu\,k_{i+1}\cdots k_{D_P}}_{k_1\cdots k_{i-1}\,k_i\,k_{i+1}\cdots k_{D_P}}}{\Delta(k_1,\ldots,k_{D_P})}, \qquad i=1,\ldots,D_P, \tag{6.99}$$

where we simply generalized what we found in Eq. (6.82). By construction, these vectors satisfy

$$v_i\cdot k_j = \delta_{ij}, \qquad i,j=1,\ldots,D_P. \tag{6.100}$$

The vectors v_i^μ therefore constitute the basis dual to the independent inflow momenta k_i^μ. This property is especially useful because the coefficient of each v_i^μ in the decomposition of an arbitrary vector is simply its projection onto k_i^μ.

When $R \le D$, it is useful to introduce the projector onto the transverse space,

$$w_\mu{}^\nu(k_1,\ldots,k_{R-1}) \equiv \frac{\delta^{k_1\cdots k_{R-1}\nu}_{k_1\cdots k_{R-1}\mu}}{\Delta(k_1,\ldots,k_{R-1})}. \tag{6.101}$$

It satisfies the standard properties of a projection operator,

$$w_\mu{}^\mu = D_T = D+1-R, \qquad k_i^\mu w_{\mu\nu} = 0, \qquad w^\mu{}_\alpha w^{\alpha\nu} = w^{\mu\nu}. \tag{6.102}$$

We denote by

$$n_r^\mu, \qquad r=1,\ldots,D_T, \tag{6.103}$$

an orthonormal basis of the transverse space. These vectors satisfy

$$n_r\cdot n_s = \delta_{rs}, \qquad k_i\cdot n_r = 0, \qquad v_i\cdot n_r = 0, \tag{6.104}$$

and the transverse metric can be written as

$$w^{\mu\nu} = \sum_{r=1}^{D_T} n_r^\mu n_r^\nu. \tag{6.105}$$

The full D-dimensional metric tensor can consequently be decomposed into its physical and transverse components,

$$g^{\mu\nu} = \sum_{i=1}^{D_P} k_i^\mu v_i^\nu + w^{\mu\nu}, \tag{6.106}$$

or, equivalently,

$$g^{\mu\nu} = \sum_{i=1}^{D_P} k_i^\mu v_i^\nu + \sum_{r=1}^{D_T} n_r^\mu n_r^\nu. \tag{6.107}$$

We can now apply this decomposition directly to the loop momentum. Contracting Eq. (6.107) with ℓ_ν gives

$$\boxed{\ell^\mu = \sum_{i=1}^{D_P} (\ell \cdot k_i) v_i^\mu + \sum_{r=1}^{D_T} (\ell \cdot n_r) n_r^\mu.} \tag{6.108}$$

The first term contains the components of the loop momentum in the physical space, whereas the second term contains its transverse components.

The physical projections can be expressed directly in terms of inverse Feynman propagators. Using

$$d_i = (\ell + q_i)^2 - m_i^2, \qquad d_{i-1} = (\ell + q_{i-1})^2 - m_{i-1}^2, \tag{6.109}$$

together with

$$k_i = q_i - q_{i-1}, \tag{6.110}$$

we obtain

$$\begin{aligned} d_i - d_{i-1} &= 2\ell \cdot (q_i - q_{i-1}) + q_i^2 - q_{i-1}^2 - m_i^2 + m_{i-1}^2 \\ &= 2\ell \cdot k_i + q_i^2 - q_{i-1}^2 - m_i^2 + m_{i-1}^2. \end{aligned} \tag{6.111}$$

Therefore,

$$\ell \cdot k_i = \frac{1}{2} \left[d_i - d_{i-1} - \left(q_i^2 - m_i^2\right) + \left(q_{i-1}^2 - m_{i-1}^2\right) \right]. \tag{6.112}$$

Substituting Eq. (6.112) into Eq. (6.108), the loop momentum can be written as

$$\ell^\mu = V_R^\mu + \frac{1}{2} \sum_{i=1}^{D_P} (d_i - d_{i-1}) v_i^\mu + \sum_{r=1}^{D_T} (\ell \cdot n_r) n_r^\mu, \tag{6.113}$$

where

$$V_R^\mu = -\frac{1}{2} \sum_{i=1}^{D_P} \left[\left(q_i^2 - m_i^2\right) - \left(q_{i-1}^2 - m_{i-1}^2\right) \right] v_i^\mu. \tag{6.114}$$

Here the cyclic convention

$$d_0 = d_R, \qquad m_0 = m_R \tag{6.115}$$

is understood.

Equation (6.113) is the central result for the applications that follow. The components of the loop momentum along the physical space are expressed in terms of inverse propagators, while only the projections onto the transverse directions remain irreducible. Consequently, once a set of propagators is placed on shell, the corresponding conditions $d_i = 0$ directly constrain the physical components of the loop momentum.

In fact, a particularly useful feature of the van Neerven–Vermaseren basis is that it provides a natural parametrization of one-loop integrands in terms of a restricted set of irreducible loop-momentum structures. In a renormalizable theory, this allows the integrand to be organized as a linear combination of terms containing four, three, two, or one Feynman denominators, with numerators of a highly constrained polynomial form.

Moreover, the same decomposition makes it particularly convenient to impose generalized unitarity conditions. Once the loop momentum has been separated into its physical and transverse components, the solutions satisfying quadruple-, triple-, double-, and single-cut on-shell conditions can be constructed systematically. The van Neerven–Vermaseren basis therefore provides a natural bridge between integrand reduction and generalized D-dimensional unitarity.

We provide a 2-dimensional example to illustrate these two features of the van Neerven–Vermaseren basis.

A rank-two bubble and the connection with unitarity. Let us consider a rank-two two-point integrand in 2-dimensional space-time,

$$\widetilde{\mathcal{I}}(k, m_1, m_2) = \frac{(\hat{n} \cdot l)^2}{d_1 d_2}, \tag{6.116}$$

where

$$d_1 = l^2 - m_1^2, \qquad d_2 = (l + k)^2 - m_2^2, \tag{6.117}$$

and

$$\hat{n} \cdot k = 0, \qquad k^2 \neq 0, \qquad \hat{n}^2 = 1. \tag{6.118}$$

Since $\hat{n}^\mu$ is orthogonal to the only independent external momentum k^μ, it spans the transverse space of the corresponding two-point function.

The rank-two two-point function in two dimensions is UV divergent. We therefore regularize it by analytically continuing the loop momentum to

$$D = 2 - 2\epsilon. \tag{6.119}$$

As the basis vector of the physical space, we choose

$$n^\mu = \frac{k^\mu}{\sqrt{k^2}}, \qquad n^2 = 1. \tag{6.120}$$

Together with $\hat{n}^\mu$, it satisfies

$$n^\mu n^\nu + \hat{n}^\mu \hat{n}^\nu = g_{(2)}^{\mu\nu}, \tag{6.121}$$

where $g_{(2)}^{\mu\nu}$ denotes the metric tensor of the two-dimensional subspace. Contracting this relation with $l_\mu l_\nu$

$$(\hat{n} \cdot l)^2 = l_{(2)}^2 - (n \cdot l)^2 = l_{(2)}^2 - \frac{(l \cdot k)^2}{k^2}. \tag{6.122}$$

Now, in order to decompose the loop momentum we exploit Eq. (6.107), also accounting for the extra-dimensional contribution:

$$l^\mu = (l \cdot n)n^\mu + (l \cdot \hat{n})\hat{n}^\mu + (l \cdot n_\epsilon)n_\epsilon^\mu, \tag{6.123}$$

where n_ϵ^μ parametrizes the additional $(D-2)$-dimensional space. Accordingly,

$$l^2 = l_{(2)}^2 + (n_\epsilon \cdot l)^2 = l_{(2)}^2 + l_\epsilon^2, \qquad l_\epsilon^2 \equiv (n_\epsilon \cdot l)^2. \tag{6.124}$$

Thus, besides the physical and transverse two-dimensional components, the loop momentum contains an additional component which disappears if the calculation is performed strictly in two dimensions.

The scalar products entering Eq. (6.122) can again be expressed through the inverse propagators. From Eq. (6.117), one obtains

$$l_{(2)}^2 = d_1 + m_1^2 - \mu^2, \qquad 2l \cdot k = d_2 - d_1 - r_1^2, \tag{6.125}$$

where we define

$$r_1^2 = k^2 + m_1^2 - m_2^2, \qquad r_2^2 = k^2 + m_2^2 - m_1^2, \tag{6.126}$$

Using these relations, the original integrand can be rewritten as

$$\begin{aligned} \widetilde{\mathfrak{I}}(k, m_1, m_2) &= \frac{(\hat{n} \cdot l)^2}{d_1 d_2} \\ &= -\frac{\lambda^2 + l_\epsilon^2}{d_1 d_2} + \frac{1}{4k^2}\left[\frac{r_1^2 - 2l \cdot k}{d_1} + \frac{r_2^2 + 2l \cdot k + 2k^2}{d_2}\right]. \end{aligned} \tag{6.127}$$

where

$$\lambda^2 = \frac{k^4 - 2k^2(m_1^2 + m_2^2) + (m_1^2 - m_2^2)^2}{4k^2}. \tag{6.128}$$

This already shows the structure expected from integrand reduction: a two-propagator contribution accompanied by two one-propagator contributions. Up to now, we have shown how the van Neerven–Vermaseren basis can be exploited in order to reduce one-loop integrands to a linear combination of terms containing Feynman denominators.

Actually, even without knowing Eq. (6.127), we could have started with a general ansatz of the form

$$\begin{aligned} \frac{(\hat{n} \cdot l)^2}{d_1 d_2} = &\frac{b_0 + b_1(\hat{n} \cdot l) + b_2(n_\epsilon \cdot l)^2}{d_1 d_2} \\ &+ \frac{a_{1,0} + a_{1,1}(n \cdot l) + a_{1,2}(\hat{n} \cdot l)}{d_1} \\ &+ \frac{a_{2,0} + a_{2,1}(n \cdot l) + a_{2,2}(\hat{n} \cdot l)}{d_2}. \end{aligned} \tag{6.129}$$

Comparing this parametrization with Eq. (6.127), one immediately finds

$$b_0 = -\lambda^2, \qquad b_1 = 0, \qquad b_2 = -1, \tag{6.130}$$

and

$$\begin{aligned} a_{1,0} &= \frac{r_1^2}{4k^2}, \qquad a_{1,1} = -\frac{1}{2\sqrt{k^2}}, \quad a_{1,2} = 0, \\ a_{2,0} &= \frac{r_2^2}{4k^2} + \frac{1}{2}, \quad a_{2,1} = \frac{1}{2\sqrt{k^2}}, \qquad a_{2,2} = 0. \end{aligned} \tag{6.131}$$

What can be shown is that the same coefficients can be obtained without performing the explicit algebraic reduction, but by exploiting generalized unitarity. We provide the computation for the b-coefficients. Multiplying Eq. (6.129) by $d_1 d_2$, we obtain

$$\begin{aligned} (\hat{n}\cdot l)^2 = \; & \left[b_0 + b_1(\hat{n}\cdot l) + b_2(n_\epsilon \cdot l)^2\right] \\ & + \left[a_{1,0} + a_{1,1}(n\cdot l) + a_{1,2}(\hat{n}\cdot l)\right] d_2 \\ & + \left[a_{2,0} + a_{2,1}(n\cdot l) + a_{2,2}(\hat{n}\cdot l)\right] d_1. \end{aligned} \tag{6.132}$$

To isolate the b-coefficients, we choose special values of the loop momentum satisfying

$$d_1(l) = d_2(l) = 0. \tag{6.133}$$

In this way, the terms proportional to d_1 and d_2 vanish identically, so that only the residue associated with the two-point topology survives. Setting these Feynman denominators to zero has precisely the meaning of putting the two propagators on shell of the bubble diagram associated with the integrand under study. Diagrammatically, this is precisely what we did in Eq. (6.59), except that here we do not have higher-point cut topologies to subtract.

For the moment, let us restrict the loop momentum to the two-dimensional subspace by setting

$$n_\epsilon \cdot l = 0. \tag{6.134}$$

Imposing the above cut conditions on the loop momentum of Eq. (6.123), two solutions emerge

$$l_c^\pm = \alpha_c n \pm i\beta_c \hat{n}, \tag{6.135}$$

where

$$\alpha_c = -\frac{r_1^2}{2\sqrt{k^2}}, \qquad \beta_c = \lambda. \tag{6.136}$$

In particular,

$$\hat{n}\cdot l_c^\pm = \pm i\lambda. \tag{6.137}$$

Substituting the two solutions into Eq. (6.132) gives

$$b_0 + b_1(\hat{n}\cdot l_c^+) = -\lambda^2, \qquad b_0 + b_1(\hat{n}\cdot l_c^-) = -\lambda^2, \tag{6.138}$$

from which

$$b_0 = -\lambda^2, \qquad b_1 = 0, \tag{6.139}$$

which correctly reproduce the first two coefficients of the integrand reduction.

Let us now consider the coefficient b_2. This coefficient cannot be determined from a strictly two-dimensional loop momentum, since in this case $n_\epsilon \cdot l = 0$. To determine it, we must allow the loop momentum to probe the additional $(D-2)$-dimensional space. The cut conditions remain the same, but we choose instead

$$l^\pm = \alpha_c n \pm i\beta_c n_\epsilon. \tag{6.140}$$

This is obtained from Eq. (6.135) simply by replacing $\hat{n} \to n_\epsilon$. The conditions

$$\hat{n} \cdot l^\pm = 0, \qquad (n_\epsilon \cdot l^\pm)^2 = -\lambda^2, \tag{6.141}$$

hold. Equation (6.132) therefore gives

$$0 = b_0 - b_2\lambda^2. \tag{6.142}$$

Using $b_0 = -\lambda^2$, we obtain

$$b_2 = -1. \tag{6.143}$$

The coefficients associated with the one-propagator terms can be determined analogously by imposing a single-cut condition. For example, the coefficients $a_{1,i}$ are isolated by requiring

$$d_1(l) = 0, \qquad d_2(l) \neq 0, \tag{6.144}$$

while the coefficients $a_{2,i}$ follow from the opposite choice. We do not display the calculation here for brevity; see Ref. [15] for the derivation.

The point of this discussion was to make the connection between integrand reduction and unitarity particularly transparent. The coefficients of the different integral topologies are obtained by evaluating the integrand at special values of the loop momentum for which selected inverse Feynman propagators vanish. Since

$$d_i(l) = 0 \tag{6.145}$$

is precisely the on-shell condition for the corresponding internal particle, the algebraic projection onto a given residue is naturally interpreted as a generalized unitarity cut.

Moreover, the role of the D-dimensional loop momentum is already visible in this simple example. In particular, the structure

$$\frac{(n_\epsilon \cdot l)^2}{d_1 d_2} \tag{6.146}$$

cannot be detected by restricting l to the original two-dimensional space. The continuation of the loop momentum to $D = 2 - 2\epsilon$ dimensions is therefore essential to reconstruct this contribution. The analogous extra-dimensional structures in four-dimensional calculations are precisely responsible for contributions to the rational part of one-loop amplitudes.

6.3.2 Integrand reduction in D dimensions

We now extend the previous discussion to D-dimensional space-time. The aim is not to reproduce the complete derivation of the reduction procedure, but rather to introduce the general parametrization of a one-loop integrand and to emphasize the role played by the D-dimensional loop momentum. This construction is known as OPP parametrization [15,55]. We consider a generic one-loop integral of the form

$$I_N = \int \frac{\mathrm{d}^D l}{(2\pi)^D} \frac{\mathrm{Num}(l)}{\prod\limits_i d_i(l)}, \tag{6.147}$$

where

$$d_i(l) = (l + q_i)^2 - m_i^2 \tag{6.148}$$

are the inverse Feynman propagators. We can decompose the numerator in the following suggestive way

$$\begin{aligned} I_N = \int \frac{\mathrm{d}^D l}{(2\pi)^D} \frac{1}{\prod\limits_i d_i(l)} \Bigg\{ & \sum_{i_1,i_2,i_3,i_4,i_5} \widetilde{e}_{i_1 i_2 i_3 i_4 i_5}(l) \prod_{j \notin \{i_1,i_2,i_3,i_4,i_5\}} d_j(l) \\ & + \sum_{i_1,i_2,i_3,i_4} \widetilde{d}_{i_1 i_2 i_3 i_4}(l) \prod_{j \notin \{i_1,i_2,i_3,i_4\}} d_j(l) \\ & + \sum_{i_1,i_2,i_3} \widetilde{c}_{i_1 i_2 i_3}(l) \prod_{j \notin \{i_1,i_2,i_3\}} d_j(l) \\ & + \sum_{i_1,i_2} \widetilde{b}_{i_1 i_2}(l) \prod_{j \notin \{i_1,i_2\}} d_j(l) \\ & + \sum_{i_1} \widetilde{a}_{i_1}(l) \prod_{j \neq i_1} d_j(l) \Bigg\}. \end{aligned} \tag{6.149}$$

The functions $\widetilde{e}$, $\widetilde{d}$, $\widetilde{c}$, $\widetilde{b}$, and $\widetilde{a}$ are respectively associated with five-, four-, three-, two-, and one-point functions.

An important feature of Eq. (6.149) is that, in the present discussion, all inverse propagators appear only to the first power. More generally, higher powers of propagators may arise, for instance in particular expansions or in multi-loop calculations after IBP reduction, but such cases will not be considered here. Therefore, by choosing special values of the loop momentum for which different subsets of inverse propagators vanish, one can project directly onto the corresponding functions. This is precisely the point at which integrand reduction naturally connects with generalized unitarity.

Parametrization of the loop momentum. The van Neerven–Vermaseren basis introduced in the previous section provides a convenient way of determining the allowed l-dependence of the functions appearing in Eq. (6.149).

Consider first a five-point function with propagators

$$d_i(l) = (l + q_i)^2 - m_i^2, \qquad i = 0, \ldots, 4, \qquad q_0 = 0. \tag{6.150}$$

The four vectors $q_1, \ldots, q_4$ span the four-dimensional physical space. The loop momentum is therefore decomposed as

$$l^\mu = \sum_{i=1}^{4} (l \cdot q_i) v_i^\mu + (l \cdot n_\epsilon) n_\epsilon^\mu. \tag{6.151}$$

The first term contains the four-dimensional components of the loop momentum, whereas n_ϵ^μ parametrizes its extra-dimensional component.

As before, the physical projections are directly related to inverse propagators,

$$l \cdot q_i = \frac{1}{2} \left[d_i - d_0 - \left(q_i^2 - m_i^2 + m_0^2 \right) \right]. \tag{6.152}$$

Consequently, the dependence of a numerator on the physical components of l^μ can be systematically traded for inverse propagators. What remains after this procedure are irreducible scalar products involving the transverse components of the loop momentum.

For a rank-five five-point function, repeated application of Eq. (6.152) shows that the corresponding five-point residue contains no irreducible dependence on l,

$$\widetilde{e}_{01234}(l) = \widetilde{e}_{01234}^{(0)}. \tag{6.153}$$

For a four-point function, the physical space is three-dimensional. The loop momentum is decomposed as

$$l^\mu = \sum_{i=1}^{3} v_i^\mu (l \cdot q_i) + (l \cdot n_4) n_4^\mu + (l \cdot n_\epsilon) n_\epsilon^\mu, \tag{6.154}$$

where n_4^μ spans the four-dimensional transverse space. For tensor integrals of rank not higher than four, the most general four-point residue can be written as [15]

$$\begin{aligned} \widetilde{d}_{0123}(l) = \widetilde{d}_0 + \widetilde{d}_1 (l \cdot n_4) + \widetilde{d}_2 (l \cdot n_\epsilon)^2 \\ + \widetilde{d}_3 (l \cdot n_\epsilon)^2 (l \cdot n_4) + \widetilde{d}_4 (l \cdot n_\epsilon)^4. \end{aligned} \tag{6.155}$$

For a three-point function, the physical space is two-dimensional and the four-dimensional transverse space is also two-dimensional. Thus,

$$l^\mu = \sum_{i=1}^{2} v_i^\mu (l \cdot q_i) + (l \cdot n_3) n_3^\mu + (l \cdot n_4) n_4^\mu + (l \cdot n_\epsilon) n_\epsilon^\mu. \tag{6.156}$$

Taking into account the relations among the different transverse components, the corresponding residue may be parametrized as

$$\begin{aligned} \widetilde{c}_{012}(l) = \widetilde{c}_0 + \widetilde{c}_1 (l \cdot n_3) + \widetilde{c}_2 (l \cdot n_4) + \widetilde{c}_3 \left[(l \cdot n_3)^2 - (l \cdot n_4)^2 \right] \\ + \widetilde{c}_4 (l \cdot n_3)(l \cdot n_4) + \widetilde{c}_5 (l \cdot n_3)^3 + \widetilde{c}_6 (l \cdot n_4)^3 \\ + \widetilde{c}_7 (l \cdot n_\epsilon)^2 + \widetilde{c}_8 (l \cdot n_\epsilon)^2 (l \cdot n_3) + \widetilde{c}_9 (l \cdot n_\epsilon)^2 (l \cdot n_4). \end{aligned} \tag{6.157}$$

Similar considerations determine the parametrization of the two-point and one-point functions. For a rank-two two-point function one finds

$$\begin{aligned} \widetilde{b}_{01}(l) = \widetilde{b}_0 &+ \widetilde{b}_1(l\cdot n_2) + \widetilde{b}_2(l\cdot n_3) + \widetilde{b}_3(l\cdot n_4) \\ &+ \widetilde{b}_4\left[(l\cdot n_2)^2 - (l\cdot n_4)^2\right] + \widetilde{b}_5\left[(l\cdot n_3)^2 - (l\cdot n_4)^2\right] \\ &+ \widetilde{b}_6(l\cdot n_2)(l\cdot n_3) + \widetilde{b}_7(l\cdot n_3)(l\cdot n_4) \\ &+ \widetilde{b}_8(l\cdot n_2)(l\cdot n_4) + \widetilde{b}_9(l\cdot n_\epsilon)^2, \end{aligned} \tag{6.158}$$

while the general numerator of a one-point function is

$$\widetilde{a}_i(l) = \widetilde{a}_0 + \widetilde{a}_1(l\cdot n_1) + \widetilde{a}_2(l\cdot n_2) + \widetilde{a}_3(l\cdot n_3) + \widetilde{a}_4(l\cdot n_4). \tag{6.159}$$

make an important feature of integrand reduction explicit. The dependence on the loop momentum is highly constrained: after all reducible scalar products have been expressed through inverse propagators, only a finite number of irreducible transverse structures remain.

The precise polynomial degree appearing in the previous expressions is a consequence of the maximal tensor rank allowed in a renormalizable theory. In an effective field theory, higher-rank numerators can occur, and the parametrizations must be enlarged accordingly. The logic of the construction, however, remains unchanged.

From the integrand to scalar integrals. We now want to make contact with the one-loop decomposition in terms of scalar integrals of Eq. (6.3). To this end, notice that not every term appearing in Eqs. (6.155)–(6.159) survives loop integration. In particular, the l-dependent four-dimensional tensor structures vanish upon performing the angular integration in the transverse space.[2]

After integration, the amplitude can therefore be written in the simplified form

$$\begin{aligned} I_N = &\sum_{i_1,i_2,i_3,i_4,i_5} \widetilde{e}^{(0)}_{i_1i_2i_3i_4i_5} I_{i_1i_2i_3i_4i_5} \\ &+ \sum_{i_1,i_2,i_3,i_4} \widetilde{d}^{(0)}_{i_1i_2i_3i_4} I_{i_1i_2i_3i_4} \\ &+ \sum_{i_1,i_2,i_3} \widetilde{c}^{(0)}_{i_1i_2i_3} I_{i_1i_2i_3} \\ &+ \sum_{i_1,i_2} \widetilde{b}^{(0)}_{i_1i_2} I_{i_1i_2} + \sum_{i_1} \widetilde{a}^{(0)}_{i_1} I_{i_1} + \mathcal{R}. \end{aligned} \tag{6.160}$$

Here $I_{i_1\ldots i_r}$ denote scalar loop integrals, while $\mathcal{R}$ contains the rational contribution. Notice that the l-dependent structures vanish and a decomposition of the form of Eq. (6.3), is precisely what remains.

[2] For example, in the four-point residue of Eq. (6.155), the terms proportional to $\widetilde{d}_1(l\cdot n_4)$ and $\widetilde{d}_3(l\cdot n_\epsilon)^2(l\cdot n_4)$ vanish after integration, since they are odd under $(l\cdot n_4)\to-(l\cdot n_4)$. In contrast, terms involving even powers of the extra-dimensional component $(l\cdot n_\epsilon)$ do not generally vanish and can contribute to the rational part of the amplitude.

The role of the D-dimensional loop momentum. Finally, we should comment more of the role of the D-dimensional loop momentum to extract the rational term contribution of an amplitude. We already hinted that the rational term is precisely the reason why the dimensionality of the loop momentum must be treated carefully. Although the external kinematics can be kept four-dimensional, the loop momentum entering the regularized integral is genuinely D-dimensional. Its extra-dimensional component is represented in the previous parametrizations by $l \cdot n_\epsilon$.

A calculation in which the loop momentum were restricted from the beginning to four dimensions would set

$$l \cdot n_\epsilon = 0 \tag{6.161}$$

and would therefore lose all information contained in structures such as

$$(l \cdot n_\epsilon)^2, \qquad (l \cdot n_\epsilon)^4, \qquad (l \cdot n_\epsilon)^2 (l \cdot n_i). \tag{6.162}$$

These terms are invisible to strictly four-dimensional cuts, but can give non-vanishing contributions after integration.

The origin of this effect can also be understood directly from PV reduction. Taking [56]

$$D = 4 - 2\epsilon, \tag{6.163}$$

the reduction coefficients may contain explicit dependence on ϵ. Rational contributions arise when such terms multiply ultraviolet poles. Schematically,

$$\text{Rational terms} \sim \epsilon B_0(p; m_i^2, m_j^2),\ \epsilon A_0(m_i^2), \tag{6.164}$$

since A_0 and B_0 are the ultraviolet-divergent scalar one-loop integrals. Indeed,

$$A_0 \sim \frac{m^2}{\epsilon} + \mathcal{O}(\epsilon^0) \qquad B_0 \sim \frac{1}{\epsilon} + \mathcal{O}(\epsilon^0), \tag{6.165}$$

so that

$$\epsilon \left(\frac{1}{\epsilon} + \mathcal{O}(\epsilon^0) \right) = 1 + \mathcal{O}(\epsilon). \tag{6.166}$$

Contributions of $\mathcal{O}(\epsilon)$ can, when mutliplied with poles in $1/\epsilon$ leave finite remainders.

This explains why the rational term cannot, in general, be reconstructed from a purely four-dimensional analysis. The missing information originates from the D-dimensional structure of the loop momentum and of the reduction coefficients. In the van Neerven–Vermaseren parametrization, this information is encoded explicitly through the n_ϵ-dependent terms, which therefore must be retained.

Chapter 7

Higgs production via gluon-fusion at one-loop

In this section, we finally apply everything we have discussed so far to the case of Higgs production via gluon fusion at one loop. This process is of extreme importance in the panorama of particle physics. Indeed, it represents the dominant Higgs production mechanism at the LHC and is therefore of central importance for testing the Higgs boson properties.

Exploiting the spinor-helicity formalism discussed in Ch. 4, we were able to determine tree-level scattering amplitudes from general principles such as little-group scaling and locality. Furthermore, we specialized these tools to the calculation of the gluon-fusion Higgs production process at tree level in Ch. 5. The general principles we relied on provide a tree-level expression that is not allowed in the SM, but which we were instead able to match onto SMEFT.

The aim of this section is to find the one-loop BSM amplitude for $gg \to h$. In doing so, we will need to bring together not only the spinor-helicity formalism, but also the characterization of one-loop amplitudes reported in Ch. 6. In particular, both the decomposition into scalar integrals and generalized unitarity methods will be implemented. Finally, we will provide a matching onto the corresponding leading-order SMEFT amplitude of Eq. (3.19).

7.1 Extending the analysis to one loop

In the SM, Higgs production via gluon fusion is loop induced. Therefore, if we want to extend the amplitude approach to one loop, we will need to recover the SM result in our expression. Recovering the SM result then provides a powerful benchmark for the calculation. Recall that in Sec. 5.1.1 we bootstrapped the hgg amplitude at tree level. There, we obtained a non-vanishing

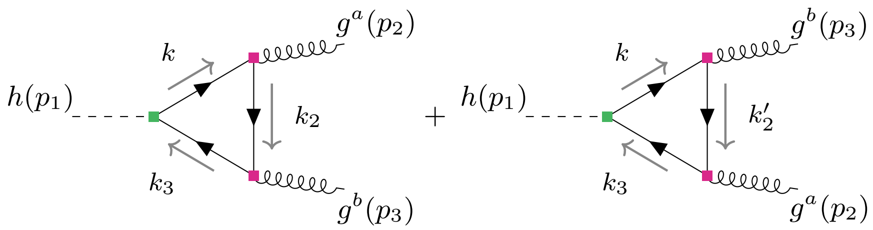

Figure 7.1: SM-like diagram contribution to Higgs production via gluon fusion.

contribution which already represents a beyond-the-Standard-Model (BSM) contribution, which we report again here for completeness,

$$\mathcal{M}\left(h, g^{a,+}(p_1), g^{b,+}(p_2)\right) = \delta^{ab}\frac{C_5^{hgg}}{\Lambda}[12]^2. \tag{7.1}$$

This refers to the case in which both gluons have positive helicity, while the opposite-helicity configuration is reported in Eq. (5.18). Recall that these are the only two non-vanishing helicity configurations, mixed gluon helicity lead to vanishing amplitudes. After evaluating this amplitude, we matched it onto SMEFT. This matching is possible because SMEFT contains specific higher-dimensional operators that are able to generate a tree-level contribution to the process of interest.

What happens at one-loop level? If we said that amplitude methods provide the model-independent contributions to a specific scattering process, why do we need to extend the analysis even further? The main point is that loop amplitudes contain more complicated non-analytic structures than in the tree-level case. Actually, since hgg is a three-point scattering amplitude, it contains no factorizable parts, namely, not even simple poles appear at tree level. Conversely, once we go to loop level, we expect the amplitude to decompose into a sum of scalar integrals, just as we saw in Eq. (6.3). Hence, divergences may also appear.

Let us outline the strategy we want to pursue. The idea is to construct the model-independent one-loop amplitude starting from the relevant model-independent lower-point tree-level amplitudes entering the process. We have already bootstrapped the relevant lower-point amplitudes for the one-loop SM-like diagrams, namely Eqs. (5.25) and (5.52). These are the $ht\bar{t}$ and $\bar{t}tg$ on-shell scattering amplitudes, respectively. They represent the basic building blocks for the two diagrams of interest, reported in Fig. 7.1. We refer to these diagrams as SM-like diagrams and assume that only the top quark flows in the loop, since it is the heaviest quark and therefore gives the dominant contribution. Notice that we are considering Higgs decay rather than Higgs production. However, the two processes are related by crossing symmetry in such a way that they are described by the same analytic amplitude. Hence, at the amplitude level, there is no distinction between considering one process or the other. Moreover, we use the same colors to denote the lower-point

Higgs-top and top-gluon interactions as those used in Appendix A.2 for the corresponding SMEFT vertices. However, here we use squared vertices to indicate that we are employing the rules obtained via the amplitude method.

From a kinematic viewpoint, we are considering

$$h(p) \to g(p_2) + g(p_3) \tag{7.2}$$

where p is the incoming Higgs momentum, while p_2 and p_3 are the outgoing momenta of the two external gluons. Therefore,

$$p^2 = m_h^2, \qquad p_2^2 = p_3^2 = 0, \tag{7.3}$$

and momentum conservation implies

$$s = 2p_2 \cdot p_3 = m_h^2, \qquad 2p \cdot p_2 = m_h^2, \qquad 2p \cdot p_3 = m_h^2. \tag{7.4}$$

Concerning the propagating internal particles, we call k the loop momentum and define

$$k_2 = k - p_2, \qquad k_2' = k - p_3, \qquad k_3 = k - p_2 - p_3, \tag{7.5}$$

as shown in the diagrams.

Now, let us consider the amplitude for the Higgs boson decay into two positive-helicity gluons,

$$\mathcal{M}_{++} = \int \frac{d^D k}{(2\pi)^D} \mu^{2\epsilon}\, \mathcal{I}_{++}(k). \tag{7.6}$$

As already discussed in Sec. 5.1.1, the negative-helicity amplitude can be readily obtained via a parity transformation. Assuming that the only diagrams contributing to the process are the two reported above, we write

$$\mathcal{I}_{++}(k) = \frac{\mathcal{A}_{++}(k)}{d_0 d_1 d_2} + \frac{\tilde{\mathcal{A}}_{++}(k)}{d_0 d_1 d_3}. \tag{7.7}$$

With the tilde notation, we denote the amplitude obtained by exchanging the two gluons, namely

$$\tilde{\mathcal{A}}_{++}(k) = \mathcal{A}_{++}(k)\big|_{p_2 \leftrightarrow p_3}. \tag{7.8}$$

The denominators d_0, d_1, d_2, and d_3 are defined as

$$\begin{aligned} d_0 &= k^2 - m^2, & d_1 &= (k - p_2 - p_3)^2 - m^2, \\ d_2 &= (k - p_2)^2 - m^2, & d_3 &= (k - p_3)^2 - m^2, \end{aligned} \tag{7.9}$$

where m denotes the top-quark mass. These are the denominators associated with the internal propagators in the diagrams.

The aim of this section is therefore clear: to determine the explicit expression of $\mathcal{M}_{++}$ by exploiting amplitude methods, without referring to a Lagrangian.

In order to evaluate $\mathcal{M}_{++}$, we first compute the numerators of the integrand, $\mathcal{A}_{++}(k)$ and consequently $\tilde{\mathcal{A}}_{++}(k)$. To approach this task, we first sew together the three lower-point amplitudes entering the first diagram in Eq. (7.1),

$$\begin{aligned}
\mathcal{A}_{++}(k) &= (-1)\, i^3\, \mathcal{M}\big(1_h, (-k)_{t_i,I}, (k_3)^L_{\bar{t}_\ell}\big) \\
&\quad \times \mathcal{M}\big(k^I_{\bar{t}_i}, (-k_2)_{t_j,J}, (-2)^{a,+}_g\big) \\
&\quad \times \mathcal{M}\big((k_2)^J_{\bar{t}_j}, (-k_3)_{t_\ell,L}, (-3)^{b,+}_g\big) \\
&= i\, \delta_{i\ell}\, \big(c^{LL}_{ht\bar{t}}\langle k^L_3| -k_I\rangle + c^{RR}_{ht\bar{t}}[k^L_3| -k_I]\big) \\
&\quad \times (T^a)_{ji} \Bigg[c_{g\bar{t}t}\, \varepsilon^+_\mu(p_2;p_3)\, \big(\langle k^I|\gamma^\mu| -k_{2,J}] + \langle -k_{2,J}|\gamma^\mu|k^I]\big) \\
&\qquad + c^{RRR}_{g\bar{t}t}[k^I| -2][-k_{2,J}| -2] \Bigg] \\
&\quad \times (T^b)_{\ell j} \Bigg[c_{g\bar{t}t}\, \varepsilon^+_\nu(p_3;p_2)\, \big(\langle k^J_2|\gamma^\nu| -k_{3,L}] + \langle -k_{3,L}|\gamma^\nu|k^J_2]\big) \\
&\qquad + c^{RRR}_{g\bar{t}t}[k^J_2| -3][-k_{3,L}| -3] \Bigg].
\end{aligned} \tag{7.10}$$

The factor (-1) in the first line is inserted because of the fermion loop, while i^3 comes from taking into account the three propagators. Notice that we choose the reference momenta of the two gluons to be $r_2 = p_3$ and $r_3 = p_2$. Moreover, we assign the little-group indices I, J, and L to the massive top quarks circulating in the loops. By employing the conventions for negative momenta inside spinors given in Eq. (4.33), and using $\mathrm{Tr}[T^aT^b] = \frac{1}{2}\delta^{ab}$ to evaluate the color factor of the diagram, we obtain

$$\begin{aligned}
\mathcal{A}_{++}(k) = i\, \frac{\delta^{ab}}{2}\, &\big(-c^{LL}_{ht\bar{t}}\langle k^L_3|k_I\rangle + c^{RR}_{ht\bar{t}}[k^L_3|k_I]\big) \\
\times &\Big[c_{g\bar{t}t}\, \varepsilon^+_\mu(p_2;p_3)\, \big(\langle k^I|\gamma^\mu|k_{2,J}] - \langle k_{2,J}|\gamma^\mu|k^I]\big) + c^{RRR}_{g\bar{t}t}[k^I|2][k_{2,J}|2] \Big] \\
\times &\Big[c_{g\bar{t}t}\, \varepsilon^+_\nu(p_3;p_2)\, \big(\langle k^J_2|\gamma^\nu|k_{3,L}] - \langle k_{3,L}|\gamma^\nu|k^J_2]\big) + c^{RRR}_{g\bar{t}t}[k^J_2|3][k_{3,L}|3] \Big],
\end{aligned} \tag{7.11}$$

where the polarizations vectors are defined in Eq. (4.60), and take the following explicit form

$$\varepsilon^+_{2,\mu} \equiv \varepsilon^+_\mu(p_2;p_3) = \frac{\langle 3|\gamma_\mu|2]}{\sqrt{2}\,\langle 32\rangle}, \qquad \varepsilon^+_{3,\nu} \equiv \varepsilon^+_\nu(p_3;p_2) = \frac{\langle 2|\gamma_\nu|3]}{\sqrt{2}\,\langle 23\rangle}. \tag{7.12}$$

They satisfy

$$\varepsilon_{+,2}^2 = \varepsilon_{+,3}^2 = 0, \qquad \varepsilon_{+,2} \cdot \varepsilon_{+,3} = \frac{[23]^2}{m_h^2}. \tag{7.13}$$

Moreover, the contractions with the external momenta always vanish,

$$p_i \cdot \epsilon_j = 0, \qquad i, j = 2, 3. \tag{7.14}$$

Now, we should multiply all terms together and perform some simplifications. These involve using much of the technology we introduced to deal with both massless and massive spinors. The aim is to make the dependence on the loop momentum k explicit. The reason for doing so will become clear when performing the calculation explicitly.

Instead of evaluating $\mathcal{A}_{++}(k)$ in its full form, it is convenient to first recover the pure SM contribution and then evaluate the remaining BSM structures.

7.1.1 Obtaining the SM contribution

Let us consider the SM contribution to $\mathcal{A}_{++}(k)$ in Eq. (7.11). To isolate this contribution, we exploit the mapping of the model-independent coefficients onto the corresponding SM ones:

$$\text{SM}: \qquad c_{ht\bar{t}}^{LL} = c_{ht\bar{t}}^{RR} = -i\frac{y_t}{\sqrt{2}}, \qquad c_{g\bar{t}t} = -ig_s, \qquad c_{g\bar{t}t}^{RRR} = 0. \tag{7.15}$$

This mapping was obtained in Ch. 5 when matching the $ht\bar{t}$ and $\bar{t}tg$ amplitudes onto the SM. Recovering the pure SM contribution allows us to benchmark the procedure and highlight the remaining BSM contribution.

Upon using the SM couplings, Eq. (7.11) reduces to a much simpler expression,

$$\begin{aligned}\mathcal{A}_{++}^{\text{SM}}(k) = &-\frac{2\pi\alpha_s m}{v}\,\delta^{ab}\left([k_3^L|k_I] - \langle k_3^L|k_I\rangle\right)\\ &\times \varepsilon_\mu^+(p_2;p_3)\left(\langle k^I|\gamma^\mu|k_{2,J}] - \langle k_{2,J}|\gamma^\mu|k^I]\right)\\ &\times \varepsilon_\nu^+(p_3;p_2)\left(\langle k_2^J|\gamma^\nu|k_{3,L}] - \langle k_{3,L}|\gamma^\nu|k_2^J]\right).\end{aligned} \tag{7.16}$$

where, in place of the Yukawa coupling we used

$$y_t = \frac{\sqrt{2}\,m}{v}, \tag{7.17}$$

with v the vacuum expectation value of the Higgs boson, measured to be $v \simeq 246\,\text{Gev}$ [2]. Moreover, we use the strong coupling constant $\alpha_s = g_s^2/(4\pi)$.

The expression above contains eight different terms we need to evaluate. The explicit computation is reported in Appendix D.1.1. We end up with the following expression

$$\begin{aligned}\mathcal{A}_{++}^{\rm SM}(k) = &- \frac{2\pi\alpha_s m}{v}\,\delta^{ab}\varepsilon_\mu^+(p_2;p_3)\,\varepsilon_\nu^+(p_3;p_2)\\ &\times\Bigg\{m\Bigg[\operatorname{Tr}\left(\bar\sigma^\alpha\sigma^\nu\bar\sigma^\beta\sigma^\mu\right)+\operatorname{Tr}\left(\sigma^\alpha\bar\sigma^\nu\sigma^\beta\bar\sigma^\mu\right)\Bigg]\left(k_{3,\alpha}k_{2,\beta}+k_\alpha k_{2,\beta}\right)\\ &\quad+m\Bigg[\operatorname{Tr}\left(\bar\sigma^\alpha\sigma^\beta\bar\sigma^\nu\sigma^\mu\right)+\operatorname{Tr}\left(\sigma^\alpha\bar\sigma^\beta\sigma^\nu\bar\sigma^\mu\right)\Bigg]k_\alpha k_{3,\beta}\\ &\quad+m^3\Bigg[\operatorname{Tr}\left(\bar\sigma^\nu\sigma^\mu\right)+\operatorname{Tr}\left(\sigma^\nu\bar\sigma^\mu\right)\Bigg]\Bigg\}.\end{aligned} \tag{7.18}$$

Notice that we have managed to achieve what was stated above, namely to isolate the dependence on the loop momentum k. To proceed further, we should evaluate the trace using Eqs. (B.36) and (B.37). This step was automated using FORM [57–59]. Moreover, exploiting the kinematic relations in Eqs. (7.3) and (7.4), we obtain

$$\begin{aligned}\mathcal{A}_{++}^{\rm SM}(k) = -\frac{8\pi\alpha_s m^2}{v}\,\delta^{ab}\Bigg\{&2\left(p_2\cdot k\right)\left(\varepsilon_2^+\cdot\varepsilon_3^+\right)+\left(\varepsilon_2^+\cdot\varepsilon_3^+\right)\left(m^2-k^2\right)\\ &+4\left(k\cdot\varepsilon_2^+\right)\left(k\cdot\varepsilon_3^+\right)-\left(\varepsilon_2^+\cdot\varepsilon_3^+\right)\frac{m_h^2}{2}\Bigg\},\end{aligned} \tag{7.19}$$

where we implemented the orthogonality of the polarization vectors to the physical space, Eq. (7.14).

At this point, we can convert this expression back to the spinor-helicity formalism. The reason for doing so is that the spinor-helicity formalism allows for a more direct implementation of generalized unitarity cuts, as we will see later. In doing so, we must take care when treating the loop momentum k. In particular, we always want it to be placed inside spinor bilinear forms. Doing so, ensures the correct implementation of the upcoming generalized unitarity algorithm. To perform the conversion, we need Eq. (4.39) to reconstruct the massless momenta in terms of spinors, Eq. (7.12) for the explicit expressions of the polarization vectors, and their dot product in Eq. (7.13). We also implement the following spinor relation

$$\langle 23\rangle\langle 32\rangle\,\frac{[23]^2}{[23]^2} = -\langle 23\rangle[32]\langle 32\rangle[23]\,\frac{1}{[23]^2} = -\frac{m_h^4}{[23]^2}, \tag{7.20}$$

which allows to collect a common $-\frac{[23]^2}{m_h^2}$ factor in front of the amplitude. We are eventually left with

$$\mathcal{A}^{\rm SM}_{++}(k) = -\frac{8\pi\alpha_s m^2}{v}\,\delta^{ab}\left(-\frac{[23]^2}{m_h^2}\right)\Bigg\{-\langle 2|\not{k}|2] - \big(m^2-k^2\big) + \frac{m_h^2}{2} + \frac{2}{m_h^2}[2|\not{k}|3\rangle[3|\not{k}|2\rangle\Bigg\}. \tag{7.21}$$

Without having to translate back to spinor variables, we could have implemented the explicit expressions of the polarization vectors in Eq. (7.16) from the outset. In this way, we would have also bypassed the evaluation of the traces. In Appendix D.1.2, we show this alternative way of performing the present calculation, in which the slashed polarization vectors are made explicit from the outset. This method, however, obscures the last term appearing in Eq. (7.21), which can still be recovered by exploiting the Schouten identity. Though still not evident here, the form obtained after applying the Schouten identity allows for the determination of the rational-term contributions, which would not otherwise emerge from the original form. Therefore, this point requires some care and is of physical importance.

Finally, we can straightforwardly obtain the expression for the numerator $\tilde{\mathcal{A}}_{++}(k)$, in which the two gluon momenta are exchanged. Equation (7.8) yields

$$\tilde{\mathcal{A}}^{\rm SM}_{++}(k) = -\frac{8\pi\alpha_s m^2}{v}\,\delta^{ab}\left(-\frac{[32]^2}{m_h^2}\right)\Bigg\{-\langle 3|\not{k}|3] - \big(m^2-k^2\big) + \frac{m_h^2}{2} + \frac{2}{m_h^2}[3|\not{k}|2\rangle[2|\not{k}|3\rangle\Bigg\}. \tag{7.22}$$

7.2 Implementation of a generalized unitarity algorithm

In this section, we make use of the techniques discussed in Ch. 6, namely generalized unitarity and the van Neerven–Vermaseren basis. The goal is to derive the expression for $\mathcal{M}_{++}$ reported in Eq. (7.6). We momentarily pause the SM derivation, since what we discuss here does not require specifying a particular theory and will also be used for the BSM terms.

Let us start by considering the following expansion in terms of scalar integrals,

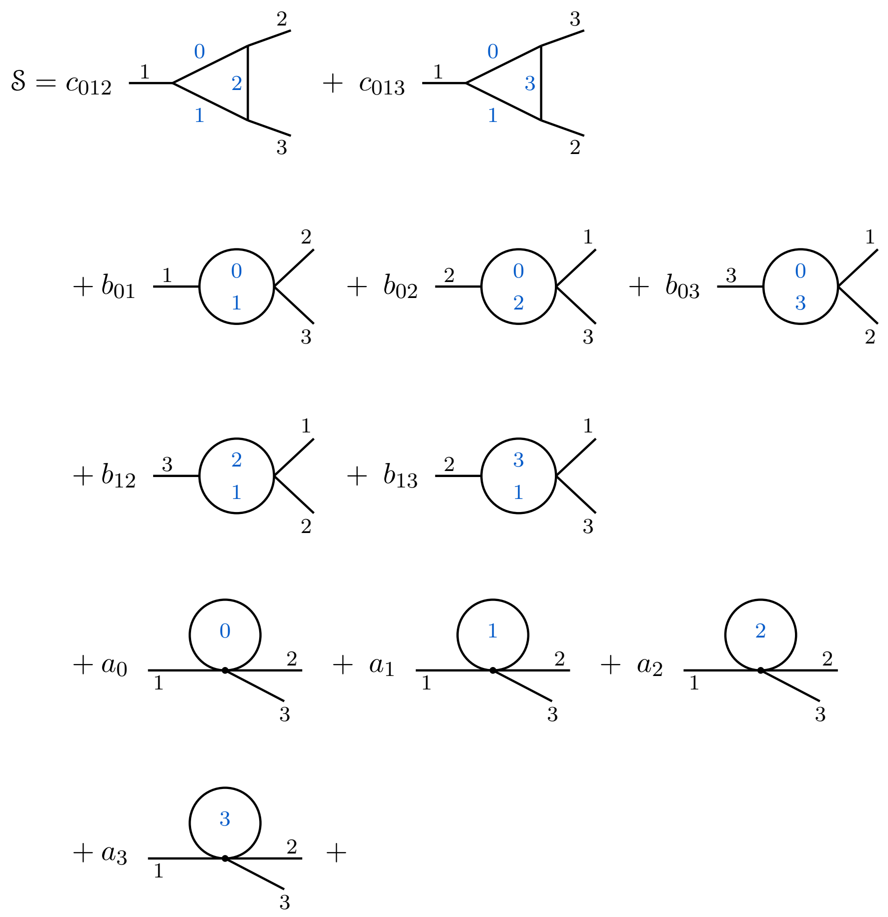

$$+\,\mathcal{R}, \tag{7.23}$$

where $\mathcal{R}$ is the rational term. The scalar triangle, bubble, and tadpole diagrams are defined as follows

$$A_0[1] \equiv$$ 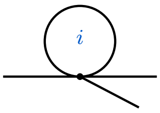

$$= \int \frac{\mathrm{d}^D k}{(2\pi)^D} \frac{\mu^{2\epsilon}}{d_i}. \tag{7.24}$$

$$B_0[1] \equiv$$ 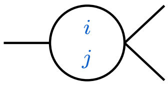

$$= \int \frac{\mathrm{d}^D k}{(2\pi)^D} \frac{\mu^{2\epsilon}}{d_i\, d_j}. \tag{7.25}$$

$$C_0[1] \equiv$$ 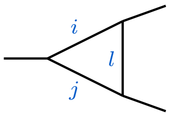

$$= \int \frac{\mathrm{d}^D k}{(2\pi)^D} \frac{\mu^{2\epsilon}}{d_i\, d_j\, d_l}, \tag{7.26}$$

where d_i, with $i \in \{0, 1, 2, 3\}$, are defined in Eq. (7.9), and the arguments of the square brackets denote the numerator of the integral. With respect to the definitions provided in Eqs. (6.4), (6.5), and (6.6), we allow for the presence of a numerator, denoted within the square brackets, which in this case is simply 1. Moreover, due to the equal masses of the internal propagators, all tadpole integrals are equal, as are the two triangle integrals, up to a redefinition of the loop momentum. The bubble integrals instead fall into two distinct classes, according to the invariant momentum flowing through them. Nevertheless, we retain all of them, since they make explicit which propagators can be cut. From now on, we label the propagators appearing in the above diagrams by the corresponding index $i \in \{0, 1, 2, 3\}$.

We use the above expansion as an ansatz for the structure of the amplitude of interest, $\mathcal{M}$:

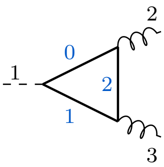

$$+$$
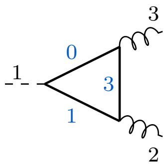

$$= \mathcal{S}. \tag{7.27}$$

This equation sets the aim of this section, namely to reconstruct the amplitude $\mathcal{M}$ by determining the explicit expressions for the coefficients of $\mathcal{S}$. Notice that we do not specify the helicities of the gluons in $\mathcal{M}$, since this procedure applies to any gluon-helicity configuration.

To exploit generalized unitarity methods for this reconstruction, we need two main ingredients: the cutting procedure discussed in Sec. 6.3 and a suitable D-dimensional parametrization of the loop momentum. Before outlining the reconstruction algorithm, we therefore specialize the van Neerven–Vermaseren basis introduced in Sec. 6.3.1 to the present process.

Van Neerven–Vermaseren parametrization of the loop momentum. In Ch. 6 we explained what a van Neerven–Vermaseren basis is, and discussed its applicability in the context of generalized unitarity. Now, we need to apply the previous construction to the process of interest. What we want to obtain is an expansion of the loop momentum similar to the one of Eq. (6.154).

We defined the kinematics of the process in Eq. (7.2), hence from momentum conservation $p_1 = p_2 + p_3$. This implies that only two external momenta are linearly independent. Hence, for the triangle topology contributing to the hgg amplitude, the four-dimensional physical space is two-dimensional, namely

$$D_P = 2, \tag{7.28}$$

where Eq. (6.92) was used. The corresponding van Neerven–Vermaseren dual vectors can be found by specializing Eq. (6.99) to the above kinematics:

$$v_1^\mu = \frac{p_3^\mu}{p_2 \cdot p_3}, \qquad v_2^\mu = \frac{p_2^\mu}{p_2 \cdot p_3}, \tag{7.29}$$

so that

$$v_1 \cdot p_2 = 1, \qquad v_1 \cdot p_3 = 0, \qquad v_2 \cdot p_2 = 0, \qquad v_2 \cdot p_3 = 1. \tag{7.30}$$

The two remaining four-dimensional directions that parametrize the transverse space, can be conveniently chosen in terms of the polarization vectors of the external gluons. For positive helicities polarization vectors we choose the ones defined in Eq. (7.12), where we chose the momentum of the other gluon as reference momentum

With this choice of reference momenta, both polarization vectors are orthogonal to the entire physical space,

$$p_i \cdot \epsilon_j = 0, \qquad i, j = 2, 3. \tag{7.31}$$

Thus, $\varepsilon^\mu_{+,2}$ and $\varepsilon^\mu_{+,3}$ provide a null basis for the two-dimensional transverse space associated with the hgg kinematics.

A D-dimensional loop momentum can consequently be decomposed as

$$k^\mu = a\, p_2^\mu + b\, p_3^\mu + c\, \varepsilon^\mu_{+,2} + d\, \varepsilon^\mu_{+,3} + k_\epsilon\, n_\epsilon^\mu, \tag{7.32}$$

where n_ϵ^μ parametrizes the extra-dimensional component of the loop momentum. The decomposition therefore separates naturally into

$$\underbrace{a\, p_2^\mu + b\, p_3^\mu}_{\text{physical space}} + \underbrace{c\, \varepsilon^\mu_{+,2} + d\, \varepsilon^\mu_{+,3}}_{\text{transverse space}} + \underbrace{k_\epsilon\, n_\epsilon^\mu}_{\text{extra-dimensional space}} . \tag{7.33}$$

This is the explicit realization of the van Neerven–Vermaseren decomposition for the hgg kinematics. The projections along p_2 and p_3 are reducible scalar products and can be expressed in terms of differences of inverse propagators. On the other hand, the projections along $\varepsilon_{+,2}$ and $\varepsilon_{+,3}$ represent the irreducible four-dimensional transverse components of the loop momentum. Finally, the component proportional to n_ε^μ contains the genuinely D-dimensional information and becomes essential for reconstructing the rational part of the one-loop amplitude. The coefficients a, b, c, and d are initially free and therefore parametrize a generic loop momentum. The unitarity cuts will constrain these coefficients by imposing the appropriate on-shell conditions on the internal propagators.

Algorithm implementation. With the van Neerven–Vermaseren parametrization at hand, the generalized-unitarity reconstruction can be summarized as follows:

1. We perform unitarity cuts on both sides of Eq. (7.27), starting from the highest number of internal propagators that can be simultaneously cut. By performing triple cuts, we obtain the coefficients c_{012} and c_{013}; cutting two propagators instead allows us to single out the contributions of b_{01}, b_{02}, b_{03}, b_{12}, and b_{13}, after subtracting the already determined higher-topology contributions; finally, single cuts allow us to evaluate a_0, a_1, a_2, and a_3.

2. Once the diagrams are cut, we are left with a set of equations involving only cut diagrams. More precisely, when we perform a cut through an internal propagator, we put the corresponding particle on shell, meaning that we replace the propagator $1/d_i$ with the Dirac delta distribution $-2\pi i\, \delta(d_i)$, as prescribed by the cutting rule in Eq. (6.44). It is therefore convenient to introduce the notation

$$\mathrm{Cut}_{i_1\cdots i_n}\left[\mathcal{M}\right] \equiv \mathcal{M}|_{\frac{1}{d_{i_r}}\to(-2\pi i)\delta(d_{i_r}),\, r=1,\ldots,n}\,. \tag{7.34}$$

The set of equations involving cut diagrams is then obtained by cutting both sides of Eq. (7.27),

$$\mathrm{Cut}_{i_1\cdots i_n}\left[\mathcal{M}\right] = \mathrm{Cut}_{i_1\cdots i_n}\left[\mathcal{S}\right]. \tag{7.35}$$

For instance, for the first triple cut, the above equation reduces to

$$\mathrm{Cut}_{012}\left[\mathcal{M}\right] = c_{012}\int\frac{d^Dk}{(2\pi)^D}\mu^{2\epsilon}\,(-2\pi i)^3\delta(d_0)\delta(d_1)\delta(d_2), \tag{7.36}$$

since, on the $\mathcal{S}$ side, only the first scalar triangle survives when propagators 0, 1, and 2 are simultaneously put on shell. Conversely, the left-hand side reads

$$\mathrm{Cut}_{012}\left[\mathcal{M}\right] = \int\frac{d^Dk}{(2\pi)^D}\mu^{2\epsilon}\,\mathcal{A}(k)\,(-2\pi i)^3\delta(d_0)\delta(d_1)\delta(d_2), \tag{7.37}$$

where $\mathcal{A}(k)$ denotes the corresponding numerator.

3. For each cut, we constrain the loop-momentum parametrization of Eq. (7.32) by imposing the appropriate on-shell conditions,

$$d_{i_1}(k) = d_{i_2}(k) = \ldots = d_{i_n}(k) = 0. \tag{7.38}$$

   These conditions imply that the parameters a, b, c, and d are no longer all independent and therefore determine the corresponding on-shell parametrization of the loop momentum for each cut. In Sec. D.2, we explain this procedure in more detail, collecting the resulting parametrizations for all the cuts in Tab. D.1.

4. Once the constrained loop momentum has been obtained, it is substituted into the corresponding numerator $\mathcal{A}(k)$. The coefficient associated with the cut can then be extracted by comparing the two sides of the cut equation, since the remaining cut measure is identical on both sides. For instance, for the triple cut 012, in the present case one obtains

$$c_{012} = \mathcal{A}(k)\big|_{d_0=d_1=d_2=0} . \tag{7.39}$$

   The same procedure is applied recursively to lower topologies, after subtracting the contributions associated with the coefficients already determined from higher cuts.

   Moreover, since the loop momentum is parametrized in $D = 4 - 2\epsilon$ dimensions, the cut solutions retain the dependence on the extra-dimensional component k_ϵ. Terms proportional to k_ϵ^2 contain the genuinely D-dimensional information and give rise, after integration, to the rational contribution $\mathcal{R}$.

The algorithm described above was implemented in MATHEMATICA [26] using the package SMASH [27]. This package provides a convenient framework for manipulating both massless and massive spinor-helicity variables, making it particularly suitable for the process under consideration.

For the SM amplitude, the calculation was first carried out analytically by hand and subsequently reproduced using the implementation described above. The agreement between the two calculations provides a non-trivial benchmark for the algorithm before applying it to the more general amplitude.

7.3 SM amplitude

Having set up the algorithm for extracting the coefficients of the scalar-integral decomposition in Eq. (7.23), we can reconstruct the SM amplitude. In Tab. 7.1, we report the expressions obtained for the triangle, bubble, and tadpole scalar coefficients. Notice that both the bubble and tadpole coefficients sum to zero, as expected, since the SM amplitude must be divergence free. As an example, in Appendix D.3, we provide a detailed derivation of the coefficient b_{01} by exploiting the algorithm described in the previous section.

Let us now reconstruct the amplitude for the hgg process in the SM. To this end, we combine the scalar-integral decomposition with the expressions for the coefficients obtained through the generalized unitarity algorithm. We obtain

$$\mathcal{M}_{++}^{\rm SM} = -\frac{8\pi\alpha_s m^2}{v}\,\delta^{ab}\left(-\frac{[23]^2}{m_h^2}\right) 2\times\left\{C_0\left(-2m^2+\frac{m_h^2}{2}\right)-\frac{i}{16\pi^2}\right\}, \quad (7.40)$$

where the two triangle scalar integrals were cast into a single $C_0(p_2, p_3; m^2, m^2, m^2)$ through loop-momentum redefinitions. We pause briefly to discuss the rational-term contribution. Computationally, its contribution, reported in the last row of Tab. 7.1, comes from performing the triple cuts 012 and 013. This means that, to extract the actual value of $\mathcal{R}$, we need to evaluate [15]

$$\mathcal{R} = -\delta^{ab}\left(-\frac{[23]^2}{m_h^2}\right)\frac{32\pi m^2\alpha_s}{v}\,C_0[k_\epsilon^2] = \delta^{ab}\left(-\frac{[23]^2}{m_h^2}\right)\frac{i\alpha_s m^2}{\pi v}, \quad (7.41)$$

in the notation introduced in Eq. (7.26). This is precisely the contribution in $\mathcal{M}_{++}^{\rm SM}$.

Now, we can exploit the following relation [60]

$$\begin{aligned} C_0(p_2, p_3; m^2, m^2, m^2) &= \int \frac{d^Dk}{(2\pi)^D}\frac{\mu^{2\epsilon}}{(k^2-m^2)[(k-p_2)^2-m^2][(k+p_3)^2-m^2]} \\ &= -\frac{i}{16\pi^2}\frac{2}{m_h^2}f(\tau), \end{aligned} \quad (7.42)$$

with $\tau \equiv \frac{4m^2}{m_h^2}$ and $f(\tau)$ defined in Eq. (A.28). Then, the above amplitude reads

$$\boxed{\mathcal{M}_{++}^{\rm SM} = i\frac{\alpha_s}{3\pi v}\,\delta^{ab}\left(-\frac{[23]^2}{m_h^2}\right)\frac{m_h^2}{2}\,F_1(\tau).} \quad (7.43)$$

This result agrees with the amplitude computed in Eq. (3.19). To see this explicitly we first set to zero all the SMEFT Wilson coefficients, then we exploit Eqs. (7.13), (7.14) and (7.4) to perform the kinematic contractions in the spinor-helicity formalism. The all-negative-helicity amplitude can be simply obtained via a parity transformation,

$$\boxed{\mathcal{M}_{--}^{\rm SM} = i\frac{\alpha_s}{3\pi v}\,\delta^{ab}\left(-\frac{\langle 23\rangle^2}{m_h^2}\right)\frac{m_h^2}{2}\,F_1(\tau).} \quad (7.44)$$

Here, we have introduced the standard form factor

$$F_1(\tau) = \frac{3}{2}\tau\left[1+(1-\tau)\,f(\tau)\right]. \quad (7.45)$$

	$\boldsymbol{c_{012}}$	$\boldsymbol{c_{013}}$
Triple cut	$\dfrac{4\pi m^2\alpha_s}{v}\left(4m^2-m_h^2\right)$	$\dfrac{4\pi m^2\alpha_s}{v}\left(4m^2-m_h^2\right)$

	$\boldsymbol{b_{01}}$	$\boldsymbol{b_{02}}$	$\boldsymbol{b_{03}}$	$\boldsymbol{b_{12}}$	$\boldsymbol{b_{13}}$
Bubble	0	0	0	0	0

	$\boldsymbol{a_0}$	$\boldsymbol{a_1}$	$\boldsymbol{a_2}$	$\boldsymbol{a_3}$
Tadpole	$-\dfrac{16\pi m^2\alpha_s}{v\,m_h^2}$	$-\dfrac{16\pi m^2\alpha_s}{v\,m_h^2}$	$\dfrac{16\pi m^2\alpha_s}{v\,m_h^2}$	$\dfrac{16\pi m^2\alpha_s}{v\,m_h^2}$

	$\boldsymbol{R_{012}}$	$\boldsymbol{R_{013}}$
Rational	$-\dfrac{16\pi m^2\alpha_s}{v}\,k_\epsilon^2$	$-\dfrac{16\pi m^2\alpha_s}{v}\,k_\epsilon^2$

Table 7.1: Triple-cut, bubble, tadpole, and rational coefficients. The common factor $\delta^{ab}\left(-[23]^2/m_h^2\right)$ has been factored out from all coefficients. The terms proportional to k_ϵ^2 have been separated from the triple-cut coefficients and collected in the rational contribution. They will lead to the rational term only once integrated.

Although the two amplitudes are not identical, since they carry opposite little-group weights, they are characterized by the same scalar form factor. Indeed, parity exchanges angle and square brackets, $\langle 23\rangle \leftrightarrow [23]$, while leaving the scalar coefficient unchanged. Therefore, in the SM, the $++$ and $--$ helicity configurations contain the same dynamical information, while the factors $\left(-[23]^2/m_h^2\right)$ and $\left(-\langle 23\rangle^2/m_h^2\right)$ only encode their different helicity structures.

For real external momenta, the two spinor structures are related by complex conjugation. Using the property reported in Eq. (4.20), one finds

$$\left(\frac{[23]^2}{m_h^2}\right)\left(\frac{[23]^2}{m_h^2}\right)^* = \frac{[23]^2\langle 32\rangle^2}{m_h^4} = \left(\frac{[23]\langle 32\rangle}{m_h^2}\right)^2 = 1. \tag{7.46}$$

Hence, these helicity-dependent factors drop out from the squared amplitude, and therefore

$$\left|\mathcal{M}_{++}^{\mathrm{SM}}\right|^2 = \left|\mathcal{M}_{--}^{\mathrm{SM}}\right|^2. \tag{7.47}$$

7.4 BSM amplitude at LO

In the previous section, we computed the SM amplitude for Higgs production via gluon fusion. We were able to set the notation and establish the method for recovering the well-known SM result. Indeed, it served as a benchmark for the algorithm based on generalized unitarity.

In this section, we instead focus on all possible BSM structures that can emerge at LO in the Λ expansion from the same SM-like diagrams reported in Eq. (7.1). Recall that, before specializing the amplitude to the SM case, we obtained the general expression for the first diagram, namely Eq. (7.11), which we report again here for completeness:

$$\begin{aligned}\mathcal{A}_{++}(k) = i\,\frac{\delta^{ab}}{2}&\left(-c^{LL}_{ht\bar{t}}\langle k_3^L|k_I\rangle + c^{RR}_{ht\bar{t}}[k_3^L|k_I]\right)\\ &\times\left[c_{g\bar{t}t}\,\varepsilon^+_\mu(p_2;p_3)\left(\langle k^I|\gamma^\mu|k_{2,J}] - \langle k_{2,J}|\gamma^\mu|k^I]\right) + c^{RRR}_{g\bar{t}t}[k^I|2][k_{2,J}|2]\right]\\ &\times\left[c_{g\bar{t}t}\,\varepsilon^+_\nu(p_3;p_2)\left(\langle k_2^J|\gamma^\nu|k_{3,L}] - \langle k_{3,L}|\gamma^\nu|k_2^J]\right) + c^{RRR}_{g\bar{t}t}[k_2^J|3][k_{3,L}|3]\right],\end{aligned} \tag{7.48}$$

This expression was obtained by sewing together the tree-level amplitudes for positive-helicity gluons. The amplitude for the second SM-like diagram, which we denote by $\tilde{\mathcal{A}}_{++}(k)$, can then be obtained by exchanging the two gluon momenta.

Since we have already computed the SM contribution to this amplitude, we can rewrite $\mathcal{A}_{++}(k)$ in a form that makes the SM and BSM structures explicit,

$$\begin{aligned}\mathcal{A}_{++}(k) = i\,\frac{\delta^{ab}}{2}&\Bigg[\frac{c^{RR}_{ht\bar{t}} + c^{LL}_{ht\bar{t}}}{2}\left(-\langle k_3^L|k_I\rangle + [k_3^L|k_I]\right)\\ &\qquad\qquad + \frac{c^{RR}_{ht\bar{t}} - c^{LL}_{ht\bar{t}}}{2}\left(\langle k_3^L|k_I\rangle + [k_3^L|k_I]\right)\Bigg]\\ &\times\left[c_{g\bar{t}t}\,\varepsilon^+_\mu(p_2;p_3)\left(\langle k^I|\gamma^\mu|k_{2,J}] - \langle k_{2,J}|\gamma^\mu|k^I]\right) + c^{RRR}_{g\bar{t}t}[k^I|2][k_{2,J}|2]\right]\\ &\times\left[c_{g\bar{t}t}\,\varepsilon^+_\nu(p_3;p_2)\left(\langle k_2^J|\gamma^\nu|k_{3,L}] - \langle k_{3,L}|\gamma^\nu|k_2^J]\right) + c^{RRR}_{g\bar{t}t}[k_2^J|3][k_{3,L}|3]\right],\end{aligned} \tag{7.49}$$

where the first two lines now resemble the parametrization of the $h\bar{t}t$ amplitude reported in Eq. (5.30). In particular, the piece proportional to $(c^{RR}_{ht\bar{t}} - c^{LL}_{ht\bar{t}})/2$ is responsible for a parity-violating interaction between the Higgs and the top quarks. Conversely, $(c^{RR}_{ht\bar{t}} + c^{LL}_{ht\bar{t}})/2$ contains the SM coupling and, at most, modifications to the Yukawa coupling.

Similarly to before, we now need to perform the spinor contractions. We can recycle much of the calculation performed in the previous section, except for the terms involving the coefficient $c^{RRR}_{g\bar{t}t}$. For convenience, we display these two parts separately.

7.4.1 Computation of the SM-like numerator

Let us consider the SM-like term contained in Eq. (7.48). In practice, we neglect the coefficient $c_{g\bar{t}t}^{RRR}$ and consider it only later. Hence,

$$\begin{aligned}\mathcal{A}_{++}^{\text{SM-like}}(k) = i\,\frac{\delta^{ab}}{2}\left(c_{ht\bar{t}}^{RR}[k_3^L|k_I] - c_{ht\bar{t}}^{LL}\langle k_3^L|k_I\rangle\right)\\ \times c_{g\bar{t}t}\,\varepsilon_\mu^+(p_2;p_3)\left(\langle k^I|\gamma^\mu|k_{2,J}] - \langle k_{2,J}|\gamma^\mu|k^I]\right)\\ \times c_{g\bar{t}t}\,\varepsilon_\nu^+(p_3;p_2)\left(\langle k_2^J|\gamma^\nu|k_{3,L}] - \langle k_{3,L}|\gamma^\nu|k_2^J]\right),\end{aligned} \tag{7.50}$$

where in the first line we factored out a minus sign. The above contribution resembles the pure SM one of Eq. (7.16), except for the use of general coefficients instead of the corresponding SM ones. For this reason, the calculation is essentially the same and is reported explicitly in Appendix D.1. We obtain

$$\begin{aligned}\mathcal{A}_{++}^{\text{SM-like}}(k) = i\frac{\delta^{ab}}{2}\,c_{g\bar{t}t}^2\,\varepsilon_\mu^+(p_2;p_3)\,\varepsilon_\nu^+(p_3;p_2)\\ \times\Bigg\{m\left[c_{ht\bar{t}}^{RR}\,\mathrm{Tr}\left(\bar{\sigma}^\alpha\sigma^\nu\bar{\sigma}^\beta\sigma^\mu\right) + c_{ht\bar{t}}^{LL}\,\mathrm{Tr}\left(\sigma^\alpha\bar{\sigma}^\nu\sigma^\beta\bar{\sigma}^\mu\right)\right]k_{3,\alpha}k_{2,\beta}\\ + m\left[c_{ht\bar{t}}^{LL}\,\mathrm{Tr}\left(\bar{\sigma}^\alpha\sigma^\nu\bar{\sigma}^\beta\sigma^\mu\right) + c_{ht\bar{t}}^{RR}\,\mathrm{Tr}\left(\sigma^\alpha\bar{\sigma}^\nu\sigma^\beta\bar{\sigma}^\mu\right)\right]k_\alpha k_{2,\beta}\\ + m\left[c_{ht\bar{t}}^{RR}\,\mathrm{Tr}\left(\bar{\sigma}^\alpha\sigma^\beta\bar{\sigma}^\nu\sigma^\mu\right) + c_{ht\bar{t}}^{LL}\,\mathrm{Tr}\left(\sigma^\alpha\bar{\sigma}^\beta\sigma^\nu\bar{\sigma}^\mu\right)\right]k_\alpha k_{3,\beta}\\ + m^3\left[c_{ht\bar{t}}^{RR}\,\mathrm{Tr}\left(\bar{\sigma}^\nu\sigma^\mu\right) + c_{ht\bar{t}}^{LL}\,\mathrm{Tr}\left(\sigma^\nu\bar{\sigma}^\mu\right)\right]\Bigg\}.\end{aligned} \tag{7.51}$$

Using Eqs. (B.36), (B.38) and (B.39), the amplitude can be rearranged as

$$\begin{aligned}\mathcal{A}_{++}^{\text{SM-like}}(k) = i\frac{c_{g\bar{t}t}^2\,m}{2}\,\delta^{ab}\,\varepsilon_\mu^+(p_2;p_3)\,\varepsilon_\nu^+(p_3;p_2)\Bigg\{\\ \frac{c_{ht\bar{t}}^{RR}+c_{ht\bar{t}}^{LL}}{2}\Bigg[\mathrm{Tr}\left(\gamma^\alpha\gamma^\nu\gamma^\beta\gamma^\mu\right)\left(k_{3,\alpha}k_{2,\beta}+k_\alpha k_{2,\beta}\right)\\ + \mathrm{Tr}\left(\gamma^\alpha\gamma^\beta\gamma^\nu\gamma^\mu\right)k_\alpha k_{3,\beta} + m^2\,\mathrm{Tr}\left(\gamma^\mu\gamma^\nu\right)\Bigg]\\ + \frac{c_{ht\bar{t}}^{RR}-c_{ht\bar{t}}^{LL}}{2}\,4i\,\epsilon^{\alpha\nu\beta\mu}\Big(-k_{3,\alpha}k_{2,\beta}+k_\alpha k_{2,\beta}-k_\alpha k_{3,\beta}\Big)\Bigg\}.\end{aligned} \tag{7.52}$$

Notice that $(c_{ht\bar{t}}^{RR}+c_{ht\bar{t}}^{LL})/2$ multiplies the same contribution obtained in the SM case of Eq. (7.18), whereas the other combination is responsible for parity violation. These behaviors were expected.

To proceed further, we need to evaluate the traces and contract the indices. We have already done this for the SM part, obtaining Eq. (7.21). On the other hand, for the epsilon-dependent term in the above equation, we implement the momentum definitions in Eq. (7.5), together with Eq. (B.43). Eventually, the expression reads

$$\mathcal{A}_{++}^{\text{SM-like}}(k) = i\,2\,c_{g\bar{t}t}^2\,m\,\delta^{ab}\left(-\frac{[23]^2}{m_h^2}\right)\left\{\frac{c_{ht\bar{t}}^{RR}+c_{ht\bar{t}}^{LL}}{2}\left[-\langle 2|\not{k}|2]-\left(m^2-k^2\right)\right.\right.$$
$$\left.\left.+\frac{m_h^2}{2}+\frac{2}{m_h^2}[2|\not{k}|3\rangle[3|\not{k}|2\rangle\right]+\frac{c_{ht\bar{t}}^{RR}-c_{ht\bar{t}}^{LL}}{2}\left[-\frac{m_h^2}{2}\right]\right\}. \tag{7.53}$$

As a crosscheck, notice that by using the SM couplings in Eq. (7.15), the above equation correctly reduces to Eq. (7.21).

7.4.2 Computation of the pure BSM factor

Let us now consider the left over pieces, namely the ones proportional to the coefficient $c_{g\bar{t}t}^{RRR}$. These terms are purely BSM. Their contribution can be extracted from Eq. (7.48), and read

$$\mathcal{A}_{++}^{c_{g\bar{t}t}^{RRR}}(k) = i\,\frac{\delta^{ab}}{2}\,c_{g\bar{t}t}\,c_{g\bar{t}t}^{RRR}\left(-c_{ht\bar{t}}^{LL}\langle k_3^L|k_I\rangle+c_{ht\bar{t}}^{RR}[k_3^L|k_I]\right)$$
$$\times\left\{\varepsilon_\mu^+(p_2;p_3)\left(\langle k^I|\gamma^\mu|k_{2,J}]-\langle k_{2,J}|\gamma^\mu|k^I]\right)[k_2^J|3][k_{3,L}|3]\right.$$
$$\left.+[k^I|2][k_{2,J}|2]\,\varepsilon_\nu^+(p_3;p_2)\left(\langle k_2^J|\gamma^\nu|k_{3,L}]-\langle k_{3,L}|\gamma^\nu|k_2^J]\right)\right\}. \tag{7.54}$$

Since we are interested in the leading-order amplitude in the $1/\Lambda$ expansion, we must retain only the contributions linear in the coupling $c_{g\bar{t}t}^{RRR}$. This is because, as already discussed in Sec. 5.1.3, dimensional analysis suggests the presence of a dimension-6 operator generating this coupling.

To perform the calculation, we first need to rewrite the two new terms in a more convenient form. This is because both $[k_2^J|3][k_{3,L}|3]$ and $[k^I|2][k_{2,J}|2]$ obscure the presence of a polarization vector that can be factored out:

$$[k_2^J|3]\,[k_{3,L}|3] = \frac{1}{2\sqrt{2}}\,\varepsilon_{3,\nu}^+\Big([k_2^J|3]\,\langle 3|\gamma^\nu|k_{3,L}]+[k_{3,L}|3]\,\langle 3|\gamma^\nu|k_2^J]\Big). \tag{7.55}$$

$$[k^I|2]\,[k_{2,J}|2] = \frac{1}{2\sqrt{2}}\,\varepsilon_{2,\mu}^+\Big([k^I|2]\,\langle 2|\gamma^\mu|k_{2,J}]+[k_{2,J}|2]\,\langle 2|\gamma^\mu|k^I]\Big). \tag{7.56}$$

These can be straightforwardly verified by using the explicit expressions of the slashed polarization vectors of Eq. (4.63).

Using Eqs. (7.55) and (7.56), we can factor out the two polarization vectors $\varepsilon^{+}_{2,\mu}$ and $\varepsilon^{+}_{3,\nu}$ to ease the computation; obtaining

$$
\begin{aligned}
\mathcal{A}^{c^{RRR}_{g\bar{t}t}}_{++}(k) = & -i\,\frac{\delta^{ab}}{2}\,c_{g\bar{t}t}\,c^{RRR}_{g\bar{t}t}\,\frac{1}{2\sqrt{2}}\,\varepsilon^{+}_{2,\mu}\,\varepsilon^{+}_{3,\nu}\left(c^{LL}_{ht\bar{t}}\langle k^{L}_{3}|k_{I}\rangle - c^{RR}_{ht\bar{t}}[k^{L}_{3}|k_{I}]\right) \\
& \times\Bigg\{\left(\langle k^{I}|\gamma^{\mu}|k_{2,J}] - \langle k_{2,J}|\gamma^{\mu}|k^{I}]\right) \\
& \qquad \times\Big([k^{J}_{2}|3]\,\langle 3|\gamma^{\nu}|k_{3,L}] + [k_{3,L}|3]\,\langle 3|\gamma^{\nu}|k^{J}_{2}]\Big) \\
& \quad + \Big([k^{I}|2]\,\langle 2|\gamma^{\mu}|k_{2,J}] + [k_{2,J}|2]\,\langle 2|\gamma^{\mu}|k^{I}]\Big) \\
& \qquad \times\left(\langle k^{J}_{2}|\gamma^{\nu}|k_{3,L}] - \langle k_{3,L}|\gamma^{\nu}|k^{J}_{2}]\right)\Bigg\}.
\end{aligned} \tag{7.57}
$$

where we collected a minus sign in the first line. In Appendix D.4, we explicitly show all the steps involved in performing the spinor contractions. Eventually, we convert the amplitude back to the spinor-helicity formalism by exploiting Eqs. (4.39), (7.12), and (7.20). We obtain the following result:

$$
\begin{aligned}
\mathcal{A}^{c^{RRR}_{g\bar{t}t}}_{++}(k) = i\,\frac{c_{g\bar{t}t}\,c^{RRR}_{g\bar{t}t}}{2\sqrt{2}}\,\delta^{ab}\left(-\frac{[23]^{2}}{m_h^{2}}\right)\Bigg\{ & m^{2}m_h^{2}\,c^{RR}_{ht\bar{t}} \\
& + c^{LL}_{ht\bar{t}}\Bigg[-\langle 2|\not{k}|2]\,[3|\not{k}|3\rangle + \langle 2|\not{k}|2]\,\left(k^{2}-m^{2}\right) \\
& \quad - \langle 2|\not{k}|2]^{2} + k^{2}m_h^{2} + \langle 2|\not{k}|3]\,\langle 3|\not{k}|2]\Bigg]\Bigg\}.
\end{aligned} \tag{7.58}
$$

An important point is that this amplitude was obtained by setting to zero all γ_5 terms appearing in the traces, as highlighted in Eq. (D.66) This corresponds to obtain the CP-conserving part of the amplitude only. In other words, we adopt the NDR-DISCARD prescription [61], in which the remaining γ_5-odd traces are set to zero. We did the same for the SMEFT amplitude of Eq. (3.19).

7.4.3 Complete amplitude

We can now combine the SM-like contribution with the term linear in $c^{RRR}_{g\bar{t}t}$. Since both contributions share the same overall kinematic factor, it is convenient to factor it out and write the complete numerator, up to linear order in $c_{g\bar{t}t}^{RRR}$, in a single expression:

$$\begin{aligned}\mathcal{A}_{++}(k) = i\, c_{g\bar{t}t}\, \delta^{ab} \left(-\frac{[23]^2}{m_h^2}\right) \Bigg\{ 2\, c_{g\bar{t}t}\, m \Bigg[\frac{c_{ht\bar{t}}^{RR} + c_{ht\bar{t}}^{LL}}{2} \Bigg(&- \langle 2|\not{k}|2] - \left(m^2 - k^2\right) \\ &+ \frac{m_h^2}{2} + \frac{2}{m_h^2} [2|\not{k}|3\rangle [3|\not{k}|2\rangle \Bigg) + \frac{c_{ht\bar{t}}^{RR} - c_{ht\bar{t}}^{LL}}{2} \left(-\frac{m_h^2}{2}\right) \Bigg] \\ + \frac{c_{g\bar{t}t}^{RRR}}{2\sqrt{2}} \Bigg[m^2 m_h^2\, c_{ht\bar{t}}^{RR} + c_{ht\bar{t}}^{LL} \Bigg(&- \langle 2|\not{k}|2]\, [3|\not{k}|3\rangle + \langle 2|\not{k}|2]\, \left(k^2 - m^2\right) \\ &- \langle 2|\not{k}|2]^2 + k^2 m_h^2 + \langle 2|\not{k}|3]\, \langle 3|\not{k}|2] \Bigg) \Bigg] \Bigg\}.\end{aligned} \tag{7.59}$$

The next step is to reconstruct the full amplitude. To this end, we employ the generalized unitarity algorithm described in Sec. 7.2. This calculation was performed completely automatically using Mathematica and its interface with SMaSH. In Tab. 7.2, we collect the expressions for the coefficients obtained. Notice that, upon using the SM couplings defined in Eq. (7.15), the BSM coefficients reduce to the corresponding SM ones reported in Tab. 7.1.

Let us now provide the full expression for the reconstructed amplitude. Inserting the coefficients of Tab. 7.2 into the amplitude expansion of Eq. (7.32), we obtain

$$\begin{aligned}\mathcal{M}_{++} = \delta^{ab} \left(-\frac{[23]^2}{m_h^2}\right) \Bigg\{ 2C_0 \Bigg[&\frac{i\, m^2 m_h^2\, c_{g\bar{t}t}\, c_{g\bar{t}t}^{RRR}\, c_{ht\bar{t}}^{RR}}{2\sqrt{2}} \\ &+ im\, c_{g\bar{t}t}^2 \left(c_{ht\bar{t}}^{LL} + c_{ht\bar{t}}^{RR}\right) \left(\frac{m_h^2}{2} - 2m^2\right) \\ &+ \frac{i}{2}\, m\, c_{g\bar{t}t}^2\, m_h^2 \left(c_{ht\bar{t}}^{LL} - c_{ht\bar{t}}^{RR}\right) \Bigg] \\ + B_0 &\frac{i\, c_{g\bar{t}t}\, m_h^2\, c_{g\bar{t}t}^{RRR}\, c_{ht\bar{t}}^{LL}}{2\sqrt{2}} \\ - \frac{i}{16\pi^2} &\left[\frac{i\, c_{g\bar{t}t}\, m_h^2\, c_{g\bar{t}t}^{RRR}\, c_{ht\bar{t}}^{LL}}{2\sqrt{2}} + 2im\, c_{g\bar{t}t}^2 \left(c_{ht\bar{t}}^{LL} + c_{ht\bar{t}}^{RR}\right) \right] \Bigg\}.\end{aligned} \tag{7.60}$$

where C_0 and B_0 indicate $C_0\left(p_2, p_3; m^2, m^2, m^2\right)$ and $B_0\left(p_1; m^2, m^2\right)$, respectively. We stress that the above expression is not the full LO result of the $h \to gg$ process. This is because, as already stated, we are taking into account the SM-like diagrams of Fig. 7.1 only. A complete expression should contain also the terms obtained from sewing four-point vertices which would appear by considering diagrams (6) and (7) of Fig. A.1.

	c_{012}	c_{013}
Triple cut	$\frac{i\,m^2 m_h^2\, c_{g\bar{t}t}\, c_{g\bar{t}t}^{RRR}\, c_{ht\bar{t}}^{RR}}{2\sqrt{2}} + im\, c_{g\bar{t}t}^2 \left(c_{ht\bar{t}}^{LL} + c_{ht\bar{t}}^{RR}\right) \times \left(\frac{m_h^2}{2} - 2m^2\right) + \frac{i}{2}\, m\, c_{g\bar{t}t}^2\, m_h^2 \left(c_{ht\bar{t}}^{LL} - c_{ht\bar{t}}^{RR}\right)$	$\frac{i\,m^2 m_h^2\, c_{g\bar{t}t}\, c_{g\bar{t}t}^{RRR}\, c_{ht\bar{t}}^{RR}}{2\sqrt{2}} + im\, c_{g\bar{t}t}^2 \left(c_{ht\bar{t}}^{LL} + c_{ht\bar{t}}^{RR}\right) \times \left(\frac{m_h^2}{2} - 2m^2\right) + \frac{i}{2}\, m\, c_{g\bar{t}t}^2\, m_h^2 \left(c_{ht\bar{t}}^{LL} - c_{ht\bar{t}}^{RR}\right)$

	b_{01}	b_{02}	b_{03}	b_{12}	b_{13}
Bubble	$\frac{i\, c_{g\bar{t}t}\, m_h^2\, c_{g\bar{t}t}^{RRR}\, c_{ht\bar{t}}^{LL}}{2\sqrt{2}}$	0	0	0	0

	a_0	a_1
Tadpole	$\frac{i}{4}\, c_{g\bar{t}t} \left(\frac{8m\, c_{g\bar{t}t}}{m_h^2} \left(c_{ht\bar{t}}^{LL} + c_{ht\bar{t}}^{RR}\right) - \frac{\sqrt{2}(x+y)}{x+y-1}\, c_{g\bar{t}t}^{RRR}\, c_{ht\bar{t}}^{LL} \right)$	$\frac{i}{4}\, c_{g\bar{t}t} \left(\frac{8m\, c_{g\bar{t}t}}{m_h^2} \left(c_{ht\bar{t}}^{LL} + c_{ht\bar{t}}^{RR}\right) + \frac{\sqrt{2}(x+y)}{x+y-1}\, c_{g\bar{t}t}^{RRR}\, c_{ht\bar{t}}^{LL} \right)$
	a_2	a_3
Tadpole	$-\frac{2im\, c_{g\bar{t}t}^2 \left(c_{ht\bar{t}}^{LL} + c_{ht\bar{t}}^{RR}\right)}{m_h^2}$	$-\frac{2im\, c_{g\bar{t}t}^2 \left(c_{ht\bar{t}}^{LL} + c_{ht\bar{t}}^{RR}\right)}{m_h^2}$

	R_{012}	R_{013}
Rational	$\frac{i\, c_{g\bar{t}t}\, m_h^2\, k_\epsilon^2\, c_{g\bar{t}t}^{RRR}\, c_{ht\bar{t}}^{LL}}{2\sqrt{2}} + 2im\, k_\epsilon^2\, c_{g\bar{t}t}^2 \left(c_{ht\bar{t}}^{LL} + c_{ht\bar{t}}^{RR}\right)$	$\frac{i\, c_{g\bar{t}t}\, m_h^2\, k_\epsilon^2\, c_{g\bar{t}t}^{RRR}\, c_{ht\bar{t}}^{LL}}{2\sqrt{2}} + 2im\, k_\epsilon^2\, c_{g\bar{t}t}^2 \left(c_{ht\bar{t}}^{LL} + c_{ht\bar{t}}^{RR}\right)$

Table 7.2: Triple-cut, bubble, tadpole, and rational coefficients. The common factor $\delta^{ab}\left(-[23]^2/m_h^2\right)$ has been omitted from all coefficients for brevity. The coefficients associated with the cuts (012) and (013) are identical for both the triple-cut and rational contributions. They will lead to the rational term only once integrated.

7.4.4 Matching onto SMEFT

In this section, we provide the matching onto SMEFT of the amplitude for Higgs production via gluon fusion obtained in Eq. (7.60). The complete LO SMEFT amplitude is reported in Eq. (A.25). However, here we focus only on the SM-like contributions, namely on diagrams (2), (3), (4), and (5) of Fig. A.1. Hence, we neglect both the $C_{\varphi G}$ contribution, which arises from the tree-level diagram, and the term proportional to $B_0(0; m^2, m^2)$, which comes from the last two diagrams of Fig. A.1.

We also take into account another modification with respect to Eq. (A.25). In order to find the correct expressions for the coefficients $c_{ht\bar{t}}^{LL}$ and $c_{ht\bar{t}}^{RR}$, we retain the CP-odd contribution to the Higgs-top interaction, namely Eq. (A.18). This means taking into account the presence of γ_5, which multiplies the imaginary part of $C_{u\varphi}^{33}$. To this end, we cannot employ the NDR-DISCARD prescription for evaluating the Dirac traces, as discussed in Sec. A.2.1. Instead, we make use of the BMHV scheme [62, 63]. Concerning the top-gluon interactions, we instead retain only the CP-even part.

Applying these modifications, the SMEFT amplitude of the SM-like diagrams of Fig. 7.1 only, can be written as

$$\boxed{\begin{aligned}\mathcal{M}_{++}^{\text{SMEFT}} = &-\frac{m[23]^2}{\Lambda^2}\,\delta^{ab}\Bigg\{\frac{8\pi\alpha_s}{m_h^2 v}\,\mathcal{X}\left[\left(4m^2-m_h^2\right)C_0+\frac{i}{8\pi^2}\right]\\ &-4i\sqrt{2}\,\pi\alpha_s v^2\,\operatorname{Im}C_{u\varphi}^{33}\,C_0\\ &+4\sqrt{2\pi\alpha_s}\,\operatorname{Re}C_{uG}^{33}\left[\left(B_0-\frac{i}{16\pi^2}\right)+2m^2C_0\right]\Bigg\},\end{aligned}} \tag{7.61}$$

where $\mathcal{X}$ is defined in Eq. (A.26), yet we report it here for completeness

$$\mathcal{X} = C_{\varphi\Box} m v^2 - \frac{1}{4} C_{\varphi D} m v^2 - \frac{1}{\sqrt{2}}\operatorname{Re}\big(C_{u\varphi}^{33}\big)\, v^3 + \Lambda^2 m. \tag{7.62}$$

We can now compare Eq. (7.61) with the corresponding amplitude obtained from the on-shell construction. The latter can be written as

$$\boxed{\begin{aligned}\mathcal{M}_{++} = &-[23]^2\delta^{ab}\Bigg\{\frac{8i\pi\alpha_s m}{m_h^2}\left(\frac{c_{ht\bar{t}}^{LL}+c_{ht\bar{t}}^{RR}}{2}\right)\left[\left(4m^2-m_h^2\right)C_0+\frac{i}{8\pi^2}\right]\\ &-8i\pi\alpha_s m\left(\frac{c_{ht\bar{t}}^{LL}-c_{ht\bar{t}}^{RR}}{2}\right)C_0\\ &+\frac{\sqrt{\pi\alpha_s}}{\sqrt{2}}\,c_{gt\bar{t}}^{RRR}\left[c_{ht\bar{t}}^{LL}\left(B_0-\frac{i}{16\pi^2}\right)+2m^2c_{ht\bar{t}}^{RR}C_0\right]\Bigg\},\end{aligned}} \tag{7.63}$$

where $c_{g\bar{t}t} = -2i\sqrt{\pi\alpha_s}$ was used. We can now match Eqs. (7.61) and (7.63).

First, matching the parity-even contribution gives

$$i\left(\frac{c_{h\bar{t}t}^{LL} + c_{h\bar{t}t}^{RR}}{2}\right) = \frac{\mathcal{X}}{\Lambda^2 v}. \tag{7.64}$$

The contribution proportional to $\mathrm{Im}\, C_{u\varphi}^{33}$ instead fixes the parity-odd combination,

$$i\left(\frac{c_{h\bar{t}t}^{LL} - c_{h\bar{t}t}^{RR}}{2}\right) = \frac{iv^2}{\sqrt{2}\Lambda^2}\,\mathrm{Im}\, C_{u\varphi}^{33}. \tag{7.65}$$

Combining these two relations and using the definition of $\mathcal{X}$, the two coefficients are independently fixed as

$$\boxed{\begin{aligned} i\, c_{h\bar{t}t}^{LL} &= \frac{m}{v} + \frac{mv}{\Lambda^2}\left(C_{\varphi\Box} - \frac{1}{4}C_{\varphi D}\right) - \frac{v^2}{\sqrt{2}\Lambda^2}\,\mathrm{Re}\, C_{u\varphi}^{33} + \frac{iv^2}{\sqrt{2}\Lambda^2}\,\mathrm{Im}\, C_{u\varphi}^{33}, \\ i\, c_{h\bar{t}t}^{RR} &= \frac{m}{v} + \frac{mv}{\Lambda^2}\left(C_{\varphi\Box} - \frac{1}{4}C_{\varphi D}\right) - \frac{v^2}{\sqrt{2}\Lambda^2}\,\mathrm{Re}\, C_{u\varphi}^{33} - \frac{iv^2}{\sqrt{2}\Lambda^2}\,\mathrm{Im}\, C_{u\varphi}^{33}. \end{aligned}} \tag{7.66}$$

Finally, the terms proportional to $\mathrm{Re}\, C_{uG}^{33}$ give

$$c_{g\bar{t}t}^{RRR}\, c_{h\bar{t}t}^{LL} = \frac{8m}{\Lambda^2}\,\mathrm{Re}\, C_{uG}^{33}, \tag{7.67}$$

$$c_{g\bar{t}t}^{RRR}\, c_{h\bar{t}t}^{RR} = \frac{8m}{\Lambda^2}\,\mathrm{Re}\, C_{uG}^{33}. \tag{7.68}$$

Since $c_{g\bar{t}t}^{RRR}$ starts at $\mathcal{O}(\Lambda^{-2})$, only the SM part of $c_{h\bar{t}t}^{LL}$ and $c_{h\bar{t}t}^{RR}$ contributes to these relations at linear order in the SMEFT expansion. In particular,

$$c_{h\bar{t}t}^{LL} = c_{h\bar{t}t}^{RR} = -\frac{im}{v} + \mathcal{O}\left(\Lambda^{-2}\right). \tag{7.69}$$

It then follows that

$$\boxed{i c_{g\bar{t}t}^{RRR} = -\frac{8v}{\Lambda^2}\,\mathrm{Re}\, C_{uG}^{33},} \tag{7.70}$$

which, as expected, is a purely BSM coefficient, since its leading contribution already appears at order $1/\Lambda^2$.

Chapter 8

Conclusions

On-shell amplitude methods provide a compelling approach to study BSM physics directly at the level of the amplitude for a given scattering process, in an EFT framework. At tree level, a satisfactory description of this approach has been developed in recent years. However, a comparably systematic bottom-up construction of model-independent one-loop amplitudes is still less developed.

In this thesis, we successfully computed the leading-order Higgs production via gluon fusion in the EFT expansion, without the need for a Lagrangian to dictate the interaction rules. Since the amplitude approach requires the helicities of the massless particles involved to be specified from the outset, we focused on the all-positive gluon-helicity configuration. The main result has been presented in Eq. (7.63). This expression considers a subset of the LO contributing diagrams, namely the SM-like triangle diagrams of Fig. 7.1. For a precise definition of all the parameters entering the amplitude, see Ch. 7.

The first part of this amplitude correctly reproduces the SM contribution in the corresponding limit, while the remaining structures are genuinely BSM. As a benchmark of the calculation, we matched our result onto its SMEFT counterpart and found complete agreement with Ref. [60].

A natural extension of this work would be to consider the other two complementary diagrams contributing to the LO amplitude for the process of interest, namely diagrams (6) and (7) of Fig. A.1. This additional contribution would be particularly interesting because the BSM vertex is now a four-point interaction and therefore contains both factorizable and non-factorizable structures.

Another possible direction would be to consider HEFT as an alternative effective description of new physics. Among other things, HEFT relaxes some of the assumptions underlying SMEFT by allowing the Goldstone bosons and the physical Higgs boson not to belong to the same linearly transforming $SU(2)$ doublet.

Furthermore, one could focus on the study of multi-Higgs production processes induced by gluon–gluon fusion. Although these processes are characterized by small cross sections, the inclusion of one-loop corrections is well motivated by ongoing experimental efforts to measure double-Higgs production [64–66] and even triple-Higgs production [67, 68].

Lastly, at the High-Luminosity Large Hadron Collider (HL-LHC), multi-dimensional differential distributions will provide increasingly detailed information on the kinematic structure of scattering processes. This may enhance the sensitivity to observables probing helicity and polarization effects, as well as spin correlations and quantum observables [12, 13]. In this context, the amplitude method provides a particularly suitable framework, since it makes the helicity and spin structure of the scattering process manifest and thereby facilitates a more direct connection with suitably designed observables.

Appendix A

SMEFT conventions and Feynman rules of interest

In this appendix, we set our notations for the definition of SMEFT Lagrangian following [20]. First, we briefly review the SM Lagrangian before the occurrence spontaneous symmetry breaking, then we present the relevant Feynman rules for the Higgs production via gluon fusion in the SMEFT framework. Finally, we evaluate the LO contribution to its scattering amplitude, using computational techniques.

A.1 The Standard Model

A quantum field theory describing elementary particles and their interactions is specified by its gauge symmetry, its field content and, possibily, by the pattern of spontaneous symmetry breaking. The Standard Model (SM) is a renormalizable and anomaly-free gauge theory based on the symmetry group

$$G_{\mathrm{SM}} = SU(3)_c \times SU(2)_L \times U(1)_Y, \tag{A.1}$$

where $SU(3)_c$ describes the strong interactions, while $SU(2)_L \times U(1)_Y$ is the gauge group of the electroweak sector. The corresponding gauge fields are denoted by G^A_μ, W^I_μ and B_μ, with $A = 1, \ldots, 8$ and $I = 1, 2, 3$.

The matter fields are arranged into three generations, labeled by $p = 1, 2, 3$. In the gauge basis, the left-handed fermions transform as doublets of $SU(2)_L$,

$$l'_{Lp} = \begin{pmatrix} \nu'_{Lp} \\ e'_{Lp} \end{pmatrix}, \qquad q'^{\alpha}_{Lp} = \begin{pmatrix} u'^{\alpha}_{Lp} \\ d'^{\alpha}_{Lp} \end{pmatrix}, \tag{A.2}$$

whereas the right-handed fermions,

$$e'_{Rp}, \qquad u'^{\alpha}_{Rp}, \qquad d'^{\alpha}_{Rp}, \tag{A.3}$$

	$SU(3)_c$	$SU(2)_L$	$U(1)_Y$
$l'_{Lp} = \begin{pmatrix} \nu'_{Lp} \\ e'_{Lp} \end{pmatrix}$	**1**	**2**	$-\frac{1}{2}$
e'_{Rp}	**1**	**1**	-1
$q'_{Lp} = \begin{pmatrix} u'_{Lp} \\ d'_{Lp} \end{pmatrix}$	**3**	**2**	$+\frac{1}{6}$
u'_{Rp}	**3**	**1**	$+\frac{2}{3}$
d'_{Rp}	**3**	**1**	$-\frac{1}{3}$
$\varphi = \begin{pmatrix} \varphi^+ \\ \varphi^0 \end{pmatrix}$	**1**	**2**	$+\frac{1}{2}$
$\widetilde{\varphi} = i\sigma_2\varphi^* = \begin{pmatrix} \varphi^{0*} \\ -\varphi^- \end{pmatrix}$	**1**	**2**	$-\frac{1}{2}$

Table A.1: Transformation properties of the Standard Model fields under $SU(3)_c \times SU(2)_L \times U(1)_Y$, where $p = 1, 2, 3$ labels the fermion generations.

are singlets under $SU(2)_L$. Here $\alpha = 1, 2, 3$ is a colour index. Notice we have used 'primed' notation for fermion fields, reserving the 'unprimed' symbols for the physical mass eigenstates basis, where flavor space rotations have been performed.

The scalar sector contains one complex $SU(2)_L$ doublet,

$$\varphi^j = \begin{pmatrix} \varphi^+ \\ \varphi^0 \end{pmatrix}, \tag{A.4}$$

whose conjugate doublet is defined as

$$\widetilde{\varphi} = i\sigma_2\varphi^*. \tag{A.5}$$

We collect in Tab. A.1 the transformation properties of the SM fields under $SU(3)_c \times SU(2)_L \times U(1)_Y$ we have just introduced.

The electric charge is related to the third component of weak isospin and to the weak hypercharge through

$$Q = T^3 + Y. \tag{A.6}$$

The gauge interactions are introduced through the covariant derivative

$$D_\mu = \partial_\mu + ig' B_\mu Y + ig W^I_\mu T^I + ig_s G^A_\mu T^A, \tag{A.7}$$

where g', g and g_s are the $U(1)_Y$, $SU(2)_L$ and $SU(3)_c$ gauge couplings, respectively.

In the fundamental representations, the generators of $SU(2)_L$ and $SU(3)_c$ respectively are

$$t^I = \frac{\sigma^I}{2}, \qquad T^A = \frac{\lambda^A}{2}, \tag{A.8}$$

with σ^I the Pauli matrices and λ^A the Gell-Mann matrices [2]. These satisfy

$$[t^I, t^J] = i\,\epsilon^{IJK} t^K, \qquad [T^A, T^B] = i\,f^{ABC} T^C, \tag{A.9}$$

and are normalized as

$$\mathrm{Tr}\big(t^I t^J\big) = \frac{1}{2}\delta^{IJ}, \qquad \mathrm{Tr}\big(T^A T^B\big) = \frac{1}{2}\delta^{AB}. \tag{A.10}$$

The generators that do not act on a given representation are understood to vanish.

With the convention adopted in Eq. (A.7), the field-strength tensors are defined through the commutator of covariant derivatives and explicitly read

$$B_{\mu\nu} = \partial_\mu B_\nu - \partial_\nu B_\mu, \tag{A.11}$$
$$W^I_{\mu\nu} = \partial_\mu W^I_\nu - \partial_\nu W^I_\mu - g\,\epsilon^{IJK} W^J_\mu W^K_\nu, \tag{A.12}$$
$$G^A_{\mu\nu} = \partial_\mu G^A_\nu - \partial_\nu G^A_\mu - g_s f^{ABC} G^B_\mu G^C_\nu. \tag{A.13}$$

Notice that the non-Abelian terms in $W^I_{\mu\nu}$ and $G^A_{\mu\nu}$ are responsible for the three- and four-gauge-boson self-interactions characteristic of Yang–Mills theories.

Finally, the complete renormalizable SM Lagrangian can be written as

$$\begin{aligned}
\mathcal{L}^{(4)}_{\mathrm{SM}} = &-\frac{1}{4}G^A_{\mu\nu}G^{A\mu\nu} - \frac{1}{4}W^I_{\mu\nu}W^{I\mu\nu} - \frac{1}{4}B_{\mu\nu}B^{\mu\nu} \\
&+ (D_\mu\varphi)^\dagger(D^\mu\varphi) + m^2\varphi^\dagger\varphi - \frac{\lambda}{2}(\varphi^\dagger\varphi)^2 \\
&+ i\left(\overline{l'_L}\not{D}l'_L + \overline{e'_R}\not{D}e'_R + \overline{q'_L}\not{D}q'_L + \overline{u'_R}\not{D}u'_R + \overline{d'_R}\not{D}d'_R\right) \\
&- \left(\overline{l'_L}\Gamma_e e'_R\varphi + \overline{q'_L}\Gamma_u u'_R\widetilde{\varphi} + \overline{q'_L}\Gamma_d d'_R\varphi + \text{h.c.}\right).
\end{aligned} \tag{A.14}$$

We can conveniently separate the different sectors as

$$\mathcal{L}^{(4)}_{\mathrm{SM}} = \mathcal{L}_{\text{gauge}} + \mathcal{L}_{\text{fermion}} + \mathcal{L}_{\text{Higgs}} + \mathcal{L}_{\text{Yukawa}}. \tag{A.15}$$

Here, the gauge kinetic terms describe the propagation and self-interactions of the gauge bosons. The fermion kinetic terms contain both the free fermion dynamics and their interactions with the gauge fields. Them scalar kinetic term generates the interactions between the Higgs doublet and the electroweak gauge bosons, while the Yukawa sector provides fermion masses and Higgs–fermion interactions after electroweak symmetry breaking.

We refer to standard textbooks [1, 2] for the realization of the electroweak symmetry breaking and the transition to the mass basis.

A.2 $gg \to h$ at leading order in SMEFT

The renormalizable Lagrangian in Eq. (A.14) contains all operators of canonical dimension equal or smaller than four that are compatible with the SM gauge symmetry and field content. It therefore provides the natural dimension-4 starting point for the construction of SMEFT, namely

$$\mathcal{L}_{\text{SMEFT}} = \mathcal{L}_{\text{SM}} + \sum_{d>4} \mathcal{L}^{(d)}, \qquad \mathcal{L}^{(d)} = \sum_i \frac{C_i^{(d)}}{\Lambda^{d-4}} Q_i^{(d)}, \tag{A.16}$$

where $Q_i^{(d)}$ are gauge-invariant operators of dimension d, while $C_i^{(d)}$ are the corresponding Wilson coefficients.

The dimension-6 operators of interest for the process under study, namely Higgs production via gluon fusion, are collected in Sec. 3.2 of the main text, specifically in Eq. (3.16).

In this section, instead, we present the relevant Feynman rules that can be obtained from those operators once spontaneous symmetry breaking has been performed. The precise steps involved in the derivation are reported in Ref. [20]. Conventionally, all momenta are taken to be incoming.

The direct Higgs–gluon interaction generated by $Q_{\varphi G}$ and $Q_{\varphi \widetilde{G}}$ is

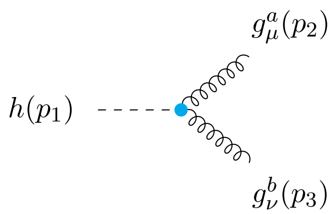

$$= \frac{4iv}{\Lambda^2}\,\delta^{ab}\Big[C_{\varphi G}\left(-p_2\cdot p_3\, g^{\mu\nu} + p_2^\nu p_3^\mu\right) + C_{\varphi\widetilde{G}}\epsilon^{\mu\nu\rho\sigma}p_{2\rho}p_{3\sigma}\Big]. \tag{A.17}$$

The Higgs–top interaction is

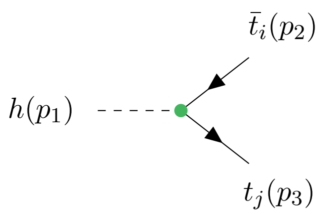

$$= -i\delta_{ji}\frac{m_t}{v}\left[1 + \frac{v^2}{\Lambda^2}\left(C_{\varphi\Box} - \frac{1}{4}C_{\varphi D}\right)\right] + i\delta_{ji}\frac{v^2}{\sqrt{2}\Lambda^2}\left[\mathrm{Re}\big(C_{u\varphi}^{33}\big) + i\,\mathrm{Im}\big(C_{u\varphi}^{33}\big)\,\gamma_5\right]. \tag{A.18}$$

The top–gluon interaction, including the chromomagnetic insertion, is

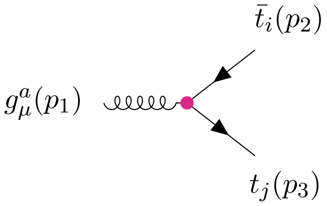

$$= -i g_s (T^a)_{ji} \gamma^\mu - \frac{\sqrt{2}v}{\Lambda^2}\, p_1^\nu (T^a)_{ji}\, \sigma^{\mu\nu} \left[\mathrm{Re}\big(C^{33}_{uG}\big) + i\ \mathrm{Im}\big(C^{33}_{uG}\big)\,\gamma_5\right]. \tag{A.19}$$

The chromomagnetic operator Q^{33}_{uG} also generates the four-point interaction $h\bar{t}tg$,

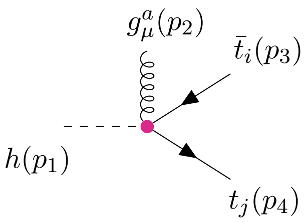

$$= -\frac{\sqrt{2}}{\Lambda^2}\, p_2^\nu (T^a)_{ji}\, \sigma^{\mu\nu} \left[\mathrm{Re}\big(C^{33}_{uG}\big) + i\ \mathrm{Im}\big(C^{33}_{uG}\big)\,\gamma_5\right]. \tag{A.20}$$

Finally, the non-Abelian term in $G^a_{\mu\nu}$ generates the contact vertices $\bar{t}tgg$ and $h\bar{t}tgg$. We omit these rules for brevity.

Notice that in the last three Feynman rules, we explicitly write the Wilson coefficients $C^{33}_{u\phi}$ and C^{33}_{uG}, splitting them into their real and imaginary parts. This makes manifest the fact that the imaginary parts of these coefficients are solely responsible for CP-odd interactions.

The Feynman rules reported in Eqs. (A.17), (A.18), (A.19), and (A.20) are those contributing to the LO $gg \to h$ amplitude in SMEFT, in the $1/\Lambda^2$ expansion.

Having specified the rules of the model, we can proceed with the explicit computation of the amplitude. This is carried out with the aid of SmeftFR v3.03 [18–20], FeynArts [21], and FeynCalc [22–24]. In particular, SmeftFR provides the Feynman rules for the process under consideration, while FeynArts is used to generate the relevant diagrams and amplitudes, and FeynCalc is used to perform the subsequent algebraic manipulations and loop reduction. The combined use of these three packages therefore provides a complete framework for the automated evaluation of the SMEFT amplitude.

A.2.1 Computational implementation

To evaluate the SMEFT amplitude for the process $gg \to h$ at LO, we start by choosing the following kinematic configuration

$$g(p_1) + g(p_2) \to h(p). \tag{A.21}$$

Then, by exploiting the `CreateTopologies` function of FeynArts the relevant diagrammatic topologies can be generated. The corresponding particle content is subsequently inserted through `InsertFields`, using the SMEFT model file employed throughout this work. The relevant amplitudes are then constructed with `CreateFeynAmp`. Schematically, this procedure takes the form

```
topsLoop = CreateTopologies[1, 2 -> 1,
    ExcludeTopologies -> {SelfEnergies, Tadpoles}];

insLoop = InsertFields[topsLoop,
    {V[4], V[4]} -> {S[1]},
    Model -> "SMEFTHgg",
    GenericModel -> "SMEFTHgg",
    InsertionLevel -> {Particles}];

ampLoopFA = CreateFeynAmp[insLoop, Truncated -> True];
```

The amplitudes generated by FeynArts are then converted into the internal FeynCalc representation by means of `FCFAConvert`. In this step we denote the loop momentum by k and perform the calculation in D dimensions. In particular, the conversion is performed according to the schematic code

```
ampLoop = FCFAConvert[ampLoopFA,
    IncomingMomenta -> {p1, p2},
    OutgoingMomenta -> {p},
    LoopMomenta -> {k},
    ChangeDimension -> D,
    UndoChiralSplittings -> True,
    DropSumOver -> True,
    Contract -> True,
    TransversePolarizationVectors -> {p1, p2}];
```

An important step involves the evaluation of the traces. To this end, we employ the NDR-Discard prescription [61]. In this prescription, traces containing an unpaired γ_5 are discarded, thus restricting the present analysis to the CP-even part of the amplitude, as done in Ref. [25]. We note that traces containing an odd number of γ_5 matrices and six or more Dirac matrices require particular care in dimensional regularization, due to the well-known reading-point ambiguity of the NDR scheme [69]. Since the corresponding CP-odd contributions are not considered in the present calculation, this ambiguity does not affect our result.

Furthermore, since the SMEFT amplitude is required only up to $\mathcal{O}(1/\Lambda^2)$, all Wilson coefficients are multiplied by an auxiliary parameter ϵ_{WC} and the resulting expression is expanded up to first order,

$$C_i \longrightarrow \epsilon_{\mathrm{WC}} C_i, \qquad \mathcal{M} = \mathcal{M}_{\mathrm{SM}} + \epsilon_{\mathrm{WC}} \mathcal{M}_{\text{dim-6}} + \mathcal{O}(\epsilon_{\mathrm{WC}}^2). \tag{A.22}$$

The auxiliary parameter is set to one only after the truncation. This procedure guarantees that products of dimension-6 Wilson coefficients, corresponding to terms beyond the linear SMEFT approximation considered here, are discarded. In Fig. A.1, we report the only contributing diagrams. Apart from the pure SM contribution shown in diagram (2), all the other diagrams contain one insertion each of a dimension-6 operator.

The resulting tensor loop integrals are reduced to the Passarino–Veltman basis (see Ch. 6.1.2) using the `TID` function,

```
ampPV = TID[ampLinear, k, ToPaVe -> True];
```

so that the result could be expressed in terms of the scalar functions B_0 and C_0, defined as

$$\begin{aligned} B_0(p; m_1^2, m_2^2) &\equiv \int \frac{d^d k}{(2\pi)^d} \frac{\mu^{2\epsilon}}{\left(k^2 - m_1^2\right)\left[(k+p)^2 - m_2^2\right]}, \\ C_0(p_1, p_2; m_1^2, m_2^2, m_3^2) &\equiv \int \frac{d^d k}{(2\pi)^d} \frac{\mu^{2\epsilon}}{\left(k^2 - m_1^2\right)\left[(k+p_1)^2 - m_2^2\right]} \\ &\qquad \times \frac{1}{\left[(k+p_1+p_2)^2 - m_3^2\right]}, \end{aligned} \tag{A.23}$$

where we are employing the definitions given in Eq. (6.7). Lorentz contractions and scalar-product simplifications were subsequently carried out using `Contract`, `ExpandScalarProduct` and `DiracSimplify`.

As a non-trivial check of the calculation, gauge invariance was verified. Denoting the tensor amplitude by $\mathcal{M}^{\mu\nu}$, we explicitly checked that

$$p_{1\mu} \mathcal{M}^{\mu\nu} = 0, \qquad p_{2\nu} \mathcal{M}^{\mu\nu} = 0. \tag{A.24}$$

These identities were verified algebraically with FeynCalc after the tensor reduction.

The non-exhaustive steps we have just sketched yield

$$\begin{aligned}\mathcal{M}^{\text{SMEFT}} &= \frac{\delta^{ab}}{2\pi^{3/2}\Lambda^2 m_h^2 v}\,\varepsilon_{1\mu}\varepsilon_{2\nu}\,[p_1^\nu p_2^\mu - (p_1\cdot p_2)g^{\mu\nu}]\Bigg\{\sqrt{2}\,\mathrm{Re}\big(C_{uG}^{33}\big)\,m m_h^2 v\sqrt{\alpha_s}\\ &\qquad\times\Big[16\pi^2 B_0(p;m^2,m^2) + 16\pi^2 B_0(p_1;m^2,m^2)\\ &\qquad\qquad + 32\pi^2 m^2 C_0(p_1,p_2;m^2,m^2,m^2) - i\Big]\\ &\quad + 4\sqrt{\pi}\,m\alpha_s\,\mathcal{X}\Big[8\pi^2(4m^2-m_h^2)C_0(p_1,p_2;m^2,m^2,m^2)+i\Big]\\ &\quad + 8i\pi^{3/2}C_{\varphi G,0}\,m_h^2 v^2\Bigg\},\end{aligned} \tag{A.25}$$

where we have introduced the convenient combination

$$\mathcal{X} = C_{\varphi\Box} m v^2 - \frac{1}{4}C_{\varphi D} m v^2 - \frac{1}{\sqrt{2}}\,\mathrm{Re}\big(C_{u\varphi}^{33}\big)\,v^3 + \Lambda^2 m. \tag{A.26}$$

The scalar integrals appearing in the amplitude can be written in the following way [25]

$$\begin{aligned} B_0(p;m^2,m^2) &= \frac{i}{16\pi^2}\,\Gamma(1+\epsilon)\left(\frac{4\pi\mu^2}{m^2}\right)^{\epsilon}\left[\frac{1}{\epsilon}+2-2g(\tau)\right]+\mathcal{O}(\epsilon),\\ B_0(p_1;m^2,m^2) &= \frac{i}{16\pi^2}\,\Gamma(1+\epsilon)\left(\frac{4\pi\mu^2}{m^2}\right)^{\epsilon}\frac{1}{\epsilon}+\mathcal{O}(\epsilon),\\ C_0(p_1,p_2;m^2,m^2,m^2) &= -\frac{i}{16\pi^2 m^2}\,\frac{\tau}{2}f(\tau)+\mathcal{O}(\epsilon),\end{aligned} \tag{A.27}$$

where $\tau \equiv 4m^2/m_h^2$ and the functions $f(\tau)$ and $g(\tau)$ read

$$\begin{aligned} f(\tau) &= \begin{cases} \arcsin^2\!\left(\dfrac{1}{\sqrt{\tau}}\right), & \tau\geq 1,\\ -\dfrac{1}{4}\left[\ln\!\left(\dfrac{1+\sqrt{1-\tau}}{1-\sqrt{1-\tau}}\right)-i\pi\right]^2, & \tau<1,\end{cases}\\ g(\tau) &= \begin{cases} \sqrt{\tau-1}\,\arcsin\!\left(\dfrac{1}{\sqrt{\tau}}\right), & \tau\geq 1,\\ \sqrt{1-\tau}\left[\ln\!\left(\dfrac{1+\sqrt{1-\tau}}{1-\sqrt{1-\tau}}\right)-i\pi\right], & \tau<1.\end{cases}\end{aligned} \tag{A.28}$$

With these definition we can rewrite Eq. (A.25) in the standard form

$$\boxed{\mathcal{M}^{\text{SMEFT}} = i\,\frac{\alpha_s}{3\pi v}\,\delta^{ab}\,\varepsilon_{1\mu}\varepsilon_{2\nu}\,[p_1^\nu p_2^\mu-(p_1\cdot p_2)g^{\mu\nu}]\,F(\tau).} \tag{A.29}$$

where, the form factor $F(\tau)$ reads

$$F(\tau) = \Gamma(1+\epsilon)\left(\frac{4\pi\mu^2}{m^2}\right)^\epsilon \left[c_t F_1(\tau) + c_{g0}F_2(\tau) + \mathrm{Re}(c_{tg})\frac{m^2}{v^2}F_{30}(\tau)\right], \tag{A.30}$$

with

$$\begin{aligned} F_1(\tau) &= \frac{3}{2}\tau\left[1+(1-\tau)f(\tau)\right], \\ F_2(\tau) &= 12, \\ F_{30}(\tau) &= \frac{6}{\epsilon} + 3\left[1 - \tau f(\tau) - 2g(\tau)\right], \end{aligned} \tag{A.31}$$

and in our notation

$$c_t = \frac{\mathcal{X}}{\Lambda^2 m}, \quad c_{g0} = \frac{\pi v^2}{\alpha_s\Lambda^2}C_{\varphi G,0}, \quad \mathrm{Re}(c_{tg}) = \frac{v^3}{\sqrt{2\pi\alpha_s}m\Lambda^2}\,\mathrm{Re}\big(C_{uG}^{33}\big). \tag{A.32}$$

The above expression of the amplitude precisely coincide with the known result obtained in Ref. [25]. The different normalization of the Wilson coefficients simply derives from using different conventions.

As a last step we should apply the renormalization procedure. Notice that the chromomagnetic form factor $F_{30}(\tau)$ contains an ultraviolet divergence of the form $1/\epsilon$. As discussed in Ref. [25], this divergence can be absorbed into the renormalization of the coefficient c_g. The bare coefficient is written as

$$c_{g0} = c_g(\mu_R) + \delta c_g, \tag{A.33}$$

where μ_R denotes the renormalization scale of c_g and the $\overline{\mathrm{MS}}$ counterterm is

$$\delta c_g = \frac{m^2}{2v^2}\,\mathrm{Re}(c_{tg})\Gamma(1+\epsilon)(4\pi)^\epsilon\left(-\frac{1}{\epsilon} - \ln\frac{\mu^2}{\mu_R^2}\right). \tag{A.34}$$

This counterterm reflects the one-loop mixing of Q_{uG}^{33} into $Q_{\varphi G}$ appearing in the SMEFT renormalization-group equations [70].

Since $F_2(\tau) = 12$, the counterterm proportional to δc_g contributes precisely to the same Lorentz structure as the chromomagnetic term. After consistently expanding the dimensional-regularization factors to order ϵ^0, the subtraction acting on F_{30} yields

$$F_3(\tau) = 3\left[1 - \tau f(\tau) - 2g(\tau) + 2\ln\frac{\mu_R^2}{m^2}\right]. \tag{A.35}$$

The $1/\epsilon$ pole has thus completely disappeared, as expected.

The final renormalized form factor can therefore be written as

$$\boxed{F(\tau) = c_t F_1(\tau) + c_g(\mu_R)F_2(\tau) + \mathrm{Re}(c_{tg})\frac{m^2}{v^2}F_3(\tau).} \tag{A.36}$$

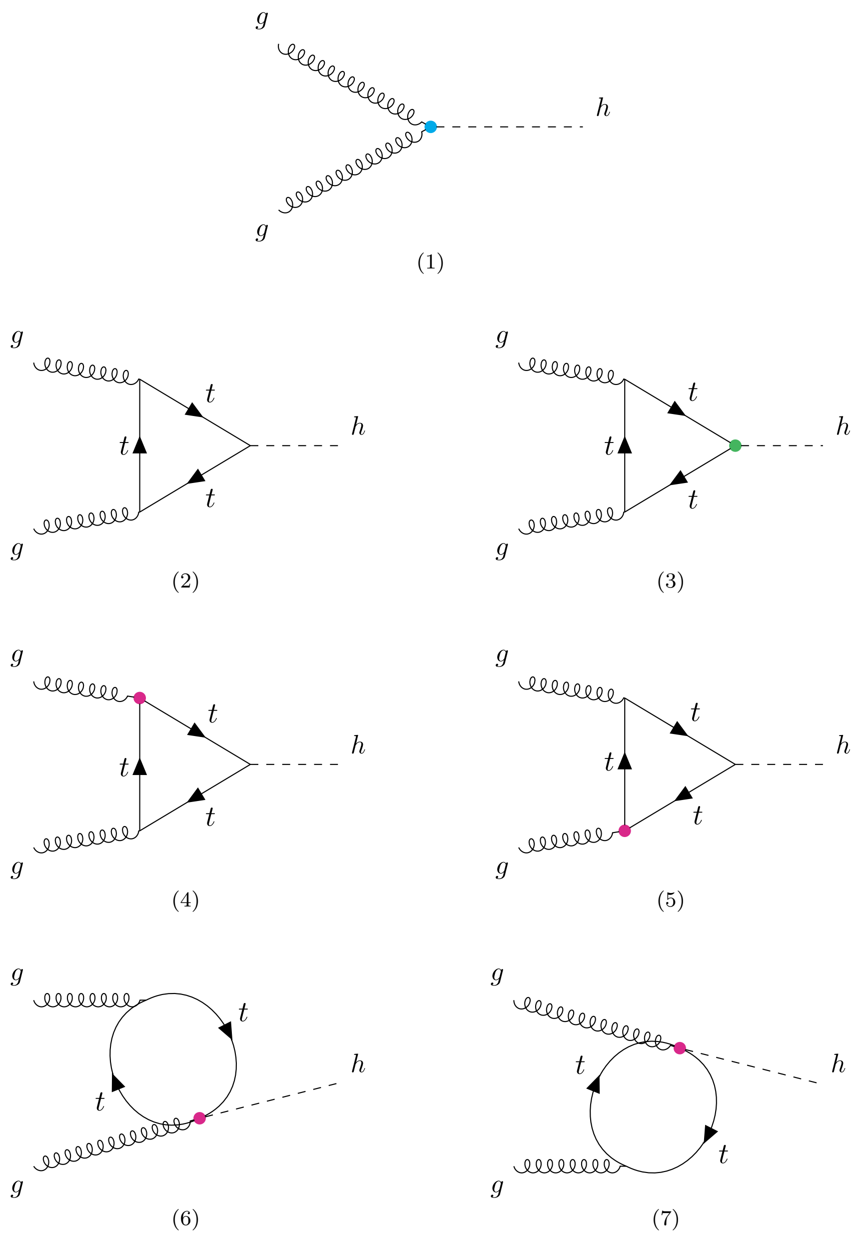

Figure A.1: Leading-order contributions to $gg \to h$ in the SMEFT at linear order in $1/\Lambda^2$. Diagram (1) corresponds to the direct Higgs–gluon interaction generated by $Q_{\varphi G}$. Diagram (2) is the pure Standard Model contribution. Diagram (3) denotes the SM-like top-loop contribution with a modified Higgs–top interaction, receiving corrections from $Q_{u\varphi}^{33}$, $Q_{\varphi\Box}$, and $Q_{\varphi D}$. Diagrams (4)–(7) arise from a single insertion of the chromomagnetic operator Q_{uG}^{33}. Standard Model vertices are left unmarked, while green, magenta, and cyan dots denote the modified Higgs–top, chromomagnetic, and direct Higgs–gluon interactions, respectively.

Appendix B

Representations of the Lorentz group

In this Appendix we briefly review the finite-dimensional representations of the Lorentz group in four spacetime dimensions following Ref. [3]. The notation that we introduce here is extensively employed in the main text, in particular in the spinor helicity formalism.

B.1 The Lorentz group

The Lorentz group can be defined as the group of transformations that leave the Minkowski metric invariant,

$$\Lambda^{\rho}{}_{\mu}\Lambda^{\sigma}{}_{\nu}g_{\rho\sigma} = g_{\mu\nu}, \tag{B.1}$$

where we use the mostly negative convention $g_{\mu\nu} = \mathrm{diag}\{+1, -1, -1, -1\}$. A generic field $\phi_A(x)$, where A denotes a generic Lorentz index, transforms according to

$$U(\Lambda)^{-1}\phi_A(x)U(\Lambda) = L_A{}^B(\Lambda)\,\phi_B(\Lambda^{-1}x), \tag{B.2}$$

where $U(\Lambda)$ acts on the Hilbert space and $L_A{}^B(\Lambda)$ is a finite-dimensional matrix acting on the Lorentz indices of the field. The matrices $L_A{}^B(\Lambda)$ form a representation of the Lorentz group, since they satisfy the composition rule

$$L_A{}^B(\Lambda')L_B{}^C(\Lambda) = L_A{}^C(\Lambda'\Lambda). \tag{B.3}$$

For an infinitesimal Lorentz transformation,

$$\Lambda^{\mu}{}_{\nu} = \delta^{\mu}{}_{\nu} + \omega^{\mu}{}_{\nu}, \qquad \omega_{\mu\nu} = -\omega_{\nu\mu}, \tag{B.4}$$

the corresponding operator acting on the Hilbert space can be written as

$$U(\mathbb{1} + \omega) = \mathbb{1} + \frac{i}{2}\omega_{\mu\nu}M^{\mu\nu}, \tag{B.5}$$

where $M^{\mu\nu}$ are the generators of Lorentz transformations. They satisfy the Lorentz algebra

$$[M^{\mu\nu}, M^{\rho\sigma}] = i\left(g^{\mu\rho}M^{\nu\sigma} - g^{\nu\rho}M^{\mu\sigma} - g^{\mu\sigma}M^{\nu\rho} + g^{\nu\sigma}M^{\mu\rho}\right). \tag{B.6}$$

It is convenient to separate rotations and boosts. We define

$$J_i = \frac{1}{2}\epsilon_{ijk}M^{jk}, \qquad K_i = M^{i0}, \tag{B.7}$$

where J_i generate spatial rotations and K_i generate boosts. The Lorentz algebra then becomes

$$[J_i, J_j] = i\epsilon_{ijk}J_k, \tag{B.8}$$
$$[J_i, K_j] = i\epsilon_{ijk}K_k, \tag{B.9}$$
$$[K_i, K_j] = -i\epsilon_{ijk}J_k. \tag{B.10}$$

The first commutation relation is the usual angular momentum algebra. The presence of the minus sign in the boost commutator reflects the non-compact nature of the Lorentz group.

The classification of finite-dimensional representations becomes simple if we define the combinations

$$N_i = \frac{1}{2}\left(J_i - iK_i\right), \qquad \overline{N}_i = \frac{1}{2}\left(J_i + iK_i\right). \tag{B.11}$$

Using the Lorentz algebra above, one finds

$$[N_i, N_j] = i\epsilon_{ijk}N_k, \tag{B.12}$$
$$[\overline{N}_i, \overline{N}_j] = i\epsilon_{ijk}\overline{N}_k, \tag{B.13}$$
$$[N_i, \overline{N}_j] = 0. \tag{B.14}$$

Therefore, the Lorentz algebra is equivalent, after complexification, to two independent $SU(2)$ algebras,

$$\mathfrak{so}(1,3)_{\mathbb{C}} \simeq \mathfrak{su}(2)_L \oplus \mathfrak{su}(2)_R. \tag{B.15}$$

As a consequence, an irreducible finite-dimensional representation of the Lorentz algebra is labelled by two angular momenta,

$$(j_L, j_R), \tag{B.16}$$

where j_L and j_R are integers or half-integers. The dimension of the representation is

$$\dim(j_L, j_R) = (2j_L + 1)(2j_R + 1). \tag{B.17}$$

Some important examples are reported in Tab. B.1.

Lorentz representation	Dimension	Field type
$(0,0)$	1	scalar representation
$\left(\frac{1}{2},0\right)$	2	left-handed Weyl spinor
$\left(0,\frac{1}{2}\right)$	2	right-handed Weyl spinor
$\left(\frac{1}{2},\frac{1}{2}\right)$	4	Lorentz vector

Table B.1: Some basic finite-dimensional representations of the Lorentz group.

B.1.1 Left- and right-handed spinor fields

We denote the left-handed Weyl spinors with a left-handed spinor index that takes on two possible values

$$\psi_a(x). \tag{B.18}$$

Whereas, we indicated a right-handed Weyl spinor as

$$\psi^\dagger_{\dot a}(x), \tag{B.19}$$

where in this case $\dot a$ is a right-handed spinor. In particular, a right-handed Weyl field is the hermitian conjugate of a field in the $\left(\frac{1}{2},0\right)$ representation, thus we write

$$[\psi_a(x)]^\dagger = \psi^\dagger_{\dot a}(x). \tag{B.20}$$

Under a Lorentz transformations, these object behave in the following way

$$U(\Lambda)^{-1}\psi_a(x)U(\Lambda) = L_a{}^b(\Lambda)\,\psi_b(\Lambda^{-1}x), \tag{B.21}$$

$$U(\Lambda)^{-1}\psi^\dagger_{\dot a}(x)U(\Lambda) = R_{\dot a}{}^{\dot b}(\Lambda)\,\psi^\dagger_{\dot b}(\Lambda^{-1}x), \tag{B.22}$$

where $L_a{}^b$ and $R_{\dot a}{}^{\dot b}$ are matrices in the $\left(\frac{1}{2},0\right)$ and $\left(0,\frac{1}{2}\right)$ representations, respectively.

We introduce another invariant symbol of the Lorentz group ϵ_{ab}, such that

$$L_a{}^c(\Lambda)L_b{}^d(\Lambda)\epsilon_{cd} = \epsilon_{ab}. \tag{B.23}$$

Notice this behavior is similar to that of the Minkowski metric $g_{\mu\nu}$ as reported in Eq. (B.1). In particular, as we use $g_{\mu\nu}$ to raise and lower vector indices, we can then use ϵ_{ab} to raise and lower left-handed spinor indices. Analogously, we can define another invariant symbol whose indices run in the right-handed field representation, namely $\epsilon_{\dot a\dot b}$, such that

$$R_{\dot a}{}^{\dot c}(\Lambda)R_{\dot b}{}^{\dot d}(\Lambda)\varepsilon_{\dot c\dot d} = \varepsilon_{\dot a\dot b}. \tag{B.24}$$

These two-component Levi-Civita tensors are defined as

$$\epsilon^{ab} = -\epsilon_{ab} = \epsilon^{\dot a\dot b} = -\epsilon_{\dot a\dot b} = \begin{pmatrix} 0 & 1 \\ -1 & 0 \end{pmatrix}. \tag{B.25}$$

With this definition, we have

$$\varepsilon_{ab}\varepsilon^{bc} = \delta_a{}^c, \qquad \varepsilon^{ab}\varepsilon_{bc} = \delta^a{}_c. \tag{B.26}$$

We can straightforwardly define

$$\psi^a(x) \equiv \varepsilon^{ab}\psi_b(x), \tag{B.27}$$

which implies that

$$\psi_a = \varepsilon_{ab}\psi^b = \varepsilon_{ab}\varepsilon^{bc}\psi_c = \delta_a{}^c\psi_c, \tag{B.28}$$

as expected. However, the antisymmetry of ε^{ab} implies that one has to be careful with minus signs. For example, the previous definition can be written in different equivalent forms:

$$\psi^a = \varepsilon^{ab}\psi_b = -\varepsilon^{ba}\psi_b = -\psi_b\varepsilon^{ba} = \psi_b\varepsilon^{ab}. \tag{B.29}$$

We must also be careful about signs when contracting indices. For instance,

$$\psi^a\chi_a = \varepsilon^{ab}\psi_b\chi_a = -\varepsilon^{ba}\psi_b\chi_a = -\psi_b\chi^b. \tag{B.30}$$

Another invariant symbol is

$$\sigma^\mu_{a\dot{a}} = (\delta_{a\dot{a}}, \vec{\sigma}_{a\dot{a}}), \tag{B.31}$$

where I is the 2×2 identity matrix, and

$$\sigma_1 = \begin{pmatrix} 0 & 1 \\ 1 & 0 \end{pmatrix}, \qquad \sigma_2 = \begin{pmatrix} 0 & -i \\ i & 0 \end{pmatrix}, \qquad \sigma_3 = \begin{pmatrix} 1 & 0 \\ 0 & -1 \end{pmatrix} \tag{B.32}$$

are the Pauli matrices. Similarly, we can also define

$$\bar{\sigma}^{\mu\,\dot{a}a} \equiv \epsilon^{ac}\epsilon^{\dot{a}\dot{d}}\sigma^\mu_{c\dot{d}}, \tag{B.33}$$

which yields

$$\bar{\sigma}^{\mu\,\dot{a}a} = \left(\delta^{\dot{a}a}, -\vec{\sigma}^{\dot{a}a}\right). \tag{B.34}$$

These two objects satisfy the following useful relations

$$\sigma^\mu_{a\dot{a}}\bar{\sigma}^{\dot{b}b}_\mu = 2\delta_a{}^b\delta_{\dot{a}}{}^{\dot{b}}, \tag{B.35}$$

$$\mathrm{Tr}(\bar{\sigma}^\mu\sigma^\nu) = (\bar{\sigma}^\mu)^{\dot{a}a}(\sigma^\nu)_{a\dot{a}} = 2g^{\mu\nu}. \tag{B.36}$$

Also,

$$\mathrm{Tr}\left(\bar{\sigma}^\alpha\sigma^\beta\bar{\sigma}^\gamma\sigma^\delta\right) + \mathrm{Tr}\left(\sigma^\alpha\bar{\sigma}^\beta\sigma^\gamma\bar{\sigma}^\delta\right) = 4(g^{\alpha\beta}g^{\gamma\delta} - g^{\alpha\gamma}g^{\beta\delta} + g^{\alpha\delta}g^{\beta\gamma}), \tag{B.37}$$

where

$$\mathrm{Tr}\left(\bar{\sigma}^{\alpha}\sigma^{\beta}\bar{\sigma}^{\gamma}\sigma^{\delta}\right) = 2(g^{\alpha\beta}g^{\gamma\delta} - g^{\alpha\gamma}g^{\beta\delta} + g^{\alpha\delta}g^{\beta\gamma} + i\epsilon^{\alpha\beta\gamma\delta}), \tag{B.38}$$

and,

$$\mathrm{Tr}\left(\sigma^{\alpha}\bar{\sigma}^{\beta}\sigma^{\gamma}\bar{\sigma}^{\delta}\right) = 2(g^{\alpha\beta}g^{\gamma\delta} - g^{\alpha\gamma}g^{\beta\delta} + g^{\alpha\delta}g^{\beta\gamma} - i\epsilon^{\alpha\beta\gamma\delta}). \tag{B.39}$$

These two equations implement the convention $\epsilon_{0123} = +1$, as in Ref. [46]. This explains why the signs in front of the Levi–Civita tensors are reversed with respect to the corresponding relations reported in Ref. [71].

Moreover, $\sigma^{\mu}_{a\dot{a}}$ and $\bar{\sigma}^{\mu\,\dot{a}a}$ can be casted in a 4×4 matrix

$$\gamma^{\mu} = \begin{pmatrix} 0 & (\sigma^{\mu})_{a\dot{a}} \\ (\bar{\sigma}^{\mu})^{\dot{a}a} & 0 \end{pmatrix}, \tag{B.40}$$

which is the chiral basis representation of the gamma matrices. In this basis the fifth gamma matrix reads

$$\gamma^5 \equiv i\gamma^0\gamma^1\gamma^2\gamma^3 = \begin{pmatrix} -I_2 & 0 \\ 0 & I_2 \end{pmatrix}, \tag{B.41}$$

which explicitly separates the two Weyl representations of the Lorentz group by means of the projector operators $\mathbb{P}_L \equiv \frac{\mathbb{1}-\gamma^5}{2}$ and $\mathbb{P}_R \equiv \frac{\mathbb{1}+\gamma^5}{2}$, namely

$$\psi_L = \mathbb{P}_L\psi = \begin{pmatrix} I_2 & 0 \\ 0 & 0 \end{pmatrix}\psi, \qquad \psi_R = \mathbb{P}_R\psi = \begin{pmatrix} 0 & 0 \\ 0 & I_2 \end{pmatrix}\psi. \tag{B.42}$$

Useful spinor relation. In this paragraph we show a useful relation which is used in Sec. 5.1.1 when matching the on-shell tree-level amplitude hgg onto SMEFT,

$$p_{1\rho}p_{2\sigma}\varepsilon^+_\mu(p_1)\varepsilon^+_\nu(p_2)\epsilon^{\mu\nu\rho\sigma} = -\frac{i}{2}[12]^2. \tag{B.43}$$

We prove it by choosing the reference momenta $r_1 = p_2$ and $r_2 = p_1$ in the definition of the polarization vectors in Eq. (4.60):

$$\begin{aligned}
&\epsilon_{\mu\nu\rho\sigma}\, p_1^\rho p_2^\sigma\, \varepsilon_1^{+\mu}(p_1;p_2)\, \varepsilon_2^{+\nu}(p_2;p_1) \\
&= \epsilon_{\mu\nu\rho\sigma}\, p_1^\rho p_2^\sigma\, \frac{[1|\bar\sigma^\mu|2\rangle}{\sqrt{2}\,\langle 12\rangle}\frac{[2|\bar\sigma^\nu|1\rangle}{\sqrt{2}\,\langle 21\rangle} \\
&= \frac{\epsilon_{\mu\nu\rho\sigma}\, p_1^\rho p_2^\sigma}{2\langle 12\rangle\langle 21\rangle}\left(|1\rangle_b[1|_{\dot a}\right)(\bar\sigma^\mu)^{\dot a a}\left(|2\rangle_a[2|_{\dot b}\right)(\bar\sigma^\nu)^{\dot b b} \\
&= \frac{\epsilon_{\mu\nu\rho\sigma}\, p_1^\rho p_2^\sigma}{2\langle 12\rangle\langle 21\rangle}\, p_{1\alpha}p_{2\beta}\,(\sigma^\alpha)_{b\dot a}(\bar\sigma^\mu)^{\dot a a}(\sigma^\beta)_{a\dot b}(\bar\sigma^\nu)^{\dot b b} \\
&= \frac{\epsilon_{\mu\nu\rho\sigma}\, p_1^\rho p_2^\sigma}{2\langle 12\rangle\langle 21\rangle}\, p_{1\alpha}p_{2\beta}\ \mathrm{Tr}\left(\sigma^\alpha\bar\sigma^\mu\sigma^\beta\bar\sigma^\nu\right) \\
&= -\frac{i\,\epsilon^{\alpha\mu\beta\nu}\epsilon_{\mu\nu\rho\sigma}}{\langle 12\rangle\langle 21\rangle}\, p_1^\rho p_2^\sigma p_{1\alpha}p_{2\beta} \qquad\qquad (\mathrm{B.44}) \\
&= -\frac{i\,\epsilon^{\mu\nu\beta\alpha}\epsilon_{\mu\nu\rho\sigma}}{\langle 12\rangle\langle 21\rangle}\, p_1^\rho p_2^\sigma p_{1\alpha}p_{2\beta} \\
&= \frac{2i}{\langle 12\rangle\langle 21\rangle}\left(\delta^\beta_\rho\delta^\alpha_\sigma - \delta^\beta_\sigma\delta^\alpha_\rho\right)p_1^\rho p_2^\sigma p_{1\alpha}p_{2\beta} \\
&= \frac{2i}{\langle 12\rangle\langle 21\rangle}\left[(p_1\cdot p_2)^2 - p_1^2p_2^2\right] \\
&= \frac{i}{2}\,\frac{\langle 12\rangle^2[21]^2}{\langle 12\rangle\langle 21\rangle} \\
&= -\frac{i}{2}[12]^2.
\end{aligned}$$

In the fifth step, we used Eq. (B.39), whereas in the seventh step we employed the contraction identity

$$\epsilon^{\mu\nu\beta\alpha}\epsilon_{\mu\nu\rho\sigma} = -2\left(\delta^\beta_\rho\delta^\alpha_\sigma - \delta^\beta_\sigma\delta^\alpha_\rho\right). \tag{B.45}$$

B.2 Particles in quantum field theory

We now turn our attention to the application of Lorentz transformations on particle states rather than field. After a brief introduction on what is meant for a particle state in quantum field theory, we will define the so-called little group of the Lorentz group.

In quantum field theory, elementary particles are described as irreducible unitary representations of the Poincaré group, which augments Lorentz group by taking into account space-time translations too. Since spacetime translations are generated by the four-momentum operator P^μ, it is convenient to choose one-particle states that are simultaneous eigenstates of all components of P^μ,

$$P^\mu|p,\sigma\rangle = p^\mu|p,\sigma\rangle. \tag{B.46}$$

Here p^μ labels the four-momentum of the state, while σ denotes any additional quantum number needed to distinguish states with the same momentum.

The commutativity of the momentum generators,

$$[P^\mu, P^\nu] = 0, \tag{B.47}$$

ensures that the four components of P^μ can be simultaneously diagonalized. In addition, the operator $P^2 = P_\mu P^\mu$ is a Casimir operator of the Poincaré algebra; see, e.g., [72]. Therefore, the subspace of states with a fixed eigenvalue of P^2 is invariant under Poincaré transformations.

Indeed, let us define the subspace of states $|\ell\rangle$

$$L_{m^2} = \left\{|\ell\rangle \ : \ P^2|\ell\rangle = m^2|\ell\rangle\right\}. \tag{B.48}$$

Since $P^2 = P_\mu P^\mu$ is a Casimir operator of the Poincaré algebra, it is invariant under Poincaré transformations

$$[P^2, U] = 0, \tag{B.49}$$

where U is the infinite-dimensional unitary representation of the Poicaré group, whose existence is assured by Wigner's theorem [72]. Therefore, for any state $|\ell\rangle \in L_{m^2}$, one has

$$\begin{aligned} P^2\left(U|\ell\rangle\right) &= UP^2|\ell\rangle \\ &= Um^2|\ell\rangle \\ &= m^2\left(U|\ell\rangle\right). \end{aligned} \tag{B.50}$$

Thus $U|\ell\rangle$ is again an eigenstate of P^2 with the same eigenvalue m^2, namely

$$U|\ell\rangle \in L_{m^2}. \tag{B.51}$$

Hence the subspace L_{m^2} is an invariant subspace of the space of physical states under Poincaré transformations.

This, however, does not guarantee apriori that the representation acting on this invariant subspace is irreducible, and indeed it is usually reducible[1].

Up to now, we are sure that the momentum of the particle should be considered as a "quantum number" of the particle state and that there may also be others adding up to its characterization. Therefore, we define a particle state via its momentum p^μ and comprise in σ all other possible labels of the state. Such a state $|p,\sigma\rangle$ clearly satisfies

$$P^2|p,\sigma\rangle = m^2|p,\sigma\rangle. \tag{B.52}$$

B.2.1 Little group

Let $U(\Lambda)$ be the unitary operator associated with a Lorentz transformation Λ. Once a reference state $|k,\sigma\rangle$ has been chosen, we define a generic one-particle state with momentum p^μ as

$$|p,\sigma\rangle \equiv U(L(p;k))\,|k,\sigma\rangle. \tag{B.53}$$

The label σ denotes the remaining degrees of freedom that are not fixed by the momentum.

We can now ask how the state $|p,\sigma\rangle$ transforms under a general Lorentz transformation Λ. Using the definition above, we have

$$\begin{aligned} U(\Lambda)|p,\sigma\rangle &= U(\Lambda)U(L(p;k))\,|k,\sigma\rangle \\ &= U(L(\Lambda p;k))\,U^\dagger(L(\Lambda p;k))\,U(\Lambda)U(L(p;k))\,|k,\sigma\rangle \\ &\equiv U(L(\Lambda p;k))\,U(W)|k,\sigma\rangle, \end{aligned} \tag{B.54}$$

where we have defined

$$W(\Lambda,p;k) \equiv L^{-1}(\Lambda p;k)\Lambda L(p;k). \tag{B.55}$$

This transformation belongs to the little group of k^μ, since

$$\begin{aligned} W(\Lambda,p;k)k &= L^{-1}(\Lambda p;k)\Lambda L(p;k)k \\ &= L^{-1}(\Lambda p;k)\Lambda p \\ &= L^{-1}(\Lambda p;k)(\Lambda p) \\ &= k. \end{aligned} \tag{B.56}$$

Hence, $W(\Lambda,p;k)$ does not change the reference momentum, so it can act non-trivially on the internal label σ. We write this action as

$$U(W(\Lambda,p;k))\,|k,\sigma\rangle = D_{\sigma'\sigma}(W(\Lambda,p;k))\,|k,\sigma'\rangle, \tag{B.57}$$

where $D_{\sigma'\sigma}(W)$ is a finite-dimensional representation of the little group.

[1] At this point one would need to introduce another Casimir of the Poincaré group which is the square of the Pauli-Lubanski opertor. For a complete discussion on the subject please see [72].

Substituting this into the transformation law gives

$$\begin{aligned} U(\Lambda)|p,\sigma\rangle &= D_{\sigma'\sigma}(W(\Lambda,p;k))\,U(L(\Lambda p;k))\,|k,\sigma'\rangle \\ &= D_{\sigma'\sigma}(W(\Lambda,p;k))\,|\Lambda p,\sigma'\rangle. \end{aligned} \tag{B.58}$$

Thus, under a Lorentz transformation, the momentum label transforms as $p \to \Lambda p$, while the remaining label σ transforms according to a representation of the little group. This is the sense in which the little group classifies the spin degrees of freedom of one-particle states.

In D spacetime dimensions, the little group for massive particles is $SO(D-1)$ [48]. For massless particles, the little group is the group of Euclidean symmetries in $(D-2)$ dimensions, namely $SO(D-2)$ augmented by $(D-2)$ translations [48]. Finite-dimensional representations require all states to have vanishing eigenvalues under these translations, and hence the relevant little group reduces to $SO(D-2)$.

Appendix C

Massive spinor conventions

This Appendix collects the relevant relations among massive spinors which are omitted from the main text for brevity. We first introduce useful relations of the formalism which are extensively used in calculations and then introduce the high energy limit, along with the massive polarization vectors. In this discussion we mainly follow Ref. [46].

C.1 Useful relations among massive spinors

In the massive spinor helicity formalism several useful bilinear forms can be obtained by using the expressions of the momentum in terms of spinor variables, Eq. (4.107), and the equations of motions, Eq. (4.111),

$$\begin{aligned} |p^I\rangle_\alpha \, \langle p_I|^\beta &= -m\, \delta_\alpha^\beta, & |p^I]^{\dot\alpha}\, [p_I|_{\dot\beta} &= m\, \delta^{\dot\alpha}_{\dot\beta}, \\ \langle p^I|p^J\rangle &= -m\, \epsilon^{IJ}, & [p^I|p^J] &= m\, \epsilon^{IJ}, \\ \langle p^I|p_J\rangle &= m\, \delta^I_J, & [p^I|p_J] &= -m\, \delta^I_J, \\ \langle p_I|p_J\rangle &= m\, \epsilon_{IJ}, & [p_I|p_J] &= -m\, \epsilon_{IJ}. \end{aligned} \tag{C.1}$$

Moreover, as for the massless case, we use the following convention for spinors of negative momentum

$$|-p^I\rangle = -|p^I\rangle, \qquad |-p_I] = +|p_I]. \tag{C.2}$$

Also, for real momenta, complex conjugation acts in the following way

$$\big(|p^I\rangle\big)^* = [p_I|, \qquad \big(|p]^I\big)^* = -\langle p|_I, \tag{C.3}$$

consistently with the wavefunctions definitions of Eq. (4.110).

C.2 The high energy limit

Let p^μ be a massive momentum satisfying $p^2 = m^2$. Choosing a reference frame in which the spatial momentum is directed along the z-axis, we write

$$p^\mu = k^\mu + q^\mu, \tag{C.4}$$

where

$$k^\mu = \frac{E+p}{2}\begin{pmatrix}1\\0\\0\\1\end{pmatrix}, \qquad q^\mu = \frac{E-p}{2}\begin{pmatrix}1\\0\\0\\-1\end{pmatrix}, \qquad p \equiv |\mathbf{p}| = \sqrt{E^2-m^2}. \tag{C.5}$$

Indeed,

$$p^\mu = \begin{pmatrix}E\\0\\0\\p\end{pmatrix}, \qquad p^2 = (k+q)^2 = E^2 - p^2 = m^2. \tag{C.6}$$

Moreover, both k^μ and q^μ are null momenta:

$$k^2 = \left(\frac{E+p}{2}\right)^2 - \left(\frac{E+p}{2}\right)^2 = 0, \tag{C.7}$$

$$q^2 = \left(\frac{E-p}{2}\right)^2 - \left(-\frac{E-p}{2}\right)^2 = 0. \tag{C.8}$$

In the high-energy limit, $E \gg m$, one finds

$$E+p = E\left(1+\sqrt{1-\frac{m^2}{E^2}}\right) = 2E - \frac{m^2}{2E} + \mathcal{O}\left(\frac{m^4}{E^3}\right) \longrightarrow 2E, \tag{C.9}$$

$$E-p = E\left(1-\sqrt{1-\frac{m^2}{E^2}}\right) = \frac{m^2}{2E} + \mathcal{O}\left(\frac{m^4}{E^3}\right) \longrightarrow \frac{m^2}{2E}. \tag{C.10}$$

Hence,

$$\boxed{q^\mu \longrightarrow 0, \qquad k^\mu \longrightarrow p^\mu \qquad \text{as} \qquad m \longrightarrow 0.} \tag{C.11}$$

Let us now formalize the high energy limit in terms of spinor helicity variables. First, the massive momentum can be written in bispinor form as

$$\begin{aligned} |p^I\rangle_a [p_I|_{\dot a} &= p_{a\dot a} = k_{a\dot a} + q_{a\dot a} \\ &= |k\rangle_a [k|_{\dot a} + |q\rangle_a [q|_{\dot a}, \end{aligned} \tag{C.12}$$

$$\begin{aligned} |p_I]^{\dot a} \langle p^I|^a &= \bar p^{\dot a a} = k^{\dot a a} + q^{\dot a a} \\ &= |k]^{\dot a} \langle k|^a + |q]^{\dot a} \langle q|^a. \end{aligned} \tag{C.13}$$

Therefore, we must have that the massive spinors can be expanded in a basis $\zeta^{\pm I}$ of the two-dimensional little-group space:

$$|p^I\rangle_a = |k\rangle_a\,\zeta^{-I} + |q\rangle_a\,\zeta^{+I}, \tag{C.14}$$
$$[p^I|_{\dot a} = [k|_{\dot a}\,\zeta^{+I} - [q|_{\dot a}\,\zeta^{-I}. \tag{C.15}$$

Here $I = 1, 2$ is an index in the fundamental representation of the massive little group $SU(2)$. For a particle of spin s, the corresponding wavefunction carries $2s$ symmetrized little-group indices as explained in the main text.

An explicit choice of basis is

$$\zeta^{+I} = \begin{pmatrix}1\\0\end{pmatrix}, \qquad \zeta^{-I} = \begin{pmatrix}0\\1\end{pmatrix}. \tag{C.16}$$

With these conventions we can verify that

$$\epsilon_{IJ}\zeta^{+I}\zeta^{+J} = 0, \qquad \epsilon_{IJ}\zeta^{-I}\zeta^{-J} = 0, \tag{C.17}$$
$$\epsilon_{IJ}\zeta^{+I}\zeta^{-J} = -1, \qquad \epsilon_{IJ}\zeta^{-I}\zeta^{+J} = 1. \tag{C.18}$$

As a consistency check we may use Eqs. (C.14) and (C.15), obtaining

$$\begin{aligned}
p_{a\dot a} &= \epsilon_{IJ}|p^I\rangle_a[p^J|_{\dot a} \\
&= \epsilon_{IJ}\left(|k\rangle_a\zeta^{-I} + |q\rangle_a\zeta^{+I}\right)\left([k|_{\dot a}\zeta^{+J} - [q|_{\dot a}\zeta^{-J}\right) \\
&= \epsilon_{IJ}\zeta^{-I}\zeta^{+J}|k\rangle_a[k|_{\dot a} - \epsilon_{IJ}\zeta^{+I}\zeta^{-J}|q\rangle_a[q|_{\dot a} \\
&= |k\rangle_a[k|_{\dot a} + |q\rangle_a[q|_{\dot a}.
\end{aligned} \tag{C.19}$$

which correctly reproduces Eq. (C.12).

C.3 Massive polarization vectors

The polarization vector associated with a massive spin-one particle of momentum p and mass m can be written in the massive spinor-helicity formalism as [46]

$$\varepsilon^{IJ}_{\mu} = \frac{\langle p^I|\sigma_\mu|p^J]}{\sqrt{2}\,m}, \qquad \text{or equivalently,} \qquad \varepsilon^{IJ}_{\alpha\dot\alpha} = \sqrt{2}\,\frac{|p^I\rangle_\alpha[p^J|_{\dot\alpha}}{m}. \tag{C.20}$$

Here $I, J = 1, 2$ are indices in the fundamental representation of the massive little group $SU(2)$. We require symmetrization over these two indices, since for a massive spin-one particle we select the symmetric triplet representation, which contains the three physical polarization states. In particular, the three independent components of the symmetric product of two little-group doublets correspond to the two transverse polarization states and the longitudinal one.

More explicitly, the positive- and negative-helicity components are

$$\varepsilon_\mu^+ \equiv \varepsilon_\mu^{11} = \frac{\langle p^1|\sigma_\mu|p^1]}{\sqrt{2}\,m}, \tag{C.21}$$

$$\varepsilon_\mu^- \equiv \varepsilon_\mu^{22} = \frac{\langle p^2|\sigma_\mu|p^2]}{\sqrt{2}\,m}, \tag{C.22}$$

whereas the longitudinal component is

$$\varepsilon_\mu^0 \equiv \varepsilon_\mu^{12} = \varepsilon_\mu^{21} = \frac{\langle p^1|\sigma_\mu|p^2] + \langle p^2|\sigma_\mu|p^1]}{2m}. \tag{C.23}$$

These polarization vectors obey the standard orthonormality relation

$$\varepsilon_\mu^i \left(\varepsilon^{j\mu}\right)^* = -\delta^{ij}, \qquad i,j = +,-,0. \tag{C.24}$$

The sum over the three physical polarization states gives

$$\sum_{i=+,-,0} \varepsilon_\mu^i \left(\varepsilon_\nu^i\right)^* = -\left(g_{\mu\nu} - \frac{p_\mu p_\nu}{m^2}\right). \tag{C.25}$$

This expression also coincides with the numerator of the propagator of a massive vector boson in unitary gauge.

Massless limit. In the high-energy or massless limit, the two transverse massive polarization vectors reduce to the corresponding massless polarization vectors. Using the decomposition introduced in the previous sections, namely Eqs. (C.14) and (C.15), the $I = J = 1$ component becomes

$$\begin{aligned} \varepsilon_{a\dot{a}}^{11} &= \sqrt{2}\,\frac{|p^1\rangle_a [p^1|_{\dot{a}}}{m} \\ &= \sqrt{2}\,\frac{|q\rangle_a [k|_{\dot{a}}}{m} \xrightarrow{m\to 0} \sqrt{2}\,\frac{|r\rangle_a [p|_{\dot{a}}}{\langle pr\rangle} \equiv \varepsilon_{a\dot{a}}^+. \end{aligned} \tag{C.26}$$

Similarly, for $I = J = 2$,

$$\begin{aligned} \varepsilon_{a\dot{a}}^{22} &= \sqrt{2}\,\frac{|p^2\rangle_a [p^2|_{\dot{a}}}{m} \\ &= -\sqrt{2}\,\frac{|k\rangle_a [q|_{\dot{a}}}{m} \xrightarrow{m\to 0} \sqrt{2}\,\frac{|p\rangle_a [r|_{\dot{a}}}{[pr]} \equiv \varepsilon_{a\dot{a}}^-. \end{aligned} \tag{C.27}$$

The massless limit was taken as prescribed by Eq. (C.11), namely the momentum q^μ vanishes as m^2, while its associated spinors vanish linearly with m; on the other hand, the momentum k^μ simply becomes p^μ. For the former momentum, we introduced the reference spinors $|r\rangle$ and $|r]$ by writing

$$|q\rangle_a = \frac{m}{\langle kr\rangle}|r\rangle_a, \qquad [q|_{\dot{a}} = \frac{m}{[rk]}[r|_{\dot{a}} = -\frac{m}{[kr]}[r|_{\dot{a}}, \tag{C.28}$$

in this way we retain the direction of the momentum q by using the reference one r. Also we explicitly highlight the high energy behavior of this momentum by introducing the mass m. In this way the massless limit $m \to 0$ can be safely taken and correctly reproduces the two massless polarization vectors reported in Eq. (4.63), as expected.

Let us finally consider the longitudinal polarization. Using the decomposition of the massive spinors introduced above, one finds

$$\begin{aligned}\varepsilon_\mu^0 &= \frac{\langle p^1|\sigma_\mu|p^2] + \langle p^2|\sigma_\mu|p^1]}{2m} \\ &= \frac{-\langle q|\sigma_\mu|q] + \langle k|\sigma_\mu|k]}{2m} \qquad \text{(C.29)} \\ &= \frac{k_\mu - q_\mu}{m}. \qquad \text{(C.30)}\end{aligned}$$

Therefore, in the high-energy limit,

$$\varepsilon_\mu^0 = \frac{p_\mu}{m} + \mathcal{O}\left(\frac{m}{E}\right). \qquad \text{(C.31)}$$

Contrary to the two transverse polarization states, the longitudinal polarization does not admit a finite massless limit. Indeed, a massless spin-one particle possesses only the two physical helicity states $h = \pm 1$, and hence there is no longitudinal polarization state in the massless theory. The singular behavior of ε_μ^0 as $m \to 0$ reflects this change in the particle's little-group representation.

C.4 Identity for an amplitude with two massive and one massless leg

In this section a relation which is needed in Sec. 5.1.3 is derived. In the context of bootstrapping the $\bar{t}tg$ tree level amplitude, the following independent structure emerges

$$[\mathbf{12}]\frac{\langle r|\not{p}_1|3]}{\langle r3\rangle}, \qquad \text{(C.32)}$$

which depends on a arbitrary reference vector r. Here, p_1 and p_2 are the two massive momenta of anti-top and top quarks, respectively. The massless momentum p_3 is instead assigned to the gluon.

We start by making use of the Schouten identity introduced in Eq. (4.53). Its analogous form for dotted spinors reads

$$|i][jk] + |j][ki] + |k][ij] = 0. \qquad \text{(C.33)}$$

Choosing

$$|i] = |\mathbf{1}], \qquad |j] = |\mathbf{2}], \qquad |k] = |3], \qquad \text{(C.34)}$$

we obtain

$$|3][\mathbf{12}] = -|\mathbf{1}][\mathbf{2}3] - |\mathbf{2}][3\mathbf{1}]. \qquad \text{(C.35)}$$

Multiplying Eq. (C.35) from the left by $\langle r|\not{p}_1$, we find

$$\begin{aligned}\langle r|\not{p}_1|3]\,[\mathbf{12}] &= -\langle r|\not{p}_1|\mathbf{1}]\,[\mathbf{2}3] - \langle r|\not{p}_1|\mathbf{2}]\,[3\mathbf{1}]\\ &= m_t\langle r1^I\rangle[3\mathbf{2}] - \langle r|\not{p}_1|\mathbf{2}]\,[3\mathbf{1}],\end{aligned}\tag{C.36}$$

where in the second line we used the massive Weyl equation $\not{p}_1|\mathbf{1}] = m_t|\mathbf{1}\rangle$, together with $[\mathbf{2}3] = -[3\mathbf{2}]$.

The second term can be further simplified by using momentum conservation,

$$p_1 = -p_2 - p_3.\tag{C.37}$$

Indeed,

$$\begin{aligned}-\langle r|\not{p}_1|\mathbf{2}]\,[3\mathbf{1}] &= \Big(\langle r|\not{p}_2|\mathbf{2}] + \langle r|\not{p}_3|\mathbf{2}]\Big)\,[3\mathbf{1}]\\ &= (m_t\langle r\mathbf{2}\rangle + \langle r3\rangle[3\mathbf{2}])\,[3\mathbf{1}]\\ &= m_t\langle r\mathbf{2}\rangle[3\mathbf{1}] + \langle r3\rangle[3\mathbf{1}][3\mathbf{2}].\end{aligned}\tag{C.38}$$

Combining Eqs. (C.36) and (C.38), we therefore obtain

$$[\mathbf{12}]\,\langle r|\not{p}_1|3] = m_t\langle r\mathbf{1}\rangle[3\mathbf{2}] + m_t\langle r\mathbf{2}\rangle[3\mathbf{1}] + \langle r3\rangle[3\mathbf{1}][3\mathbf{2}].$$

Finally, dividing by $\langle r3\rangle$ and suppressing the massive little-group indices through the bold notation gives

$$[\mathbf{12}]\,\frac{\langle r|\not{p}_1|3]}{\langle r3\rangle} = m_t\,\frac{\langle r\mathbf{1}\rangle[3\mathbf{2}] + \langle r\mathbf{2}\rangle[3\mathbf{1}]}{\langle r3\rangle} + [\mathbf{13}][\mathbf{23}].\tag{C.39}$$

Appendix D

Explicit computations for hgg at one loop

In this Appendix, we collect some non-trivial calculations involving both massless and massive spinor-helicity relations, which we exploit in Ch. 7. The aim is to obtain the full LO amplitude for the process of Higgs production via gluon fusion using amplitude methods.

To benchmark the computation, we first compute the SM amplitude, providing two different procedures which eventually lead to the same result. Furthermore, we introduce the loop-momentum parametrizations for the triple, double, and single cuts, which we exploit in the generalized unitarity algorithm discussed in Sec. 7.2.

Eventually, we display the relevant calculations involved in the BSM contribution to the amplitude.

D.1 Computation of SM integrand

D.1.1 SM integrand–way 1

In Sec. 7.1 of the main text, we aim to find the complete SM expression for the hgg process at one loop. In order to do so, we implement the lower-point tree-level amplitudes that make up the two relevant Feynman diagrams of Fig. 7.1. By doing so, we obtain Eq. (7.16), which we report here for completeness:

$$\begin{aligned}\mathcal{A}_{++}(k) = &-\frac{2\pi\alpha_s m}{v}\,\delta^{ab}\left([k_3^L|k_I] - \langle k_3^L|k_I\rangle\right)\\ &\times \varepsilon_\mu^+(p_2;p_3)\left(-\langle k_{2,J}|\gamma^\mu|k^I] + \langle k^I|\gamma^\mu|k_{2,J}]\right)\\ &\times \varepsilon_\nu^+(p_3;p_2)\left(-\langle k_{3,L}|\gamma^\nu|k_2^J] + \langle k_2^J|\gamma^\nu|k_{3,L}]\right),\end{aligned} \tag{D.1}$$

In this section we perform the explicit calculation of the eight resulting terms. Eventually, we will obtain Eq. (7.18) of the main text. The calculation reads

$$\begin{aligned}[k_I|k_3^L]\langle k_{2J}|\gamma^\mu|k^I]\langle k_{3L}|\gamma^\nu|k_2^J] &= [k_I|k_3^L]\langle k_{3L}|\gamma^\nu|k_2^J]\langle k_{2J}|\gamma^\mu|k^I] \\ &= [k_I|_{\dot a}\,|k_3^L]^{\dot a}\,\langle k_{3L}|^b(\sigma^\nu)_{b\dot c}|k_2^J]^{\dot c}\,\langle k_{2J}|^d(\sigma^\mu)_{d\dot e}|k^I]^{\dot e} \\ &= k_{3,\alpha}k_{2,\beta}\,|k^I]^{\dot e}[k_I|_{\dot a}\,(\bar\sigma^\alpha)^{\dot a b}(\sigma^\nu)_{b\dot c}(\bar\sigma^\beta)^{\dot c d}(\sigma^\mu)_{d\dot e} \\ &= m\,k_{3,\alpha}k_{2,\beta}\ \mathrm{Tr}\left(\bar\sigma^\alpha\sigma^\nu\bar\sigma^\beta\sigma^\mu\right). \qquad \text{(D.2)}\end{aligned}$$

$$\begin{aligned}-[k_I|k_3^L]\langle k_{2J}|\gamma^\mu|k^I][k_{3L}|\gamma^\nu|k_2^J\rangle &= -[k_I|k_3^L][k_{3L}|\gamma^\nu|k_2^J\rangle\langle k_{2J}|\gamma^\mu|k^I] \\ &= -[k_I|_{\dot a}|k_3^L]^{\dot a}[k_{3L}|_{\dot b}(\bar\sigma^\nu)^{\dot b c}|k_2^J\rangle_c\langle k_{2J}|^d(\sigma^\mu)_{d\dot e}|k^I]^{\dot e} \\ &= m^2\,[k_I|_{\dot b}(\bar\sigma^\nu)^{\dot b d}(\sigma^\mu)_{d\dot e}|k^I]^{\dot e} \\ &= m^2\,|k^I]^{\dot e}[k_I|_{\dot b}(\bar\sigma^\nu)^{\dot b d}(\sigma^\mu)_{d\dot e} \\ &= m^3\,(\bar\sigma^\nu)^{\dot e d}(\sigma^\mu)_{d\dot e} \\ &= m^3\ \mathrm{Tr}\,(\bar\sigma^\nu\sigma^\mu)\,. \qquad \text{(D.3)}\end{aligned}$$

$$\begin{aligned}-[k_I|k_3^L][k_{2J}|\gamma^\mu|k^I\rangle\langle k_{3L}|\gamma^\nu|k_2^J] &= -[k_I|k_3^L]\langle k_{3L}|\gamma^\nu|k_2^J][k_{2J}|\gamma^\mu|k^I\rangle \\ &= -[k_I|_{\dot a}|k_3^L]^{\dot a}\langle k_{3L}|^b(\sigma^\nu)_{b\dot c}|k_2^J]^{\dot c}[k_{2J}|_{\dot d}(\bar\sigma^\mu)^{\dot d e}|k^I\rangle_e \\ &= m\,[k_I|_{\dot a}\,\bar k_3^{\dot a b}(\sigma^\nu)_{b\dot d}(\bar\sigma^\mu)^{\dot d e}|k^I\rangle_e \\ &= m\,|k^I\rangle_e[k_I|_{\dot a}\,\bar k_3^{\dot a b}(\sigma^\nu)_{b\dot d}(\bar\sigma^\mu)^{\dot d e} \\ &= m\,k_{e\dot a}\,\bar k_3^{\dot a b}(\sigma^\nu)_{b\dot d}(\bar\sigma^\mu)^{\dot d e} \\ &= m\,k_\alpha k_{3,\beta}\,(\sigma^\alpha)_{e\dot a}(\bar\sigma^\beta)^{\dot a b}(\sigma^\nu)_{b\dot d}(\bar\sigma^\mu)^{\dot d e} \\ &= m\,k_\alpha k_{3,\beta}\ \mathrm{Tr}\left(\sigma^\alpha\bar\sigma^\beta\sigma^\nu\bar\sigma^\mu\right). \qquad \text{(D.4)}\end{aligned}$$

$$\begin{aligned}[k_I|k_3^L][k_{2J}|\gamma^\mu|k^I\rangle[k_{3L}|\gamma^\nu|k_2^J\rangle &= [k_I|k_3^L][k_{3L}|\gamma^\nu|k_2^J\rangle[k_{2J}|\gamma^\mu|k^I\rangle \\ &= [k_I|_{\dot a}|k_3^L]^{\dot a}[k_{3L}|_{\dot b}(\bar\sigma^\nu)^{\dot b c}|k_2^J\rangle_c[k_{2J}|_{\dot d}(\bar\sigma^\mu)^{\dot d e}|k^I\rangle_e \\ &= -m\,k_{2,\alpha}\,|k^I\rangle_e[k_I|_{\dot b}(\bar\sigma^\nu)^{\dot b c}(\sigma^\alpha)_{c\dot d}(\bar\sigma^\mu)^{\dot d e} \\ &= m\,k_{2,\alpha}k_\beta\ \mathrm{Tr}\left(\sigma^\beta\bar\sigma^\nu\sigma^\alpha\bar\sigma^\mu\right). \qquad \text{(D.5)}\end{aligned}$$

$$\begin{aligned}-\langle k_I|k_3^L\rangle\langle k_{2J}|\gamma^\mu|k^I]\langle k_{3L}|\gamma^\nu|k_2^J] &= -\langle k_I|k_3^L\rangle\langle k_{3L}|\gamma^\nu|k_2^J]\langle k_{2J}|\gamma^\mu|k^I] \\ &= -\langle k_I|^a|k_3^L\rangle_a\langle k_{3L}|^b(\sigma^\nu)_{b\dot c}|k_2^J]^{\dot c}\langle k_{2J}|^d(\sigma^\mu)_{d\dot e}|k^I]^{\dot e} \\ &= m\,k_{2,\alpha}\,\langle k_I|^b(\sigma^\nu)_{b\dot c}(\bar\sigma^\alpha)^{\dot c d}(\sigma^\mu)_{d\dot e}|k^I]^{\dot e} \\ &= m\,k_{2,\alpha}k_\beta\ \mathrm{Tr}\left(\bar\sigma^\beta\sigma^\nu\bar\sigma^\alpha\sigma^\mu\right). \qquad \text{(D.6)}\end{aligned}$$

$$\begin{aligned}\langle k_I|k_3^L\rangle\langle k_{2J}|\gamma^\mu|k^I][k_{3L}|\gamma^\nu|k_2^J\rangle &= \langle k_I|k_3^L\rangle[k_{3L}|\gamma^\nu|k_2^J\rangle\langle k_{2J}|\gamma^\mu|k^I]\\ &= \langle k_I|^a|k_3^L\rangle_a[k_{3L}|_{\dot b}(\bar\sigma^\nu)^{\dot b c}|k_2^J\rangle_c\langle k_{2J}|^d(\sigma^\mu)_{d\dot e}|k^I]^{\dot e}\\ &= m\,k_{3,\alpha}k_\beta\ \mathrm{Tr}\left(\bar\sigma^\beta\sigma^\alpha\bar\sigma^\nu\sigma^\mu\right)\\ &= m\,k_{3,\beta}k_\alpha\ \mathrm{Tr}\left(\bar\sigma^\alpha\sigma^\beta\bar\sigma^\nu\sigma^\mu\right).\end{aligned}\tag{D.7}$$

$$\begin{aligned}\langle k_I|k_3^L\rangle[k_{2J}|\gamma^\mu|k^I\rangle\langle k_{3L}|\gamma^\nu|k_2^J] &= \langle k_I|k_3^L\rangle\langle k_{3L}|\gamma^\nu|k_2^J][k_{2J}|\gamma^\mu|k^I\rangle\\ &= \langle k_I|^a|k_3^L\rangle_a\langle k_{3L}|^b(\sigma^\nu)_{b\dot c}|k_2^J]^{\dot c}[k_{2J}|_{\dot d}(\bar\sigma^\mu)^{\dot d e}|k^I\rangle_e\\ &= m^3\ \mathrm{Tr}\left(\sigma^\nu\bar\sigma^\mu\right).\end{aligned}\tag{D.8}$$

$$\begin{aligned}-\langle k_I|k_3^L\rangle[k_{2J}|\gamma^\mu|k^I\rangle[k_{3L}|\gamma^\nu|k_2^J\rangle &= -\langle k_I|k_3^L\rangle[k_{3L}|\gamma^\nu|k_2^J\rangle[k_{2J}|\gamma^\mu|k^I\rangle\\ &= -\langle k_I|^a|k_3^L\rangle_a[k_{3L}|_{\dot b}(\bar\sigma^\nu)^{\dot b c}|k_2^J\rangle_c[k_{2J}|_{\dot d}(\bar\sigma^\mu)^{\dot d e}|k^I\rangle_e\\ &= m\,k_{3,\alpha}k_{2,\beta}\ \mathrm{Tr}\left(\sigma^\alpha\bar\sigma^\nu\sigma^\beta\bar\sigma^\mu\right).\end{aligned}\tag{D.9}$$

In these equations we exploited the massive momentum spinor variables defined in Eq. (4.107), as well as the relations contained in Eq. (C.1).

Applying these equations, we obtain

$$\begin{aligned}\mathcal{A}_{++}(k) =\ & -\frac{2\pi\alpha_s m}{v}\,\delta^{ab}\varepsilon^+_\mu(p_2;p_3)\,\varepsilon^+_\nu(p_3;p_2)\\ &\times\Bigg\{m\Bigg[\mathrm{Tr}\left(\bar\sigma^\alpha\sigma^\nu\bar\sigma^\beta\sigma^\mu\right)+\mathrm{Tr}\left(\sigma^\alpha\bar\sigma^\nu\sigma^\beta\bar\sigma^\mu\right)\Bigg]\left(k_{3,\alpha}k_{2,\beta}+k_\alpha k_{2,\beta}\right)\\ &+m\Bigg[\mathrm{Tr}\left(\bar\sigma^\alpha\sigma^\beta\bar\sigma^\nu\sigma^\mu\right)+\mathrm{Tr}\left(\sigma^\alpha\bar\sigma^\beta\sigma^\nu\bar\sigma^\mu\right)\Bigg]k_\alpha k_{3,\beta}\\ &+m^3\Bigg[\mathrm{Tr}\left(\bar\sigma^\nu\sigma^\mu\right)+\mathrm{Tr}\left(\sigma^\nu\bar\sigma^\mu\right)\Bigg]\Bigg\},\end{aligned}\tag{D.10}$$

which is Eq. (7.18) of the main text. After performing the traces using FORM [57–59], we contracted the indices using Eqs.(7.13) and (7.14), and performed some spinor manipulations. The expression then reads

$$\begin{aligned}\mathcal{A}_{++}(k) =\ & -\frac{8\pi\alpha_s m^2}{v}\,\delta^{ab}\left(-\frac{[23]^2}{m_H^2}\right)\Bigg\{-\langle 2|\not{k}|2]-\left(m^2-k^2\right)+\frac{m_H^2}{2}\\ &+\frac{2}{m_H^2}[2|\not{k}|3\rangle[3|\not{k}|2\rangle\Bigg\},\end{aligned}\tag{D.11}$$

namely Eq. (7.21) of the main text. For a more detailed derivation of this last part, see the main text.

D.1.2 SM amplitude–way 2

In this section, we provide an alternative derivation of the integrand $\mathcal{A}_{++}(k)$ in Eq. (7.19). In the main text, we factor out the polarization vectors ε_2^+ and ε_3^+ and make them explicit only at the end, when converting the expression back to spinor-helicity variables. In this section, we instead use the slashed polarization vectors defined in Eq. (4.63) from the outset. We will obtain the same result as in the main text, but only after applying the Schouten identity to one term.

We start from the integrand expression for the SM contribution, in which, with respect to Eq. (7.16), the polarization vectors are contracted with the γ matrices,

$$\begin{aligned}\mathcal{A}_{++}(k) = & -\frac{2\pi\alpha_s m}{v}\,\delta^{ab}\left([k_3^L|k_I] - \langle k_3^L|k_I\rangle\right)\\ & \times\left(-\langle k_{2,J}|\not{\varepsilon}_2^+|k^I] + \langle k^I|\not{\varepsilon}_2^+|k_{2,J}]\right)\\ & \times\left(-\langle k_{3,L}|\not{\varepsilon}_3^+|k_2^J] + \langle k_2^J|\not{\varepsilon}_3^+|k_{3,L}]\right)\\ = & \frac{4\pi\alpha_s m}{v}\,\delta^{ab}\,\frac{[23]^2}{m_h^4}\left([k_3^L|k_I] - \langle k_3^L|k_I\rangle\right)\\ & \times\left(-\langle k_{2,J}|3\rangle[2|k^I] + \langle k^I|3\rangle[2|k_{2,J}]\right)\\ & \times\left(-\langle k_{3,L}|2\rangle[3|k_2^J] + \langle k_2^J|2\rangle[3|k_{3,L}]\right),\end{aligned} \tag{D.12}$$

As before, eight terms need to be evaluated. We report the explicit calculation below

$$\begin{aligned}[2|k^I]\,[k_I|k_3^L]\,\langle k_{3L}|2\rangle\,[3|k_{2J}]\,\langle k_2^J|3\rangle &= m\,[2|\not{k}|2\rangle\,[3|\not{k}_2|3\rangle\\ &= m\left([2|\not{k}|2\rangle - [23]\langle 32\rangle\right)\left([3|\not{k}|3\rangle - [32]\langle 23\rangle\right)\\ &= m\left([2|\not{k}|2\rangle - m_H^2\right)\left([3|\not{k}|3\rangle - m_H^2\right).\end{aligned} \tag{D.13}$$

$$\begin{aligned}-[k_I|k_3^L]\,\langle k_{2J}|3\rangle\,[2|k^I]\,[k_{3L}|3]\,\langle 2|k_2^J\rangle &= -m^3[23]\langle 32\rangle\\ &= -m^3 m_H^2.\end{aligned} \tag{D.14}$$

$$\begin{aligned}-[3|k_2^J]\,[k_{2J}|2]\,\langle k_{3L}|2\rangle\,[k_I|k_3^L]\,\langle 3|k^I\rangle &= -m[32]\,\langle 2|\not{k}_3\not{k}|3\rangle\\ &= -m[32]\left(\langle 2|\not{k}\not{k}|3\rangle - \langle 23\rangle[3|\not{k}|3\rangle\right)\\ &= -m[32]\left(k^2\langle 23\rangle - \langle 23\rangle[3|\not{k}|3\rangle\right)\\ &= -m\,m_H^2\left(k^2 - [3|\not{k}|3\rangle\right).\end{aligned} \tag{D.15}$$

$$[k_I|k_3^L]\,[k_{2J}|2]\,\langle 3|k^I\rangle\,[k_{3L}|3]\,\langle 2|k_2^J\rangle = m\,[3|\not{k}|3\rangle\,[2|\not{k}|2\rangle.$$

$$
\begin{aligned}
-\langle k_I|k_3^L\rangle\,\langle k_{2J}|3\rangle\,[2|k^I]\,\langle k_{3L}|2\rangle\,[3|k_2^J] &= m\,[3|\not{k}_2|3\rangle\,[2|\not{k}|2\rangle \\
&= m\,([3|\not{k}|3\rangle - [32]\langle 23\rangle)\,[2|\not{k}|2\rangle \\
&= m\left([3|\not{k}|3\rangle - m_H^2\right)[2|\not{k}|2\rangle. \qquad \text{(D.16)}
\end{aligned}
$$

$$
\begin{aligned}
\langle k_I|k_3^L\rangle\,\langle k_{2J}|3\rangle\,[2|k^I]\,[k_{3L}|3]\,\langle 2|k_2^J\rangle &= -m\,[2|\not{k}\not{k}_3|3\rangle\,\langle 32\rangle \\
&= -m\,([2|\not{k}\not{k}|3\rangle - [2|\not{k}|2\rangle[23])\,\langle 32\rangle \\
&= -m\left(k^2[23]\langle 32\rangle - [2|\not{k}|2\rangle[23]\langle 32\rangle\right) \\
&= -m\,m_H^2\left(k^2 - [2|\not{k}|2\rangle\right). \qquad \text{(D.17)}
\end{aligned}
$$

$$
\begin{aligned}
\langle k_I|k_3^L\rangle\,[k_{2J}|2]\,\langle 3|k^I\rangle\,\langle k_{3L}|2\rangle\,[3|k_2^J] &= -m^3[23]\langle 32\rangle \\
&= -m^3 m_H^2. \qquad \text{(D.18)}
\end{aligned}
$$

$$
\begin{aligned}
-\langle k_I|k_3^L\rangle\,[k_{2J}|2]\,\langle 3|k^I\rangle\,[k_{3L}|3]\,\langle 2|k_2^J\rangle &= m\,[3|\not{k}_2|3\rangle\,[2|\not{k}|2\rangle \\
&= m\,([3|\not{k}|3\rangle - [32]\langle 23\rangle)\,[2|\not{k}|2\rangle \\
&= m\left([3|\not{k}|3\rangle - m_H^2\right)[2|\not{k}|2\rangle. \qquad \text{(D.19)}
\end{aligned}
$$

Hence, we end up with

$$
\begin{aligned}
\mathcal{A}_{++}(k) = \frac{4\pi\alpha_s m}{v}\,\delta^{ab}\,\frac{[23]^2}{m_h^4}\Bigg\{ & m\,m_H^4 + 4m\,[3|\not{k}|3\rangle[2|\not{k}|2\rangle \\
& - 2m^3 m_H^2 - 2m\,k^2 m_H^2 - 2m\,m_H^2[2|\not{k}|2\rangle\Bigg\}. \qquad \text{(D.20)}
\end{aligned}
$$

Although this method is more straightforward than the one adopted in the main text, notice that the result we found seems to differ from that of Eq. (7.21). The above expression contains a term of the form $[3|\not{k}|3\rangle[2|\not{k}|2\rangle$, whereas the one in the main text interchanges 2 and 3 in the following way: $[2|\not{k}|3\rangle[3|\not{k}|2\rangle$. When performing the unitarity cuts, this difference is essential, since in the former case we cannot recover the rational-term contribution. Fortunately, these two forms are related by the following identity:

$$
\begin{aligned}
[3|\not{k}|3\rangle\,[2|\not{k}|2\rangle &= -[3|k_I]\,[k_J|2]\,\langle k^I|3\rangle\langle k^J|2\rangle \\
&= -\left([3|2]\,[k_J|k_I] + [3|k_J]\,[k_I|2]\right)\langle k^I|3\rangle\langle k^J|2\rangle \qquad \text{(Schouten)} \\
&= -[k_J|k_I]\,[32]\,\langle k^I|3\rangle\langle k^J|2\rangle - [3|k_J]\,\langle k^J|2\rangle[k_I|2]\,\langle k^I|3\rangle \\
&= [32]\,\langle 2|k^J\rangle[k_J|k_I]\langle k^I|3\rangle + [3|\not{k}|2\rangle[2|\not{k}|3\rangle \\
&= [32]\,\langle 2|\not{k}\not{k}|3\rangle + [3|\not{k}|2\rangle[2|\not{k}|3\rangle \\
&= k^2[32]\langle 23\rangle + [3|\not{k}|2\rangle[2|\not{k}|3\rangle \\
&= k^2 m_H^2 + [3|\not{k}|2\rangle[2|\not{k}|3\rangle, \qquad \text{(D.21)}
\end{aligned}
$$

where, in the second step, we used the Schouten identity reported in Eq. (4.59). Employing this relation and collecting a common factor of $2m$, we obtain

$$
\begin{aligned}
\mathcal{A}_{++}(k) = -\frac{8\pi\alpha_s m^2}{v}\,\delta^{ab}\left(-\frac{[23]^2}{m_H^2}\right)\Bigg\{ &-\langle 2|\not{k}|2] - \left(m^2 - k^2\right) + \frac{m_H^2}{2} \\
&+ \frac{2}{m_H^2}[2|\not{k}|3\rangle[3|\not{k}|2\rangle\Bigg\}, \qquad \text{(D.22)}
\end{aligned}
$$

which precisely coincides with Eq. (7.21). This not only benchmarks our calculation, but also allows us to select one of the two methods. Since the method presented here involves Schouten rearrangements that may obscure important contributions, the one reported in the main text is preferable. For this reason, when computing the complete BSM amplitude arising from the two SM-like diagrams, we will follow a procedure similar to the one adopted in the main text. In particular, the term $[2|\not{k}|3\rangle[3|\not{k}|2\rangle$ becomes of fundamental importance for the evaluation of rational terms, see Sec. D.3.

D.2 Loop-momentum parametrization

To find the complete expression of the amplitude for the one-loop hgg process, we exploit generalized unitarity. This requires cutting through the internal propagators of the diagrams, which amounts to putting the particles flowing through them on shell. Therefore, as implied by the cutting rule in Eq. (6.44), each propagator denominator is replaced by a Dirac delta. As a consequence, once a given set of propagators is cut, the loop momentum is constrained by the corresponding on-shell conditions.

In this appendix, we collect the loop-momentum parametrizations that solve these constraints for the different cuts used in the calculation. Rather than displaying the derivation separately for each cut, we summarize the results in terms of a common parametrization.

The on-shell conditions associated with the four propagators are

$$\begin{aligned} d_0 = 0 \quad &\Longleftrightarrow \quad k^2 = m^2, \\ d_1 = 0 \quad &\Longleftrightarrow \quad (k - p_2 - p_3)^2 = m^2, \\ d_2 = 0 \quad &\Longleftrightarrow \quad (k - p_2)^2 = m^2, \\ d_3 = 0 \quad &\Longleftrightarrow \quad (k - p_3)^2 = m^2. \end{aligned} \tag{D.23}$$

Using the loop-momentum decomposition introduced in Eq. (7.32), we choose throughout

$$c = \frac{m_h^2}{[23]^2}\, z, \tag{D.24}$$

for convenience. Therefore, the momentum associated with a generic cut $\mathcal{C}$ can be written as

$$k_{\mathcal{C}}^{\mu} = a\, p_2^{\mu} + b\, p_3^{\mu} + \frac{m_h^2}{[23]^2}\, z\, \varepsilon_2^{+\mu} + d\, \varepsilon_3^{+\mu} + k_\epsilon\, n_\epsilon^{\mu}. \tag{D.25}$$

The corresponding spinor representation is given by

$$\boxed{\begin{aligned} \not{k}_{\mathcal{C}} = {}& a\, (|2\rangle[2| + |2]\langle 2|) + b\, (|3\rangle[3| + |3]\langle 3|) \\ &+ \frac{m_h^2}{[23]^2}\, z\, \frac{\sqrt{2}}{\langle 23\rangle}\, (|2]\langle 3| + |3\rangle[2|) \\ &+ d\, \frac{\sqrt{2}}{\langle 32\rangle}\, (|3]\langle 2| + |2\rangle[3|) + k_\epsilon\, \not{n}_\epsilon. \end{aligned}} \tag{D.26}$$

The resulting parametrizations for the triple, double, and single cuts are collected in Tab. D.1. The triple, double, and single cuts leave one, two, and three free parameters, respectively.

D.3 Implementation of the generalized unitarity algorithm for the b_{01} coefficient

In Sec. 7.2, we qualitatively explained the algorithm used to implement generalized unitarity as a tool for reconstructing the one-loop hgg scattering amplitude. Here, we provide the explicit derivation of the coefficient b_{01} as an example. In particular, we first discuss the physical interpretation of the corresponding double cut in terms of cut diagrams, and then perform the actual computation required to extract the coefficient. As discussed in the main text, the same algorithm was also implemented in MATHEMATICA [26] using the package SMASH [27].

We evaluate the coefficient b_{01} in the SM for the helicity configuration in which both gluons have positive helicity. The amplitude is

$$\mathcal{M}_{++}^{\rm SM} = \int \frac{d^D k}{(2\pi)^D}\, \mu^{2\epsilon}\, \mathcal{I}_{++}^{\rm SM}(k), \tag{D.27}$$

Cut $\mathcal{C}$	$\boldsymbol{a}$	$\boldsymbol{b}$	$\boldsymbol{d}$	$\boldsymbol{k_{\mathcal{C}}^2}$
		Triple cuts		
012	1	0	$\frac{m^2-k_\epsilon^2}{2z}$	m^2
013	0	1	$\frac{m^2-k_\epsilon^2}{2z}$	m^2
		Double cuts		
01	x	$1-x$	$\frac{m^2-k_\epsilon^2+x(x-1)m_h^2}{2z}$	m^2
02	x	0	$\frac{m^2-k_\epsilon^2}{2z}$	m^2
03	0	y	$\frac{m^2-k_\epsilon^2}{2z}$	m^2
12	1	y	$\frac{m^2-k_\epsilon^2}{2z}$	$m^2+y\,m_h^2$
13	x	1	$\frac{m^2-k_\epsilon^2}{2z}$	$m^2+x\,m_h^2$
		Single cuts		
0	x	y	$\frac{m^2-k_\epsilon^2-m_h^2xy}{2z}$	m^2
1	x	y	$\frac{m^2-k_\epsilon^2-m_h^2(1-x)(1-y)}{2z}$	$m^2+(x+y-1)m_h^2$
2	x	y	$\frac{m_h^2y(1-x)+m^2-k_\epsilon^2}{2z}$	$m^2+y\,m_h^2$
3	x	y	$\frac{m_h^2x(1-y)+m^2-k_\epsilon^2}{2z}$	$m^2+x\,m_h^2$

Table D.1: Loop-momentum parametrizations for the triple, double, and single cuts. Here, we have defined $c=\frac{m_h^2}{[23]^2}\,z$ for all cuts. The free parameters x, y, and z are in general complex, as the cut conditions are solved in complexified momentum space.

with

$$\mathcal{I}^{\mathrm{SM}}_{++}(k) = \frac{\mathcal{A}^{\mathrm{SM}}_{++}(k)}{d_0 d_1 d_2} + \frac{\tilde{\mathcal{A}}^{\mathrm{SM}}_{++}(k)}{d_0 d_1 d_3}. \tag{D.28}$$

The direct numerator $\mathcal{A}^{\mathrm{SM}}_{++}(k)$ and the inverted one $\tilde{\mathcal{A}}^{\mathrm{SM}}_{++}(k)$ were obtained in Eqs. (7.21) and (7.22), respectively. We report them here again for completeness:

$$\begin{aligned}\mathcal{A}^{\mathrm{SM}}_{++}(k) = &-\frac{8\pi\alpha_s m^2}{v}\,\delta^{ab}\left(-\frac{[23]^2}{m_h^2}\right)\Bigg\{-\langle 2|\not{k}|2] - \left(m^2-k^2\right) + \frac{m_h^2}{2}\\ &\qquad\qquad\qquad\qquad + \frac{2}{m_h^2}[2|\not{k}|3\rangle[3|\not{k}|2\rangle\Bigg\},\end{aligned} \tag{D.29}$$

and

$$\begin{aligned}\tilde{\mathcal{A}}^{\mathrm{SM}}_{++}(k) = &-\frac{8\pi\alpha_s m^2}{v}\,\delta^{ab}\left(-\frac{[32]^2}{m_h^2}\right)\Bigg\{-\langle 3|\not{k}|3] - \left(m^2-k^2\right) + \frac{m_h^2}{2}\\ &\qquad\qquad\qquad\qquad + \frac{2}{m_h^2}[3|\not{k}|2\rangle[2|\not{k}|3\rangle\Bigg\}.\end{aligned} \tag{D.30}$$

D.3.1 Physical interpretation of the double cut (01)

Before performing the explicit computation, it is useful to consider the physical meaning of the double cut through propagators 0 and 1. This cut does not isolate the bubble coefficient directly, since the same two propagators also belong to both triangle topologies contributing to the physical amplitude. Therefore, in order to extract b_{01}, the higher-topology contributions already determined from the triple cuts must first be subtracted.

Diagrammatically, the corresponding cut equation takes the form

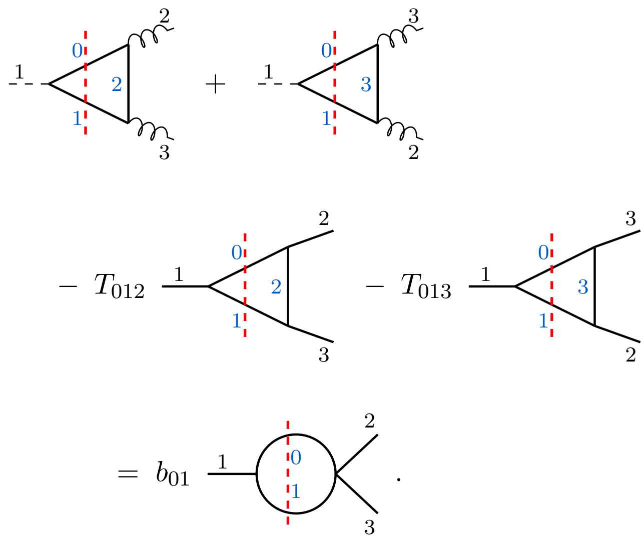

(D.31)

Here, T_{012} and T_{013} denote the complete D-dimensional residues associated with the triple cuts (012) and (013), respectively. In terms of the notation used in the scalar-integral decomposition, they contain both the four-dimensional triangle coefficient and its k_ϵ^2-dependent part,

$$T_{012} = c_{012} + R_{012}, \qquad T_{013} = c_{013} + R_{013}. \tag{D.32}$$

These coefficients are reported in Tab. (7.1) and read

$$T_{012} = T_{013} = \delta^{ab} \left(-\frac{[23]^2}{m_h^2} \right) \frac{4\pi m^2 \alpha_s}{v} \left(4m^2 - m_h^2 - 4k_\epsilon^2 \right), \tag{D.33}$$

This distinction is useful here because the full D-dimensional residue must be subtracted before the lower-topology coefficient can be isolated.

Using the explicit form of the integrands in Eq. (D.28), the diagrammatic relation (D.31) becomes

$$\begin{aligned} &\int \frac{d^D k}{(2\pi)^D} \mu^{2\epsilon} \left[\frac{\mathcal{A}_{++}^{\mathrm{SM}}(k) - T_{012}}{d_2} + \frac{\tilde{\mathcal{A}}_{++}^{\mathrm{SM}}(k) - T_{013}}{d_3} \right] (-2i\pi)^2 \delta(d_0)\delta(d_1) \\ &\quad = b_{01} \int \frac{d^D k}{(2\pi)^D} \mu^{2\epsilon} (-2i\pi)^2 \delta(d_0)\delta(d_1). \end{aligned} \tag{D.34}$$

Since the cut measure is common to both sides, the bubble coefficient is therefore obtained from

$$b_{01} = \left[\frac{\mathcal{A}_{++}^{\mathrm{SM}}(k) - T_{012}}{d_2} + \frac{\tilde{\mathcal{A}}_{++}^{\mathrm{SM}}(k) - T_{013}}{d_3} \right] \Bigg|_{d_0 = d_1 = 0}. \tag{D.35}$$

D.3.2 Explicit evaluation

We now evaluate Eq. (D.35). The first step is to determine the loop momentum compatible with the double-cut conditions

$$d_0(k) = d_1(k) = 0. \tag{D.36}$$

To this end we use the general van Neerven–Vermaseren parametrization introduced in Eq. D.26 and the coefficients for the cut $\mathcal{C} = 01$ reported in Tab. D.1. We obtain

$$\begin{aligned} \not{k}_{01} &= x \left(|2\rangle[2| + |2]\langle 2| \right) + (1 - x) \left(|3\rangle[3| + |3]\langle 3| \right) \\ &\quad + \frac{m_h^2}{[23]^2} z \frac{\sqrt{2}}{\langle 23 \rangle} \left(|2]\langle 3| + |3\rangle[2| \right) \\ &\quad + \frac{m^2 - k_\epsilon^2 + x(x-1)m_h^2}{2z} \frac{\sqrt{2}}{\langle 32 \rangle} \left(|3]\langle 2| + |2\rangle[3| \right) + k_\epsilon \not{n}_\epsilon, \end{aligned} \tag{D.37}$$

which represents the constrained momentum that can flow in the diagrams cut through 0 and 1. Conversely, the two propagators that remain uncut are easily obtained from this parametrization. Since

$$d_2 = (k - p_2)^2 - m^2, \qquad d_3 = (k - p_3)^2 - m^2, \tag{D.38}$$

and $k^2 = m^2$ on the cut, we find

$$d_2 = -2k_{01} \cdot p_2 = (x-1)m_h^2, \tag{D.39}$$
$$d_3 = -2k_{01} \cdot p_3 = -x\, m_h^2. \tag{D.40}$$

In particular,

$$d_2 + d_3 = -m_h^2, \qquad d_2 d_3 = x(1-x)m_h^4. \tag{D.41}$$

We now evaluate the spinor structures entering Eqs. (D.29) and (D.30). From Eq. (D.37), one immediately obtains

$$\langle 2|\not{k}_{01}|2] = -d_2, \qquad \langle 3|\not{k}_{01}|3] = -d_3. \tag{D.42}$$

Moreover, using the standard spinor identities and the explicit transverse part of the cut momentum,

$$[2|\not{k}_{01}|3\rangle[3|\not{k}_{01}|2\rangle = m_h^2\left[k_\epsilon^2 - m^2 - x(x-1)m_h^2\right]. \tag{D.43}$$

The same expression is obtained after exchanging $2 \leftrightarrow 3$.

Hence, using $k_{01}^2 = m^2$, the direct numerator becomes

$$\begin{aligned}\mathcal{A}_{++}^{\mathrm{SM}}(k_{01}) = &- \frac{8\pi\alpha_s m^2}{v}\,\delta^{ab}\left(-\frac{[23]^2}{m_h^2}\right)\\ &\times\left[d_2 + \frac{m_h^2}{2} + 2k_\epsilon^2 - 2m^2 - 2x(x-1)m_h^2\right],\end{aligned} \tag{D.44}$$

while for the inverted contribution we obtain

$$\begin{aligned}\tilde{\mathcal{A}}_{++}^{\mathrm{SM}}(k_{01}) = &- \frac{8\pi\alpha_s m^2}{v}\,\delta^{ab}\left(-\frac{[23]^2}{m_h^2}\right)\\ &\times\left[d_3 + \frac{m_h^2}{2} + 2k_\epsilon^2 - 2m^2 - 2x(x-1)m_h^2\right].\end{aligned} \tag{D.45}$$

Subtracting Eq. (D.33) from the two numerators gives

$$\mathcal{A}_{++}^{\mathrm{SM}}(k_{01}) - T_{012} = -\frac{8\pi\alpha_s m^2}{v}\,\delta^{ab}\left(-\frac{[23]^2}{m_h^2}\right)\left[d_2 - 2x(x-1)m_h^2\right], \tag{D.46}$$

$$\tilde{\mathcal{A}}_{++}^{\mathrm{SM}}(k_{01}) - T_{013} = -\frac{8\pi\alpha_s m^2}{v}\,\delta^{ab}\left(-\frac{[23]^2}{m_h^2}\right)\left[d_3 - 2x(x-1)m_h^2\right]. \tag{D.47}$$

Equation (D.35) therefore becomes

$$\begin{aligned} b_{01} = & -\frac{8\pi\alpha_s m^2}{v}\,\delta^{ab}\left(-\frac{[23]^2}{m_h^2}\right)\left[\frac{d_2 - 2x(x-1)m_h^2}{d_2} + \frac{d_3 - 2x(x-1)m_h^2}{d_3}\right] \\ = & -\frac{8\pi\alpha_s m^2}{v}\,\delta^{ab}\left(-\frac{[23]^2}{m_h^2}\right)\left[2 - 2x(x-1)m_h^2\left(\frac{1}{d_2} + \frac{1}{d_3}\right)\right] \\ = & -\frac{8\pi\alpha_s m^2}{v}\,\delta^{ab}\left(-\frac{[23]^2}{m_h^2}\right)\left[2 - 2x(x-1)m_h^2\left(-\frac{1}{x(1-x)m_h^2}\right)\right] \\ = & \ 0 \end{aligned} \tag{D.48}$$

The vanishing of b_{01} therefore results from a cancellation between the direct and inverted triangle contributions after the higher-topology residues have been subtracted. This provides a useful illustration of the top-down nature of the generalized-unitarity reconstruction: the double cut alone does not directly determine the bubble coefficient, but does so only once the information obtained from the triple cuts has been removed. The same procedure is applied to the remaining double and single cuts in the complete reconstruction of the amplitude.

D.4 Computation of BSM integrand

In Sec. 7.4.2 of the main text, we perform the calculation of the pure BSM contribution in Eq. (7.57), which we report here for completeness:

$$\begin{aligned}\mathcal{A}_{++}^{c_{g\bar{t}t}^{RRR}}(k) = & -i\,\frac{\delta^{ab}}{2}\,c_{g\bar{t}t}\,c_{g\bar{t}t}^{RRR}\frac{1}{2\sqrt{2}}\,\varepsilon_{2,\mu}^{+}\,\varepsilon_{3,\nu}^{+}\left(c_{ht\bar{t}}^{LL}\langle k_3^L|k_I\rangle - c_{ht\bar{t}}^{RR}[k_3^L|k_I]\right)\\ & \times\Bigg\{\left(\langle k^I|\gamma^\mu|k_{2,J}] - \langle k_{2,J}|\gamma^\mu|k^I]\right)\\ & \qquad\times\Big([k_2^J|3]\,\langle 3|\gamma^\nu|k_{3,L}] + [k_{3,L}|3]\,\langle 3|\gamma^\nu|k_2^J]\Big)\\ & \quad+\Big([k^I|2]\,\langle 2|\gamma^\mu|k_{2,J}] + [k_{2,J}|2]\,\langle 2|\gamma^\mu|k^I]\Big)\\ & \qquad\times\left(\langle k_2^J|\gamma^\nu|k_{3,L}] - \langle k_{3,L}|\gamma^\nu|k_2^J]\right)\Bigg\}.\end{aligned}\tag{D.49}$$

Similarly to the procedure adopted in the SM case, we want to perform the calculation in such a way as to single out the dependence on the loop momentum k. Hence, the sixteen resulting terms are evaluated as follows:

$$[2|k^I]\,[k_I|k_3^L]\,\langle k_{3L}|\gamma^\nu|k_2^J]\,[k_{2J}|\gamma^\mu|2\rangle = -m^2 k_{3,\alpha}p_{2,\beta}\;\mathrm{Tr}\Big[\mathbb{P}_L\gamma^\beta\gamma^\alpha\gamma^\nu\gamma^\mu\Big]\,.\tag{D.50}$$

$$-[2|k^I]\,[k_I|k_3^L]\,[k_{3L}|\gamma^\nu|k_2^J\rangle\,\langle k_{2J}|\gamma^\mu|2\rangle = -m^2 k_{2,\gamma}p_{2,\beta}\;\mathrm{Tr}\Big[\mathbb{P}_L\gamma^\beta\gamma^\nu\gamma^\gamma\gamma^\mu\Big]\,.\tag{D.51}$$

$$-[2|k_{2J}]\,[k_2^J|\gamma^\nu|k_{3L}\rangle\,[k_3^L|k_I]\,[k^I|\gamma^\mu|2\rangle = m^2 k_{3,\alpha}p_{2,\beta}\;\mathrm{Tr}\Big[\mathbb{P}_L\gamma^\beta\gamma^\nu\gamma^\alpha\gamma^\mu\Big]\,.\tag{D.52}$$

$$[2|k_{2J}]\,\langle k_2^J|\gamma^\nu|k_{3L}]\,[k_3^L|k_I]\,[k^I|\gamma^\mu|2\rangle = m^2 k_{2,\gamma}p_{2,\beta}\;\mathrm{Tr}\Big[\mathbb{P}_L\gamma^\beta\gamma^\gamma\gamma^\nu\gamma^\mu\Big]\,.\tag{D.53}$$

$$-[2|k^I]\,\langle k_I|k_3^L\rangle\,\langle k_{3L}|\gamma^\nu|k_2^J]\,[k_{2J}|\gamma^\mu|2\rangle = -m^2 k_\delta p_{2,\beta}\;\mathrm{Tr}\Big[\mathbb{P}_L\gamma^\beta\gamma^\delta\gamma^\nu\gamma^\mu\Big]\,.\tag{D.54}$$

$$[2|k^I]\,\langle k_I|k_3^L\rangle\,[k_{3L}|\gamma^\nu|k_2^J\rangle\,[k_{2J}|\gamma^\mu|2\rangle = -k_\delta k_{3,\alpha}k_{2,\gamma}p_{2,\beta}\;\mathrm{Tr}\Big[\mathbb{P}_L\gamma^\beta\gamma^\delta\gamma^\alpha\gamma^\nu\gamma^\gamma\gamma^\mu\Big]\,.$$

$$[2|k_{2J}]\,[k_2^J|\gamma^\nu|k_{3L}\rangle\,\langle k_3^L|k_I\rangle\,[k^I|\gamma^\mu|2\rangle = m^2 k_\delta p_{2,\beta}\;\mathrm{Tr}\Big[\mathbb{P}_L\gamma^\beta\gamma^\nu\gamma^\delta\gamma^\mu\Big]\,.\tag{D.55}$$

$$\begin{aligned} &-[2|k_{2J}]\,\langle k_2^J|\gamma^\nu|k_{3L}]\,\langle k_3^L|k_I\rangle\,[k^I|\gamma^\mu|2\rangle \\ &\quad = k_\delta k_{2,\gamma} k_{3,\alpha} p_{2,\beta}\;\mathrm{Tr}\left[\mathbb{P}_L \gamma^\beta\gamma^\gamma\gamma^\nu\gamma^\alpha\gamma^\delta\gamma^\mu\right]. \end{aligned} \tag{D.56}$$

$$\begin{aligned} &[3|k_2^J]\,\langle k_{2J}|\gamma^\mu|k^I]\,\langle k_I|k_3^L\rangle\,[k_{3L}|\gamma^\nu|3\rangle \\ &\quad = -m^2 k_{2,\gamma}\,[3|\gamma^\gamma\gamma^\mu\gamma^\nu|3\rangle \\ &\quad = -m^2 k_{2,\gamma} p_{3,\rho}\;\mathrm{Tr}\,[\mathbb{P}_L\gamma^\rho\gamma^\gamma\gamma^\mu\gamma^\nu]\,. \end{aligned} \tag{D.57}$$

$$\begin{aligned} &[3|k_{3L}]\,[k_3^L|k_I]\,[k^I|\gamma^\mu|k_{2J}\rangle\,[k_2^J|\gamma^\nu|3\rangle \\ &\quad = -m^2 k_{2,\delta}\,[3|\gamma^\mu\gamma^\delta\gamma^\nu|3\rangle \\ &\quad = -m^2 k_{2,\delta} p_{3,\rho}\;\mathrm{Tr}\left[\mathbb{P}_L\gamma^\rho\gamma^\mu\gamma^\delta\gamma^\nu\right]. \end{aligned} \tag{D.58}$$

$$\begin{aligned} &-[3|k_2^J]\,[k_{2J}|\gamma^\mu|k^I\rangle\,[k_I|k_3^L]\,[k_{3L}|\gamma^\nu|3\rangle \\ &\quad = -m^2 k_\delta\,[3|\gamma^\mu\gamma^\delta\gamma^\nu|3\rangle \\ &\quad = -m^2 k_\delta p_{3,\rho}\;\mathrm{Tr}\left[\mathbb{P}_L\gamma^\rho\gamma^\mu\gamma^\delta\gamma^\nu\right]. \end{aligned} \tag{D.59}$$

$$\begin{aligned} &-[3|k_{3L}]\,[k_3^L|k_I]\,\langle k^I|\gamma^\mu|k_{2J}]\,[k_2^J|\gamma^\nu|3\rangle \\ &\quad = -m^2 k_\delta\,[3|\gamma^\delta\gamma^\mu\gamma^\nu|3\rangle \\ &\quad = -m^2 k_\delta p_{3,\rho}\;\mathrm{Tr}\left[\mathbb{P}_L\gamma^\rho\gamma^\delta\gamma^\mu\gamma^\nu\right]. \end{aligned} \tag{D.60}$$

$$\begin{aligned} &-[3|k_2^J]\,\langle k_{2J}|\gamma^\mu|k^I]\,\langle k_I|k_3^L\rangle\,[k_{3L}|\gamma^\nu|3\rangle \\ &\quad = -k_{2,\gamma} k_\delta k_{3,\alpha}\,[3|\gamma^\gamma\gamma^\mu\gamma^\delta\gamma^\alpha\gamma^\nu|3\rangle \\ &\quad = -k_{2,\gamma} k_\delta k_{3,\alpha} p_{3,\rho}\;\mathrm{Tr}\left[\mathbb{P}_L\gamma^\rho\gamma^\gamma\gamma^\mu\gamma^\delta\gamma^\alpha\gamma^\nu\right]. \end{aligned} \tag{D.61}$$

$$\begin{aligned} &-[3|k_{3L}]\,\langle k_3^L|k_I\rangle\,[k^I|\gamma^\mu|k_{2J}\rangle\,[k_2^J|\gamma^\nu|3\rangle \\ &\quad = -k_{2,\gamma} k_\delta k_{3,\alpha} p_{3,\rho}\;\mathrm{Tr}\left[\mathbb{P}_L\gamma^\rho\gamma^\alpha\gamma^\delta\gamma^\mu\gamma^\gamma\gamma^\nu\right]. \end{aligned} \tag{D.62}$$

$$[3|k_2^J]\,[k_{2J}|\gamma^\mu|k^I\rangle\,\langle k_I|k_3^L\rangle\,[k_{3L}|\gamma^\nu|3\rangle = -m^2 k_{3,\alpha} p_{3,\rho}\;\mathrm{Tr}[\mathbb{P}_L\gamma^\rho\gamma^\mu\gamma^\alpha\gamma^\nu]\,. \tag{D.63}$$

$$[3|k_{3L}]\,\langle k_3^L|k_I\rangle\,\langle k^I|\gamma^\mu|k_{2J}]\,[k_2^J|\gamma^\nu|3\rangle = -m^2 k_{3,\alpha} p_{3,\rho}\ \mathrm{Tr}[\mathbb{P}_L \gamma^\rho \gamma^\alpha \gamma^\mu \gamma^\nu]\,. \tag{D.64}$$

Notice also that the choice of globally factoring out the polarization vectors in the amplitude of Eq. (D.49) closely follows the method adopted in Sec. D.1.1. In this way, we managed to express the result in terms of traces of γ matrices. We obtain

$$\begin{aligned}
\mathcal{A}_{++}^{c_{g\bar{t}t}^{RRR}}(k) = &-i\,\frac{\delta^{ab}}{2}\,c_{g\bar{t}t}\,c_{g\bar{t}t}^{RRR}\frac{1}{2\sqrt{2}}\,\varepsilon^+_{2,\mu}\,\varepsilon^+_{3,\nu}\Bigg\{\\
&c_{ht\bar{t}}^{RR}\Bigg[-m^2 k_{3,\alpha}p_{2,\beta}\ \mathrm{Tr}\left[\mathbb{P}_L\gamma^\beta\gamma^\alpha\gamma^\nu\gamma^\mu\right]\\
&\quad - m^2 k_{2,\gamma}p_{2,\beta}\ \mathrm{Tr}\left[\mathbb{P}_L\gamma^\beta\gamma^\nu\gamma^\gamma\gamma^\mu\right]\\
&\quad + m^2 k_{3,\alpha}p_{2,\beta}\ \mathrm{Tr}\left[\mathbb{P}_L\gamma^\beta\gamma^\nu\gamma^\alpha\gamma^\mu\right]\\
&\quad + m^2 k_{2,\gamma}p_{2,\beta}\ \mathrm{Tr}\left[\mathbb{P}_L\gamma^\beta\gamma^\gamma\gamma^\nu\gamma^\mu\right]\\
&\quad - m^2 k_{2,\gamma}p_{3,\rho}\ \mathrm{Tr}\left[\mathbb{P}_L\gamma^\rho\gamma^\gamma\gamma^\mu\gamma^\nu\right]\\
&\quad - m^2 k_{2,\delta}p_{3,\rho}\ \mathrm{Tr}\left[\mathbb{P}_L\gamma^\rho\gamma^\mu\gamma^\delta\gamma^\nu\right]\\
&\quad - m^2 k_{\delta}p_{3,\rho}\ \mathrm{Tr}\left[\mathbb{P}_L\gamma^\rho\gamma^\mu\gamma^\delta\gamma^\nu\right]\\
&\quad - m^2 k_{\delta}p_{3,\rho}\ \mathrm{Tr}\left[\mathbb{P}_L\gamma^\rho\gamma^\delta\gamma^\mu\gamma^\nu\right]\Bigg]\\
&+c_{ht\bar{t}}^{LL}\Bigg[-m^2 k_{\delta}p_{2,\beta}\ \mathrm{Tr}\left[\mathbb{P}_L\gamma^\beta\gamma^\delta\gamma^\nu\gamma^\mu\right]\\
&\quad - k_\delta k_{3,\alpha}k_{2,\gamma}p_{2,\beta}\ \mathrm{Tr}\left[\mathbb{P}_L\gamma^\beta\gamma^\delta\gamma^\alpha\gamma^\nu\gamma^\gamma\gamma^\mu\right]\\
&\quad + m^2 k_{\delta}p_{2,\beta}\ \mathrm{Tr}\left[\mathbb{P}_L\gamma^\beta\gamma^\nu\gamma^\delta\gamma^\mu\right]\\
&\quad + k_\delta k_{2,\gamma}k_{3,\alpha}p_{2,\beta}\ \mathrm{Tr}\left[\mathbb{P}_L\gamma^\beta\gamma^\gamma\gamma^\nu\gamma^\alpha\gamma^\delta\gamma^\mu\right]\\
&\quad - k_{2,\gamma}k_\delta k_{3,\alpha}p_{3,\rho}\ \mathrm{Tr}\left[\mathbb{P}_L\gamma^\rho\gamma^\gamma\gamma^\mu\gamma^\delta\gamma^\alpha\gamma^\nu\right]\\
&\quad - k_{2,\gamma}k_\delta k_{3,\alpha}p_{3,\rho}\ \mathrm{Tr}\left[\mathbb{P}_L\gamma^\rho\gamma^\alpha\gamma^\delta\gamma^\mu\gamma^\gamma\gamma^\nu\right]\\
&\quad - m^2 k_{3,\alpha}p_{3,\rho}\ \mathrm{Tr}\left[\mathbb{P}_L\gamma^\rho\gamma^\mu\gamma^\alpha\gamma^\nu\right]\\
&\quad - m^2 k_{3,\alpha}p_{3,\rho}\ \mathrm{Tr}\left[\mathbb{P}_L\gamma^\rho\gamma^\alpha\gamma^\mu\gamma^\nu\right]\Bigg]\Bigg\}.
\end{aligned} \tag{D.65}$$

To evaluate the traces, we adopt the NDR-DISCARD scheme [61], in which the γ_5-odd traces are set to zero, thus retaining only the CP-even part of the

BSM amplitude. Explicitly,

$$\mathrm{Tr}[\mathbb{P}_L\,\Gamma] \overset{\text{NDR-discard}}{=} \frac{1}{2}\,\mathrm{Tr}[\Gamma]\,, \tag{D.66}$$

with Γ generically denoting a product of an even number of γ matrices. Evaluating the traces using FORM [57–59], and using the contractions in Eqs. (7.13) and (7.14), yields

$$\begin{aligned}
\mathcal{A}_{++}^{c_{g\bar{t}t}^{RRR}}(k) = &-i\,\frac{\delta^{ab}}{2}\,c_{g\bar{t}t}\,c_{g\bar{t}t}^{RRR}\frac{1}{2\sqrt{2}}\Bigg\{2m^2m_h^2\,c_{ht\bar{t}}^{RR}\,\frac{[23]^2}{m_h^2}\\
&-8\,(k\cdot p_2)(k\cdot p_3)\,c_{ht\bar{t}}^{LL}\,\frac{[23]^2}{m_h^2}+4\,(k\cdot p_2)\,k^2\,c_{ht\bar{t}}^{LL}\,\frac{[23]^2}{m_h^2}\\
&-4\,(k\cdot p_2)\,m^2\,c_{ht\bar{t}}^{LL}\,\frac{[23]^2}{m_h^2}-8\,(k\cdot p_2)^2\,c_{ht\bar{t}}^{LL}\,\frac{[23]^2}{m_h^2}\\
&+2\,k^2m_h^2\,c_{ht\bar{t}}^{LL}\,\frac{[23]^2}{m_h^2}-4m_h^2\,c_{ht\bar{t}}^{LL}\left(k\cdot\,\varepsilon_2^+\right)\left(k\cdot\,\varepsilon_3^+\right)\Bigg\}.
\end{aligned} \tag{D.67}$$

Using Eqs. (4.39), (7.12), and (7.20), we can convert the amplitude into spinor variables, obtaining

$$\begin{aligned}
\mathcal{A}_{++}^{c_{g\bar{t}t}^{RRR}}(k) = i\,\frac{c_{g\bar{t}t}\,c_{g\bar{t}t}^{RRR}}{2\sqrt{2}}\,\delta^{ab}\left(-\frac{[23]^2}{m_h^2}\right)\Bigg\{&m^2m_h^2\,c_{ht\bar{t}}^{RR}\\
&+c_{ht\bar{t}}^{LL}\Bigg[-\langle 2|\not{k}|2]\,[3|\not{k}|3\rangle+\langle 2|\not{k}|2]\,\left(k^2-m^2\right)\\
&\quad-\langle 2|\not{k}|2]^2+k^2m_h^2+\langle 2|\not{k}|3]\,\langle 3|\not{k}|2]\Bigg]\Bigg\}.
\end{aligned} \tag{D.68}$$

This is precisely Eq. (7.58) of the main text.

Bibliography

[1] M. E. Peskin and D. V. Schroeder, *An Introduction to quantum field theory*. Addison-Wesley, Reading, USA, 1995.

[2] M. D. Schwartz, *Quantum Field Theory and the Standard Model*. Cambridge University Press, 3, 2014.

[3] M. Srednicki, *Quantum field theory*. Cambridge University Press, 1, 2007.

[4] A. V. Manohar, "Introduction to Effective Field Theories," 2018. `https://arxiv.org/abs/1804.05863`.

[5] D. B. Kaplan, "Five lectures on effective field theory," 2005. `https://arxiv.org/abs/nucl-th/0510023`.

[6] R. Bartocci, A. Biekötter, and T. Hurth, "A global analysis of the SMEFT under the minimal MFV assumption," 2023. `https://arxiv.org/abs/2311.04963`.

[7] J. Ellis, C. W. Murphy, V. Sanz, and T. You, "Updated global SMEFT fit to Higgs, diboson and electroweak data," *Journal of High Energy Physics* **2018** no. 6, (2018) . `http://dx.doi.org/10.1007/JHEP06(2018)146`.

[8] J. de Blas, A. Goncalves, V. Miralles, L. Reina, L. Silvestrini, and M. Valli, "Constraining new physics effective interactions via a global fit of electroweak, Drell-Yan, Higgs, top, and flavour observables," *Journal of High Energy Physics* **2026** no. 3, (Mar., 2026) . `http://dx.doi.org/10.1007/JHEP03(2026)013`.

[9] J. ter Hoeve, L. Mantani, A. N. Rossia, J. Rojo, and E. Vryonidou, "Connecting Scales: RGE Effects in the SMEFT at the LHC and Future Colliders," 2025. `https://arxiv.org/abs/2502.20453`.

[10] I. Brivio, R. Gröber, and K. Schmid, "The Art of Counting: a reappraisal of the HEFT expansion," *JHEP* **04** (2026) 202.

[11] G. Buchalla, O. Catà, and C. Krause, "On the power counting in effective field theories," *Physics Letters B* **731** (Apr., 2014) 80–86. `http://dx.doi.org/10.1016/j.physletb.2014.02.015`.

[12] G. A. e. a. ATLAS Collaboration, "Observation of quantum entanglement with top quarks at the ATLAS detector," *Nature* **633** no. 8030, (2024) 542–547. `http://dx.doi.org/10.1038/s41586-024-07824-z`.

[13] CMS Collaboration, "Observation of quantum entanglement in top quark pair production in proton–proton collisions at $\sqrt{s} = 13$ TeV," *Reports on Progress in Physics* **87** no. 11, (Oct., 2024) 117801. `https://doi.org/10.1088/1361-6633/ad7e4d`.

[14] N. Arkani-Hamed, T.-C. Huang, and Y. tin Huang, "Scattering Amplitudes For All Masses and Spins," 2021. `https://arxiv.org/abs/1709.04891`.

[15] R. K. Ellis, Z. Kunszt, K. Melnikov, and G. Zanderighi, "One-loop calculations in quantum field theory: From Feynman diagrams to unitarity cuts," *Physics Reports* **518** no. 4-5, (2012) 141–250. `http://dx.doi.org/10.1016/j.physrep.2012.01.008`.

[16] R. Britto, F. Cachazo, and B. Feng, "Generalized unitarity and one-loop amplitudes in N=4 super-Yang-Mills," *Nucl. Phys. B* **725** (2005) 275–305, `arXiv:hep-th/0412103`.

[17] C. Anastasiou, R. Britto, B. Feng, Z. Kunszt, and P. Mastrolia, "D-dimensional unitarity cut method," *Phys. Lett. B* **645** (2007) 213–216, `arXiv:hep-ph/0609191`.

[18] A. Dedes, M. Paraskevas, J. Rosiek, K. Suxho, and L. Trifyllis, "SmeftFR – Feynman rules generator for the Standard Model Effective Field Theory," *Comput. Phys. Commun.* **247** (2020) 106931, `arXiv:1904.03204 [hep-ph]`.

[19] A. Dedes, J. Rosiek, M. Ryczkowski, K. Suxho, and L. Trifyllis, "SmeftFR v3 – Feynman rules generator for the Standard Model Effective Field Theory," *Comput. Phys. Commun.* **294** (2024) 108943, `arXiv:2302.01353 [hep-ph]`.

[20] A. Dedes, W. Materkowska, M. Paraskevas, J. Rosiek, and K. Suxho, "Feynman Rules for the Standard Model Effective Field Theory in R_ξ-gauges," *Journal of High Energy Physics* **2017** no. 6, (2017) 143, `arXiv:1704.03888 [hep-ph]`.

[21] T. Hahn, "Generating Feynman Diagrams and Amplitudes with FeynArts 3," *Comput. Phys. Commun.* **140** (2001) 418–431, `arXiv:hep-ph/0012260`.

[22] R. Mertig, M. Böhm, and A. Denner, "Feyn Calc: Computer-algebraic calculation of Feynman amplitudes," *Comput. Phys. Commun.* **64** (1991) 345–359.

[23] V. Shtabovenko, R. Mertig, and F. Orellana, "New Developments in FeynCalc 9.0," *Comput. Phys. Commun.* **207** (2016) 432–444, `arXiv:1601.01167 [hep-ph]`.

[24] V. Shtabovenko, R. Mertig, and F. Orellana, "FeynCalc 9.3: New features and improvements," *Comput. Phys. Commun.* **256** (2020) 107478, `arXiv:2001.04407 [hep-ph]`.

[25] M. Grazzini, A. Ilnicka, M. Spira, and M. Wiesemann, "Modeling BSM effects on the Higgs transverse-momentum spectrum in an EFT approach," *JHEP* **03** (2017) 115, `arXiv:1612.00283 [hep-ph]`.

[26] Wolfram Research, Inc., "Mathematica." Version 14.3, 2025.

[27] A. Kumar, A. Rudra, and R. Shaw, "SMaSH: Simplify Massive Spinor Helicity," `arXiv:2606.27928 [hep-th]`.

[28] B. Gripaios, "Lectures on Physics Beyond the Standard Model," 2015.

[29] Q. R. Ahmad *et al.*, "Measurement of the Rate of $\nu_e + d \to p + p + e^-$ Interactions Produced by ^8B Solar Neutrinos at the Sudbury Neutrino Observatory," *Phys. Rev. Lett.* **87** (2001) 071301, `arXiv:nucl-ex/0106015`.

[30] Q. R. Ahmad *et al.*, "Direct Evidence for Neutrino Flavor Transformation from Neutral Current Interactions in the Sudbury Neutrino Observatory," *Phys. Rev. Lett.* **89** (2002) 011301, `arXiv:nucl-ex/0204008`.

[31] P. A. R. Ade *et al.*, "Planck 2015 Results. XIII. Cosmological Parameters," 2015.

[32] A. D. Sakharov, "Violation of CP Invariance, C Asymmetry, and Baryon Asymmetry of the Universe," *Pisma Zh. Eksp. Teor. Fiz.* **5** (1967) 32–35.

[33] G. Degrassi, S. Di Vita, J. Elias-Miro, J. R. Espinosa, G. F. Giudice, G. Isidori, and A. Strumia, "Higgs mass and vacuum stability in the Standard Model at NNLO," *JHEP* **08** (2012) 098, `arXiv:1205.6497 [hep-ph]`.

[34] C. Abel *et al.*, "Measurement of the Permanent Electric Dipole Moment of the Neutron," *Phys. Rev. Lett.* **124** no. 8, (2020) 081803, `arXiv:2001.11966 [hep-ex]`.

[35] A. Manohar and H. Georgi, "Chiral Quarks and the Nonrelativistic Quark Model," *Nucl. Phys.* **B234** (1984) 189.

[36] H. Georgi, "Effective Field Theory," *Ann. Rev. Nucl. Part. Sci.* **43** (1993) 209–252.

[37] A. Falkowski, "Saclay Lectures on Effective Field Theories," 2017. `https://userswww.pd.infn.it/~feruglio/Falkowski.pdf`. Lecture notes, version of June 14, 2017.

[38] A. V. Manohar, "Introduction to Effective Field Theories," in *Effective Field Theory in Particle Physics and Cosmology*, S. Davidson *et al.*, eds. Oxford University Press, 2018. `arXiv:1804.05863 [hep-ph]`.

[39] D. B. Kaplan, "Effective Field Theories," 1995. Lectures given at the Seventh Summer School in Nuclear Physics: Symmetries.

[40] I. Z. Rothstein, "TASI Lectures on Effective Field Theories," 2003. Lectures given at TASI 2002.

[41] R. Penco, "An Introduction to Effective Field Theories," 2020. Lecture notes prepared for the 2nd Joint ICTP-Trieste/ICTP-SAIFR School on Particle Physics.

[42] T. Cohen, "As Scales Become Separated: Lectures on Effective Field Theory," *PoS* **TASI2018** (2019) 011, `arXiv:1903.03622 [hep-ph]`.

[43] A. V. Manohar, "Introduction to Effective Field Theories," in *Effective Field Theory in Particle Physics and Cosmology*, S. Davidson, P. Gambino, M. Laine, M. Neubert, and C. Salomon, eds., pp. 47–135. Oxford University Press, 2020. `arXiv:1804.05863 [hep-ph]`.

[44] B. Grzadkowski, M. Iskrzynski, M. Misiak, and J. Rosiek, "Dimension-Six Terms in the Standard Model Lagrangian," *JHEP* **10** (2010) 085, `arXiv:1008.4884 [hep-ph]`.

[45] I. Brivio and M. Trott, "The Standard Model as an Effective Field Theory," *Phys. Rept.* **793** (2019) 1–98, `arXiv:1706.08945 [hep-ph]`.

[46] G. Durieux, T. Kitahara, Y. Shadmi, and Y. Weiss, "The electroweak effective field theory from on-shell amplitudes," *Journal of High Energy Physics* **2020** no. 1, (2020) 119, `arXiv:1909.10551 [hep-ph]`.

[47] H. Elvang and Y.-t. Huang, "Scattering Amplitudes," 2014.

[48] N. Arkani-Hamed, T.-C. Huang, and Y. tin Huang, "Scattering Amplitudes For All Masses and Spins," 2021. `https://arxiv.org/abs/1709.04891`.

[49] R. Gröber, A. N. Rossia, and M. Ryczkowski, "Multi-Higgs Amplitudes Bootstrapped: Dissecting SMEFT and HEFT," *JHEP* **02** (2026) 245, arXiv:2509.02680 [hep-ph].

[50] Y. Shadmi and Y. Weiss, "Effective Field Theory Amplitudes the On-Shell Way: Scalar and Vector Couplings to Gluons," *JHEP* **02** (2019) 165, arXiv:1809.09644 [hep-ph].

[51] G. Durieux, T. Kitahara, C. S. Machado, Y. Shadmi, and Y. Weiss, "Constructing massive on-shell contact terms," *JHEP* **12** (2020) 175, arXiv:2008.09652 [hep-ph].

[52] G. Passarino and M. J. G. Veltman, "One-Loop Corrections for e+ e- Annihilation Into mu+ mu- in the Weinberg Model," *Nucl. Phys. B* **160** (1979) 151–207.

[53] R. E. Cutkosky, "Singularities and Discontinuities of Feynman Amplitudes," *J. Math. Phys.* **1** (1960) 429–433.

[54] W. L. van Neerven and J. A. M. Vermaseren, "Large Loop Integrals," *Phys. Lett. B* **137** (1984) 241–244.

[55] G. Ossola, C. G. Papadopoulos, and R. Pittau, "Reducing full one-loop amplitudes to scalar integrals at the integrand level," *Nucl. Phys. B* **763** (2007) 147–169, arXiv:hep-ph/0609007.

[56] S. D. Badger, "Direct Extraction Of One Loop Rational Terms," *JHEP* **01** (2009) 049, arXiv:0806.4600 [hep-ph].

[57] J. A. M. Vermaseren, "New features of FORM," 2000. https://arxiv.org/abs/math-ph/0010025.

[58] J. Kuipers, T. Ueda, J. Vermaseren, and J. Vollinga, "FORM version 4.0," *Computer Physics Communications* **184** no. 5, (May, 2013) 1453–1467. http://dx.doi.org/10.1016/j.cpc.2012.12.028.

[59] B. Ruijl, T. Ueda, and J. Vermaseren, "FORM version 4.2," 2017. https://arxiv.org/abs/1707.06453.

[60] M. Grazzini, A. Ilnicka, and M. Spira, "Higgs boson production at large transverse momentum within the SMEFT: analytical results," *Eur. Phys. J. C* **78** no. 10, (2018) 808, arXiv:1806.08832 [hep-ph].

[61] V. Shtabovenko, R. Mertig, and F. Orellana, "FeynCalc 9.3: New features and improvements," *Comput. Phys. Commun.* **256** (2020) 107478, arXiv:2001.04407 [hep-ph].

[62] G. 't Hooft and M. J. G. Veltman, "Regularization and Renormalization of Gauge Fields," *Nucl. Phys. B* **44** (1972) 189–213.

[63] P. Breitenlohner and D. Maison, "Dimensional Renormalization and the Action Principle," *Commun. Math. Phys.* **52** (1977) 11–38.

[64] ATLAS Collaboration, "Combination of Searches for Higgs Boson Pair Production in pp Collisions at $\sqrt{s} = 13$ TeV with the ATLAS Detector," *Physical Review Letters* **133** no. 10, (2024) 101801, `arXiv:2406.09971 [hep-ex]`.

[65] ATLAS Collaboration, "Study of Higgs boson pair production in the $HH \to b\bar{b}\gamma\gamma$ final state with 308 fb^{-1} of data collected at $\sqrt{s} = 13$ TeV and 13.6 TeV by the ATLAS experiment," `arXiv:2507.03495 [hep-ex]`.

[66] CMS Collaboration, "Constraints on the Higgs boson self-coupling from the combination of single and double Higgs boson production in proton-proton collisions at $\sqrt{s} = 13$ TeV," *Physics Letters B* **861** (2025) 139210, `arXiv:2407.13554 [hep-ex]`.

[67] ATLAS Collaboration, "Search for triple Higgs boson production in the $6b$ final state using pp collisions at $\sqrt{s} = 13$ TeV with the ATLAS detector," *Physical Review D* **111** no. 3, (2025) 032006, `arXiv:2411.02040 [hep-ex]`.

[68] CMS Collaboration, "Search for triple Higgs production in Run 2 data of CMS using $4b2\gamma$ final state," Tech. Rep. CMS-PAS-HIG-24-015, CERN, Geneva, 2025. `https://cds.cern.ch/record/2937680`.

[69] S. Di Noi, R. Gröber, G. Heinrich, J. Lang, and M. Vitti, "γ_5 schemes and the interplay of SMEFT operators in the Higgs-gluon coupling," *Phys. Rev. D* **109** no. 9, (2024) 095024, `arXiv:2310.18221 [hep-ph]`.

[70] E. E. Jenkins, A. V. Manohar, and M. Trott, "Renormalization Group Evolution of the Standard Model Dimension Six Operators II: Yukawa Dependence," *JHEP* **01** (2014) 035, `arXiv:1310.4838 [hep-ph]`.

[71] H. K. Dreiner, H. E. Haber, and S. P. Martin, "Two-component spinor techniques and Feynman rules for quantum field theory and supersymmetry," *Phys. Rept.* **494** (2010) 1–196, `arXiv:0812.1594 [hep-ph]`.

[72] G. Costa and G. Fogli, *Symmetries and Group Theory in Particle Physics: An Introduction to Space-Time and Internal Symmetries*, vol. 823 of *Lecture Notes in Physics*. Springer Berlin, Heidelberg, 2012.